Energy transfer in a DNA-based π-array – On the use as light-harvesting antenna systems

Inauguraldissertation
der Philosophisch-naturwissenschaftlichen Fakultät
der Universität Bern

vorgelegt von

Florian Garo

von Tschugg BE

Leiter der Arbeit:

Prof. Dr. R. Häner

Universität Bern

Energy transfer in DNA-based π-arrays – On the use as light-harvesting antenna systems

Inauguraldissertation
der Philosophisch-naturwissenschaftlichen Fakultät
der Universität Bern

vorgelegt von

Florian Garo

von Tschugg BE

Leiter der Arbeit:

Prof. Dr. R. Häner

Universität Bern

Von der philosophisch-naturwissenschaftlichen Fakultät angenommen.

Der Dekan

Bern, 1.6.2012
Prof. Dr. S. Decurtins

II. Acknowledgements

First of all I would like to thank Prof. Dr. Robert Häner for giving me the opportunity to do my PhD thesis in his research group. I had the chance to elaborate interesting and challenging projects. The door to the office of Prof. Häner was always open for problem-solving discussions. Second, I like to thank Prof. Dr. Stefan Vogel and Prof. Dr. Silvio Decurtins for being referees of my PhD work. In addition I'd like to thank Dr. Kerstin Giessler for critically reviewing and proofreading this manuskript.

A special thank goes to the current and past members of the Häner and Leumann research groups for a stimulating and fruitful working athmosphere and to Stefan Keller from the Decurtins research group for his help with cyclic volrammetry experiments. The supporting services in-house (Ausgabe, MS, NMR) and financial support of the Swiss National Science Fonudation (SNF) are greatfully acknowledged.

My bigest gratefulness belongs to my family and friends who always supported me during my studies. Things would have been less encouraging without their reinforcements.

Für Kerstin.
Für Brigitte.
Für Dave und Benj.

Für Papa, ich werde dich für immer in meinem Herzen tragen.

III. Content

Page

1. Introduction 1

1.1 DNA – Besides its natural role 3
1.2 Chromophores – Organization into predictable arrays 5
1.3 DNA-assisted organization of chromophores 7
1.4 DNA-templated energy transfer in multi-chromophoric systems 12

2. Aim of the study 17

3. Results and Discussion 19
3.1 Energy transfer in a phenanthrene stack – DNA-based light-harvesting antenna 19
3.1.1 Synthesis of the required building blocks **P** and **S** 19
3.1.2 System design 20
3.1.3 Spectroscopic investigation and discussion 21
3.1.4 Summary 33
3.2 Energy transfer in a phenanthrene stack – A second channel for energy conversion 35
3.2.1 System design 35
3.2.2 Spectroscopic investigation and discussion 37
3.2.3 Summary 47
3.3 Energy transfer in a phenanthrene stack – Probing the excitation delocalization between **S** and **P** 49
3.3.1 System design 49
3.3.2 Spectroscopic investigation and discussion 51
3.3.3 Summary 57
3.4 New chromophores – The 2,1,3-benzothiadiazole-based building blocks **W** and **V** 59
3.4.1 Synthesis of the new chromophores **W** and **V** 59
3.4.1.1 Spectroscopic investigation of the monomeric building blocks 61
3.4.2 System design 64
3.4.3 Spectroscopic investigation and discussion 65
3.4.4 Summary 71
3.4.4.1 Note on other non-nucleosidic building blocks derivatived from BTD 72

3.5 Energy transfer in a pyrene stack – Quenching of the pyrene excimer by **W** 75
3.5.1 System design 76
3.5.2 Spectroscopic investigation and discussion 77
3.5.3 Summary 83

4. Summary 85

5. Outlook and Conclusion 89

6. Experimental Part 93

7. Appendix 110

8. References 123

1. Introduction

Deoxyribonucleic acids (DNA) pocess a central role for the structure, function and reproduction of living organisms and the importance of DNA in biology and biochemistry is indisputable. More than 80 years after its discovery in the late 19th century by *Friedrich Miescher* and the description of its role as carrier of the genetic information by *Oswald Avery* and *Colin McLeod* in the middle of the 20th century, the three scientists *James Watson*, *Francis Crick* and *Maurice Wilkins* revealed the double helical structure of DNA.[1] By correctly combining the findings of *Erwin Chargaff* with the X-ray diffraction patterns *Rosalind Franklin* determined from DNA fibers provided by *Rudolf Signer*, they proposed the double helical structure of DNA in 1953 which was awarded with the Noble Prize in 1962.[2] Structural as well as functional aspects initiated the search for a chemical way to synthesized DNA oligomers. *Marvin Caruthers* and *Hubert Koester* pioneered with their work the development of automated solid phase DNA synthesis based on phosphoramidite chemistry and opened the gate for a whole new area of chemical research.[3] In 2001, *Craig Venter* and co-workers fully described the sequence of the human genome.[4]

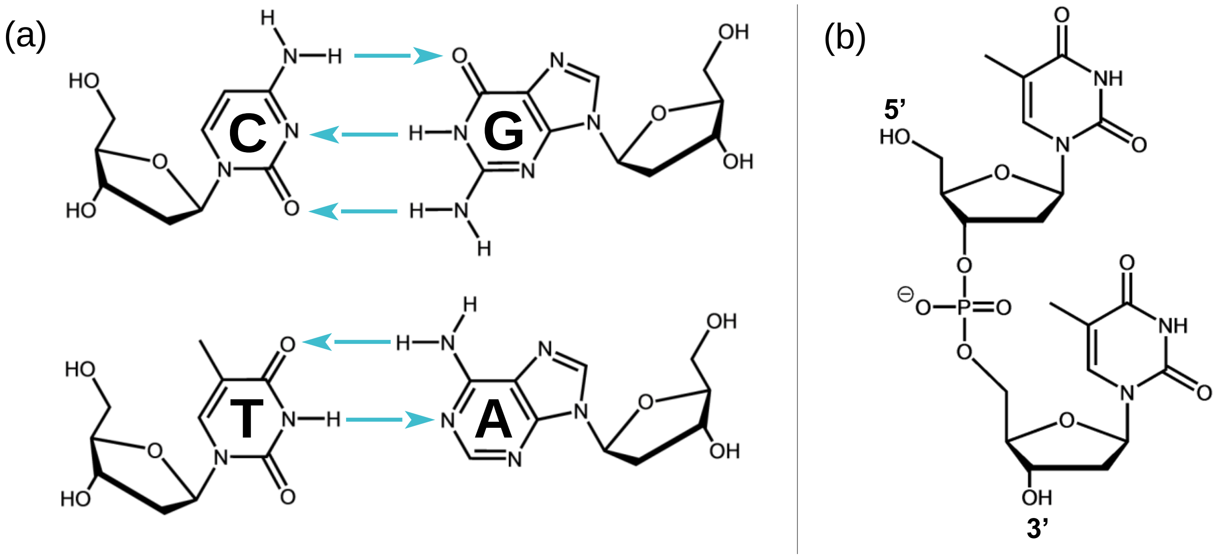

Figure 1. (a) The monomeric DNA building blocks (= nucleosides) with the D-desoxyribose sugar sub-unit (pentose, five-membered ring) and the heterocyclic nucleobases (G = guanine, C = cytosine, T = thymine and A = adenine). The nucleobases are attached via an *N*-glycosidic bond to the 1'-position of the sugar. (b) The nucleosides are connected via a negatively charged phosphodiester bond (= phosphate group).

The central monomeric unit which forms a DNA polymer is called nucleoside. It has two important parts; a D-desoxyribose sugar unit and a heteroaromatic nucleobase. The nucleobase is attached via an *N*-glycosidic bond to the 1'-position of the sugar unit (**Figure 1**). DNA has four different nucleobases ('canonical nucleobases'): adenine (A), guanine (G), thymine (T) and cytosine (C). They are grouped into pyrimidine bases (T and C) and purine bases (A and G). In RNA polymers, the ribonucleic acid analogue of DNA, thymine is replaced by the mainly identical uracil (U). The only difference between U and T is the CH_3-group in the 5-position of the nucleobase. The nucleobases have a particular hydrogen bonding pattern. Two H-bonds are formed between A and T and three H-bonds are formed between G and C. This allows a specific recognition of matching sequences since only two pairs of binding partners exist. The complementary AT and GC recognition is called Watson-Crick base pairing. Nucleosides are linked together via a phosphodiester bond between the 5'-hydroxy group of one monomer and the 3'-hydroxy group of the second monomer. A directionality is generated as both ends of the dimer have different substitution patterns. A DNA strand is normally considered in the 5'-3' direction.[5] A linear oligo- or polymer with the alternating sugar-phosphate motive is called single strand. Pairing of a second single strand with the correct sequence forms a double stranded DNA hybrid. Different factors influence the two-state model between free single strands and bound double strands. The formation of the double strand is favored by the enthalpy of interstrand H-bonds, the enthalpy of nucleobase stacking and the entropy of water molecules released after hybrid formation. To remain in the free single strand state is favored by the entropy of free bond rotation and free translation and the enthalpy of H-bonds with water.[6]

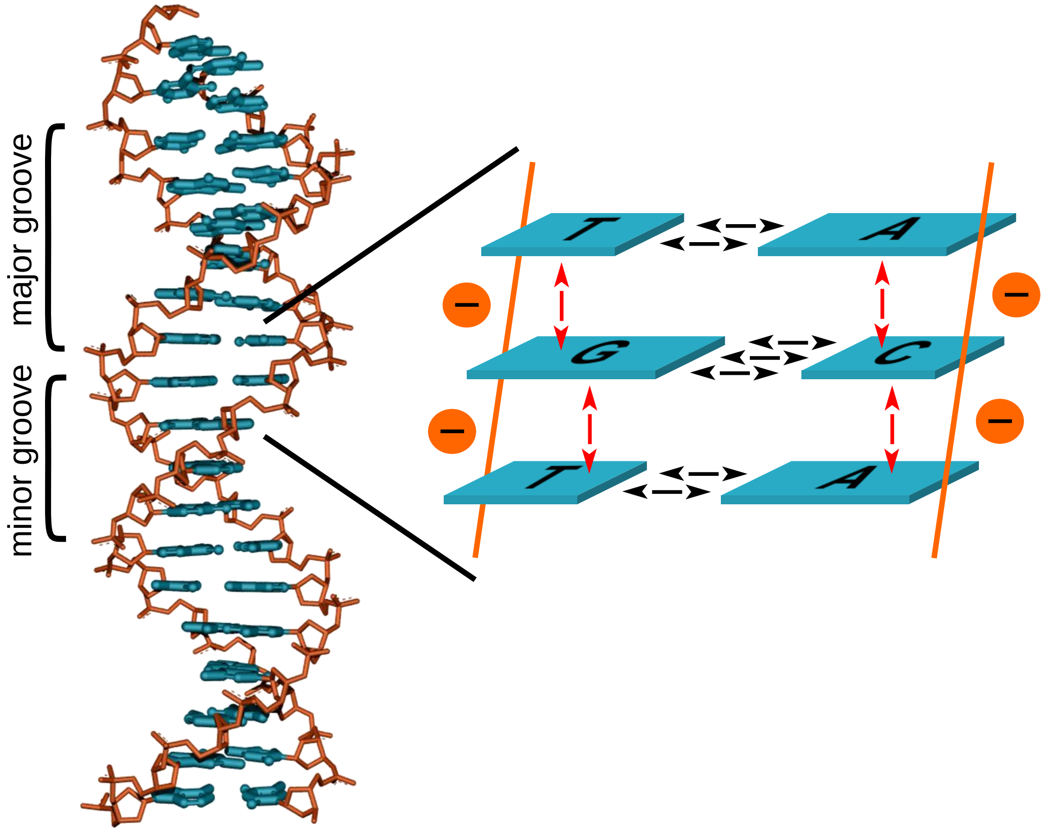

Figure 2. (Left) A right-handed (B-shaped) DNA double helix with the hydrophilic sugar-phosphate backbone (orange) at the outside and the hydrophobic nucleobase stack in the inside (cyan). The particular recognition via H-bonds (black arrows) between the nucleobases A and T (two H-bonds) and between G and C (three H-bonds) brings the two polyanionic (negative charge of the phosphodiester bond) strands together. (Right) Besides the interstrand H-bonds (black arrows) the π-π-stacking interactions between nucleobases (red arrows) are a central stabilizing force for the formation of DNA hybrids.

Two intertwined single strands form the double-helical structure (**Figure 2**). The DNA double helix has two faces, a deep major groove (22 Å) and a shallow minor groove (12 Å). Three major conformations of DNA double helices exist: The B-form (under normal physiological conditions, right handed double helix), the A-form (under dehydrated conditions, compressed compared to the B-form, right handed double helix) and the Z-form (in GC alternating sequences under high salt concentrations, stretched compared to the B-form, left handed double helix).[7] Not only double helical DNA strands are observed but also triple- [8] and multiple helical DNA constructs are found. In this context the so called G-quadruplexes (or G-tetrades) are most prominent.[9] They form the telomeres and protect the chromosomes from being degraded. Thus, G-tetrades are important in cell division and proliferation.[10]

Three important forces are responsible for the stabilization of DNA double (and multi) strands:

(1) Hydrogen bonds (H-bonds) are non-covalent interactions between an electron donor (electronegative atom) and an acidic hydrogen atom. The strength of an H-bond is between the strength of a covalent bond and van der Waals interactions. The nucleobases A and T have both one H-bond acceptor and one donor (blue arrows in **Figure 5**). The nucleobases G and C have a different H-bond pattern, C has two acceptors and one donor whereas G has the opposite.

(2) π-π-Stacking interactions are attractive forces between aromatic units (see section 1.2.1). They are considered to be as important as H-bonds in the stabilization of DNA double strands. Mainly bases in the same strand profit from this force even though the twist of the double helix also allows interstrand interactions.

(3) The hydrophobic effect describes the tendency of hydrophobic units to shield themselves from the exposure to the water environment. Water molecules which dissolve the surface of an aromatic molecule are higher in energy than water in a bulk. The aromatic nucleobases are therefore found in the inner shell part of the DNA double strand to reduce their exposure to water.

1.1 DNA – Besides its natural role

1.1.1 Chemical modification of DNA

With the possibility to chemically synthesize DNA oligomers, scientists started to wonder which consequences certain modifications or changes of the natural form would give concerning the shape, the recognition mode or the function of DNA. Not only curiosity drove this new area of research but also important scientific tasks. To better understand DNA chemistry and to find applications of DNA strands besides its natural role, this research was highly requested.[11]

Three main locations are found where DNA can be modified and were changes are introducible (**Figure 3**): (a) At the nucleobases. It is obvious that the aromatic purine or pyrimidine units are basically alterable. Small changes at the natural base like additional substituents or deletion of heteroatoms can cause different physical properties or can severely change the binding properties of the canonical bases.

To expand the four-letter code of the genetic alphabet, it was tried to find new selective DNA base pairs by altering the H-bond motive.[12] The introduction of completely new and entirely unnatural base surrogates let to particular results. Insertion of fluorescent and larger base analogues let to important diagnostic tools.[13] (b) At the sugar sub-unit. The five-membered sugar ring of the canonical nucleobases resulting from the pentose D-desoxyribose was intensively investigated in the last decades. The different ring size and the additional carbon atom in homo – DNA (six-membered ring and a total of six carbon atoms = hexopyranosyl) caused a much higher thermodynamic stability resulting in only self-pairing of the strands.[14] No cross-pairing of homo – DNA to natural DNA or RNA is possible. Many other analogues were prepared and analyzed.[15] Approaches were undertaken to lock the conformation of D-ribose into a desired position. Conformationally restricted sugar units like the locked nucleic acids family (LNA) [16] or the bi- and tricyclo-DNA analogues were prepared and analyzed. The very high binding affinity of LNA to RNA was unprecedented. (c) At the sugar-phosphate backbone. Modifications of the backbone are difficult to classify. The backbone can be seen as a bridge composed of the repeating sequence P-O-CH-CH-CH_2-O-P which obviously includes parts of the sugar unit. The simplified glycol-DNA (GNA) is focusing on only this backbone and places the nucleobase as a substituent of the main glycol backbone chain.[17] Only homo pairing of (S) - and (R)-GNA and no pairing to DNA was found. A neutral analogue of natural DNA is a peptide nucleic acid (PNA) which uses an amide bond as linkage between monomers.[18] Hybrid formation between PNA and DNA is possible. Other examples exist were the phosphate backbone was modified by replacing the phosphodiester bond.[19]

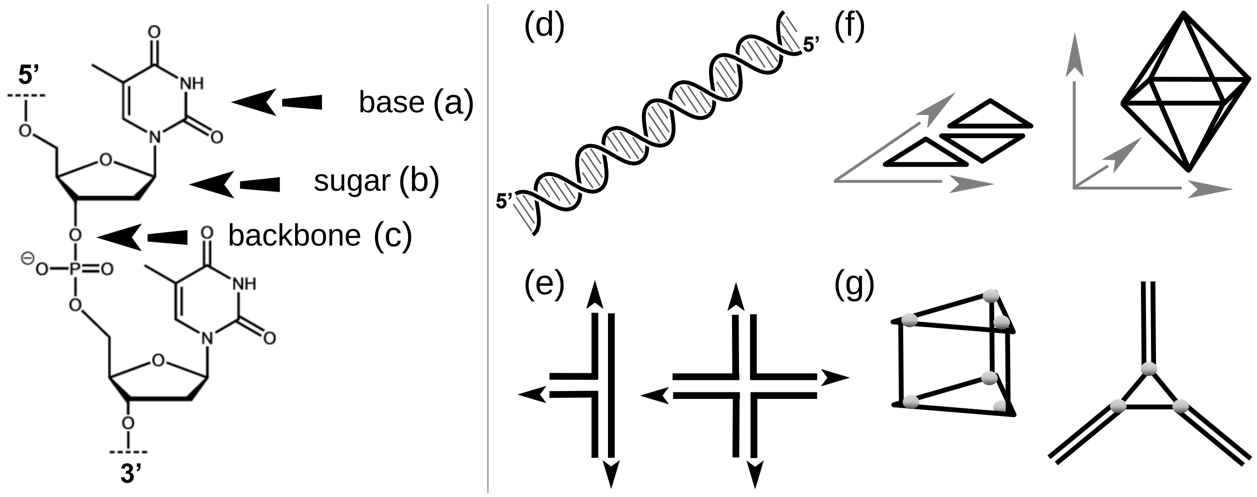

Figure 3. (Left) Possible points were the DNA strand can be modified. (a) The nucleobase can be chemically modified or completely replaced (= base surrogate). (b) The sugar unit can be substituted, extended or reduced in size. (c) During chemical synthesis the backbone can be changed by introducing additional units. In addition the whole phosphate backbone is replaceable. (Right) From the linear oligomer to the construction of three-dimensional objects. (d) The sequences of a linear DNA double helix with two strands in antiparallel direction can be adapted to form (e) three- and four-way junctions composed of multiple strands. (f) A smart sequence design allows the formation of two- and three-dimensional objects. (g) The modification of DNA single strands with metal-binding ligands or other functional objects (grey spheres) allows the construction of other 2D and 3D objects.

1.1.2 DNA nanoarchitectures

DNA single strands form double stranded hybrids by complementary binding to each other in an antiparallel fashion (**Figure 3**d). The distinct binding and the sequence specificity allows the formation of higher ordered constructs like three-way [20] and four-way junctions [21] (holiday junction, **Figure 3**e). This design with its simple and bottom-up approach allows the formation of two- and three-dimensional constructs with a huge variety where nearly no limitations are made concerning shape, complexity and creativity (**Figure 3**f).[22] The precision and reliability which is required from DNA in its role as carrier of the genetic information made it as well the ideal tool for the assembly and precise organization of different components in the nanometer scale. The very high selectivity of one DNA single strand to find the corresponding complementary counter strand allowed the precise and directed organization and orientation of functional materials into higher-ordered constructs (**Figure 3**g). In such complex structures the architecture and the organization are often the key elements for sophisticated and advanced functions and performances.[23]

1.2 Chromophores – Organization into predictable arrays

Chromophores have an essential importance for our daily life. They are central in the photosynthetic energy production of plants [24] and bacteria [25] and they act as dyes and pigments in many technological applications.[26] The ordered arrangement and the proper orientation of chromophores are important in order to control the electronic interactions of adjacent units.[27] Multi-arrays of chromophores often possess significantly different spectroscopic properties than their monomeric sub-units which makes such array attractive for advanced functional materials.[28] The archetype and probably the most elegant and outstanding example of an ordered multi-chromophoric assembly is the light-harvesting antenna complex of photosystems in plants and bacteria.[29] The high degree of ordering and the efficient accomplishment of its duty inspired scientists to design and create artificial systems to organize chromophores.[30]

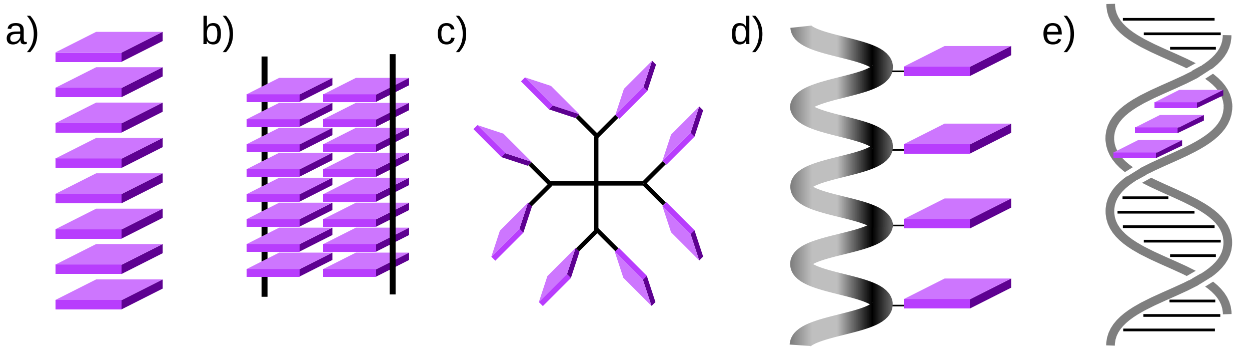

Figure 4. Different approaches to organize and assemble chromophores (violet plates). (a) Supramolecular columnar stacks with strong π-π-stacking interactions and H-bonds between individual units can also be (b) polymerized to higher ordered structures by the guidance of a backbone (black line). (c) Dendrimer-based approach. (d) A helical polymer is functionalized with chromophores on the backbone. (e) DNA double strands are used to assemble chromophres.

1.2.1 π-Functional materials

Self-assembly of π-functional materials is achieved by using supramolecular design rules defined by Jean-Marie Lehn (**Figure 4**a/b).[31] Non-covalent bonds like π-π-stacking interactions and H-bonds thereby stabilize the conjugated constructs built out of repeating monomeric units. These monomers are often extended aromatic units where side-chains are functionalized with H-bond acceptors or donors. The approach of programmed self-assembly of aromatic molecules is straight forward.[32] H-bonds are the ideal construction tool for the formation of secondary structures. They are highly selective and are guidable. Obviously, π-π-stacking interactions are always present in aromatic compounds, but the strength strongly depends on the used solvent. In the model proposed by *Sanders* and *Hunter* the σ-framework of the aromatic unit is considered as a positively charged scaffold sandwiched between two negatively charged π-clouds.[33] The resulting favorable σ-π-attraction between adjacent units is the driving force for the formation of π-functional materials. These materials are broadly used in electronics and sensors.[34] Despite their numerous applications, columnar stacks have certain drawbacks for the organization of chromophores. The length of these nanostructures is not controllable and the exact positioning of the chromophores with nanometric precision is difficult.

1.2.2 Dendritic materials

The shape of a dendrimer is the origin of its name (**Figure 4**c). The name is derived from the Greek word Dendron (tree). Dendrimers have certain advantages compared to π-functional materials in terms of chromophore organization.[35] They have a monodisperse structure (all particles with the same size), they are flexible and the shape of the dendrimer can undergo distortion. Two main synthetic strategies are possible: The divergent strategy starts at the core unit and adds the braching units step-by-step to the periphery. The convergent approach starts at the end groups and builds up the skeleton from the outside. The two different synthetic ways allow the precise placement of specific functionalities and the preprogramed positioning of desired units. Even though dendrimers are monodisperse, the organization within one macromolecule is weak.

1.2.3 Helical polymers

A repeating structural motive with a constant persistence is important for the organization of chromophores. Therefore, helical polymers gained considerable attraction (**Figure 4**d).[36] Among this class of helical polymers polyisocyanates, polysilanes and polyacetylenes are the most frequently used. The rigid polymer backbone is ideal for the placement and organization of chromophores.[37] The control over the interchromophoric interactions is guaranteed by the stiffness of the backbone and the repetitive architecture. As the classes of π-functional materials and denrimers, also helical polymers have certain disadvantages. The control over the polymer's chain length is difficult and the placement or mixing of different chromophores is randomly achieved.

1.2.4 DNA oligomers

It was already pointed out that the helicity and the stiffness of the scaffold were important features for the proper organization of chromophores. Obviously, this makes DNA an ideal tool for the purpose of organizing chromophores. Over a long range of several nanometers a DNA double strand is very rigid and stiff. The complementarity of the two single strands enables a directed assembly and a precise placement of chromophores into a desired position (**Figure 4**e).[38] The length of the array can be controlled by the automation of the synthesis. In addition this automated synthesis protocol allows site-specific insertion and mixing of different types of chromophores. Another important point that makes DNA an ideal tool for the placement of chromophores is the distance between adjacent DNA base pairs. The gap of approximately 3.5 Å is ideal for the insertion of foreign units, for example aromatic chromophores.

1.3 DNA-assisted organization of chromophores

In the last two decades a huge variety of modifications and functionalization of DNA with all types of chromophores for diverse approaches were made.[38, 39] A lot of information about structural aspects and functional details was generated. The following section will give a short introduction on the topic of chromophore organization assembled by DNA double strands.

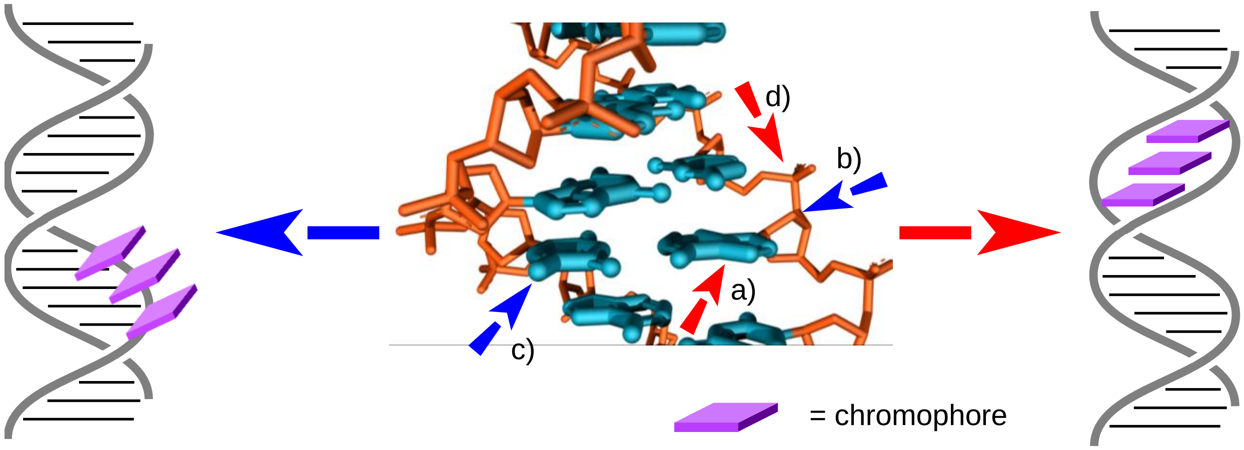

Figure 5. Colored arrows indicate the points where chromophores can be attached. (a) Chromophores can be introduced as base surrogate or by (b) substituting the desoxyribose sugar at the 2'-position. (c) Another approach is the direct attachment of chromophores to the nucleobase from the face where no hydrogen bonds are formed, for example at the CH_3 group of T. (d) The automated synthesis protocol allows for the insertion of completely artificial units into the DNA backbone. Depending on the site where the units are introduced, the chromophores are stacked in the base stack (red arrows) or at the outside of the DNA double helix, in the major or minor groove (blue arrows).

Chapter 1.1.1 dealt with the topic of chemical modification of DNA and where such modifications could be introduced. Chromophores can be introduced at the same positions, namely at the base, on the sugar unit and in between two natural units in the phosphate backbone. The location, where the chromophore is covalently attached to, highly influences the stacking mode of the aromatic chromophores. There are two main modes of stacking: In the interior of the DNA base stack or at the exterior, in one of the two grooves (minor or major groove). Thus, the decision about the point of attachment affects where the chromophore finally is located in the hybrid. **Figure 5** shows the enlarged region of natural base pairs in a B-DNA hybrid. The sugar is twisted against the nucleobase, they are almost perpendicular to each other and the 2'-position of the sugar is pointing to the major groove. It seems to be obvious that a modification of the sugar unit at the 2'-position will bring the chromophore in the major groove. By modifying the nucleobase itself, the mode of stacking can be guided. Stacking into the major as well as into the minor groove is possible depending on the position where the nucleobase is modified.[37, 38] To keep the natural duty of the nucleobase, functionalization is made from the face where no H-bonds are formed. A common way is to functionalize the CH_3 group of T (see later 1.4). This modification can also be seen as a substitution of U. Modifications at the sugar unit or at the nucleobases are made to not further disturb the natural pairing mode of the canonical bases. The 3D model (**Figure 5**) demonstrates that there are no severe interactions expected by modifying DNA at the indicated positions. In contrast to this idea, structural changes and direct interactions with the natural pairing mode are intended by modifying the backbone or by replacing a canonical DNA nucleobase. It is easily understood that the replacement of the nucleobase by a flat aromatic unit shouldn't change the placement of the base surrogate. It has the same position in the DNA base stack like the natural base with the difference that the Watson-Crick H-bonds are no longer possible. Thus, base surrogates are internally stacked like canonical bases.

The automated DNA synthesis protocol is performed on a functionalized solid support (normally on controlled pore size glass (CPG) or polystyrene). The monomeric units are natural nucleosides which are functionalized with a 2-cyanoethyl-*N*,*N*-diisopropylphosphoramidte (CEP) group at the 3'-hydroxy group of the sugar and a 4,4'-dimethoxytrityl (DMT) group at the 5'-hydroxy group. This monomer is is often denoted as natural phosphoramidite building block for chemical DNA synthesis. This building blocks is added to the growing single strand by activating the *N*,*N*-diisopropylamine group of the phosphoramidite with 5-ethylthio-1-H-tetrazole (ETT) or 4,5-dicyanoimidazole (DCI). After oxidation (aqueous iodine and pyridine) of the phosphotriester bond to the corresponding phosphate and acidic deprotection (di- or trichloroacetic acid) of the DMT group, the next cycle begins. The cyanoethyl group remains on the oligomer as protecting group. The oligomer is realeased from the solid phase by basic treatment (ca. 30 % NH_4OH at 55 °C) which also deprotects the phosphate group (β-elimination) and the exocyclic protecting group of the nucleobases (**Figure 6**).[40] The CEP and the DMT functionalities are also chemically introducible into other molecules, as long as two free hydroxyl groups are available (see later in **Scheme 3**). Thus, DNA sequences can be modified by designer units which have no relation to natural building blocks by simply replacing the natural phosphoramidite building blocks in the synthetic cycle.

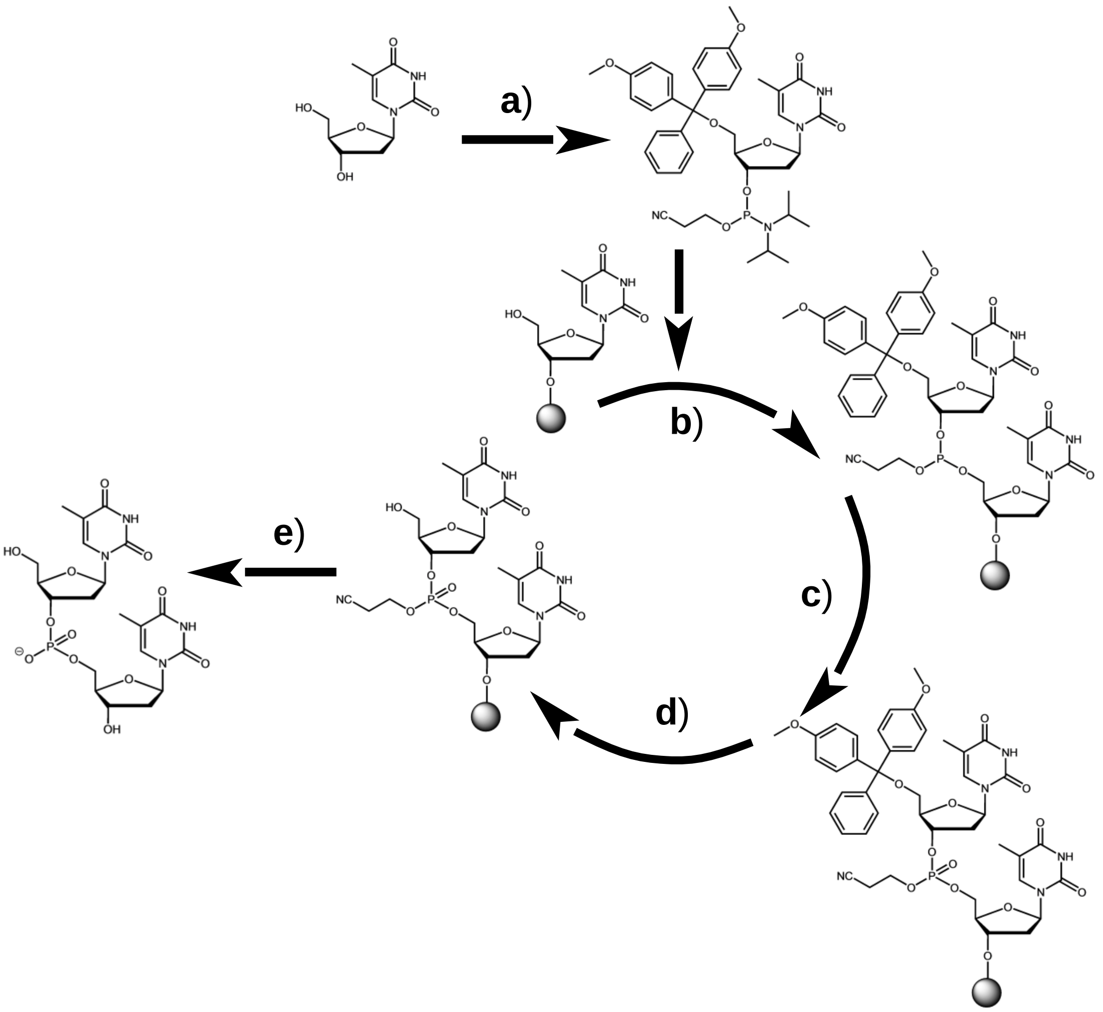

Figure 6. Synthetic scheme for the chemical preparation of DNA. (a) 4'4-Dimethoxytrityl (DMT) protection at the 5'-end and 2-cyanoethyl-*N*,*N*-diisopropylphosphoramidte (CEP) functionalization at the 3'-end of a natural nucleoside. These are the key functionalities for the synthetic cycle. (b) Elongation of an immobilized oligonucleotide (on a solid support, grey sphere) and the formation of a phosphotriester bond. (c) Oxidation of the phosphotriester to a phosphate bond protected with a cyanoethyl group. (d) Acidic deprotection of the DMT group to release a free hydroxyl group. (e) The cycle can start again with (b) or the oligomer can be released and deprotect by basic treatment.

1.3.1 Multi-chromophore arrays on the basis of DNA

Three examples of different types of chromophore attachments and their introduction into DNA hybrids are considered in more detail. The focus is on pyrene as a chromophore which is introduced in different ways. The research development from a single incorporation in the beginning to the multi-chromophore arrays and the potential application in the end is presented. It is well recognized that this part is highly condensed and much more examples of brilliant and smart examples would exist.

Eric Kool and co-workers used building blocks bearing a polyaromatic hydrocarbon unit in the 1'-position of the sugar unit instead of the canonical nucleobase (**Figure 7**). Pyrene derivatives of this kind were the first ones to be incorporated into DNA hybrids.[41] It was found that abasic site analogues (a sugar unit without a nucleobase, see chapter 3.1) in the counter strand were better tolerated by the designer unit than natural bases.[42] The stability of the DNA hybrids didn’t suffer from the presence of this pyrene-abasic site pair. In the following the pyrene modified building blocks were also used for the screening of point mutations (single nucleotide polymorphisms, SNP’s). An important property of pyrene was the key element in this approach. Pyrene excimer formation (see chapter 3.3) was the spectroscopic response which allowed the differentiation between mutations and wild type sequences.[43] Many derivatives with other base surrogates such as naphthalene, phenanthrene, perylene, and benzopyrene were synthesized.[44] By providing extended chains with different sequences (so called ‘oligodesoxyfluorosides’ = ODF) with these units next to each other and by reducing step-by-step the amount of natural DNA, an imaging tool was generated which allowed for the excitation and detection by one single wavelength. The π-π-stacking interactions of the extended aromatic units and the hydrophobic effect caused a strong interaction between adjacent units and allowed different energy transfer mechanisms like FRET (see later in chapter 3.1), excimer and exciplex formation.[45] ODF’s were also used to tag antibodies.[46] In addition they were able to penetrate into the cell plasma.

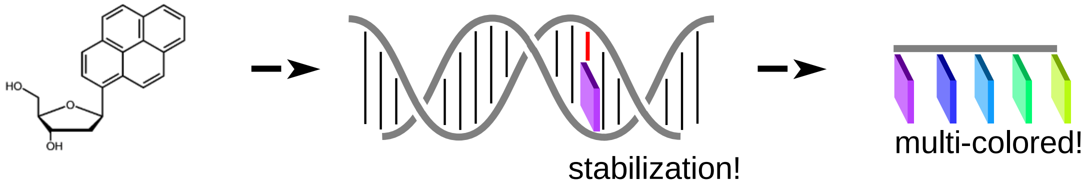

Figure 7. The flat, polyaromatic hydrocarbon pyrene as a nucleobase surrogate in the 1’-position of the sugar unit and its first application as efficient stabilizer of abasic sites (red). Long sequences incorporating related units (benzopyrene, perylene and others) are used as multicolor labelling tool in different approachs.

The group of *Hans-Achim Wagenknecht* introduced a different building block which used the natural binding mode of an AT base pair to organize pyrene units in the major groove. The chromophore was introduced via a Suzuki-cross coupling reaction between pyrenyl boronic acid and a 5-iodo-2’-desoxyuridine (Py-dU).[47] Fist applications of this building block were made by using it for the injection of electrons into the DNA base stack (**Figure 8**). The electrons were transported via the aromatic stack to a 5-bromouridine unit (Br-dU). This behavior was shown by transient absorption measurements and by imaging the DNA strand cleavage at Br-dU.[48, 49] The helical DNA double strand provided an ideal scaffold for the organization of the rigid Py-dU unit. The Watson-Crick base pair between A and Py-dU was not disturbed and the multiply introduced chromophores were helically arranged along the major groove.[50, 51] The same approach was used by other research groups for the organization of different chromophores in the same way.[52]

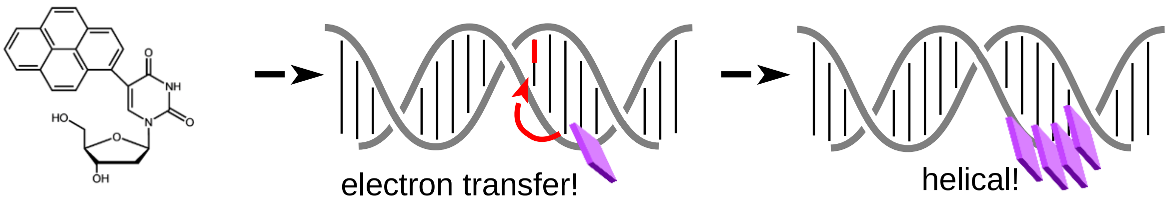

Figure 8. Pyrene as extension of the nucleobase thymine/uracile (T/U). This building block was first used as electron injector for DNA charge transfer approaches. Multiple incorporations of these units revealed the helical arrangement of pyrene along the major groove of the DNA double helix.

The research group of *Robert Häner* used pyrene in a different way. The aim was to introduce pyrene into the DNA backbone with flexible linker units between the phosphodiester bond and the aromatic core.[53] These modifiers were generally called ‘non-nucleosidic’ aromatic building blocks (**Figure 9**).[54] The term non-nucleosidic refers to the fact that no structural aspects from natural nucleosides were present. The high flexibility of the linker chains allowed pyrene to be introduced into the DNA base stack. In a first approach two units were introduced into a DNA hybrid, one unit in each strand. The DNA base stack was interrupted by these two units but the thermal stability of the modified duplex was not decreased. The favorable interstrand stacking interaction between the two pyrene units was not only seen by the high stability of the hybrid but also from pyrene excimer fluorescence emission (see chapter 3.3). In order to test the influence on the total hybrid length and its thermal stability as well as to get structurally organized chromophores, multiple incorporations of the flexible aromatic building blocks into DNA hybrids were performed.[55] It was found that the achiral pyrene building blocks were helically organized within the ‘DNA sandwich’.[56] In contrast to the previously described helical organization of pyrene units in the major groove of DNA hybrids (**Figure 8**), the twisted assembly of the pyrene molecules in this approach happened independently and without the help of natural base pairs.[57] It was shown that the helical arrangement of oligomers entirely composed of non-nucleosidic pyrene molecules and no DNA part was as well possible.[58]

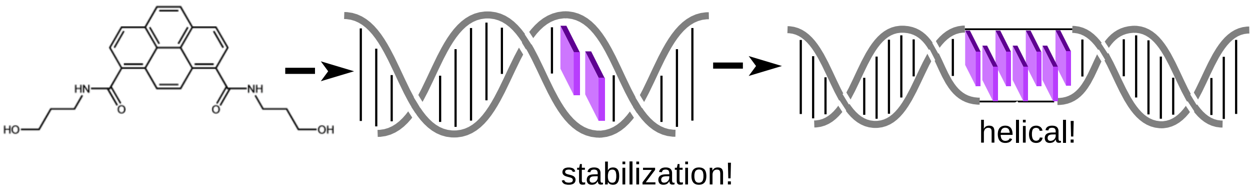

Figure 9. Pyrene with flexible linker units in the 1,8-position. Two units in both strands next to each other stabilize the DNA hybrid by a considerable amount. Multiple incorporated units self-assemble and form helical stacks within the DNA duplex.

The distinct and precise organizing properties of non-nucleosidic aromatic DNA building blocks revealed them a versatile tool for several specialized applications. In the last few years structural aspects of short[59] or extended[55, 56] π-arrays built with non-nucleosidic units gained more and more attraction in the DNA-based organization of chromophores. Several applications and tools were reported recently including general and specific DNA detection probes.[60, 61] The characteristic spectroscopic properties, especially monomer- as well as exciplex- or excimer fluorescence emission, ascribed the aromatic cores of phenanthrene and pyrene a particular role.[62] The placement of a self-assembled stack of up to fourteen phenanthrene units within a DNA double strand (*tri-segmental* design) did not disturb the right-handed helicity of DNA and an extended duplex length was found. Replacement of phenanthrene by pyrene units revealed the helical organization of non-nucleosidic units within the DNA hybrid. In the course of the discussion about the independency of this process it was possible to show that the helical organization of pyrene units was largely independent (*bi-segmental* and *non-DNA* designs). Mixing of different chromophore types in DNA hybrids and, thus, generating disproportional situations not only disrupted the homogeneity of the stacks but also introduced new possibilities. New fluorescent species[53, 63], selective excitation of individual units, selective fluorescence signal quenching[64] and selective aggregation was reported. In this context, one should explicitly mention the description of the first pyrene-phenanthrene exciplex. Excimer emission of pyrene was known since decades[65, 66] and many fluorescent exciplexes[67, 68] with derivatives of phenanthrene are described.[69-72] A triple helical DNA construct revealed for the first time the formation of an exciplex between phenanthrene and pyrene.[62, 73] The intense fluorescence emission at a distinct wavelength was exceptional. It can be hypothesized that the close relationship between the used pyrene and phenanthrene building blocks concerning scaffold and geometry was the reason for the strong fluorescence emission and an excimer-like exciplex could be postulated.[70]

1.4 DNA-templated energy transfer in multi-chromophoric systems

In section 1.3 the DNA-templated organization of chromophores was discussed. Three examples were presented which used fundamentally different approaches to get defined and predictable arrays of chromophores.

The correct and oriented arrangement of chromophores in the antennas complexes and reaction centers of photosystems in plants and bacteria is the reason for the very high and unique efficiency of photosynthetic energy production.[74] In this process electromagnetic energy from the sunlight is absorbed and collected in the antenna complexes, transferred to the reaction center and converted to chemical energy by charge separation across a bilayer. Apparently, three important events are crucial during this process: (1) *light harvesting* and energy collection by the antenna complexes to maximize the overall efficiency of the process, (2) *transfer of the energy* in several steps to the reaction center and (3) *charge separation* combined with the storage of chemical energy. The quest for artificial photosynthetic systems gained more and more attraction and was driven by the aim to mimic this natural photovoltaic device on a molecular level.[75] For each of the three individual processes different approaches were undertaken to mimic photosynthesis.[76] In the following section the focus will be kept on DNA-templated energy transfer processes in multi-chromophoric arrays.

Förster resonance energy transfer (FRET, often also refered to as fluorescence resonance energy transfer) was first described and explored by *Theodor Förster*.[77] The mechanism is described in chapter 3.1. This non-radiative energy transfer process from an excited donor molecule to an acceptor molecule in the ground state highly depends on the distance between the two molecules and on their relative angular distortion. The FRET efficiency depends on the distance (R) between the chromophores by:

$$\frac{1}{1+\left(\frac{R}{R_0}\right)^6}$$

In other words, the efficiency decreases by a factor of $1/R^6$ the longer the distance between donor and acceptor is. This makes the FRET concept a versatile tool to measure and describe distances between two locations. In a different consideration, one could also say that the FRET concept allows the transport of excitation energy over a defined distance.

One of the first who tested DNA structures by using FRET-based approaches was *Robert Clegg*.[78] He and his co-workers investigated the FRET efficiency between fluorescein as energy donor and rhodamine as energy acceptor molecule to see the helicity of double stranded DNA (**Figure 10**).[79] Fluorescein was placed at different positions in one strand whereas rhodamine was kept constant in the counter strand. The expected $1/R^6$ dependence of the FRET efficiency was indeed found, but the helical DNA hybrid disturbed the expectation slightly. A constant efficiency by increasing the distance from 10 to 14 base pairs was found. The rise per twist in a B-shaped DNA hybrid is 10 base pairs. Therefore, the increasing distance between fluorescein and rhodamine was compensated when the chromophores were almost parallel in space to each other.

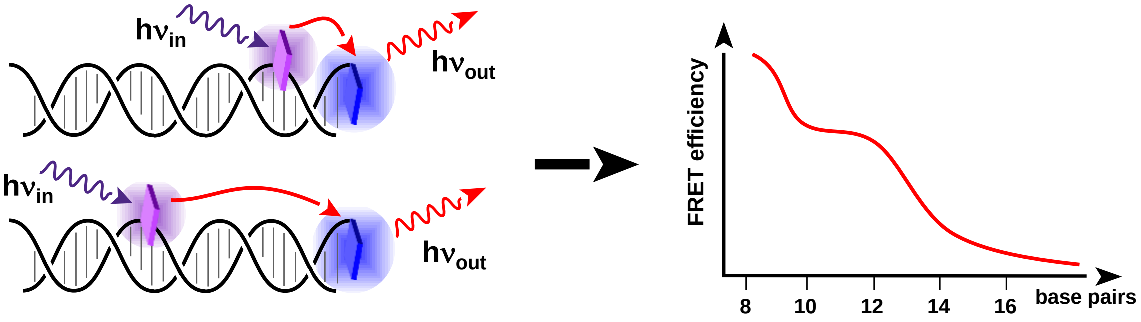

Figure 10. FRET event from fluorescein (donor chromophore, violet) to rhodamine (acceptor chromophore, blue). The efficiency of the transfer process decreased by a factor of $1/R^6$ by increasing the distance between fluorescein and rhodamine. The shape of the curve represented the helicity of the DNA hybrid.

Tedafumi Uchimaru and co-workers found that the FRET efficiency was increased by adding a third chromophore as mediator between donor and acceptor unit. A hexachlorocarboxyfluorescein had the function of a mediating unit between carboxyfluorescein (FAM) and carboxyrhodamine.[80] With his preliminary work *Uchimaru* initiated a fascinating process of amelioration and advancement of the efficiency in long-range energy transfer processes. Independently, the research groups of *Stephen*

Quake[81] and *Yuichi Ohya*[82] took up the *Uchimaru* approach and placed up to three mediator chromophores between donor and acceptor units (**Figure 11**). Even if the experimental design was slightly different, the outcome was largely the same. The *Ohya* approach used a multi-stranded DNA system with eosin as donor chromophore, two tetramethylrhodamines as mediators and TexasRed as final acceptor unit. *Quake* used a two-stranded DNA system with FAM as donor, up to three tetramethylrhodamine-carboxamides (TAMRA) as mediators and Cy5 (cyanine dye family) as acceptor chromophore. The fundamental approach of *Clegg* was virtually inefficient at a distance of 20 base pairs between donor and acceptor. With the introduction of mediator chromophores this distance was almost doubled. The energy was now efficiently transported over a distance of up to 40 base pairs.

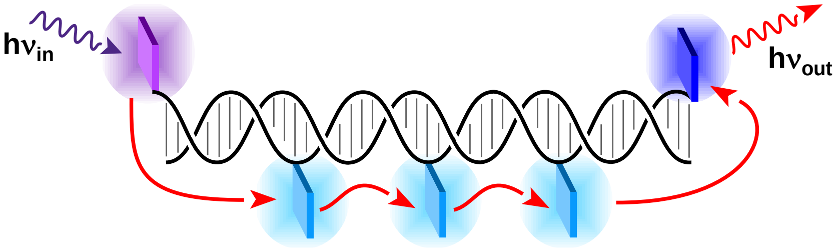

Figure 11. Mediator chromophores (light blue) to overcome the decrease in FRET efficiency and to increase the distance between donor (violet) and acceptor unit (blue).

Markus Sauer and co-workers made one step further by using the general approach of *Clegg* and the advancements of the other research groups and constructed an energy cascade from the initial donor to the final acceptor unit (**Figure 12**). The multistranded DNA system with a four-step energy cascade involved rhodamine green (RhG) as energy donor, tetramethylrhodamine, Atto 590 and LightCycler Red as mediators and Atto 680 as final acceptor unit.[83] Several advantages were achieved in using this approach: First, a spectral range of more than 200 nm was covered between excitation of RhG at 488 nm and fluorescence emission of Atto 680 at 700 nm. Second, a unidirectional energy transfer path was given by the spectral properties and the arrangement of the chromophores.

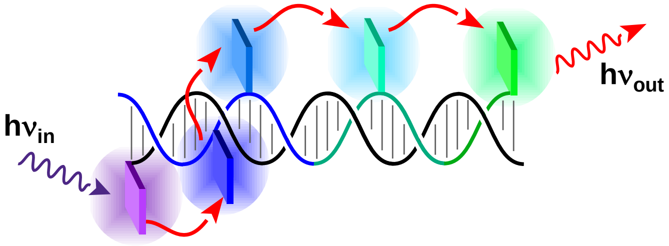

Figure 12. A spectral range of more than 200 nm is covered in the energy cascade from rhodamine green (violet) to Atto 680 (green) in a multi-chromophoric DNA array.

So far the presented examples combined a common concept: One fluorophore was excited and the energy was constantly transported across the cascades to the final acceptor unit. A virtual monomer excitation transfer took place. *Kool* and co-workers attached their multi-colored tag arrays to DNA hybrids and used the ‘secondary fluorescence species’ as FRET donors and a convenient fluorophore on the other end of the double strand as acceptor (**Figure 13**).[84] In this context the term ‘secondary fluorescence species’ is used to summarize fluorophores which are the product of one excited species forming an excited complex with a second species in the ground state (e.g. excimers and exciplexes, see chapter 3.1 and 3.3). The architecture included pyrene, perylene, dimethylaminostilbene and benzopyrene in the multi-colored arrays and TAMRA or Cy5 as FRET acceptors. For the first time excimers and exicplexes were used as FRET donors.

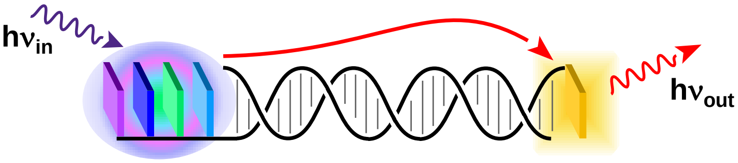

Figure 13. FRET energy transfer from ‘secondary fluorescent species’ (e.g. exciplexes and excimers in violet, blue, green and light blue) to the final acceptor moiety (yellow).

A recent example from the group of *Albertus Schenning* used a supramolecular approach to organize chromophores and afterwards to transfer their excitation energy to an acceptor unit. An oligo-T DNA single strand was used as a template in order to complex monomeric building blocks via H-bonds (**Figure 14**).[85] The helical arrangement of such constructs is remarkable even if the energy transfer efficiency is not outstanding. The monomers were based on naphthalenes. Thus, the energy transfer was from naphthalene to a Cy3.5 acceptor.

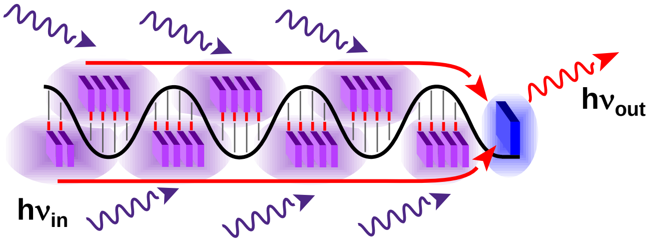

Figure 14. Energy transfer from multiple naphthalene units (violet) complexed via H-bonds (red) to a single stranded DNA template (oligo-T sequene, black) with an acceptor unit (blue) on top.

In summary it can be concluded that energy transfer phenomena between chromophores in close proximity or spatially separated from each other are well understood and explored in detail. Different chromophores were used and especially fluorescein derivatives seemed to be efficient energy donors. Apart from the design of *Albertus Schenning* the waste majority of the studies used one-by-one chromophore assemblies which means that a single molecule absorbed energy and transferred it via several mediators units to the final single acceptor chromophore.

2. Aim of the study

Besides the substantial amount of spectroscopic data dealing with structural and self-assembly aspects of stacks with non-nucleosidic aromatic building blocks, only a small set of data is available which focuses on the energetics and dynamics in such constructs.[86] The introduction of this thesis showed different approaches for the assembly and organization of chromophores into extended stacks (1.2 and 1.3) in order to study the energy transfer properties of such arrays (1.4, **Figure 15**a).

The aim of this thesis was to get more insight into the energy transfer properties of extended stacks built with non-nucleosidic aromatic building blocks. For this approach, extended stacks of phenanthrene units are sandwiched between two DNA segments. Each phenanthrene unit in the stack is an energy donor in analogy to the design of *Schenning* (see section 1.4). A pyrene unit is placed on one end of the phenanthrene stack to form a phenanthrene-pyrene exciplex (**Figure 15**b).[62] This 'secondary fluorophore' (see 1.4) acts as energy acceptor. Unlike the design of previous studies, the used architecture for this work has one main difference. The energy donating moiety (the phenanthrene units) is directly connected and linked to the final acceptor which is not a single unit but an excited complex (exciplex, **Figure 15**c). Thus, one phenanthrene unit has a key role as it is both, part of the energy donor and part of the energy acceptor. The concept is justified by the early work of *Uchimaru*, *Ohya* and *Quake* (see section 1.4) who reported energy transfer events over several steps between equal units.

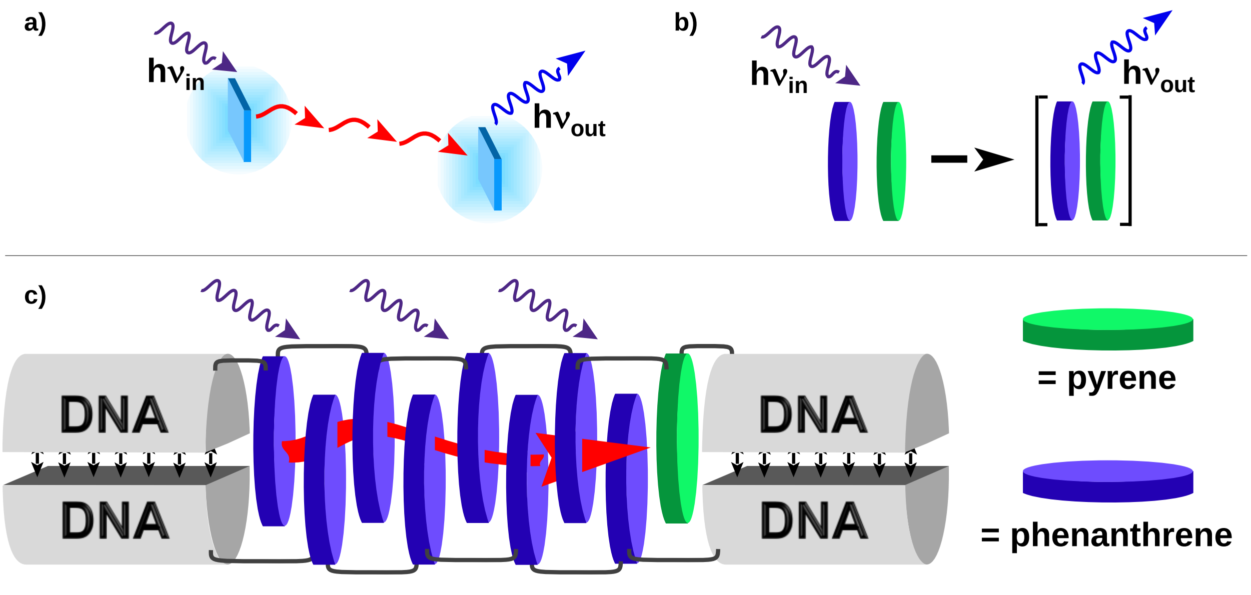

Figure 15. Aim of the study. (a) Several approaches during the last few years used FRET-based systems to transport the initial energy of excitation ($h\nu_{in}$) over several similar units to an acceptor unit where energy was converted to fluorescence emission ($h\nu_{out}$). (b) Pyrene (green disc) and phenanthrene (blue disc) in close proximity can form an exciplex (black clamp) which shows fluorescence emission at a distinct wavelength. (c) Combination of the self-assembly approach of non-nucleosidic aromatic units in DNA frameworks to build an extended stack of phenanthrene units with a pyrene exciplex on one end to test the energy transfer behavior between similar phenanthrene units.

3. Results and Discussion

3.1 Energy transfer in a phenanthrene stack – DNA-based light-harvesting antenna

The results discussed in this chapter let to the following publication: F. Garo, R. Häner, *Angew. Chem. Int. Ed.* **2012**, *51*, 916-919.

3.1.1 Synthesis of the required building blocks **P** and **S**

The synthesis of the required pyrene and phenanthrene phosphoramidite building blocks was performed in close analogy to previously published procedures.[53, 87] Detailed synthetic procedures are described in the experimental part (chapter 5.3).

The flexible aliphatic carbon-three linker (C3) for the attachment of pyrene and phenanthrene to the DNA backbone was synthesized by first protecting the amine group of 3-hydroxypropylamine **1** with phthalic anhydride to give intermediate **2**. 4,4'-Dimethoxytrityl (DMT) protection of the hydroxyl group (compound **3**) was subsequently followed by cleaving the phthalic protecting group under the treatment with hydrazine hydrate to yield DMT-protected 3-hydroxypropylamine **4** (**Scheme 1**).

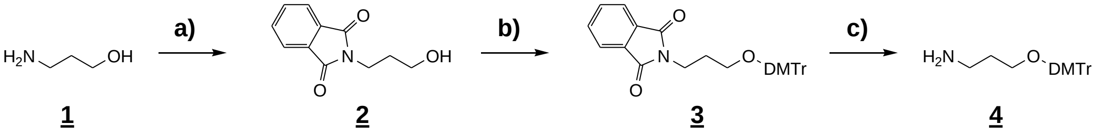

Scheme 1. Route for the synthesis of the carbon-three linker (C3) for the attachment of the aromatic cores to the DNA backbone. Reagents and conditions: (a) phthalic anhydride, 140 °C (99 %); (b) 4,4'-dimethoxytrityl chloride, pyridine, RT, overnight (87 %); (c) hydrazine hydrate, MeOH, 50 °C, overnight (90 %). For the structure of DMTr see scheme 2.

The phenanthrene building block was synthesized according to the described route. Methyl-4-(bromomethyl)benzoate **5** was converted to the corresponding *Wittig* triphenylphosphonium salt and subsequently reacted with methyl-4-formylbenzoate **6** to give a cis:trans isomeric mixture of stilbene **7**. Photocyclization of stilbene **7** gave phenanthrene-3,6-dimethylester **8** which was hydrolyzed to the phenanthrene-3,6-dicarboxylic acid **9**. Amide formation involved the treatment of **9** with a 1:1 mixture of **1** and **4** to give the mono-DMT protected phenanthrene intermediate **10**. Phosphitylation of compound **10** provided the phenanthrene phosphoramidite building block **11** with carboxamide-C3-linker chains attached in the 3,6 position of phenanthrene (**Scheme 2** upper part).

The pyrene building block was synthesized according to the described route (**Scheme 2** lower part). Starting from pyrene **12** the 1,8 functionalization of the aromatic core was reached by a *Friedel-Crafts* acylation with chloroacetylchloride to give 1,8-dichloroacetylated intermediate **13** (the 1,6 isomer was separated off, see experimental part) which was hydrolyzed to pyrene 1,8-dicarboxylic acid **14** by a haloform reaction. Amide formation was reached in the same way as for the phenanthrene building block. Treatment of **14** with a 1:1 mixture of **1** and **4** gave mono-DMT protected intermediate **15**.

Phosphitylation of compound **15** gave the pyrene phosphoramidite building block **16** with carboxamide-C3-linker chains attached to the 1,8 position of pyrene. The synthesized phosphoramidite building blocks **11** and **16** were introduced into DNA oligomers by conventional automated phosphoramidite chemistry (see chapter 1.3).

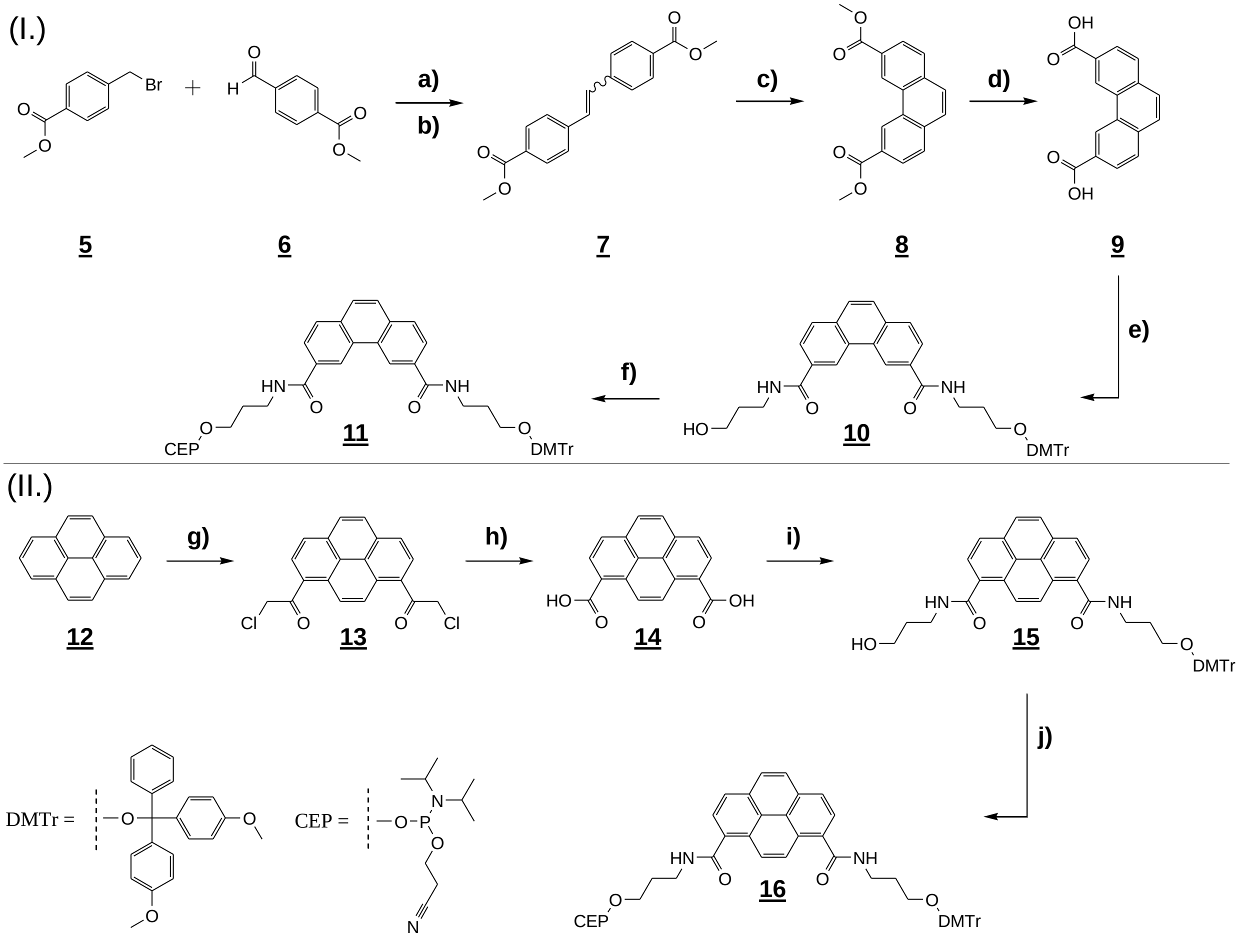

Scheme 2. (I) Synthetic route for the preparation of the phenanthrene phosphoramidite building block **11**. Reagents and conditions: (a) triphenylphosphine, toluene, reflux, 5 hrs. (97 %); (b) sodium methoxide, toluene, MeOH, reflux, 30 min. (76 %); (c) hν, iodine, toluene, RT (56 %); (d) NaOH, EtOH, reflux, 1 h (92 %); (e) **4** and **1** (1:1), *N*,*N*-diisopropylethylamine, HBTU, pyridine, DMF, RT, 2 hrs. (31 %); (f) 2-cyanoethyl *N*,*N*-diisopropylchlorophosphoramidite, *N*,*N*-diisopropylethylamine, DCM, RT, 1 h (45 %). (II) Synthetic route for the preparation of the pyrene phosphoramidite building block **16**. Reagents and conditions: (g) $AlCl_3$, chloroacetyl chloride, DCM, 0 °C (20 min.) then RT, overnight; (h) sodium hypochlorite, Na_2CO_3, n-butanol, EtOH, water, 90 °C, 2 hrs. (91 %); (i) 4 and 3-hydroxypropylamine (1:1), *N*,*N*-diisopropylethylamine, HBTU, pyridine, DMF, RT, 2 hrs. (39 %); (j) 2-cyanoethyl *N*,*N*-diisopropylchlorophosphoramidite, *N*,*N*-diisopropylethylamine, DCM, RT, 1 h (62 %).

3.1.2 System design

The sequences of the DNA hybrids were designed to have three important segments. The core segment was a π-array composed of the unnatural non-nucleosidic phenanthrene (**P**) and pyrene (**S**) building blocks. In this core segment of the hybrid, interstrand aromatic π-π-stacking interactions were the stabilizing forces. The two outer segments were composed of natural DNA base pairs (**Figure 16** and

Table 1). The stabilizing forces between natural base pairs (e.g. H-bonds and π-π-stacking interactions) were described in the introduction.

The number of phenanthrene units in the core segment increased constantly and was doubled from hybrid to hybrid. The core included a stack of zero, two, four or eight **P** units and one **S** unit at one end of the **P**-stack. Next to the **S** unit in the counter strand, an abasic site analogue φ was introduced to keep the sequence length of both strands constant and to reduce positional isomers of the pyrene unit. The DNA hybrid with zero phenanthrene units acted as control hybrid to investigate the spectroscopic properties of pyrene alone and to generate a good reference probe. The flanking DNA parts on both sides of the core segments had an important function. Their role was to bring the non-nucleosidic aromatic phenanthrene and pyrene building blocks into close proximity and to fix them in the desired position. Thus, a clamp-like function was ascribed to the DNA parts in the system presented here. It was desired that the DNA parts and the bases next to the core segment did not, in a first approach, interfere with the core segment at all. It was important to find the fundamental fluorescence properties of the system without external challenges. Therefore the sequences of the outer DNA segments included no guanine (G) units and were composed of entirely AT base pairs. Guanine is known as a fluorescence quencher (see later in chapter 3.2 and 3.4) and could based on this property proposea challenge by quenching the system. An agreement between the loss of hybrids stability because of the absence of GC base pairs and the minimization of fluorescence quenching, especially from G, was made. It was calculated [88] in advance that nine AT base pair on both sides of the core segment guaranteed a stable hybrid.

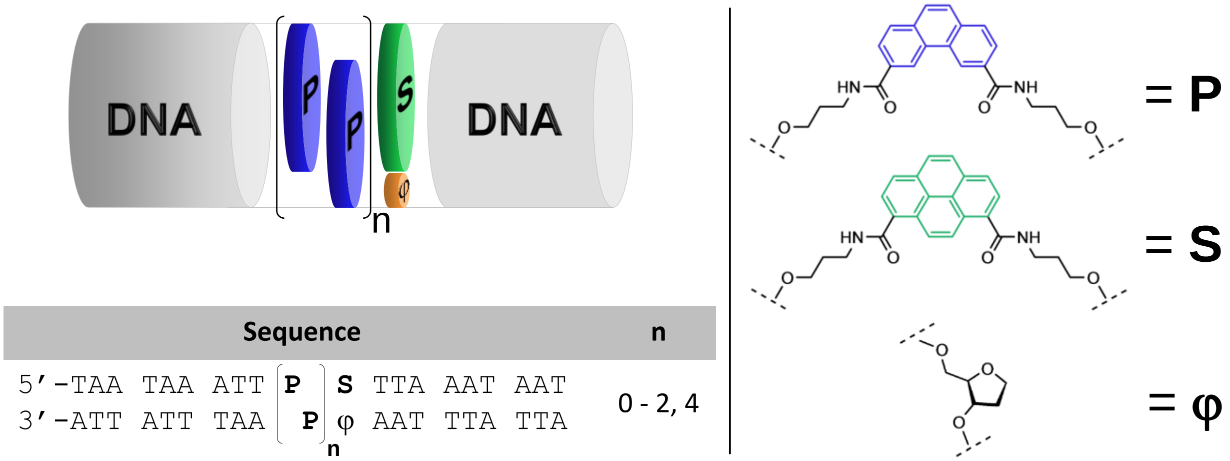

Sequence	n
5′-TAA TAA ATT [**P**]$_n$ **S** TTA AAT AAT 3′-ATT ATT TAA [**P**]$_n$ φ AAT TTA TTA	0 - 2, 4

Figure 16. Design of the DNA-based system in chapter 3.1. The core segment was composed of zero, two, four or eight phenanthrene units (**P**, blue discs) and one pyrene unit (**S**, green disc) which was next to an abasic site analogue (φ, brown disc). The flanking DNA parts were composed of entirely AT base pairs. The chemical structures of the building blocks are shown on the right side.

3.1.3 Spectroscopic investigation and discussion

The single strands were analyzed first by UV/VIS absorbance spectroscopy. All spectroscopic measurements were performed under physiological conditions (aqueous solution with 100 mM sodium chloride and 10 mM sodium phosphate buffer at pH 7.0). The absorbance spectra were composed of two important regions. The DNA nucleobases have a maximum absorption at 260 nm (DNA region). The incorporated chromophores normally absorb in the far ultraviolet (UV) or visible (VIS) region of the electromagnetic spectrum, typically at wavelengths between 300 nm and 450 nm (chromophore region). As the only function of the DNA parts was to hold the core segment in the desired order and to stabilize the whole construct, the DNA region of the UV/VIS spectrum was only important for the determination of the thermal stability (see later). Otherwise, analytical considerations concentrated on the chromophore region.

Table 1. Oligonucleotides **17** – **24** synthesized for chapter 3.1

Nr.	***Sequence***	***ε value (260 nm)***	***Mass [g/mol]***	***Tm [°C]***[a]
17	5‛- TAA TAA ATT **S** TTA AAT AAT	233600	5970.1	27.0
18	3‛- ATT ATT TAA φ AAT TTA TTA	212400	5665.8	
19	5‛- TAA TAA ATT **P S** TTA AAT AAT	260500	6412.5	34.5
20	3‛- ATT ATT TAA **P**φ AAT TTA TTA	239300	6108.2	
21	5‛- TAA TAA ATT **P P S** TTA AAT AAT	287400	6855.0	36.5
22	3‛- ATT ATT TAA **P P**φ AAT TTA TTA	266200	6550.6	
23	5‛- TAA TAA ATT **P P P P S** TTA AAT AAT	341200	7739.7	37.0
24	3‛- ATT ATT TAA **P P P P**φ AAT TTA TTA	320000	7435.4	

[a] 2 µM DNA double strand (4 µM total oligonucleotides concentration), 100 mM sodium chloride, 10 mM sodium phosphate buffer at pH 7.0

The single strands were separated into two groups of different types. One group had two different chromophores in the sequence, namely pyrene **S** and phenanthrene **P**. The other group of single strands included only **P** units. Single strand **17** with only one **S** unit acted as a control. The first group of single strands (**19**, **21** and **23**) and the control strand **17** were considered first (**Figure 17**a). The pyrene unit in single strand **17** had a broad and structureless maximum absorption band around 360 nm. Strands **19**, **21** and **23** showed two distinguishable absorption bands in the chromophore region. The first maximum around 320 nm originated from the **P** units and the second maximum around 360 nm from the **S** unit. A small effect was observed by increasing the content of phenanthrene units from one (**19**) to two (**21**) and four (**23**) units per strand. A slight hypsochromic shift (blue shift) in the maximum absorbance band of the phenanthrene units from 330 nm (**19** with one **P**) to 320 nm (**23** with four **P**) was found. The increased number of hydrophobic interactions between the aromatic **P** units as well as the stronger stacking interactions between them could be reasons for this observation.

The UV/VIS absorbance spectra of the second group of single strands (**20**, **22** and **24**) with only phenanthrene units in the sequence were considered next (**Figure 17**b). Only one absorbance band around 320 nm with a steadily increasing absorbance intensity was observed. A slight broadening of the absorbance bands as well as better resolved vibronic structure were found. The two groups of single strands (**Figure 17**a/b) showed that the lowest energy absorbance bands of phenanthrene (320 nm) and pyrene (360 nm) were well speareted form each other. The overlap of the curves was minimal as the absorbance band of pyrene had a minimum around 320 nm and the phenanthrene aborbance band was tailing off around 360 nm.

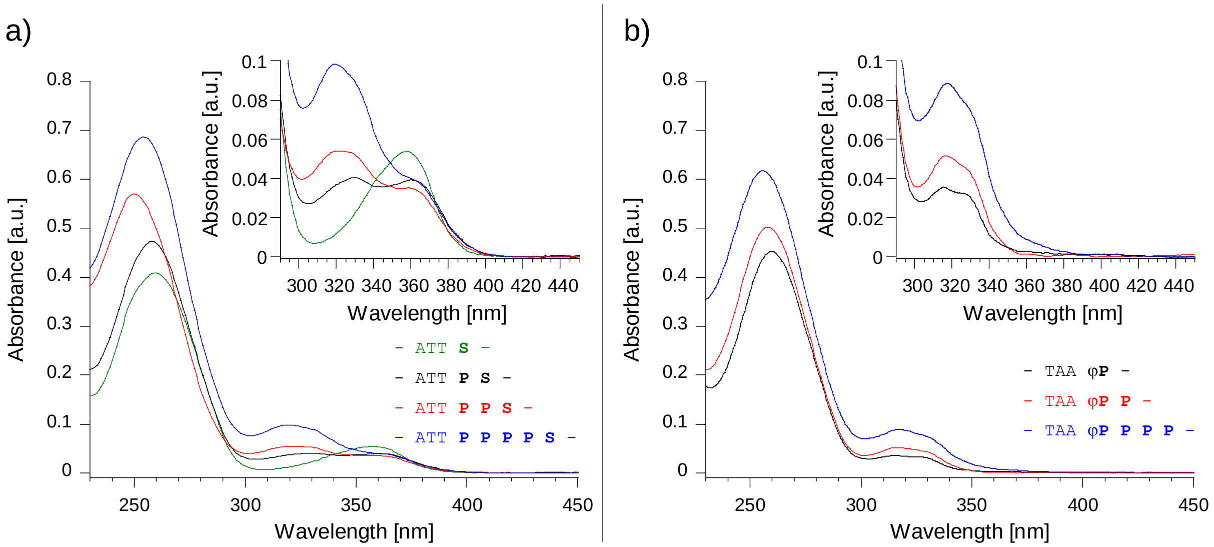

Figure 17. (a) UV/VIS absorbance spectra of the single strands containing **S** and **P**. The abbreviations only indicate the core segment with one neighboring DNA base triplet in the 5' – 3' direction. (b) UV/VIS absorbance spectra of all single strands containing only **P** units and the abasic site analogue φ.

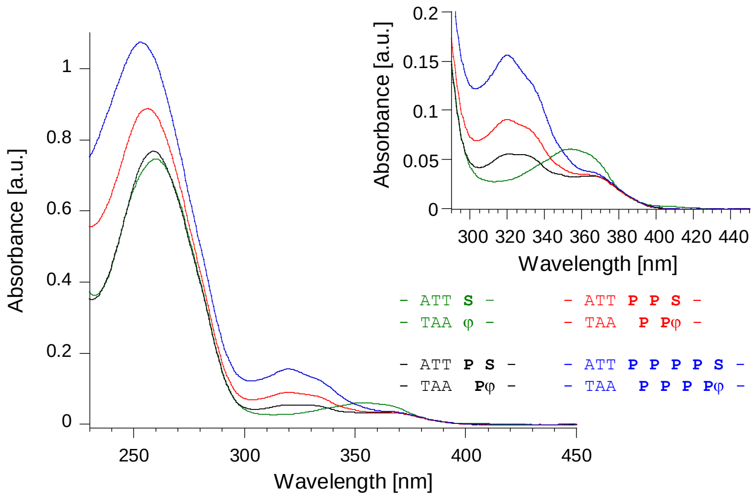

Figure 18. UV/VIS spectra of all hybrids from chapter 3.1.

Sample preparation before measuring the double stranded systems was performed as follows: Annealing of two complementary DNA single strands involved mixing of the strands in the aqueous solution and heating the solution up to 90 °C. This ensured complete separation of the two strands and minimized miss-folded structures. Cooling of the solution to room temperature annealed the double stranded DNA hybrid and the sample was afterwards ready for spectroscopic measurements. The UV/VIS absorbance spectra of all hybrids were investigated (**Figure 18**). The control hybrid **17*****18** showed a broad and structureless absorption band with a maximum at 355 nm (**Figure 18** green line). No remarkable changes of the properties of pyrene after inclusion into the DNA base stack were found. Hybrid **19*****20** (black line), **21*****22** (red line) and **23*****24** (blue line) showed a linear increase of the absorbance intensity at 320 nm. At this wavelength, hybrid **19*****20** had a broad and unstructured band which was only slightly more intense than the second absorption band around 365 nm. Hybrid **23*****24** showed a slightly structured band at 320 nm. A better resolved vibronic structure of an absorption band can be attributed to less rotational freedom of the absorbing units and a more constrained aggregation.[57, 89] Thus, longer phenanthrene stacks provided organized and fixed chromophore constructs (see **24**, **21*****22** and **23*****24**). The absorbance band at 365 nm was attributed to the pyrene unit. All three hybrids with different numbers of **P** units and one **S** unit had the same absorptivity at 365 nm. In all three hybrids the intensity of the absorbance at 365 nm was decreased by a considerable amount compared to control hybrid **17*****18**. This was attributed to the interplay between pyrene and phenanthrene units and the increased stacking interactions between the units. It was important to see that pyrene was well tolerated and integrated on top of the aromatic stack of phenanthrene units.

The thermal stability of all hybrids was determined by UV/VIS assisted thermal denaturation experiments. The temperature dependent absorbance value was measured and gave a melting temperature (Tm) for each hybrid. It is known that the organization of molecules and their transition moments in a molecular aggregate causes changes in the absorption spectrum. Organization of randomly oriented transition moments to colinear or parallel arranged aggregates results in a hyperchromic or hypochromic effect in the absorbance value.[90] Therefore, DNA hybrids have less intense absorbance intensities at 260 nm (maximum absorption of the DNA nucleobases) than the corresponding randomly distributed and non-oriented single strands. This effect can easily be followed by changing the temperature. At high temperatures the strands are separated and unorganized. Hybridization of the strands at lower temperatures therefore causes a hypochromic effect in the absorbance spectrum. The Tm value of a DNA hybrid is calculated from the maximum of the first derivative of its sigmoidal temperature-dependent absorbance curve.[91]

The Tm values of the four hybrids were between 27.0 °C and 37.0 °C (see **Table 1**). Not surprisingly, hybrid **17*****18** had the lowest thermal stability. It was found previously that **S** units can stabilize abasic sites and compensate their disadvantageous effect on the hybrid stability compared to natural DNA bases in the same place.[92] The abasic site analogue φ in hybrid **17*****18** reduced the Tm by a considerable value and was not completely compensated by the presence of **S**. The AT rich flanking DNA sequences were also not advantageous for the thermal stability. The two factors (abasic site analogue, high AT content) were the main reasons for the low thermal stability. The other three hybrids reached higher thermal stabilities. The introduction of **P** units and the resulting interstrand stacking interactions caused a considerable increase in the Tm values as described in the introducation (1.3). This higher stability indicated a beneficial interplay between aromatic units in the core segment. Overall, the Tm values were high enough to ensure a proper arrangement and organization of all hybrids under normal temperature conditions. The following experiments were performed at 15 °C.

The thermal denaturation was determined at two absorbance wavelengths, at 260 nm to follow the denaturation of the DNA part and at 320 nm to follow the denaturation of the core segment. It was interesting to see whether the hybrids were constantly stable over all three segments and denatured at once or if each segment had its own dynamic. The sigmoidal curves (**Figure 19**, blue lines) indicate that strand separation at elevated temperatures occurred at once. The 1st derivatives (**Figure 19**, black lines) of the two curves had the maximum value at the same temperature for both interrogated wavelengths. The chromophore region had exactly the same stability as the DNA region. These results also showed that strong stacking interactions between the chromophores were present.

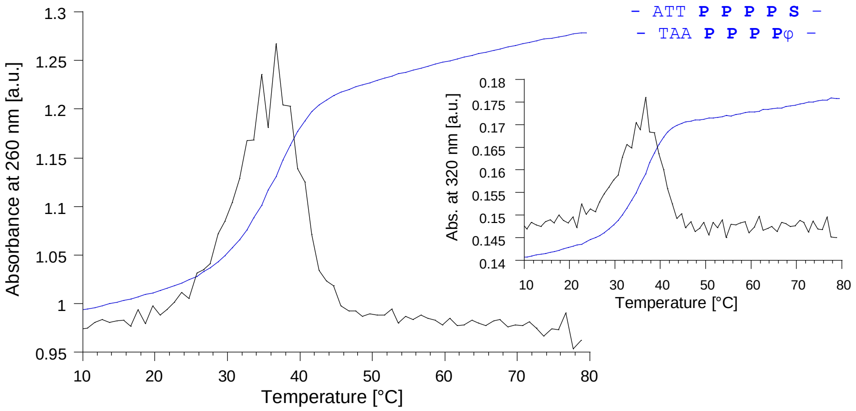

Figure 19. Tm curve of hybrid **23*24** (blue lines) at 260 nm and 320 nm (inset) and the corresponding 1st derivatives (black lines).

The UV/VIS spectra revealed that the hybrids were excitable at two sites in the core segment for fluorescence emission analysis. One site was the part of the core segment with multiple phenanthrene units (excitable at 320 nm) and the other site was the single pyrene unit (excitable at 365 nm). Pyrene and phenanthrene are both moderate to good fluorophores. Therefore, different fluorescent species were possible from hybrids or from single strands.[93] It was possible to find pyrene or phenanthrene monomer emission from hybrids or single strands where only one kind of chromophore was present.Pyrene-phenanthrene exciplex emission was possible from hybrids and single strands where both chromophores were present in close proximity. From previous studies it was known that the maximum emission wavelengths of the fluorescent species were approximately 400 nm (**S** monomer)[89, 94], 370 nm – 400 nm (**P** monomer)[95] and 450 nm (**SP** exciplex)[62]. Hence, not only the absorption bands of the two chromophores were nicely separated but also the maximum fluorescence emission bands of the monomers and the exciplex were easily distinguishable (**Figure 20**).

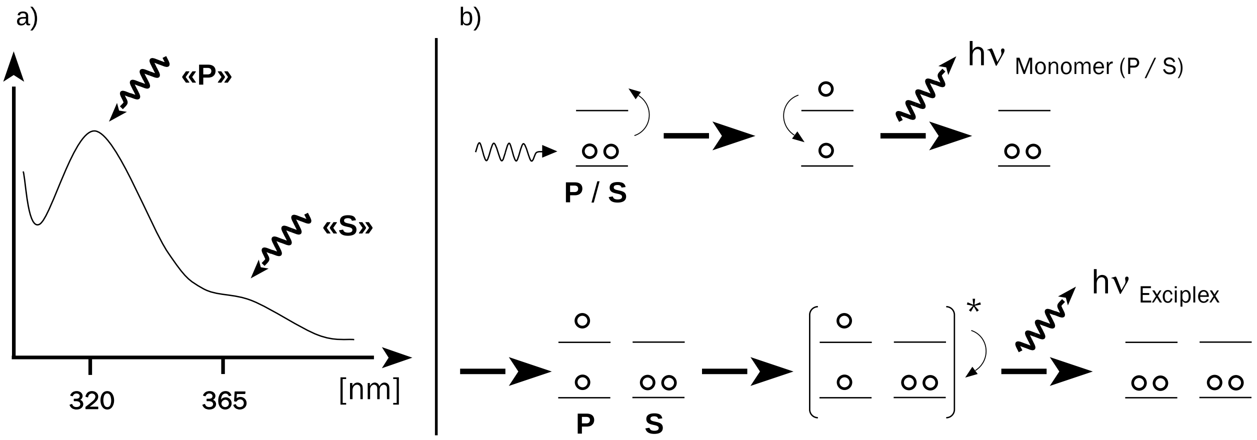

Figure 20. (a) Excitation at the two sites in the DNA hybrids. The absorbance bands of **S** and **P** were well separated from each other. A predominant excitation of one species at the indicated wavelength (320 nm for **P** and 365 nm for **S**) was possible while the other species remained mainly unaffected. (b) The principle of fluorescence emission (open circles represent electrons): After excitation of an electron in the highest occupied molecular orbital (HOMO), relaxation to the ground state leads to emission of light at a specific wavelength (monomer emission of **S** or **P**, upper part). If a complex is formed between the excited state of one species and the ground state of another species ('excited complex' = exciplex) relaxation of this interaction leads to fluorescence emission at batochromically shifted wavelengths compared to monomer emission (**PS**-exciplex, bottom).

The fluorescence properties of the control hybrid **17*18** after excitation at 320 nm were tested. Single strand **17** (**Figure 21**a, black line) had an emission maximum at the typical pyrene monomer emission wavelength of 400 nm. Hybrid formation by adding counter strand **18** to form hybrid **17*18** did not significantly change the spectrum (**Figure 21**a, red line). The emission intensity as well as the position of the emission maximum remained the same as for the single strand alone. No additional fluorescence emission lines were found. No exciplex formation between pyrene and one of the nucleobases was expected. Such complexes mostly occur between pyrene and guanine.[96, 97] It was shown that excitation of pyrene in **17** or **17*18** at 320 nm emitted a considerable amount of fluorescence even if the pyrene had a minimal absorbance at this wavelength. After excitation at 320 nm, the single strands with only **P** units in the sequence (**20**, **22** and **24**) had an emission maximum between 380 nm and 410 nm (**Figure 21**b/c/d, blue lines). The emission intensity was low and increased steadily from one to four units. This fluorescence emission was attributed to phenanthrene monomer emission. Even if there are certain examples in the literature of phenanthrene building blocks that formed excimers[98], the red-shift of only 30 nm of the emission maxima from the hybrid with one **P** unit (**20**) to the hybrid with four **P** units (**24**) was quite small. A larger shift is often seen in the transition from monomer emission to excimer emission (see later in chapter 3.3). In addition, excimer emission bands are often lower in intensity compared to the monomeric species. Nevertheless, it was not excluded that **P**-excimers were present in single strand **22** or **24**. A final conclusion on this topic couldn't be made.

The other single strands (**Figure 21**b/c/d, black lines) and all hybrids (**Figure 21**b/c/d, red lines) had both chromophores in the sequence and showed a broad and mainly structurless emission band with a maximum centered at 450 nm. This was the typical maximum emission wavelength of the phenanthrene-pyrene exciplex. The emission curves of some single strands had a very slight shoulder around 400 nm. This shoulder was attributed to a remaining amount of pyrene or phenanthrene monomer emission. The emission curves of the hybrids did not show this feature around 400 nm. They showed a perfectly structureless and symmetrical emission envelope. The intensities of the exciplex emission curves in hybrids **19*20**, **21*22** and **23*24** increased constantly.

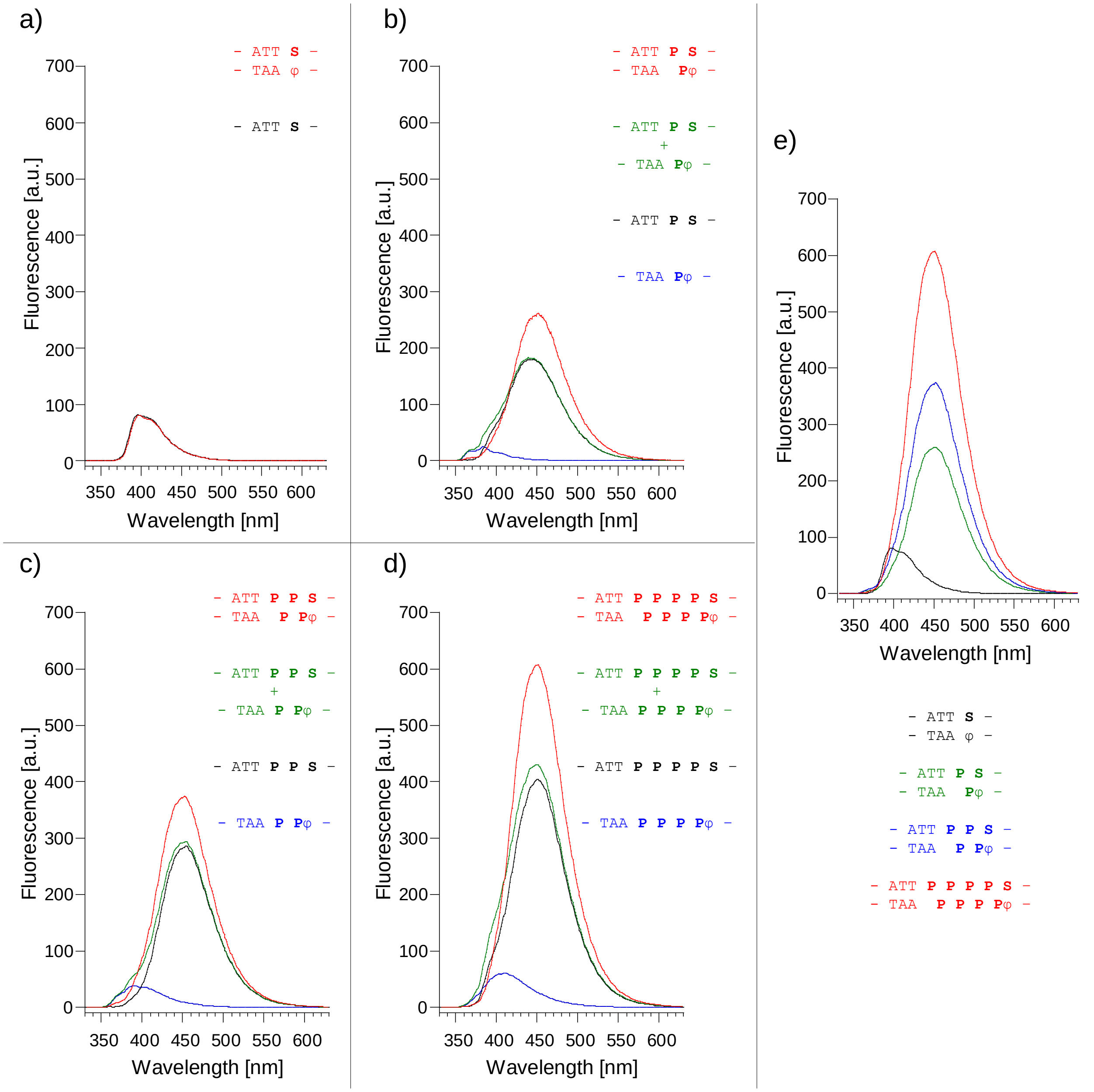

Figure 21. Fluorescence spectra of all hybrids and single strands after excitation at 320 nm. (a) Control hybrid **17***18 with one pyrene unit; (b) hybrid **19*20** with two phenanthrene units and one pyrene unit; (c) hybrid **21***22 with four phenanthrene units and one pyrene unit; (d) hybrid **23***24 with eight phenanthrene units and one pyrene unit. Hybrid emission spectra are shown in red, emission from single strands in black or blue and the sum of the emission spectra of single strands in green (calculation). (e) Summary of the emission curves of the first four hybrids after excitation at 320 nm.

Roughly speaking, the more phenanthrene units a hybrid included, the higher was the exciplex emission intensity. The intensities of the curves were much higher than initially expected. The emission curves of hybrids were not simply the sum (**Figure 21**b/c/d, green lines) of the emission curves of the corresponding single strands but significantly changed after hybridization. For example, hybrid formation between single strand **20** (low intensity phenanthrene monomer emission at 400 nm, **Figure 21**b, blue line) and single strand **19** (phenanthrene-pyrene exciplex emission at 450 nm, **Figure 21**b, black line) to double strand **19*****20** resulted in a pronounced exciplex emission curve(**Figure 21**b, red line). On the other hand, the sum of the emission curves of the mentioned single strands (**Figure 21**b, green line) expected a less intense emission. This trend was found for all hybrids. As soon as the phenanthrene-containing single strand was added, the exciplex emission increased.

At 365 nm all hybrids had the same UV/VIS absorptivity. This was expected because all hybrids included only one pyrene unit. Excitation of this pyrene unit at 365 nm therefore should lead to simple and straight forward results. The control hybrid **17*****18** had an emission maximum centered at 400 nm after excitation at 365 nm (**Figure 22**a, orange line). The emission intensity was higher than after excitation at 320 nm which was expected based on the UV/VIS spectrum. Excitation at 365 nm of the other hybrids with phenanthrene units gave an emission maximum at 450 nm. The curves of all three hybrids were superimposable (**Figure 22**a, black/red/blue lines).

The emission curves after excitation at 320 nm and after excitation at 365 nm were identical in shape and position. This was visualized by normalization of the two emission curves of hybrid **23*****24** after excitation at the two different wavelengths. The normalized emission curve after excitation at 365 nm was superimposable with the normalized emission curve after excitation at 320 nm. This revealed that the exciplex formed after excitation at either of the two wavelengths was in both cases the same. Whether an excited **P** formed a complex with a ground state **S** or vice versa had no influence on the position of the emission maximum. Exciplex emission always took place at 450 nm. This seemed to be obvious, but examples in the literature showed that this does not necessarily need to be the case. Different exciplex emission wavelengths were found depending on the excitation wavelength and the ratio of the chromophores in a two-component system.[99] In the example described here, exciplex formation between pyrene and phenanthrene always gave an emission curve centered at 450 nm irrespective of the excitation wavelength and the total number of involved chromophores. The hybrid emission spectra had no shoulder around 400 nm. If a shoulder would be detected, an ‘inefficient’ exciplex formation could be stated because energy would be lost by phenanthrene or pyrene monomer emission. The number of excitable phenanthrene units had no influence on the position of the emission curve. All hybrids were centered at 450 nm irrespective of the number of excited phenanthrene units. Even if this number was increasing from two to eight units the emission maximum was always centered at 450 nm. This fact was as well not this obvious. Examples in the literature showed that red-shifted emission curves were formed when the number of excited units was increased in relation to the unit which was in the ground state.[100]

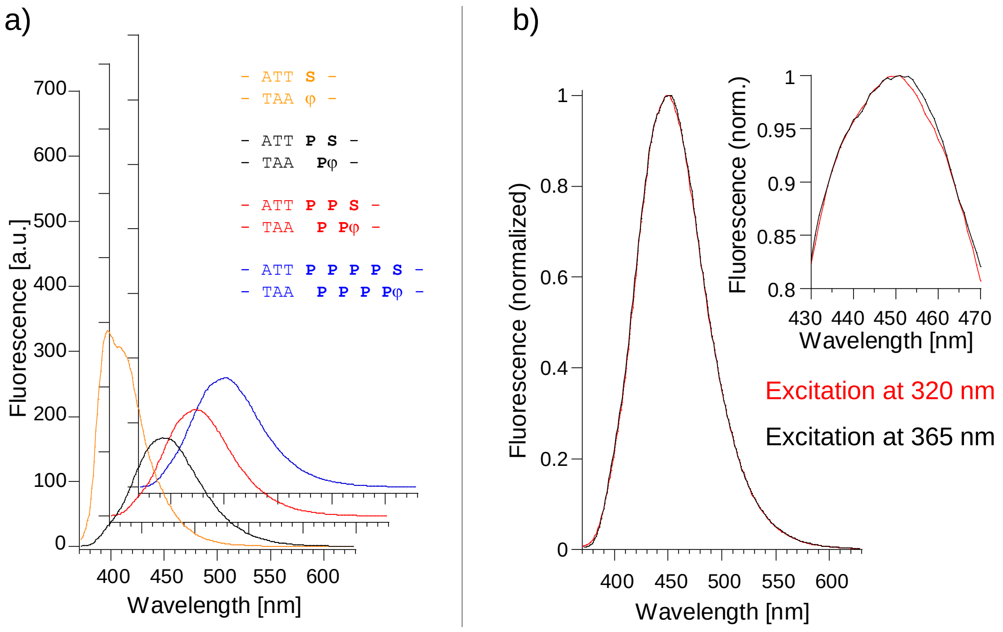

Figure 22. (a) Perspective view on the fluorescence spectra of all hybrids after excitation at 365 nm. (b) Normalized emission curves of hybrid **23*24** from different excitation wavelength.

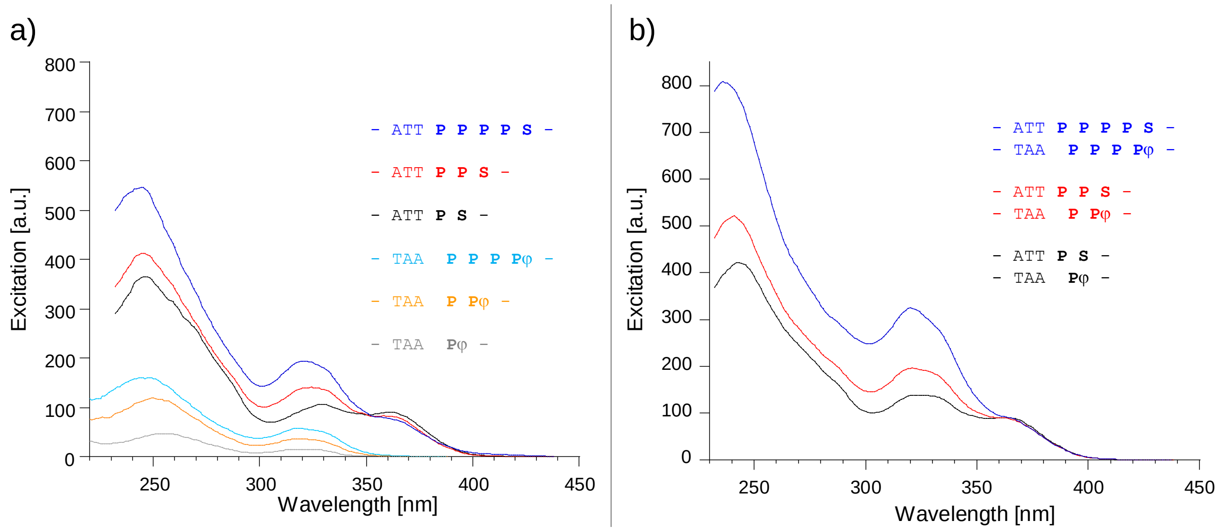

Figure 23. (a) Excitation spectra of single strands. (b) Excitation spectra of hybrid **19*20**, **21*22** and **23*24**. The emission wavelength was 450 nm.

Excitation spectra of single strands and of the three hybrids with two (**19***20**), four (**21***22**) or eight (**23***24**) phenanthrene units were collected at the maximum emission wavelength of the exciplex (450 nm, **Figure 23**). Single strands with only **P** units in the sequence showed no excitation at wavelength longer than 360 nm. Around 320 nm the intensity increased constantly with increasing number of **P** units. Single strands with sequences including **P** and **S** units had two maxima, one at 320 nm (**P** units) and one at

365 nm (**S** units). Of course, the excitation spectra of hybrids were analogous to the spectra from single strands with **S** and **P**. At 365 nm all hybrids showed the same excitation intensity. At 320 nm the excitation intensity increased linearly and hybrid **23*24** was the most intense. At 240 nm the third maximum of the excitation curves was located. Also here, a constant increase of the intensity was found. It was concluded that the exciplex was a composition of a constant number of pyrene units and an increasing number of phenanthrene units. This was in agreement with the findings from the emission curves and their linear increase of the intensities.

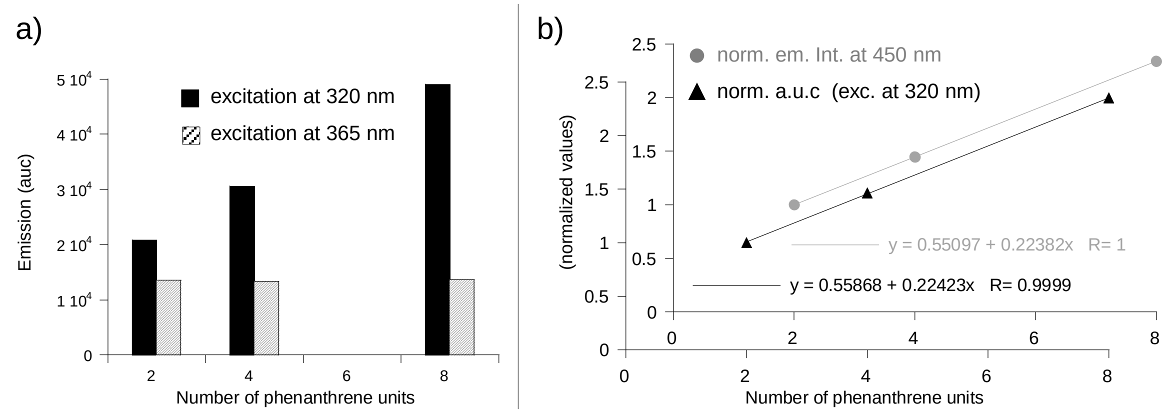

Figure 24. (a) Area under the emission curves (a.u.c) of hybrids as a function of phenanthrene units. Excitation at 320 nm (black bars) resulted in a linear increase of intensity upon increasing number of phenanthrene units whereas excitation at 365 nm (black shaded bars) gave a constant value of all hybrids upon increasing number of phenanthrene units. (b) Comparison between areas under the emission curve (black triangles, excitation at 320 nm) and the effective intensity at 450 nm (grey circles). The values were normalized (also see **Table 2**)

The increase of the emission intensity upon increasing number of phenanthrene units after excitation at 320 nm was investigated in more details. The area under the emission curves (a.u.c) of hybrid **19*20**, **21*22** and **23*24** after excitation at 320 nm or 365 nm were calculated and plotted against the number of phenanthrene units (**Figure 24**a). A linear increase of the values for emission curves after excitation at 320 nm was found whereas the values were constant after excitation at 365 nm. These two facts were expected based on the obtained fluorescence emission curves. It was of course recognized that this consideration included the whole emission envelope, thus, also other not directly detected fluorescent processes (monomer emission from both building blocks around 400 nm). It was possible that monomer emission signals were covered by the broad emission curve of the exciplex and would therefore not be detected. On the other hand, fluorescence emission between 450 nm and 500 nm came to a waste majority from the exciplex as monomer emission form **S** and **P** was tailing off at these wavelengths (see emission curve from single strand with only **P** units and the monomer emission curve of the **S** unit in hybrid **17*18** in **Figure 21**). Therefore the normalized fluorescence intensities at 450 nm and the normalized areas under the emission curves were plotted against the number of phenanthrene units (**Figure 24**b). The points linearly increased and the slopes of the two regression lines were identical. The signal amplification factors (normalization to the value of hybrid **19*20**) were all the same irrespective whether the areas under the curves or the emission intensities were taken (see **Table 2**). The quantum yields of the exciplex emission were determined. The highest value was detected for hybrid **19*20** (0.46) and the lowest for hybrids **23*24** (0.41). Even if the values were not similar, the deviations were within an experimental error. The quantum yield was basically constant within the three hybrids. The fluorescence properties of the three hybrids were summarized (**Table 2**).

Table 2. Fluorescence properties of hybrids **19*20**, **21*22** and **23*24**

	19*20	***21*22***	***23*24***
number of phenanthrenes	2	4	8
a.u.c (excitation at 320 nm)	20877	30612	49038
amplification factor of a.u.c [a]	1	1.46	2.35
Increase of a.u.c per additional **P** unit [%]	-	23.0	22.5
a.u.c (excitation at 365 nm)	13504	13375	13699
amplification factor [a]	1	0.99	1.01
fluorescence intensity at 450 nm [a.u.] [b]	259	374	607
amplification factor at 450 nm [a]	1	1.44	2.34
fluorescence intensity at 500 nm [a.u.] [b]	91	133	212
amplification factor at 500 nm [a]	1	1.46	2.33
quantum yield Φ	0.46	0.42	0.41

[a] normalized to the value of hybrid **19*20**; [b] emission curves after excitation at 320 nm.

The more **P** units a hybrid included the more pronounced was the exciplex emission. This was the core finding of this first set of hybrids. Areas under the emission curves and fluorescence emission intensities at 450 nm and 500 nm increased perfectly in parallel. Hybrid **23*24** had an approximately 2.3-fold more intense exciplex emission intensity than hybrid **19*20**. The increase of fluorescence emission was approximately 23 % per **P** unit. It was shown that only the exciplex caused this increase in emission intensity and other fluorescent species, which could potentially be present as well, were irrelevant for the observed behavior. It was tried to find a possible mechanism to explain the findings.

A hypothetical mechanism is proposed and shown (**Figure 25**). The mechanism for the results after excitation at the pyrene units (365 nm) was straight forward. The excited pyrene **S** formed a complex with the phenanthrene **P** next to it in the ground state. This excited complex (exciplex) relaxed back to the ground state by emitting light at a maximum wavelength of 450 nm (exciplex fluorescence emission). The number of additional **P** units next to the exciplex was unimportant (one, three or seven remaining **P** units). The excitation of a single molecule (the **S** units) gave three times the same emission event. Therefore only the **P** unit which formed the exciplex was important and the other **P** units remained untouched.

If all **P** units were excited at once (excitation at 320 nm) the exciplex emission increased linearly with increasing number of excited molecules. It was concluded that each excited phenanthrene unit had to deliver its excitation to the exciplex and no phenanthrene monomer emission occurred. If some of the excited **P** units were “lost” by relaxing back to the ground state via fluorescence monomer emission, a less intense exciplex signal should be the result. Different considerations excluded this mechanism. Only the extreme case of the **P** unit which was farthest away from the exciplex is shown (**Figure 25**). The excitation moved from one **P** unit to the next one. The transfer of excitation from one unit to the next can be explained by a conventional resonance energy transfer by the Förster-Dexter mechanism (**Figure 26**).[93, 101] The excitation finally reached the last **P** unit which was next to **S**. This excited **P** formed a complex with the **S** unit in the ground state. This excited complex relaxed back to the ground states of **S** and **P** by fluorescence emission at 450 nm (exciplex emission). Needless to say that each excited **P** followed this pathway. Obviously more **P** units could deliver more excitation and therefore more exciplex emission was detected for hybrids with more **P** units in the sequence.

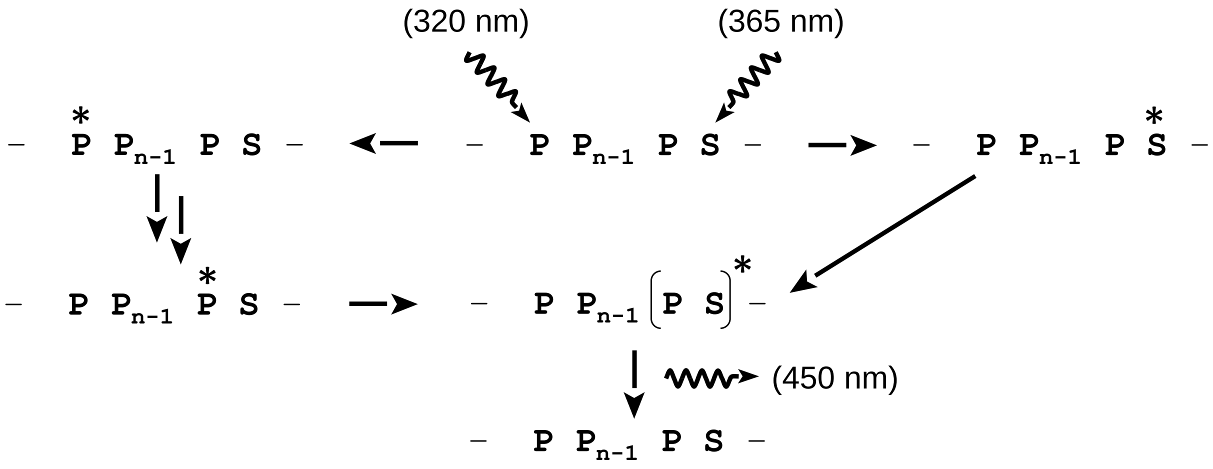

Figure 25. The two pathways of energy transfer followed by fluorescence emission. The two extreme cases of excitation at one end of the phenanthrene stack (320 nm) and at the single pyrene unit (365 nm) are shown. Energy transfer from other phenanthrene units to the exciplex took place in the same way. Abbreviations: * = unit in the excited state; [ ]* = exciplex state; n = 1, 3, 7

The proposed mechanism postulated an energy transfer process from **P** to the **PS**-exciplex. In other words, **P** units acted as energy-harvesting species (collector) and formed an energy-transferring channel. The collected energy (light with a wavelength of 320 nm) was funneled to the reaction center (exciplex) and converted to light (450 nm).

The proposed energy transfer mechanism considered the process as a step-by-step event from one unit to the next. Each unit is treated as single and independent species. Energy transfer can happen via different pathways. The Förster and Dexter mechanisms are the most common ones. Both processes are non-radiative energy transfers between an excited species (donor) and a ground state species (acceptor). The Förster process describes a dipole-dipole interaction. Thereby the relaxation of the excited donor unit to the ground state generates an electric field (transition dipole). This transition dipole is interacting with the ground state of the acceptor unit and stimulates its excitation (**Figure 26**a).

The Förster mechanism is an interchromophore relaxation process and describes the energy transfer between two individual molecules. As soon as donor and acceptor units are no longer single molecules but rather aggregates, the generalized Förster theory needs to be applied.[102] The donor aggregate is excited as a whole and the single components (individual molecules) are no longer treated independently. The excited state of the effective donor (the aggregate) is a linear combination of the excited states of the individual species that build the aggregate. A delocalization of the excitation takes place (**Figure 26**b). The requirements for such aggregated donors are strongly coupled molecules in a confined geometry. Extended stacks of aromatic units are well known to form highly ordered and regularly oriented aggregates. In particular, it was shown that the **S** building block and other pyrene derivatives adapted helical conformations by exciton coupling within a DNA framework.[50, 56, 103] It is thus not speculative if the findings from chapter 3.1 are explained and described by the generalized Förster theory. For our purpose, the simplified model in **Figure 25** gives enough information for better understanding of the working principle.

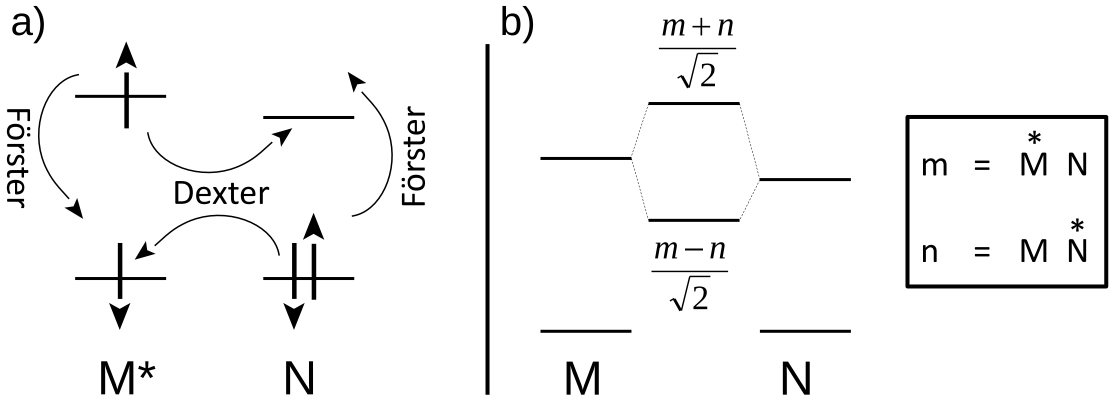

Figure 26. (a) Förster-Dexter mechanism of energy transfer from M to N. The transition dipole generated from M* by relaxing back to the ground state excites N to N*. (b) Generalized Förster theory. Coupling of two molecules results in the delocalization of the excited state.

3.1.4 Summary

The most precious findings from this first chapter were summarized and a mechanism was proposed (**Figure 27**). Excitation at 320 nm of hybrid **23*24** let to an energy transfer process from the phenanthrene units (blue discs) to the phenanthrene-pyrene exciplex (one blue disc and the green disc) which emitted light with a maximum intensity at 450 nm. The energy transfer was in one direction towards the exciplex. The system was named “A DNA-based light harvesting antenna” as energy from light was collected and transferred to a defined location and therefore reminded of the the inicial prcesses during photosynthesis.

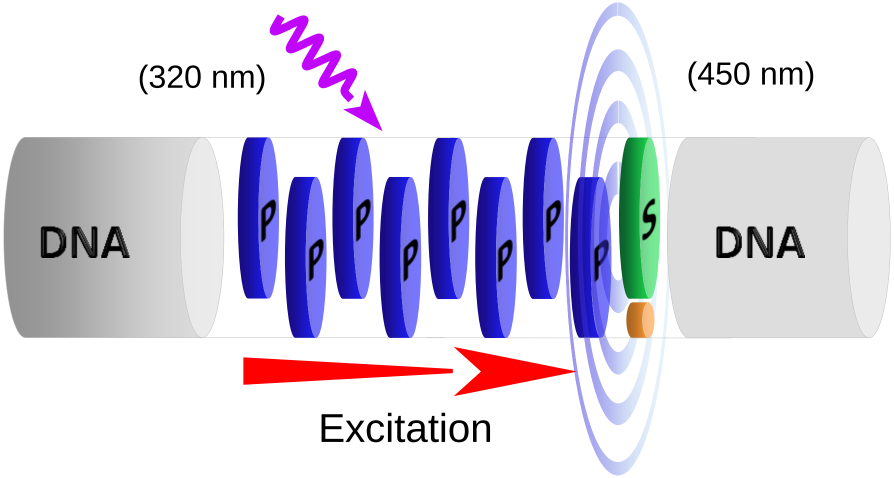

Figure 27. Summary of the working principle of the system described in chapter 3.1.

The exciplex was the only species which accepted excitation energy and converted it to fluorescence emission. Therefore the energy transfer in the phenanthrene stack was only in one direction. The idea was to introduce a second channel where an additional conversion could take place. What will be the outcome if two pathways are possible? Is it possible to seriously disturb the transfer in one direction or are the energy-accepting properties of the exciplex to strong?

3.2 Energy transfer in a phenanthrene stack – A second channel for energy conversion

The last chapter 3.1 dealt with the topic of energy transfer in one direction and the light harvesting properties of a phenanthrene (**P**) stack embedded in a DNA framework. In the phenanthrene π-arrays light with a wavelength of 320 nm was absorbed by the phenanthrene units (**P**) and the absorbed energy was transferred to the collection center, a phenanthrene-pyrene (**PS**) exciplex, where energy conversion to fluorescence emission at 450 nm took place. The direction of the energy transfer was uniform, always towards the exciplex. To further investigate these transferring properties it was aimed to introduce another channel where excitation energy originating from **P** units could be converted. The question was whether the energy transfer towards the exciplex could be challenged.

3.2.1 System design

To introduce a second channel where energy conversion could take place, different approaches were possible. It seemed to be obvious that the only position for the introduction of this second energy-converting channel was at the opposite side of pyrene across the phenanthrene stack. The **P**-stack would then be flanked on one side by the pyrene unit (‘exciplex former’, first channel) and on the other side by a newly introduced other unit (‘challenger’, second channel). There were several possibilities how energy conversion in this second channel could be reached, for example the use of a third chromophore to form a second exciplex was considered. The arising complexity and the scientifically delicious task such new modifications would initiate were numerous. Therefore, a simple but by far not unjustified new set of hybrids was designed by using the natural DNA building blocks.

Guanine (G) has the lowest oxidation potential of the four natural DNA nucleobases and can therefore act as a fluorescence quencher.[104] Fluorescence quenching by electron transfer is a well-known a widely used principle and finds application in different areas.[105-107] A schematic representation of the mechanism is shown (**Figure 28**). A detailed consideration of this topic is given in chapter 3.4. During the charge transfer process an electron from a donor molecule (e.g. a guanine base) reduces the excited state of an acceptor molecule (e.g. an excited chromophore, **P** or **S**). The charge-separated state between donor and acceptor relaxes back to the two ground states (**Figure 28**a). The relaxation is non-fluorescent. This non-fluorescent relaxation causes a quenched fluorescence signal. The amount of quenching depends on different aspects as for example on the life time of the different states (fluorescent state versus charge separated state). In the context of DNA chemistry the most prominent examples of fluorescence quenching by a guanine base were provided by *Frederick. D. Lewis* and co-workers. They were the first who showed that the fluorescence of different chromophores was quenched across an AT-rich DNA hybrid by the presence of a GC-base pair.[108] The reverse way of electron transfer is possible as well. In this mechanism the excited state of the chromophore acts as electron donor (**Figure 28**b). This mechanism is important for excess-electron transfer pathways in DNA hybrids.[48, 109] For the design investigated in this chapter this mechanism is not relevant.

After the insertion of a guanine base, two channels are therefore present where an excited phenanthrene **P** unit potentially can be relaxed (**Figure 28**c). The close proximity to pyrene **S** can form an exciplex and leads to exciplex fluorescence emission. If a guanine is next to an excited **P** to formation of a charge separated state leads to a non-radiative relaxation and therefore a quenched fluorescence emission.

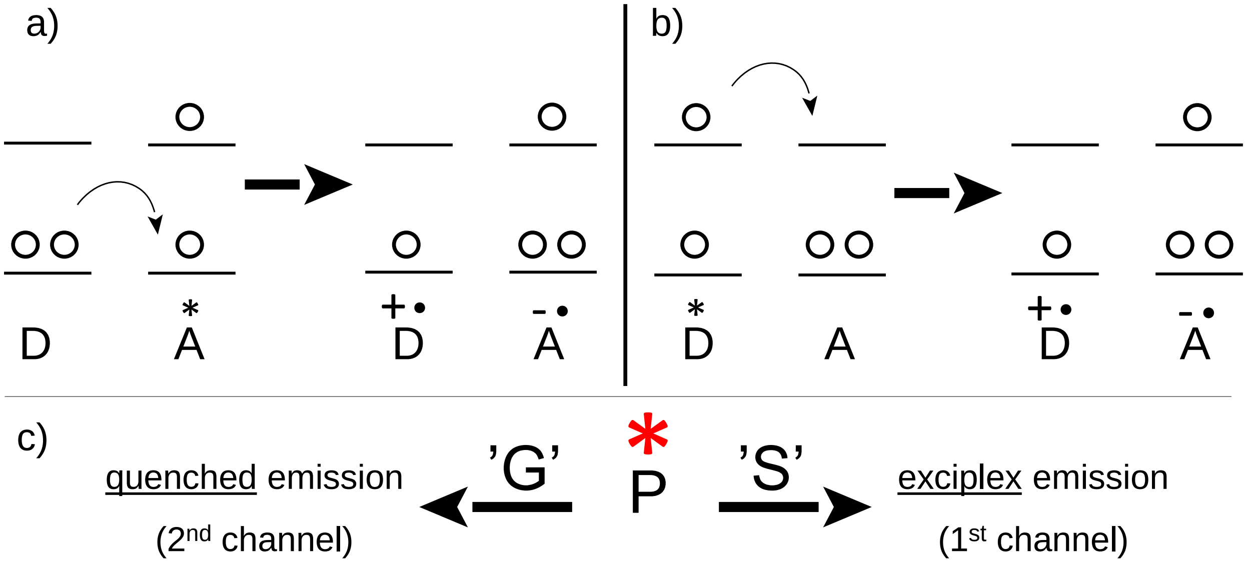

Figure 28. (a) Schematic illustration of the electron transfer from a donor molecule D in the ground state (e.g. guanine) to an acceptor molecule A in the excited state (e.g. **P** unit). (b) The reverse way where the excited state of a chromophore D acts as electron donor for an acceptor molecule A in the ground state is also possible. (c) Relaxation channels for an excited **P** unit. Close proximity to an **S** unit leads to exciplex emission. A guanine (G) base next to an excited **P** can form a charge-separated state which relaxes back to the ground states without fluorescence emission.

The essential design of the new sequences in chapter 3.2 remained constant as introduced in chapter 3.1. The core segment of the DNA hybrids was composed of a stack of phenanthrene units **P** with a pyrene unit **S** at one side of the stack. Next to pyrene in the counter strand an abasic site analogue φ was introduced to keep the length of the two corresponding strands constant and to reduce positional isomers of the **S** unit. The outer DNA parts which flanked the core segment included only AT-base pairs. The base pair directly next to the phenanthrene stack on the opposite side of pyrene was crucial for the system. A GC-base pair was introduced in this position. This GC-base pair acted as second energy converging channel. Excitation energy from the **P** units could be transferred to the exciplex as shown in chapter 3.1 or to the guanine unit on the other side of the **P**-stack (**Figure 29**).

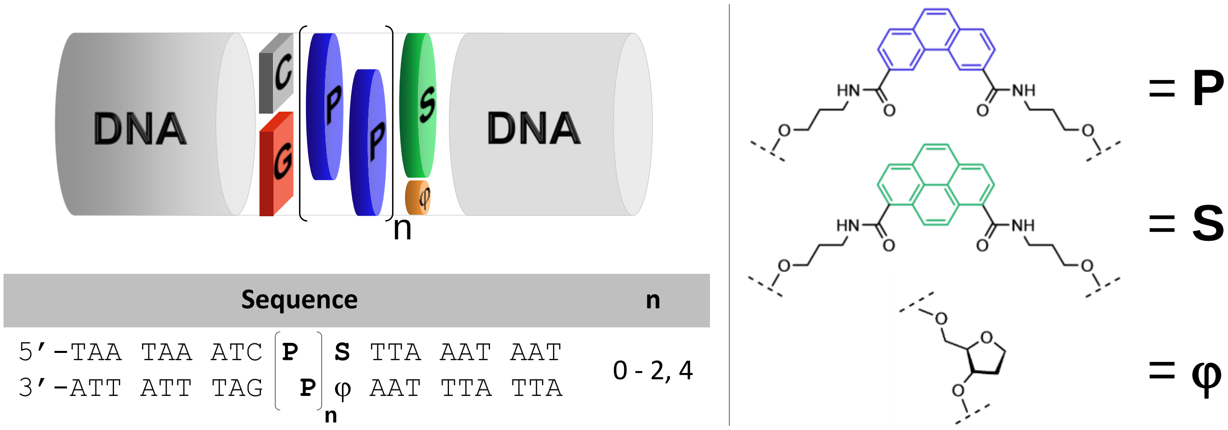
DNA
C
G
P
P
S
φ
n
DNA
Sequence
n
5′-TAA TAA ATC P S TTA AAT AAT
3′-ATT ATT TAG P φ AAT TTA TTA
n
0 - 2, 4
HN
O
NH
O
O
O
= P
HN
O
NH
O
O
O
= S
O
O
O
= φ

Figure 29. System design in chapter 3.2. The basic design remained constant. The crucial change was performed by replacing the AT base pair next to the core segment (see **Figure 16**) by a GC base pair. The unnatural building blocks remained unchanged.

3.2.2 Spectroscopic investigation and discussion

The spectroscopic properties of the hybrids composed of the newly synthesized oligonucleotides were investigated. The slightly higher Tm values and the better thermal stability of the hybrids were in agreement with the changes in the sequences (**Table 3**). The replacement of the AT base pair directly next to the core segment by a GC base pair was expected to cause a higher stability. Nevertheless, the temperature for the following spectroscopic measurements was kept as in chapter 3.1 at 15 °C.

Table 3. Oligonucleotides **25** – **32** prepared for chapter 3.2

Nr.	*Sequence*	*ε value (260 nm)*	*Mass [g/mol]*	*Tm [°C]* [a]
25 **26**	5'- TAA TAA ATC **S** TTA AAT AAT 3'- ATT ATT TAG φ AAT TTA TTA	232000 208800	5955.1 5681.8	31.0
27 **28**	5'- TAA TAA ATC **P S** TTA AAT AAT 3'- ATT ATT TAG **P**φ AAT TTA TTA	258900 235700	6397.5 6124.2	40.0
29 **30**	5'- TAA TAA ATC **P P S** TTA AAT AAT 3'- ATT ATT TAG **P P**φ AAT TTA TTA	285800 262600	6839.9 6566.6	41.5
31 **32**	5'- TAA TAA ATC **P P P P S** TTA AAT AAT 3'- ATT ATT TAG **P P P P**φ AAT TTA TTA	339600 316400	7724.7 7451.4	41.0

[a] 2 μM DNA double strand (4 μM total oligonucleotide concentration), 100 mM sodium chloride, 10 mM sodium phosphate buffer at pH 7.0

The UV/VIS absorbance spectra were in perfect analogy to the spectra of hybrids from chapter 3.1. No deviations from the expected result or new features were found (**Figure 30**). The absorbance at 365 nm was slightly higher in hybrid **25*26** compared to the hybrids with a phenanthrene stack. At 320 nm a steadily increasing absorptivity was detected. This was in agreement with the increasing number of phenanthrene units.

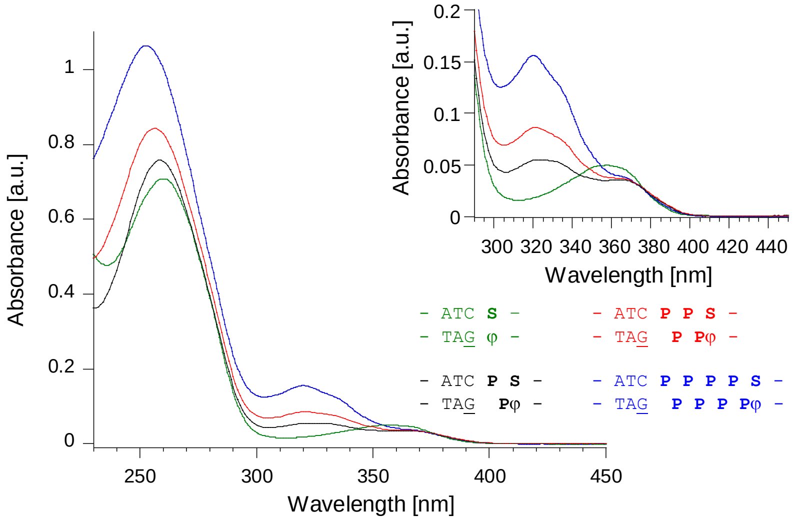

Figure 30. UV/VIS absorbance spectra of hybrids **25*****26**, **27*****28**, **29*****30** and **31*****32**.

It was shown in the last chapter that excitation of pyrene **S** at 320 nm resulted in a small signal with a maximum at 400 nm. At that point this consideration was important for the argumentation afterwards. It was possible to show that excitation at 320 nm of hybrids with **S** and **P** formed a pure exciplex and no side effects of **S** were found. It was shown that the proposed energy transfer was very efficient and no monomer emission of pyrene or phenanthrene was present. The excitation wavelength had a minor importance in the control hybrid **17*****18**. Thus, in this chapter the control sequences with no phenanthrene stack between **S** and G could be excited at 355 nm. In addition the expected low emission intensity was partially compensated by shifting the excitation wavelength to the absorbance maximum of pyrene.

Comparison of the fluorescence emission spectra of single strand **25** and the corresponding hybrid **25*****26** revealed the first important fact for this chapter (**Figure 31**a). Single strand **25** had an emission maximum at the normal pyrene monomer emission wavelength of 400 nm. The influence of cytosine (C) at the 5'-end of **S** was marginal (data not shown). Nor C neither A (adenine, chapter 3.1) quenched the emission of **S**. The formation of the double strand by adding **26** to **25** to form hybrid **25*****26** considerably changed the emission behavior. The emission intensity of hybrid **25*****26** was highly quenched compared to single strand **25** alone. As expected, G had a strong influence on the fluorescence emission of **S**. Despite the behavior of related compounds no formation of a fluorescent exciplex species between pyrene and guanine was found in hybrid **25*****26**.[96] Single strands and hybrids with **P** and **S** units were again excited at 320 nm (**Figure 31**b-d). Single strands **28** and **30** with one and two **P** units in the sequence did not show phenanthrene monomer emission. Guanine at the 3'-end directly next to the chromophores quenched the emission almost completely. In single strand **32** a slight emission with a maximum intensity at 410 nm was detected (**Figure 31**b-d, blue lines). The three single strands **27**, **29** and **31** with the sequences 5'-C-P$_n$-S (n = 1, 2, 4) in the core segment had the same emission intensities at 450 nm (**Figure 31**b-d, black lines) as their parent strands from chapter 3.1 (5'-A-P$_n$-S, **Figure 21**b-d, black lines). No additional signals were found. The replacement of adenine (in **19**, **21** and **23**) by cytosine (in **27**, **29** and **31**) had no influence on the fluorescence emission.

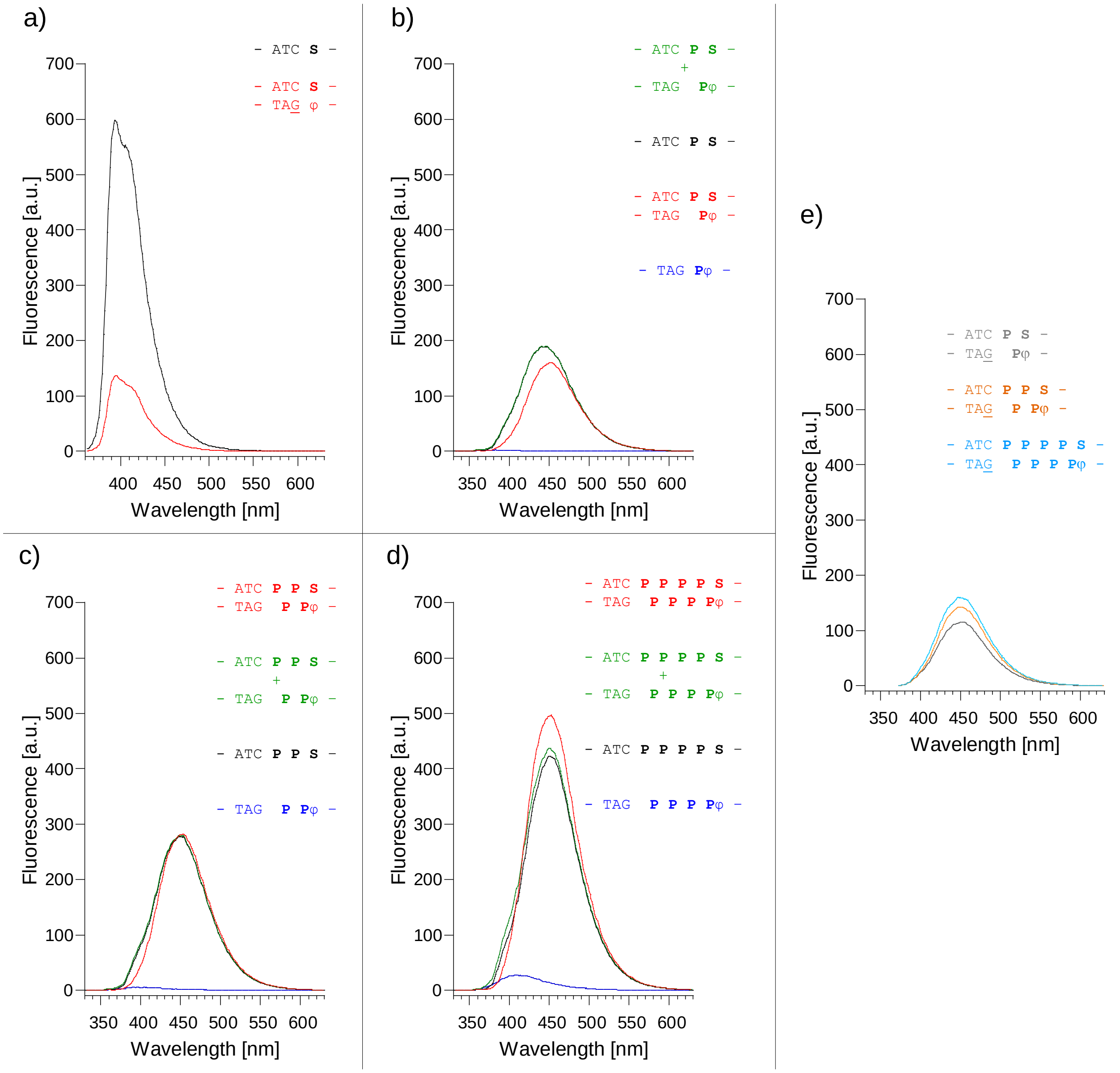

Figure 31. Fluorescence spectra of single strands and hybrids. (a) Control hybrid with single strand **25** and **25*****26** excited at 355 nm. A strong quenching effect of the pyrene monomer emission was observed after the formation of the hybrid. (b-d) All samples were excited at 320 nm. (e) Fluorescence spectra of all hybrids excluding control hybrid **25*****26** after excitation at 365 nm.

Hybrid formation by adding the corresponding single strands changed the emission. A guanine unit was now present next to the core segment. Hybrid **27*28** performed the most significant change in the spectrum. In contrast to its parent hybrid in the last chapter (**19*20**) the exciplex emission of hybrid **27*28** was not increased compared to single strand **27** alone. The addition of G caused a significant change also in the exciplex emission. The change in hybrid **29*30** after double strand formation was not as significant as in the case of hybrid **27*****28**. The emission curve of hybrid **29*****30** and single strand **29** showed almost the same intensity. As a slight deviation from the trend in the first two hybrids, **31*****32** had a slightly increased emission intensity at 450 nm compared to single strand **31**. This increase was by far not as explicit as for the parent hybrid **23*****24** compared to single strand **23** in chapter 3.1.

The hybrids were in a second consideration excited at 365 nm (**Figure 31**e). This was the direct excitation of the pyrene unit. Hybrids with only one channel for excitation energy conversion (**19*****20**, **21*****22** and **23*****24**) did not show differences in the emission intensity during this experiment. However, hybrids shown in this chapter exhibited significantly different exciplex emission intensities to each other after excitation at 365 nm. Hybrid **27*****28** with the shortest phenanthrene stack showed the weakest signal, followed by a slightly more pronounced signal in hybrid **29*****30**. The most intense exciplex emission after excitation at 365 nm was detected for hybrid **31*****32**. Summarized for these three hybrids, a length dependence of the exciplex emission intensity upon increasing number of **P** units was found after excitation at the **S** unit.

The fluorescence properties of the four new hybrids during these experiments were different from the behavior of the hybrids in chapter 3.1. The single strands alone did not differ in their emission behavior from each other. All single strands with **S** (and **P**) had the same emission intensity. This result disclosed that C and A had the same effect on the fluorescence emission of the single strands. Arguments were needed to explain the fluorescence properties of the hybrids by only focusing on the effects of G. A closer look was taken at the effective influence of the different base pair next to the core segment. A comparison of the emission curves of all hybrids from chapter 3.1 and 3.2 was made (**Figure 32**).

As long as no **P**-stack was placed between **S** and G (control hybrids **17*****18** and **25*****26**, **Figure 32**a) the explanation of the results was straight forward. **Figure 28** explained the mechanism of fluorescence quenching by G in detail. It was shown several times that this quenching effect of G on the fluorescence emission of **S** was based on charge transfer from G to **S**.[94, 95, 106] Introduction of **P** units let to two different excitation sites, the **P**-stacks (at 320 nm) or the **S** unit (at 365 nm). The situation after excitation at 320 nm was considered first (**Figure 32**b). Hybrid **27*****28** (n = 1, red line) exhibited an exciplex emission which was reduced by 40 % compared to the emission of parent hybrid **19*****20** (blue line). The exciplex emission intensities of hybrid **29*****30** (n = 2, red line) and **31*****32** (n = 4, red line) were reduced by 27 % and 20 % compared to **21*****22** and **23*****24** (also see **Table 4**).

The emission curves of these six hybrids after excitation at 365 nm were compared (**Figure 32**c). The continuous and uniform emission intensity of all three hybrids in chapter 3.1 after excitation at 365 nm was not a conflict for the explanation of a potential mechanism. It was shown that a simple explanation for this result was found (**Figure 25**). Only one **S** unit was excited in all three hybrids and they formed an exciplex with one **P** unit. Thus, other results than the reported ones would have been difficult to explain. In chapter 3.2, the hybrids with **P**-stacks between **S** and G (**27*****28**, **29*****30** and **31*****32**) revealed different emission intensities after excitation at 365 nm. It seemed that the G unit across the **P**-stack on the opposite site of the exciplex indeed had an influence on the fluorescence of the exciplex. This effect depended on the number of **P**-units which is nicely shown (**Figure 32**c, red lines). A clear difference was seen between a GC or an AT base pair next to the core segment in the emission spectrum of the two hybrids with the short **P**-stack (n = 1, **Figure 32**c). The distinctiveness of this effect diminished the longer the **P**-stack was. The quenching ratio was 32 % (n = 1), 15 % (n = 2) and 6 % (n = 4).

All areas under the emission curves (a.u.c) were determined and plotted against the number of phenanthrene units (**Figure 32**d). A linear increase of the bars after excitation at 320 nm was already seen for hybrids **19*****20**, **21*****22** and **23*****24** which was attributed to the light-harvesting and energy transferring properties of the **P**-stacks. The same linear increase after excitation at 320 nm was seen for hybrids **27*****28**, **29*****30** and **31*****32** which had a GC base next to the core segment. The linear regressions for both hybrid sets had very similar slopes, albeit not identical. Nevertheless, the similarity of the slopes was surprising. No length dependent effect upon increasing number of **P** units was seen in the set with the GC base pair next to the core. The bars seemed to be constantly reduced by a fixed value, irrespective of the number of **P** units. The second excitation wavelength at 365 nm let to a uniform emission intensity over the set in chapter 3.1 (**Figure 32**d, grey bars). With the GC base pair next to the core segment, again, a linear increase of the emission intensity was found (**Figure 32**d, red bars).**Table 4** summarizes all the data from fluorescence emission analysis. To visualize the actual shape of the presented hybirds an amber-minimized HyperChem® model[110] of hybrid **31*****32** was made (**Figure 33**).

Table 4. Fluorescence properties of hybrids from chapter 3.1 and 3.2

	19*20	***27*28***	***21*22***	***29*30***	***23*24***	***31*32***
number of phenanthrenes	2	2	4	4	8	8
number of channels	1	2	1	2	1	2
a.u.c (excitation at 320 nm)	20877	12506	30612	22262	49038	39424
amplification factor of a.u.c [a]	1	1	1.46	1.78	2.35	3.15
Relative amplification [b]	1.00	0.60	1.00	0.73	1.00	0.80
a.u.c (excitation at 365 nm)	13504	9228	13375	11351	13699	12810
Relative amplification [b]	1.00	0.68	1.00	0.85	1.00	0.94
fluorescence intensity at 450 nm [a.u.] [c]	259	160	374	282	607	497
amplification factor at 450 nm [a]	1	1	1.44	1.76	2.34	3.11
fluorescence intensity at 500 nm [a.u.] [c]	91	56	133	102	212	178
amplification factor at 500 nm [a]	1	1	1.46	1.82	2.33	3.17

[a] normalized to the values of hybrid **19*****20** and **27*****28**; [b] normalized to the value of the hybrid with one channel [c] emission curves after excitation at 320 nm.

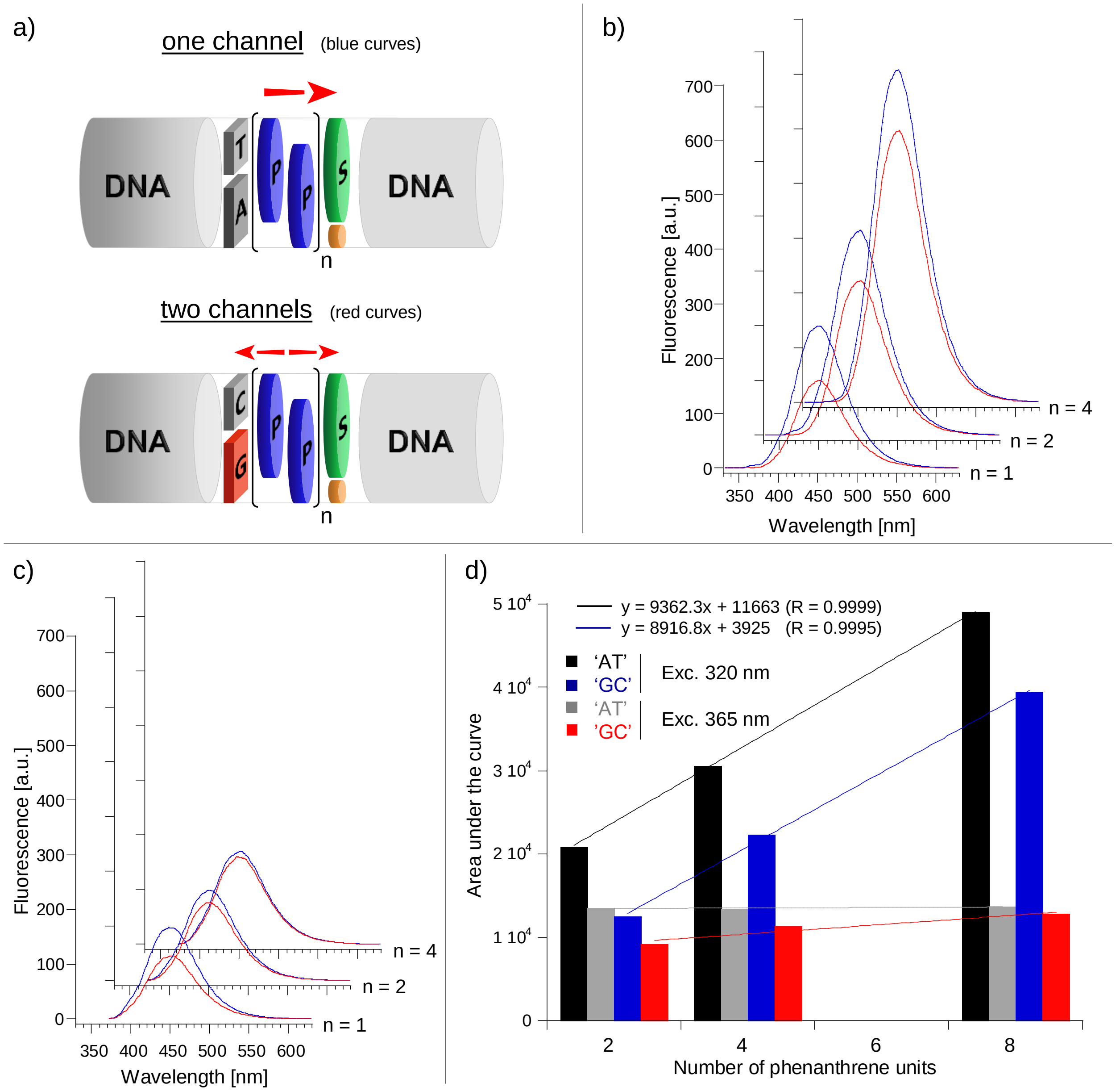

Figure 32. Summary of the two systems in chapter 3.1 and 3.2. (a) Cartoon of the antenna systems with one or with two channels where energy conversion could take place (one channel: exciplex; two channels: exciplex and guanine). (b) Emission spectra of hybrids with two (n=1), four (n=2) and eight (n=4) phenanthrene units. The excitation wavelength was 320 nm. Red emission curves represent hybrids with two channels (GC base pair next to the core segment) and blue emission curves represent hybrids with one channel (AT base pair next to the core segment). (c) The excitation wavelength for fluorescence emission was 365 nm. Red curves represent hybrids with two channels (GC base pair) and blue curves represent hybrids with one channel (AT base pair). (d) Area under the emission curves of all hybrids. Black and grey bars represent the three hybrids with an AT base pair next to the core segment, blue and red bars represent hybrids with a GC base pair in this position.

Excitation spectra were determined to get more insight into the specific aspects of the results. The excitation spectra in chapter 3.1 revealed that the exciplexes were composed of always the same fraction of pyrene (constant excitation intensity for hybrids **19*20**, **21*22** and **23*24** at 365 nm) and for each hybrid a changing fraction of phenanthrene excitation (excitation at 320 nm increased with increasing number of **P** units). This was attributed to the excitation energy transfer from phenanthrene to the phenanthrene-pyrene exciplex. The excitation spectra of hybrids **27*28**, **29*30** and **31*32** (**Figure 34**a) shown in this chapter did not fundamentally differ from the ones measured in the last chapter 3.1. Nevertheless, by taking a closer look at the important aspects, clear differences appeared.

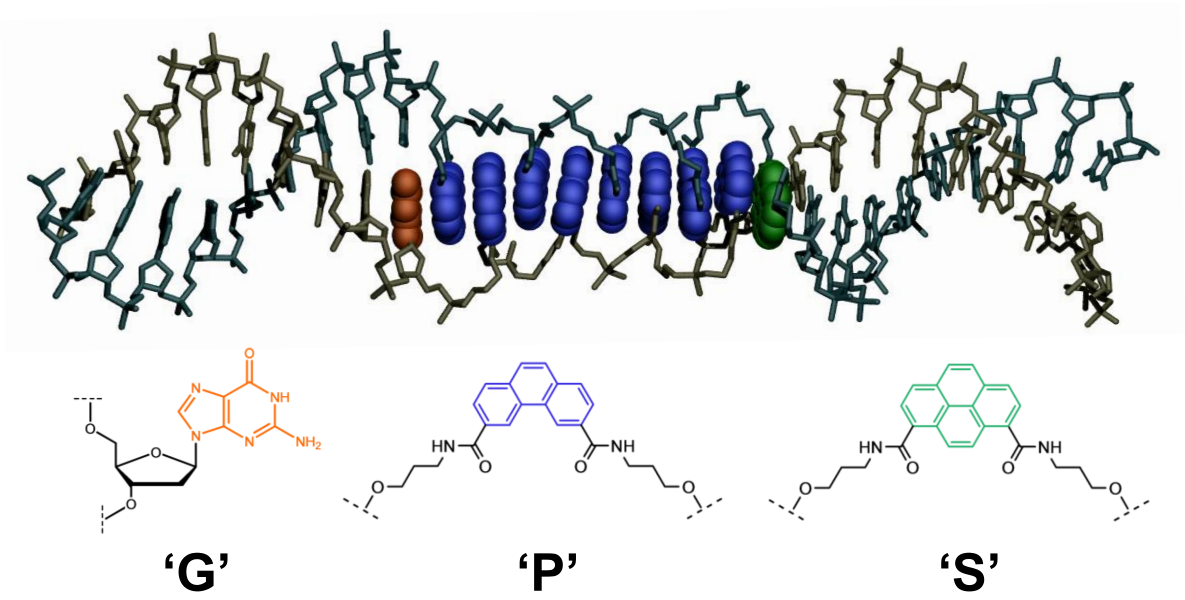

Figure 33. Amber-minimized HyerChem model of hybrid **31*32** with guanine G in orange, phenanthrene **P** in blue and pyrene **S** in green.

The ratio between the excitation bands were calculated by dividing the value of the excitation intensity at 320 nm (phenanthrene) by the value at 365 nm (pyrene, see **Table 5**). Why was it the best choice? The only fluorescent species detected in all six hybrids was the exciplex emitting at 450 nm. To form this exciplex, pyrene and phenanthrene units were required. Pyrene was a constant and repeating unit in all six hybrids and therefore a good reference point in all spectra. Irrespective of the quenching mechanism (see later) pyrene always added a constant fraction of energy to the exciplex. On the other hand, the number of phenanthrene units changed from hybrid to hybrid and the influence of the GC base pair onto the **P**-units or onto the **PS**-exciplex was still unclear. By dividing the excitation intensity at 320 nm (**P**) by the value at 365 nm (**S**) all ratios were normalized to a constant parameter.

The data revealed that the values of the calculated ratios in hybrids with the AT base pair next to the core (hybrids from chapter 3.1) were higher than the ratios in hybrids with the GC base pair next to the core. A smaller value in the ratio calculated here indicated less excitation energy at 320 nm. In other words, exciplexes from hybrids with the AT base pair next to the core segment were composed of a higher fraction of energy originating for **P** compared to hybrids with the GC base pair next to the core. In these hybrids **P** units added less excitation energy to the exciplex. It was concluded that the reduced exciplex emission intensity in hybrids with the GC base pair next to the core segment was a consequence of the interaction between guanine and the **P** unit next to it and not based on a direct interaction between G and the **PS**-exciplex.

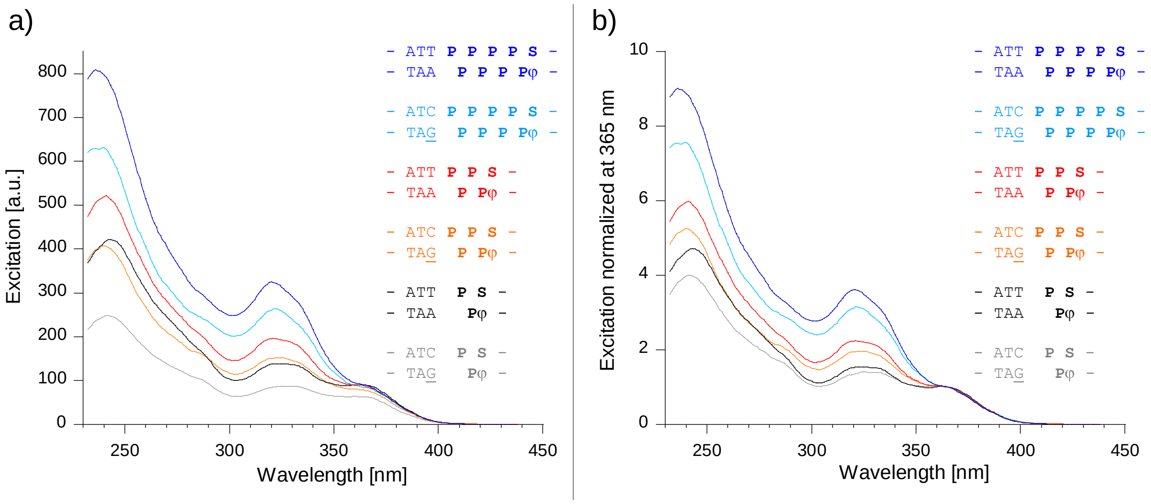

Figure 34. Excitation specta of all hybrids. (a) Measured intensities at an emission wavelength of 450 nm. (b) Excitation spectra normalized at 365 nm.

Table 5. Analysis of the excitation spectra

hybrid	*intensity at 320 nm*	*intensity at 365 nm*	*ratio (320/365)*	*amplification*	*relative [%]*
19*20	138.0	89.5	1.54	1	100
27*28	86.8	62.0	1.40	1	91
21*22	195.8	87.2	2.25	1.46	100
29*30	152.4	77.5	1.97	1.41	88
23*24	324.8	89.7	3.62	2.35	100
31*32	263.5	83.5	3.16	2.26	87

Chapter 3.1 proposed an efficient mechanism of energy transfer from **P** units to the **PS**-exciplex and light harvesting properties were postulated for such hybrids. The results in chapter 3.2 showed a slight deviation from the uniform behavior in the last chapter. Nevertheless it was expected that the fundamental mechanism of energy transfer via the **P** units remained constant. Therefore, the mechanism to explain the results in chapter 3.2 was proposed based on the mechanism in chapter 3.1 (**Figure 25**).

Two possible mechanisms were considered how guanine could quench the exciplex fluorescence emission: First, a direct interaction between guanine and the exciplex could take place which would imply an electron superexchange between guanine and the exciplex. Second, the observed lower exciplex emission intensity in the presence of the GC base pair could be a consequence of less energy that was transported to the exciplex, hence, a constant quenching of excitation energy from **P** by G.

What should be the spectroscopic outcome of the superexchange mechanism? This was closer investigated (**Figure 35**). A short distance between quencher G and the exciplex fluorophore must result in a highly quenched fluorescence emission. The probability that an electron is introduced into the exciplex is high as the distance between quencher (guanine) and fluorophore (exciplex) is short (**Figure 35**a). This probability of electron transfer decreases by a factor of $1/r^6$ the longer the distance is (**Figure 35**a/b/c).[111] The distance dependence of the superexchange mechanism is similar to the dependence of the FRET-efficiency on the interchromophore distance (see 1.4). The slopes of the regression lines of the areas under the emission curves of hybrids with or without a quencher must consequently differ from each other (**Figure 35**d). The regression line from hybrids with the quencher should be steeper compared to the regression line form hybrids without the quencher. In one point the regression lines must cross each other because the distance between fluorophore and quencher will be too long at a certain point and the electron transfer can no longer take place. Excitation of the hybrids in chapter 3.1 and 3.2 at 320 nm did not show such a distance dependent behavior (see **Figure 32**). The regression lines of the areas under the emission curves from hybrids with an AT base pair or a GC base pair next to the core segment were in parallel. It was concluded that direct introduction of an electron into the exciplex and direct quenching of the fluorescence emission by guanine via a superexchange mechanism was unlikely to happen.

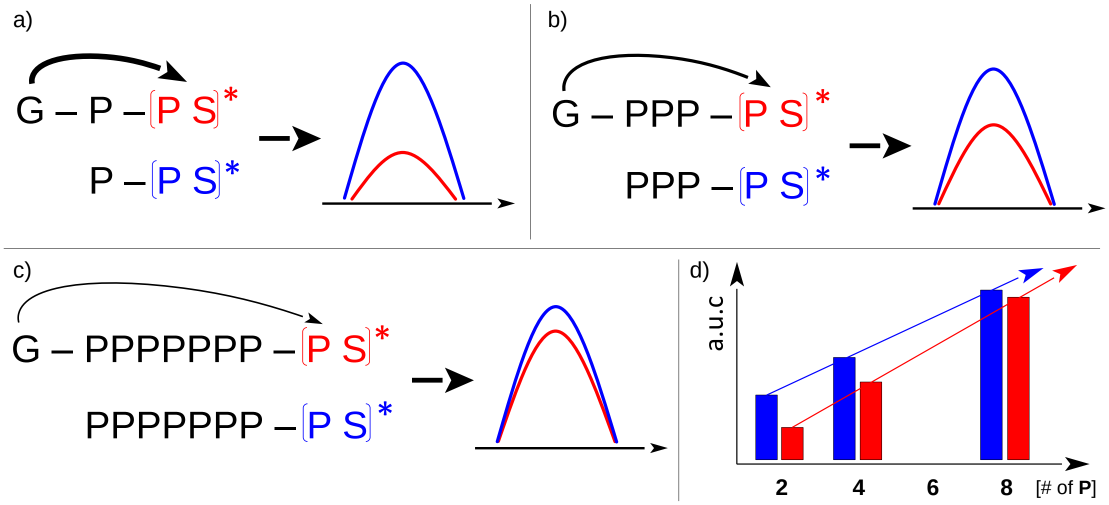

Figure 35. Model behavior of the fluorescence curves (blue and red lines) if the quenching by G was based on a direct interaction between G and the exciplex (superexchange). A length dependent effect should be detected. (a) Short distance = high quenching. (b) Intermediate distance = considerable quenching. (c) long distance = low quenching. (d) Regression lines of a.u.c-values from quenched (red bars) and unquenched (blue bars) hybrids must have different slopes.

Apart from the superexchange mechanism a second possibility was proposed to explain the results. It seemed that this mechanism was, based on the results reported in chapter 3.1 and 3.2 and based on theoretical investigations, the most reasonable one.

First, the direct excitation of the **P** units was considered (excitation at 320 nm). It was expected that all **P** units were excited at once. The two **P** units next to G had the key roles for the explanation of the mechanism. The excited state of the first **P** in the core segment (directly next to G) was quenched by G via the formation of a charge separated state (also see **Figure 28**). This charge separated state relaxed back to the ground state via a non-fluorescent decay. The excitation of the second **P** unit in the core segment was transferred (in analogy to the mechanism in **Figure 25**) to the last **P** unit next to **S**. Formation of an exciplex and relaxation to the ground states by fluorescence emission terminated the process. Each **P** unit (in longer stacks, especially **P** = 4 and **P** = 8), which was sandwiched between the first two **P** units of the core and **S**, transferred its excitation to the exciplex, as shown in chapter 3.1. As a consequence, only the excitation of one **P** unit was lost by the formation of a charge separated state between the first **P** and G. This explained why the a.u.c-values of hybrids with the GC base pair next to the core were reduced by a constant value over all hybrids. This finding was comparable to previous findings where the dynamics in extended pyrene stacks were investigated.[86] The key conclusion of this study was that the inner elements of the extended **S**-stacks were shielded from the DNA bases by the **S** unit at the periphery. Quenching by electron transfer was blocked. In a different approach this was now also shown with the results in chapter 3.2. The **P** unit next to the GC base pair shielded the inner **P** elements. Thanks to this shielding effect of the **P** unit at the periphery the other **P** units could still efficiently transport their excitation energy to the exciplex.

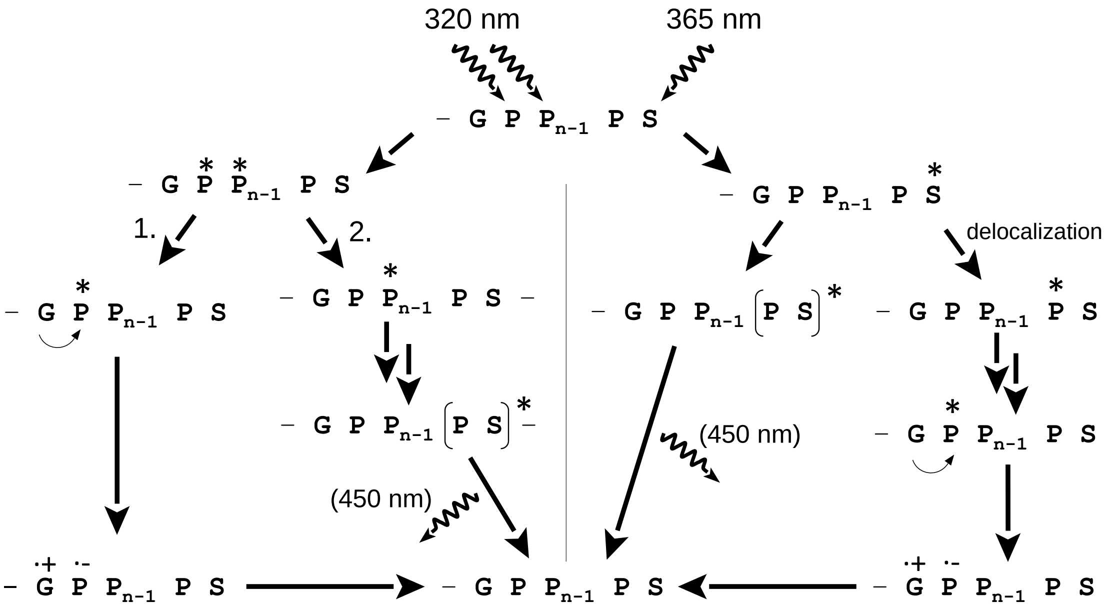

Figure 36. The proposed mechanisms for fluorescence quenching of hybrids with a GC base pair next to the core segment (n = 1, 3, 7). Left route = excitation at 320 nm, right route = excitation at 365 nm. For the mechanisms with the AT base pair in this position (see **Figure 25**).

Direct pyrene excitation at 365 nm let to a uniform exciplex fluorescence emission intensity over the whole set in chapter 3.1. The number of **P** units was not important in these cases. However, the data in chapter 3.2 clearly showed that G on the other hand indeed influenced the exciplex emission if hybrids **27*****28**, **29*****30** and **31*****32** were excited at 365 nm (**Figure 32**). The quenching effect of G was less important the longer the **P**-stack between the exciplex and G was. I other words, a length-dependent effect between hybrids with the AT base pair next to the core segment and hybrids with the GC base pair in this position was observed. Based on this observation, it was expected that the excited state of **S** could be translated to **P** and from there on the excitation could be transported to the bottom of the core segment. Arrived at the end of the core segment (excitation of the first **P** unit of the core segment), formation of a charge separated state between **P** and G took place. This step quenched the fluorescence emission of the exciplex (**Figure 36**). This behavior denoted a delocalization of the excitation between **S** and **P**. This was only possible if the excitation was not localized on one unit (**S**) but was moving in between. The longer the **P**-stack was the lower was the probability for the excitation to reach the bottom. Therefore, a length-dependent effect of the fluorescence quenching was observed. Nevertheless, experimental support for the proposed delocalization between **S** and **P** was needed.

3.2.3 Summary

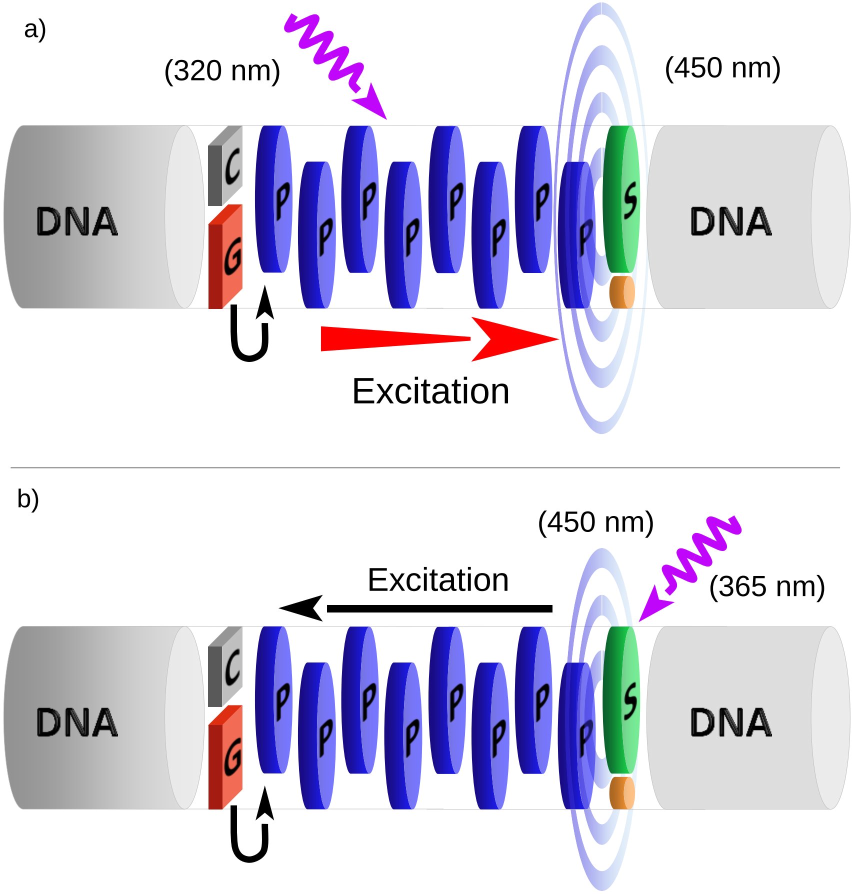

Figure 37. The model of the influence of the GC base pair next to the core is presented. (a) Irradiation at 320 nm let to the excitation of all **P** units. All excited **P** units, except for one, transferred their excitation to the exciplex where energy conversion to fluorescence emission at 450 nm took place. The excitation of the **P** unit next to G on the other hand was quenched by the formation of a charge separated state between G and **P**. (b) Irradiation at 365 nm let to the excitation of **S**. The excitation was delocalized between **S** and **P**. Predominant formation of an exciplex was observed (emission at 450 nm). Once the excitation was localized on **P**, it could travel in the counter direction down to the first **P** unit of the core segment where charge separation between G and **P** took place. The whole process was in concurrence with exciplex formation and depended on the length of the **P** stack.

Figure 3 summarizes the proposed model of chapter 3.2. It was found that the energy transfer direction remained mainly towards the exciplex even if a second channel for energy conversion was present. The GC base pair next to the core segment trapped the excitation of one **P** unit. The rest of the excitation energy was transported to the exciplex where energy conversion to fluorescence emission took place. The data also showed that excitation energy introduced at the pyrene side was transported to the other end of the core segment where it was trapped by the G unit. This implemented a delocalization of the excited state between **S** and **P**. The next chapter will look into this question in more details.

3.3 Energy transfer in a phenanthrene stack – Probing the excitation delocalization between **S** and **P**

The proposed mechanism in chapter 3.2 contained steps which were well understood and were explainable. The energy transfer from **P** units to the phenanthrene-pyrene exciplex was shown in both approaches (with one channel and with two channels) and the explanation was clear. A constant fraction of reduced exciplex emission in hybrids with the GC base pair next to the core segment (two channels) compared to hybrids with the AT base pair in this position (one channel) was observed. This quenching effect of the GC base pair on the phenanthrene-pyrene exciplex fluorescence was explained by trapping of excitation energy from the first **P** unit in the core segment by guanine. Excitation at 365 nm of hybrids with the GC base pair next to the core resulted in a length-dependent quenching effect of the exciplex emission compared to hybrids with the AT base pair next to the core. This observation was explained by a beneficial delocalization between **S** and **P**. Once the excitation was localized on **P** it could travel (in 'counter direction' of the usual way, see chapter 3.1) via other **P** units down to the first unit of the core segment. Formation of a charge separated state between this first **P** unit and G finally quenched the excited state and let to a quenched exciplex emission. The longer the **P**-stack was the smaller was the probability that the excitation reached the bottom. Therefore, longer **P**-stacks showed less fluorescence quenching compared to shorter **P**-stacks when excited at 365 nm. The delocalization between **S** and **P** was only a possible explanation for the observed results but a clear experimental evidence was still missing. Therefore, it was tried to find another system which could add more support for this mechanism.

3.3.1 System design

Figure 20b explained the formation of exciplexes. The IUPAC definition of an exciplex is:[112]

> "An electronically excited complex of definite stoichiometry, 'non-bonding' in the ground state. For example, a complex formed by the interaction of an excited molecular entity with a ground state counterpart of a different structure."

The words '… counterpart of a different structure …' are the important terms of this definition. If, by definition, the mechanism of exciplex formation is kept constant but the word 'different' is replaced by the word 'same', the definition of another important fluorescent species is generated:[112]

> "An electronically excited dimer, 'non-bonding' in the ground state. For example, a complex formed by the interaction of an excited molecular entity with a ground state partner of the same structure."

This is the IUPAC definition of an excimer, a special case of an exciplex. The classical excimer former since decades is pyrene.[66] A wide variety of applications in different research fields used the principle of pyrene excimer formation. Up to date, pyrene excimer formation remains a topic of high interest. Thereby, the specific fluorescence behavior and the easily distinguishable pyrene monomer and pyrene excimer emission wavelengths play an important role. Upon excitation of pyrene (typically at wavelengths between 340 nm and 360 nm) a Stoke's shift [93, 113] of almost 150 nm after excimer formation can be found. The pyrene monomer has a typical maximum emission wavelength of 400 nm whereas the excimer has its maximum emission at wavelength longer than 500 nm. This makes pyrene an interesting and attractive candidate for fluorescence studies. The scheme for exciplex emission (**Figure 20**) is now extendable (**Figure 38**).

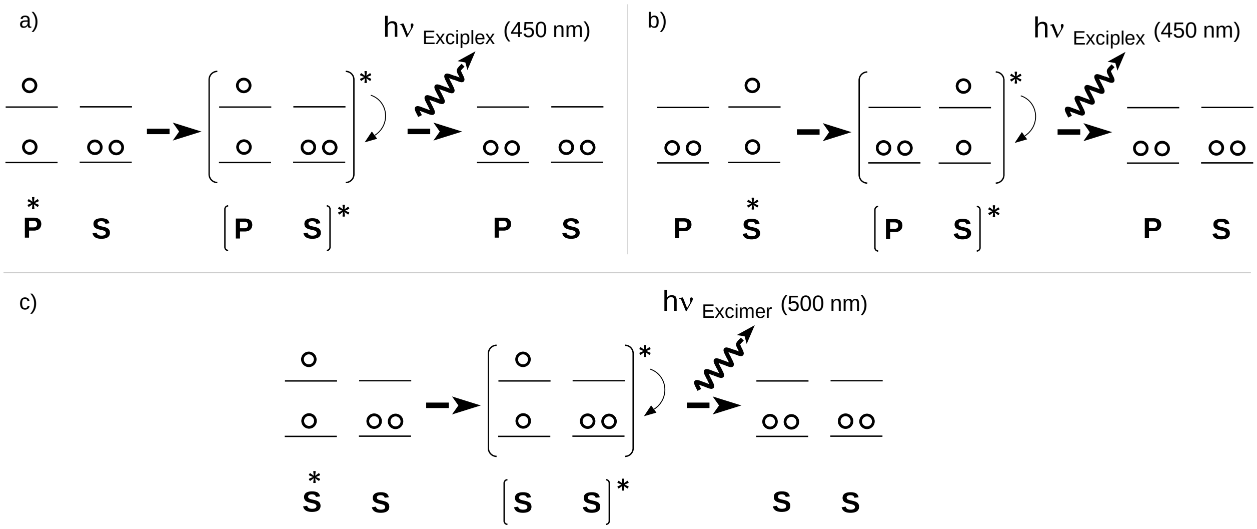

Figure 38. Exciplex versus excimer fluorescence emission. (a/b) The exciplex is formed either by exciting the **P** unit which subsequently forms a complex with **S** in the ground state (or vice versa). The excited complex relaxes back to the ground state by emitting light with a maximum intensity at 450 nm. (c) The excimer is formed if an excited **S** unit forms an excited dimer with another **S** unit in the ground state. The excited complex relaxes back to the ground state by emitting light with a maximum intensity around 500 nm.

Excimer formation in hybrids reported in the last two chapters offered new possibilities. The design of the previous systems was reinvestigated. The DNA hybrids contained an abasic site analogue φ next to **S** in the counter strand to keep the length of the strands constant. This left slightly more space to the **S** unit and reduced the formation of positional isomers. The linked tetrahydrofuranyl-unit φ did not have any spectroscopic functions. By replacing this abasic site analogue φ a relatively small intervention into the global design of the hybrids would be made and spectroscopic results from the last two chapters could still be easily used for argumentations. It was decided to replace the abasic site analogue φ by an **S** unit. This implicated the potential formation of an excimer between the **S** units in the two strands. Examples in the literature supported this intention.[53] Why should this new fluorescent species give deeper insight into the present systems?

It was a central question in chapter 3.2 whether a delocalization of the excitation between **S** and **P** was present. The idea was to introduce a second S unit behind the exciplex to probe whether this position was reached by the traveling excited state. In other words, if a delocalization between **P** and **S** was present, an excimer state should be possible with this design. **Figure 39** summarizes the preliminary thoughts.

Figure 40 shows the design of the hybrids investigated in this chapter. The central design remained constant. Only the abasic site analogue φ was replaced by a second **S** unit.

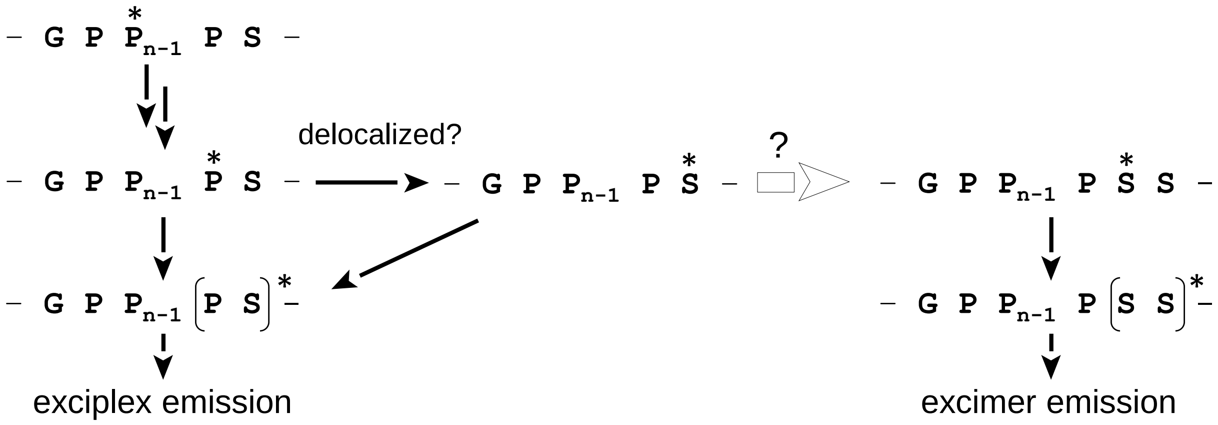

Figure 39. Energy transfer from **P** to the **P**-**S** exciplex. The excitation reaches the **P** unit next to **S**. Formation of an exciplex with **S** in the ground state is followed by relaxation via exciplex emission (the known normal pathway). The central question is whether the excitation is delocalized between **S** and **P**. The question could be possibly answered by the introduction of a second **S** unit. Two **S** units in close proximity can form an excimer. The emission maximum is red-shifted compared to the exciplex and thus is clearly distinguishable.

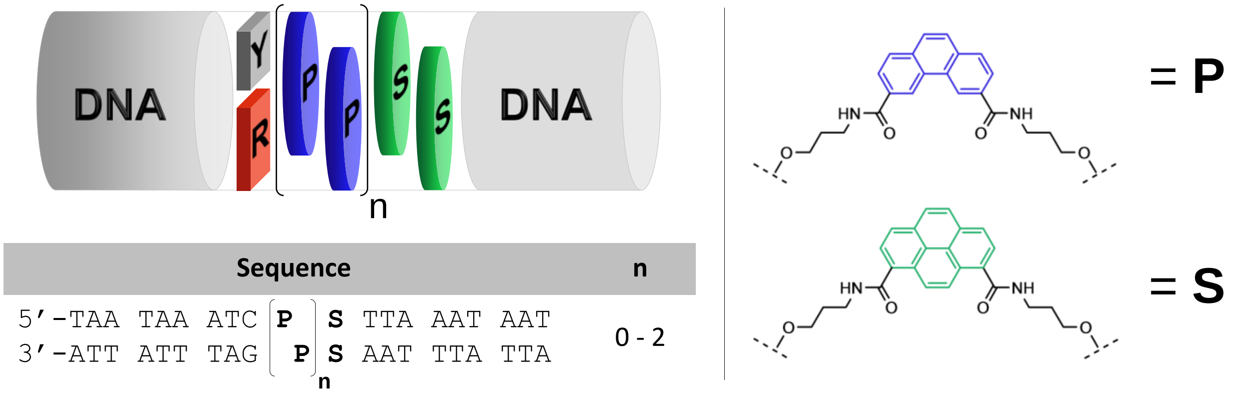

Sequence	n
5′-TAA TAA ATC (P)$_n$ S TTA AAT AAT 3′-ATT ATT TAG (P)$_n$ S AAT TTA TTA	0 - 2

Figure 40. System design of the hybrids in chapter 3.3. The core segment remained constant, just the abasic site analoge φ was replaced by an additional **S** unit.

3.3.2 Spectroscopic investigation and discussion

The thermal stability (Tm values) of the three new hybrids was investigated (**Table 6**). The Tm values roughly matched the expected outcome. Nor a special stabilization neither destabilization which would be worth to notice was found. The additional **S** unit compared to hybrids in chapter 3.1 and 3.2 had no special effect on the thermal stability.

The UV/VIS spectra of the three new hybrids were investigated. The changes compared to the spectra of hybrids with only one **S** unit but equal amount of **P** units (see chapter 3.1 and 3.2) were obvious. The control hybrid **25*33** with two **S** units next to each other had a broad and structureless absorbance band centered at 355 nm. This maximum absorbance was slightly blue-shifted compared to the control hybrids

17***18** and **25*****26** (one **S** unit) in chapter 3.1 and 3.2. Hybrid **27*****34** had a broad and slightly structured absorbance band between 420 nm and 300 nm. From the previous chapters the positions of the pyrene and the phenanthrene absorbance bands were known. Two slight shoulders at 360 nm and 330 nm were found in hybrid **27*****34**. As the number of **S** and **P** units was equal in this hybrid almost no differentiation of the two absorbance bands was possible. On the other hand such a differentiation was possible for hybrid **29*****35**. The double amount of **P** units compared to **S** units in hybrid **29*****35** clearly separated the intensities of the absorbance bands

Table 6. Oligonucleotides **33** – **35** (and **25**, **27** and **29**) of chapter 3.3

Nr.	*Sequence*	*ε value (260 nm)*	*Mass [g/mol]*	*Tm [°C]* [a]
25	5'- TAA TAA ATC **S** TTA AAT AAT	232000	5955.1	37.0
33	3'- ATT ATT TAG **S** AAT TTA TTA	217400	5968.1	
27	5'- TAA TAA ATC **P S** TTA AAT AAT	258900	6397.5	37.0
34	3'- ATT ATT TAG **P S** AAT TTA TTA	244300	6410.5	
29	5'- TAA TAA ATC **P P S** TTA AAT AAT	285800	6566.6	38.0
35	3'- ATT ATT TAG **P P S** AAT TTA TTA	271200	6852.9	

[a] 2 μM DNA double strand (4 μM total oligonucleotide concentration), 100 mM sodium chloride, 10 mM sodium phosphate buffer at pH 7.0

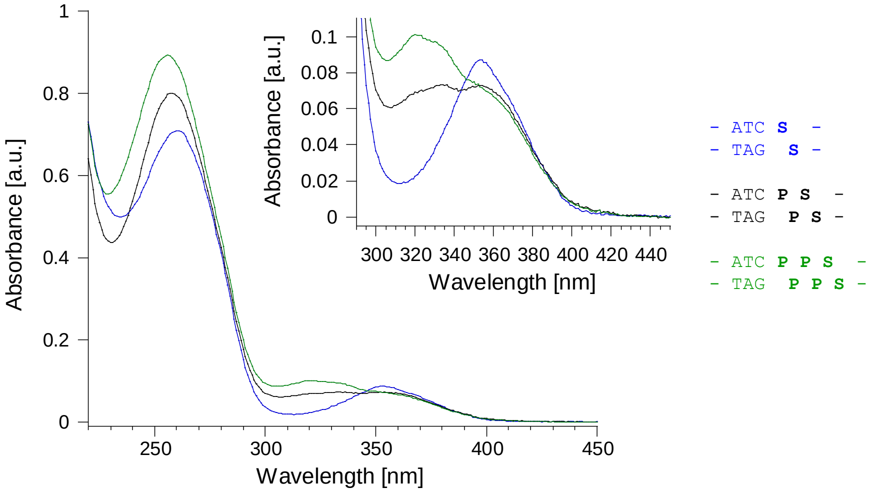

Figure 41. UV/VIS spectra of the hybrids **25*****33**, **27*****34** and **29*****35**.

First, a proof-of-principle was made to clearly show the working principle of the system. Hybrid **25*****33** acted as a control hybrid and was the direct counterpart to hybrid **25*****26** from chapter 3.2. Except for the replaced abasic site analogue φ the hybrids were identical. Hybrid **25*****26** showed pyrene monomer emission with a maximum emission wavelength at 400 nm (**Figure 31**a). Excitation of hybrid **25*****33** at 355 nm gave two distinct emission maxima, one centered at 400 nm and one centered at 500 nm respectively. The introductory part to this chapter announced a clear separation of pyrene monomer and excimer emission. The experimental proof for this behavior was shown by comparing these two hybrids (**Figure 42**a, blue and grey line). The formation of an excimer clearly indicated a close proximity of the two pyrene units and an interstrand interaction between them.

Hybrids **27***34** and **29***35** offered the possibility of excitation at two different sites, namely at **P** units and at **S** units. The excitation wavelengths were kept constant at 320 nm and 365 nm even if the maxima of the absorbance bands were slightly shifted. For homology and comparability with the results from previous chapters this seemed to be a reasonable decision. Hybrid **27***34** showed a broad emission band with a maximum at 500 nm after excitation at 320 nm (**Figure 42**b, black line). The term ‘centered at’ was no longer correct in this case. The emission intensity started to steadily increase at 380 nm until the maximum at 500 nm was reached. The decrease of the emission intensity was steeper compared to the increase which gave a slightly unsymmetrical emission envelope. The emission maximum at 485 nm of hybrid **29***35** (**Figure 42**b, green line) was slightly blue-shifted compared to the emission maximum of hybrid **27***34**. The maximum emission intensity was slightly higher and the envelope was broader. As a comparison the emission curves of hybrid **27***28** (**Figure 42**b, orange line) and **29***30** (**Figure 42**b, red line) were also plotted. The intensity of the two new hybrids was considerably less intense. The position as well as the overall shape of the curves was also different compared to the hybrids with only one **S** unit but the same amount of **P** units. The most impressive change was found when the emission curve of hybrid **25***33** after excitation at 320 nm (**Figure 42**b, blue line) was compared to the emission curves of the other two hybrids **27***34** and **29***35**. The emission band at 500 nm (indicative for pyrene excimer emission) was highly increased by factors of 9 (**27***34**) and 13 (**29***35**) compared to hybrid **25***33**. Hybrid **25***33** was excited at an absorption minimum, therefore, areas under the emission curves (a.u.c) were calculated and divided by the absorbance value at the excitation wavelength. This relative quantum yield showed that hybrid **27***34** revealed a 2.44 times brighter fluorescence emission whereas hybrid **29***35** had a 2.5 times brighter fluorescence emission compared to hybrid **25***33**.

The UV/VIS absorbance spectra indicated that hybrid **27***34** and **29***35** had the same absorptivity at 365 nm. Based on this fact, the almost same maximum emission intensity was not an outstanding observation (**Figure 42**c, green and black lines). A small difference between the two emission curves was still found. Hybrid **29***35** had a shoulder around 450 nm compared to hybrid **27***34**. The maximum intensity was red-shifted compared to the emission maximum after excitation at 320 nm.

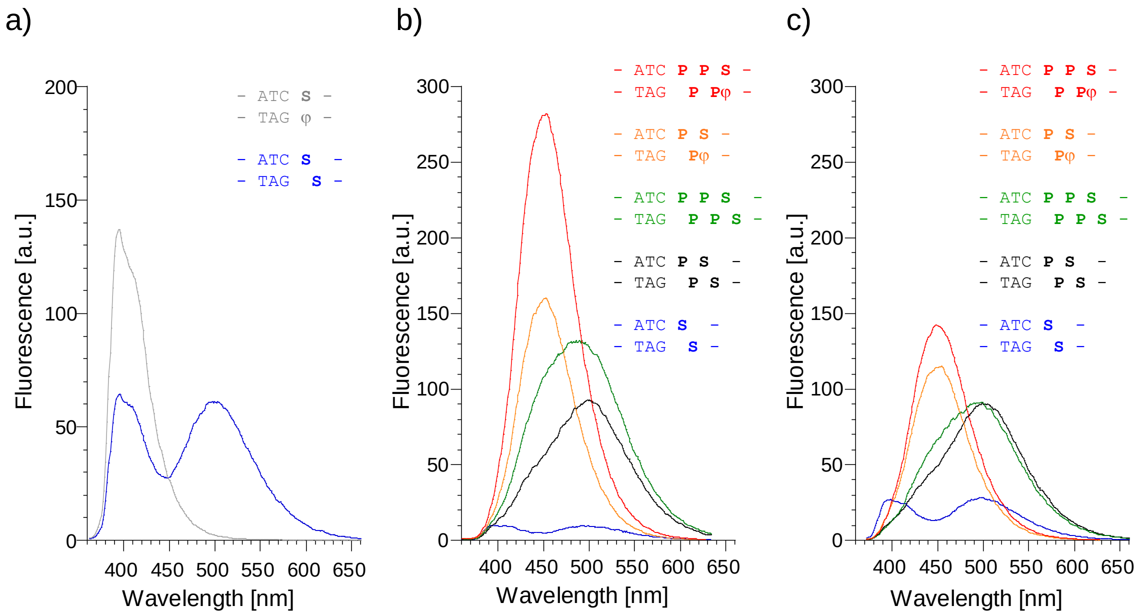

Figure 42. Fluorescence spectra of hybrids from chapter 3.3. (a) Control hybrids after excitation at 355 nm. (b) Hybrids with one or two pyrene units after excitation at 320 nm and (c) after excitation at 365 nm.

Table 7. Fluorescence data of hybrids from chapter 3.3

	25*33	***27*34***	***29*35***
a.u.c (excitation at 320 nm)	1444	10906	16339
Relative quantum yield (a.u.c / Abs.)	$6.45 \cdot 10^4$	$15.8 \cdot 10^4$	$16.2 \cdot 10^4$
Amplification	1	2.44	2.51
Max.intensity at excimer emission (500 nm)	10	93	132
a.u.c (excitation at 365 nm)	4004	10680	11157
Maximum excimer emission	29	91	91

The question at the beginning of this chapter was whether the excitation between **P** and **S** was delocalized. If a significant difference between control hybrid **25*33** and the two hybrids **27*34** and **29*35** after excitation at 320 nm was found a considerable support for the delocalization could be stated.

It was clearly shown that excimer formation was achieved after excitation of hybrid **27*34** and **29*35** at 320 nm. The comparison of the emission spectra from hybrids of the last two chapters and the spectra determined in this chapter clearly showed the formation of a new fluorescent species. Clearly, the emission maxima of hybrid **27*34** and **29*35** were red shifted compared to the emission curves of hybrid **27*28** and **29*30**. The maxima around 500 nm supported pyrene excimer emission. However, excimer formation was not fully accomplished. Exciplex emission at 450 nm was still an important fraction of the emission curve. Shape analysis indicated that probably different fractions of exciplex emission were present (see **Figure 43**b). The asymmetric emission curve originating from hybrid **27*34** could be interpreted as a sum of a major fraction of pyrene excimer emission and a minor fraction of pyrene-phenanthrene exciplex emission. The emission curve of hybrid **29*35** was fairly symmetrical. Thus, equal amounts of exciplex and excimer emissions should be present. The blue-shifted emission maximum at 485 nm in hybrid **29*35** would then be a clear consequence. The most significant support for the delocalization was seen when the emission curve of control hybrid **25*33** after excitation at 320 nm was compared to the curve of hybrid **27*34** and **29*35**. A huge difference in the emission intensities at 500 nm (pyrene excimer emission) was found. Hybrid **25*33** had only a very low emission intensity at 500 nm after excitation at 320 nm. Hybrids **27*34** and **29*35** showed a highly increased emission intensity at 500 nm after excitation at 320 nm (**Figure 43**c). This was an indication that excited **P** units (after excitation at 320 nm) transported their excitation energy to the exciplex where delocalization between **P** and **S** took place. This delocalization let to the formation of a pyrene excimer.

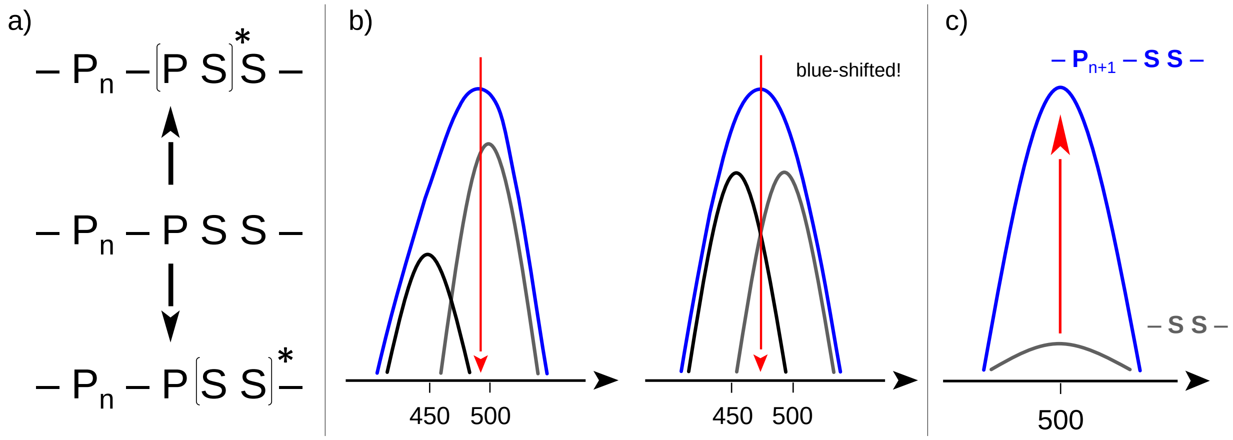

Figure 43. (a) Possible fluorescent species in hybrids from chapter 3.3. A **S**-**P**-exciplex as well as an **S**-**S**-excimer were possible. (b) Different emission intensities of the exciplex (450 nm) or the excimer (500 nm) let to an asymmetrical emission envelope. If the emission intensities were almost equal, a symmetrical envelope was found with a blue-shifted maximum compared to the asymmetrical curve. (c) A highly increased emission intensity at 500 nm after excitation at 320 nm was found in hybrids with a **P** stack next to the excimer.

The fluorescence emission data suggested that different excitation wavelengths let to changing emission curves. This was an indication that excitation at different sites caused different fluorescence species and different intensity ratios. To investigate this behavior hybrid **27*34** and **29*35** were excited between 310 nm and 350 nm in 10 nm steps and the resulting emission curves were compared. The range between 310 nm and 350 nm was in the region where the major absorption of **P** and the minor absorption of **S** changed to the inverse situation. The collected emission curves were normalized at their maximum intensity to get a better picture for comparison (**Figure 44**a/b). For both hybrids it became evident that a substantial change of the emission spectra occurred between 420 nm and 480 nm. In both hybrids the shoulder in this region decreased while the excitation wavelength was increased. In hybrid **27*34** the shoulder was located more in the flank of the emission curve whereas in hybrid **29*35** the effect was seen rather in the upper part of the curve near the maximum. The shoulder was in both hybrids centered at 450 nm. Therefore, this effect was ascribed to the exciplex emission which was present.

A similar effect was expected when the emission wavelength in excitation experiments was shifted from higher to lower energy. Only the excitation data from the emission wavelength at 440 nm, 500 nm and 540 nm were plotted (**Figure 44**c/d). The excitation band at 320 nm and 360 nm showed different intensities depending on the investigated emission wavelength. The ratio between the two bands was calculated. The value of the intensity at 365 nm was divided by the value at 320 nm (**Figure 44**e). Hybrid **27*****34** had ratios which were around 1.0, hybrid **29*****35** had ratios which were around 0.7. Values below 1.0 denoted a higher intensity of the 320 nm excitation band whereas values above 1.0 denoted a higher excitation intensity at 365 nm. The ratio overall increased from values of approximately 0.9 (**27*****34**) and 0.6 (**29*****35**) to 1.0 and 0.7 by increasing the emission wavelength. This reported that at longer emission wavelengths pyrene added a higher amount of excitation energy to the emission spectrum. In other words: At longer emission wavelengths (longer than 500 nm) the emission included a higher fraction from the excimer whereas at shorter wavelengths (shorter than 500 nm) the emission curve contained a higher ammount from the exciplex.

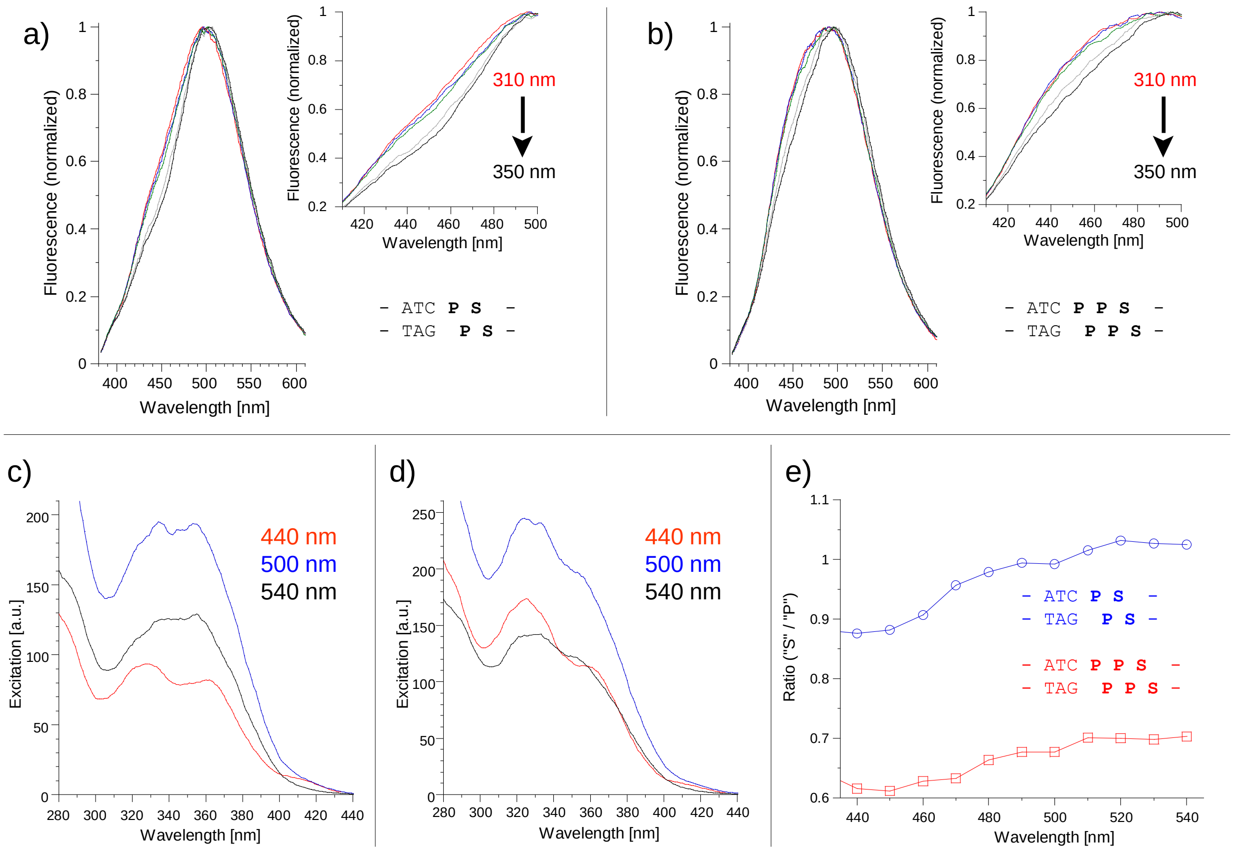

Figure 44. (a) Emission curves of hybrid **27*34** after excitation from 310 nm (red line) to 350 nm (black line) normalized at the emission maximum. The inset illustrates the decrease at 450 nm by increasing the excitation wavelength. (b) Emission curves of hybrid **29*35** after excitation between 310 nm to 350 nm normalized at the emission maximum. (c) Excitation curves of hybrid **27*34** at different emission wavelengths (440 nm, 500 nm and 540 nm). (d) Excitation curves of hybrid **29*35** at different emission wavelengths (440 nm, 500 nm and 540 nm). (e) Plot of the ratios between the excitation bands at 365 nm and 320 nm against the emission wavelength.

A mechanism was formulated in analogy to the mechanisms from the previous chapters (**Figure 25** and **Figure 36**). Energy transfer in the **P**-stack was well understood during the last two chapters. Thus, the mechanism started when the excitation already reached the **P** unit next to the two **S** units. From here on, two pathways were formulated. The first main pathway included the normal and well-known formation of an exciplex an emission at 450 nm. It was supposed that the excitation was delocalized between **S** and **P**. From the localized situation when the excitation was on **S** the second main pathway started. Excimer formation by forming a complex with the second **S** unit in the ground state was followed by excimer emission at 500 nm (**Figure 45**).

It was well recognized that the design of the hybrids could have be chosen in a better way. In chapter 3.2 the influence of G next to the core segment was analyzed and discussed in detail. It was found that the excitation of only one **P** was trapped by G and all other **P** units transferred their excitation to the exciplex. However, the used sequence design in chapter 3.3 was building on the design and the conclusions of chapter 3.2 and the influence of G was kept in mind by analyzing the results here. Nevertheless, a different result if an AT base pair was next to the core segment instead of the GC base pair was not expected.

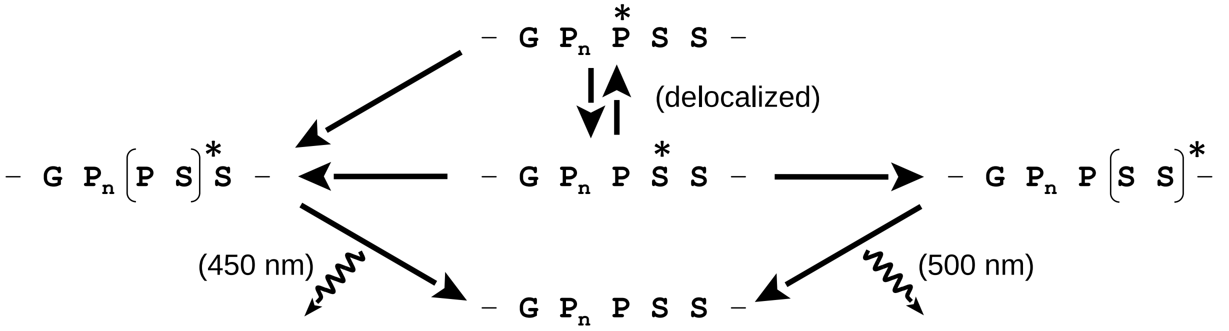

Figure 45. Mechanism of exciplex and excimer emission after excitation at 320 nm. The excitation localized on **P** next to the two **S** units could take two pathways: The first pathway included exciplex formation and emission at 450 nm. The second pathway built on the idea of an excitation delocalization between **S** and **P**. Once the excitation was localized on **S** the pathway was terminated by excimer emission at 500 nm.

3.3.3 Summary

It was concluded that delocalization of the excitation between **S** and **P** was possible. The formation of an excimer between two adjacent **S** units after excitation at 320 nm was best explained via a delocalized state. Therefore, the mechanism proposed in chapter 3.2 was supported by substantial experimental evidence (**Figure 46**).

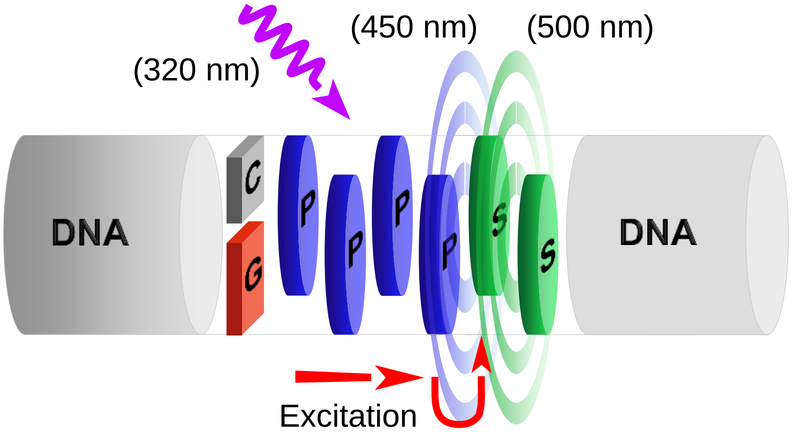

Figure 46. Model of excitation energy transfer to the fluorescent species and the delocalization between **P** and **S**. Phenanthrene-pyrene exciplex as well as pyrene excimer emission were possible.

In the last three chapters fundamental aspects of energy transfer phenomena between multiple π-stacked phenanthrene units (**P**) were investigated. It was shown that excitation energy was efficiently transferred via the **P** units to the phenanthrene-pyrene (**S**) exciplex. The introduction of a second channel where the excitation energy potentially could be transferred to and released from there did not significantly disturb the transfer direction towards the exciplex. A GC base pair next to the core segment only trapped the excitation of one **P** unit. Furthermore, a delocalization of the excitation between **S** and **P** was experimentally shown.

In order to provide and describe the energy transfer properties in π-stacked aromatic arrays in a more general purpose, the use of a different building block than phenanthrene in the absorbing part of the array was envisioned. To make the concept more general a new chromophore had to be introduced to considerably red-shift the absorbance bands.

3.4 New chromophores – The 2,1,3-benzothiadiazole-based building blocks **W** and **V**

The results discussed in this chapter let to the following publication: F. Garo, R. Häner, *Eur. J. Org. Chem.* **2012**, , .

A proof-of-principle was made by demonstrating the fundamental aspects of DNA-based light-harvesting antenna systems. The next step was to extend the cross-section of light absorption. The area of 320 nm is not in the visible region of the electromagnetic spectrum and potential applications to harvest sunlight are therefore not yet possible. To achieve a red-shift of the excitation wavelength of DNA-based antenna systems, the block where light absorption took place had to be composed of a different chromophore than phenanthrene. As could be seen, pyrene has a maximum absorbance around 360 nm. A DNA-based antenna composed of pyrene in the collecting part of the core segment and a new chromophore on top could then at least collect light which is red-shifted by approximately 30 – 40 nm compared to the previous design. This idea initiated the search for a new chromophore with a lowest absorption band between 400 nm and 450 nm.

The scaffold of 2,1,3-benzothiadiazole (BTD) is a versatile building block and widely used in numerous applications. BTD units are used as central components in photovoltaic devices [114], as linker unit in different polymers [115] and oligomers [116, 117] and as as key unit of fluorophores [118]. BTD derivatives are good fluorophores and they previously showed interesting spectroscopic properties, for example high quantum yields and large Stoke's shift in combination with a high molar absorptivity. The electron-accepting properties promoted BTD as an ideal component in donor-acceptor constructs based on π-conjugated polymers. Furthermore, the molecule's polarization supported the formation of highly ordered structures with strong π-π interactions.[119] Because of these structural and electronic properties, BTD presents itself as an ideal building block for DNA-based functional materials. The mentioned properties like strong electron accepting and preferred structural organization rendered BTD an ideal new building block for the use in antenna systems. In this chapter the synthesis and the general properties of new BTD-based building blocks in combination with DNA are described.

3.4.1 Synthesis of the new chromophores **W** and **V**

In previous studies the use of triple bond linker for non-nucleosidic DNA building blocks showed interesting and beneficial properties in DNA hybrids.[63, 120] Literature search revealed that triple bond extended BTD derivatives had absorption spectra which perfectly matched the described requirements of a new chromophore. Thus, the use of a 4,7-dialkynyl BTD derivative as new energy collecting center in the antenna systems might bring the whole project one step further. Nevertheless, for completeness the synthetic strategy for a 4,7-carboxamide-linked BTD core, in analogy to the well-known pyrene and phenanthrene units, was also designed.

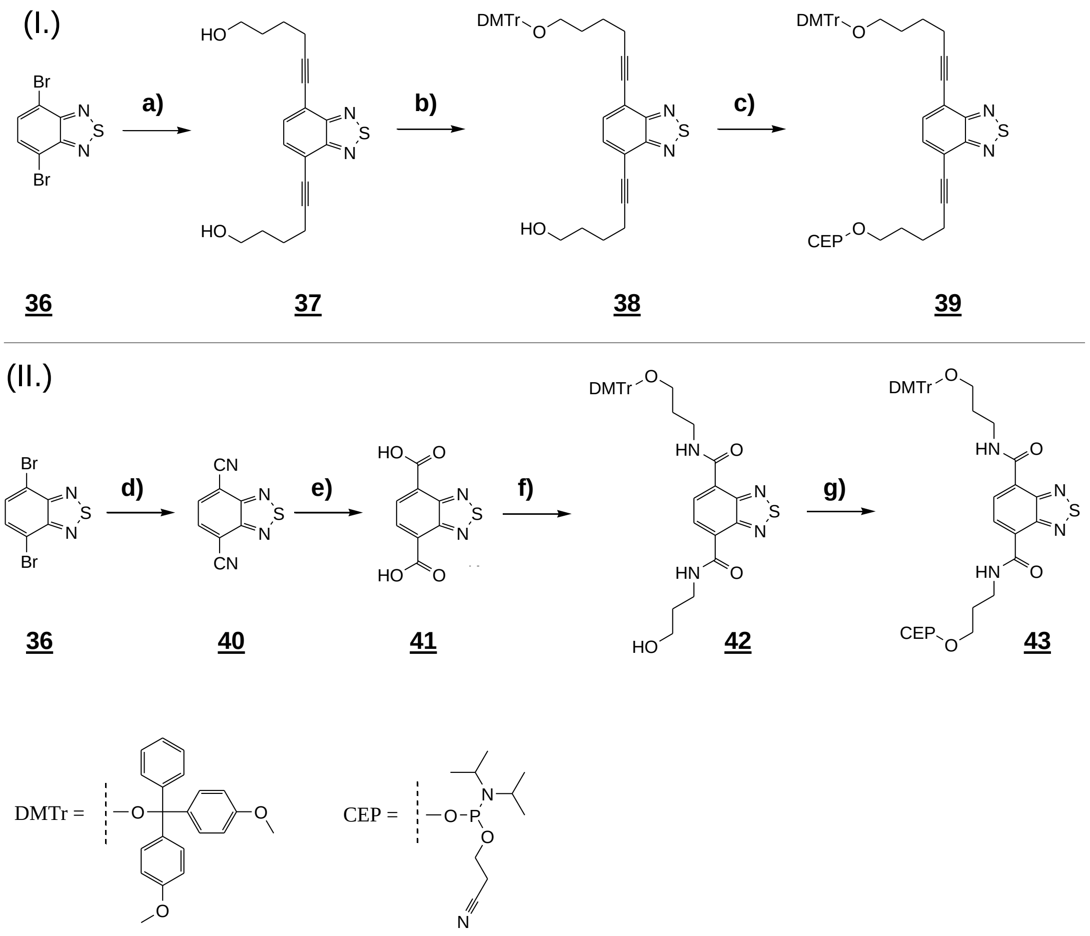

Scheme 3. (I) Synthetic scheme for the preparation of 4,7-dihexynyl BTD phosphoramidite **39**. Reagents and conditions: (a) 5-hexyn-1-ol, Cu(I)I, bis(triphenylphosphine)palladium(II) dichloride, Et$_3$N, dioxane, 60 °C, 1 h (92 %); (b) 4,4'-dimethoxytrityl chloride, pyridine, DMAP, CH$_2$Cl$_2$, r.t., 4 h (45 %); (c) 2-cyanoethyl *N*,*N*-diisopropylchlorophosphoramidite, *N*,*N*-diisopropylethylamine, DCM, r.t., 1 h (90 %). (II) Synthetic scheme for the preparation of 4,7-dicarboxamide BTD phosphoramidite **43**. Reagents and conditions: (d) Cu(I)CN, pyridine, NaI, DMF, 180 °C, 6 h (80 %); (e) 25 % NaOH in water, 100 °C, 2 h (85 %); (f) **4** and **1** (1:1), HBTU, *N*,*N*-diisopropylethylamine, DMF, r.t., 2 h (33 %); (g) 2-cyanoethyl N,N-diisopropylchlorophosphoramidite, *N*,*N*-diisopropylethylamine, DCM, r.t., 1 h (75 %).

The same starting material for the synthesis of 4,7-dihexynyl- and 4,7-dicarboxamide BTD building blocks was required, namely commercially available 4,7-dibromo-2,1,3-benzothiadiazole **36** (4,7-dibromo BTD). The alkynyl linker chains were introduced via the *Sonogashira* cross coupling reaction with 5-hexyn-1-ol to yield diol **37**. One hydroxyl group was subsequently protected by treatment of **37** with 4,4'-dimethoxytityl (DMT) chloride to give mono-DMT protected 4,7-dihexynyl BTD **38**. Finally, phosphitylation of the second hydroxyl group gave the required 4,7-dihexynlyl BTD phosphoramidite building block **39**. (**Scheme 3**, upper part)

The carboxamide linker chains were introduced by first converting 4,7-dibromo BTD **36** via the *Rosenmund – von Braun* reaction to 4,7-dicarbonitrile BTD **40** [121] followed by hydrolysis to yield 4,7-dicarboxylic acid BTD **41**.[122] Amide formation involved treatment of **41** with a 1:1 mixture of **1**and **4**. The resulting mono-DMT protected 4,7-dicarboxamide BTD **42** was subsequently transferred to the 4,7-

dicarboxamide BTD phosphoramidite building block **43** by phosphitylation of the free hydroxyl group. Synthetic and analytical details are listed in the experimental section (3.5). The phosphoramidite building blocks were incorporated into DNA oligomers by conventional phosphoramidite chemistry in analogy to chapters 3.1 – 3.3 (see **Figure 49** and **Table 10**)

3.4.1.1 Spectroscopic investigation of the monomeric building blocks

The monomeric building blocks **37** and **41** were characterized by UV/VIS absorbance and fluorescence emission spectroscopy. The absorbance properties of the two new building blocks were very diverse. Compound **37** was red-shifted by approximately 70 nm compared to **41** and showed structured and resolved vibronic bands. The absorbance band with a maximum at 387 nm was ascribed to the intramolecular charge transfer from the phenyl part to the thiadiazole part within the BTD molecule. Compound **37** had broad and unstructured absorbance bands. The fluorescence emission intensity was highly increased in compound **37** compared to the emission of **41** if both chromophores were excited at 350 nm. This excitation wavelength was nor for **37** neither for **41** the maximum of the absorbance band. The advantage was that at 350 nm both chromophores had the same absorptivity and thus emission data could be directly compared. The quantum yield of compound **37** was highly increased compared to compound **41** which was ascribed to the presence of the triple bond linkers. It is known from several studies that the introduction of triple bonds into aromatic molecules can significantly change the spectroscopic properties.[123] Red-shifted absorption bands as well as increased fluorescence emission intensities were mostly the direct consequences of the introduction of triple bonds. Pyrene as well as fluorene building blocks showed exactly this behavior. Hence, the data presented (see **Figure 47**) were in good agreement with previous findings.

Table 8. Electronic properties of compound **37** and **41**

	compound 37	***compound 41***
Absorption band λ_{max} [nm] [a]	242; 260; *270* [b]; 309; 322; 387	230; 316
ε [L mol^{-1} cm^{-1}] [a]	16390; 22880; 26110; 8660; 12660; 7950	12430; 11270
Emission λ_{max} [nm] [a]	515	460
Quantum yield [c]	0.230	0.046
reduction potential [V] [d]	-1.12	-0.67

[a] 10 μM in water; [b] underlined values indicate main absorbance bands; [c] quinine sulfate as fluorescence standard; [d] vs. Ag/AgCl in acetonitrile.

BTD is known as a strong electron acceptor and is often used for this purpose. On this basis the determination of the reduction potentials of **37** and **41** was the most straight-forward approach. Cyclic voltammetry experiments revealed values of -1.12 V for **37** and -0.67 V for **41** (vs. Ag/AgCl in acetonitrile, for details see the experimental part 5.2). The reduction potential of **41** was in good agreement with previous studies of similar compounds. Ethyl and butyl esters of **41** had reduction potentials of -0.9 V (vs. SCE in acetonitrile).[124] The lower potential of **41** compared to the potentials of the esters might be a reason of the higher electron affinity of the core unit (BTD) when the ester groups are hydrolyzed to the free carboxylic acid.

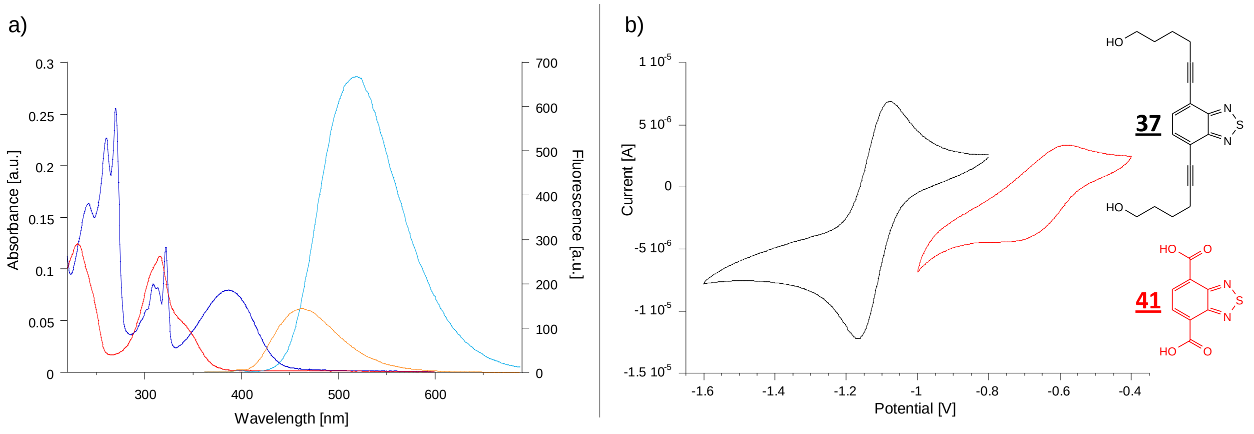

Figure 47. (a) UV/VIS and fluorescence spectra of compound **37** (blue and light-blue line) and **41** (red and orange line) in water (both 10 μM). (b) Cyclic voltammetry experiments of compounds **37** (black line) and **41** (red line) in acetonitrile (**37** = 1.0 mM and **41** = 0.5 mM; 0.1 M ammonium hexafluorophosphate).

The interplay between fluorescent labels and the four DNA nucleobases was investigated in many examples and represents a well investigated topic.[104, 107, 125] For example genetic diagnostic tool to detect single-nucleotide-polymorphisms (SNP) or sequence-specific screening of DNA samples often benefit from such interactions.[126] A smart probe design includes a preliminary study of the chromophore – DNA base interaction to minimize or maximize the fluorescent signal, depending on the approach. If response of the designed probe to an external input (e.g. molecular beacon probes for the detection of DNA sequences) releases the chromophore from the DNA-base environment and increases the fluorescence signal, a strong quenching interaction between chromophore and DNA bases is required. If binding of the chromophore probe to the DNA double strand and subsequent fluorescence signal read-out is performed, quenching of the DNA-bases should be as small as possible. The mechanism of fluorescence quenching by electron transfer was described previously in chapter 3.2. The kinetics of the electron transfer process between an electron donor and an electron acceptor molecule can be estimated by using the *Weller* equation:[127]

$$\Delta G_{CS} = E_{ox\ (base)} - E_{red\ (label)} - E_{0,0\ (label)} + C$$

where ΔG_{CS} is the free *Gibbs* energy (reported in eV), E_{ox} and E_{red} are redox potentials (in Volts) and $E_{0,0}$ is the electronic excitation energy (in eV). The constant *C* is negligible in polar solvents (e.g. water and acetonitrile). Therefore, the probability for the formation of a charge separated state between donor and acceptor is predictable if the redox properties of the two molecules are known. A simple determination of $E_{0,0}$ is possible based on steady-state spectroscopic data of the chromophores.[128] $E_{0,0}$ is the crossing point of the absorption and the emission spectrum. The simple and easy-to-use *Weller* formula allows a first approximation of possible quenching effects and reveals support for experimental data afterwards. A negative ΔG_{CS} value represents an event which is exergonic, thus, charge separation is favorable for this process whereas positive values are endergonic processes and are unfavorable (**Figure 48**a). ΔG_{CS} values for charge separation between the four canonical DNA nucleobases dG, dA, dT and dC and the two new chromophores **37** and **41** were determined (**Table 9**).

Table 9. Calculation of ΔG_{CS} between chromophore **37** and **41** and the four canonical DNA nucleobases

	E_{red} [V] [a]	*excitation energy $E_{0,0}$ [eV]* [b]	*E_{ox} [V]* [a]	*ΔG_{CS} (vs. X)*	*ΔG_{CS} (vs. X)*
compound **37**	-1.17	2.80	-		
compound **41**	-0.71	3.10	-		
guanine (dG)	-	-	1.25	-0.40	-1.16
adenine (dA)	-	-	1.72	0.07	-0.69
thymine (dT)	-	-	1.87	0.22	-0.54
cytosine (dC)	-	-	1.90	0.25	-0.51

[a] vs. SCE (standard calomel electrode) in acetonitrile; [b] 2.80 eV = 443 nm, 3.10 eV = 400 nm.

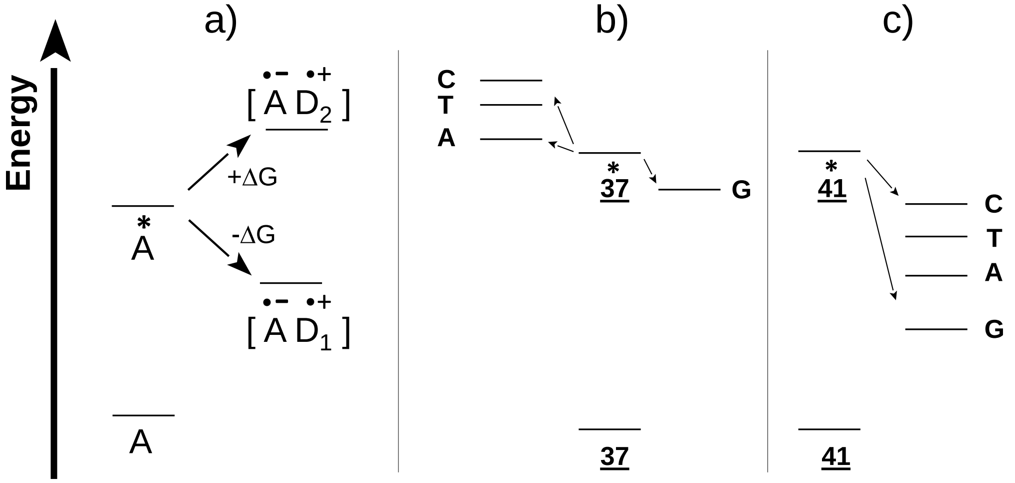

Figure 48. Relative energies for the formation of charge separated states. (a) General consideration: An excited chromophore A* forms a charge separate state with donor D_1 (exergonic = - ΔG) and D_2 (endergonic = + ΔG). (b) and (c) Energy diagrams (based on calculated ΔG_{CS} values, see **Table 9**) for charge separation between the chromophores **37** and **41** and the four canonical DNA nucleobases. Only charge separation between **37** and G was exergonic whereas for the other three bases ΔG_{CS} was positive. Charge separation between compound **41** and all four DNA bases was favorable (exergonic).

The calculated ΔG_{CS} values between compound **41** and the nucleobases were all negative. It was expected that irrespective of the used DNA sequence as soon as **41** was introduced into DNA oligonucleotide sequences, the fluorescence of **41** will be highly quenched (**Figure 48**c). For the other building block **37** only the value for charge separation between G and **37** was negative and all other values were slightly endergonic (**Figure 48**b). This was interesting because it provided **37** as a potentially valuable building block for the specific detection of DNA bases.

3.4.2 System design

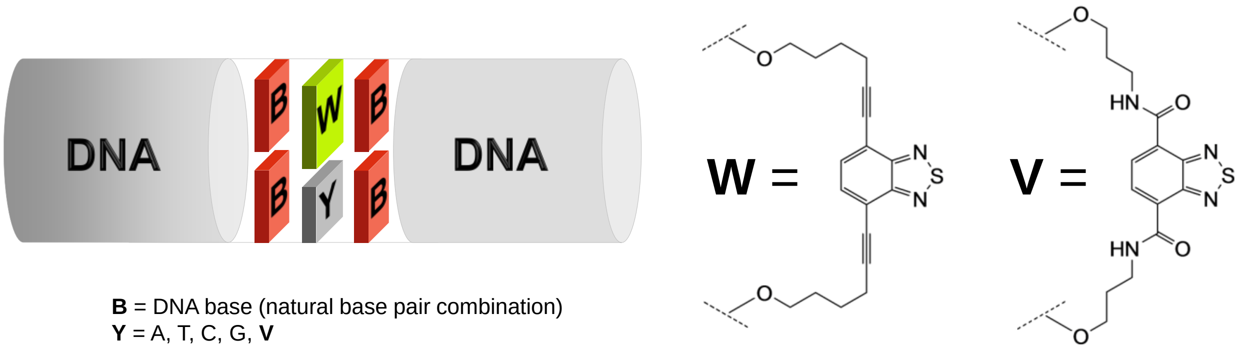

Figure 49. Design of the hybrid set for the study of the spectroscopic properties of building blocks **W** and **V** (for detailed sequences see **Table 10**)

Table 10. Oligonucleotides **44** – **67** prepared for chapter 3.4

	Hybrid	*oligomer number (Y)* [a]				
Pool 1	5'- TAA TAA TAA ATA **W** ATA AAT AAT AAT	**44**				
	3'- ATT ATT ATT TAT **Y** TAT TTA TTA TTA	**45** (A)	**46** (T)	**47** (C)	**48** (G)	**49**(V)
Pool 2	5'- TAA TAA TAA ATA **Y** ATA AAT AAT AAT	**50** (A)	**51** (T)	**52** (C)	**53** (G)	**54** (V)
	3'- ATT ATT ATT TAT **W** TAT TTA TTA TTA	**55**				
Pool 3	5'- TAA TAA TAA ATC **W** ATA AAT AAT AAT	**56**				
	3'- ATT ATT ATT TAG **Y** TAT TTA TTA TTA	**57** (A)	**58** (T)	**59** (C)	**60** (G)	**61** (V)
Pool 4	5'- TAA TAA TAA ATC **Y** ATA AAT AAT AAT	**62** (A)	**63** (T)	**64** (C)	**65** (G)	**66** (V)
	3'- ATT ATT ATT TAG **W** TAT TTA TTA TTA	**67**				

[a] modified oligomers (ε-value at 260 nm / Mass [g/mol]): **44** (357050 / 7773.1); **49** (275546 / 7711.2); **54** (325946 / 7783.3); **55** (286525 / 7700.9); **56** (349150 / 7748.9); **61** (278246 / 7736.2); **66** (318046 / 7759.3); **67** (289225 / 7725.9)

To test the predictions (see **Table 9**), a DNA-based system was designed (**Figure 49**). Chromophore **37** introduced in a DNA hybrid will be abbreviated in the following as **W**. The calculations of ΔG_{CS} values between the four DNA nucleobases and **37** predicted a strong quenching effect of G on the fluorescence of **37**. Therefore the chromophore was introduced in the middle of an AT-sequence and G was omitted entirely in the whole sequence. Because of the expected sensitivity of **W** in combination with DNA, the fluorescence behavior of **W** in changing nucleobase base environments was tested. For this purpose the sequence of the corresponding counter strands had in the position next to **W** one of the four DNA nucleobases. For the resulting four hybrids, the microenvironment of **W** was constant except for the base next to it in the counter strand. The system was closer inverted by providing a set of hybrids where the positions of **W** and the four bases were exchanged. This extended the test by keeping the microenvironment constant but putting **W** in the mirror-inverted position (hybrid pool 1 and hybrid pool 2, **Table 10**). To challenge the system in two additional pools, a GC base pair was introduced directly next to the positions of **W**. To look for the system's borderline and for the fluorophore's strength this was a straight forward approach. A total of four different hybrid pools (one pool with four hybrids) were prepared.

The calculation of the ΔG_{CS} values between **41** and the four DNA bases predicted highly exergonic values and therefore strong quenching effects on the fluorescence of **41**. No special behavior was expected for **41** in combination with DNA bases as all excitation energy for subsequent fluorescence emission would be "destroyed" by accepting an electron from each of the DNA bases. Nevertheless **41** was incorporated into DNA oligonucleotides as base surrogate and positioned in the counter strand next to **W**. Chromophore **41** introduced in a DNA hybrid will be abbreviated in the following as **V** This broadened the four hybrid pools by one strand. A total of five strands per pool were now available.

3.4.3 Spectroscopic investigation and discussion

The melting temperature (Tm) values of all hybrids were investigated first (**Table 11**). A reference for the study, the Tm values of hybrid **51*****45** and **52*****48** were determined. These two hybrids were good representatives for fully natural DNA hybrids; **51*****45** had an AT base pair in the center of the hybrid (in the position where **W** was otherwise introduced) and **52*****48** had a GC base pair in this position. Hybrid **51*****45** had a Tm of 41.5 °C and hybrid **52*****48** of 44.5 °C. The GC base pair stabilized the hybrid by 3.0 °C.

The introduction of **W** caused a considerable destabilization when **W** was next to a natural DNA base. Hybrids from pool 1 and pool 2 were structurally the same except for the position of **W** in the strands. When **W** was facing a natural base all Tm values were equal in these two pools (around 32 °C), except for a slight experimental deviation. The base in the counter strand next to **W** seemed to have no influence on the stability of the hybrids as within the two pools no deviation of the Tm values was found. The constant Tm value within the two hybrid pools revealed that probably no interaction between the base and **W** in the counter strand took place. Hybrids from pool 3 and 4 also showed the same stabilities within the pool and compared to each other when a natural base was next to **W**. Hybrids from pool 3 and 4 had a GC base pair next to **W** and the Tm values were slightly higher (3 – 4 °C) compared to the hybrids from pool 1 and 2. This was in agreement with the determined Tm values from the two reference hybrids **51*****45** and **52*****48**.

The hybrid stability was highly increased when **W** was facing another **W** or **V** unit. Hybrids with a **W*****W** pair were slightly more stable (1 – 2 °C) compared to hybrids with a **W*****V** pair. "Homo-hybrids" (**44*****55** and **56*****67**) with the same modification in both strands seemed to have an even more favored interaction between the BTD units than "hetero-hybrids" with different modifications. The highest stability was determined for hybrid **56*****67**. The Tm value was 46.5 °C which was 2 °C more stable than the reference hybrid **52*****48**. This was a remarkable result and let to further questions. What was the driving force that caused such a high stabilization of the hybrids with two BTD units next to each other? A closer look at the stabilizing effect of BTD units on DNA hybrids revealed that this stabilizing effect was in the same range as other polyaromatic units previously showed. Pyrene, phenanthrene, phenanthroline and other investigated units had big aromatic surfaces compared to the reported BTD core. It could be stated that the high stabilization of BTD was exceptional.

Table 11. Tm values and quantum yield for all hybrid combinations of chapter 3.4

Pool 1

```
5′-TAATAATAAATA W ATAAATAATAAT
3′-ATTATTATTTAT Y TATTTATTATTA
```

Hybrid	pair	Quantum yield	Tm value [°C] [a]
51*45	T*A	-	41.5
52*48	C*G	-	44.5
44*45	W*A	0.119	32.0
44*46	W*T	0.120	32.0
44*47	W*C	0.118	31.5
44*48	W*G	0.017	32.5
44*49	W*V	0.008	39.5

Pool 2

```
5′-TAATAATAAATA Y ATAAATAATAAT
3′-ATTATTATTTAT W TATTTATTATTA
```

Hybrid	Pair	Quantum yield	Tm value [°C] [a]
50*55	A*W	0.131	32.0
51*55	T*W	0.161	32.5
52*55	C*W	0.199	32.0
53*55	G*W	0.031	32.0
54*55	V*W	0.006	40.0
44*55	W*W	0.110	41.5

Pool 3

```
5′-TAATAATAAATC W ATAAATAATAAT
3′-ATTATTATTTAG Y TATTTATTATTA
```

Hybrid	pair	Quantum yield	Tm value [°C] [a]
56*57	W*A	0.034	36.0
56*58	W*T	0.070	35.5
56*59	W*C	0.074	35.0
56*60	W*G	0.016	36.5
56*61	W*V	0.016	44.0

Pool 4

```
5′-TAATAATAAATC Y ATAAATAATAAT
3′-ATTATTATTTAG W TATTTATTATTA
```

Hybrid	Pair	Quantum yield	Tm value [°C] [a]
62*67	A*W	0.011	35.5
63*67	T*W	0.012	35.5
64*67	C*W	0.011	35.0
65*67	G*W	0.007	35.0
66*67	V*W	0.003	44.5
56*67	W*W	0.010	46.5

[a] 1 μM DNA double strand (2 μM total oligonucleotide concentration), 100 mM sodium chloride, 10 mM sodium phosphate buffer at pH 7.0

The high hybrid stability was attributed to the strong polarization within the BTD molecule (**Figure 50**a). As mentioned in the introductory part of chapter 3.4, the polarization in BTD is not only responsible for the strong electron accepting behavior (also seen as low reduction potentials of **37** and **41**) but also for the formation of highly ordered and well-arranged structures. Molecular modeling studies (with HyperChem®) supported the importance of the polarization. Twisted arrangements of the BTD building blocks stacked on each other as starting point let to a parallelization of the molecules after geometry optimization with the polarization in contrary directions. A nearly collinear stack of the two units was proposed (**Figure 50**b). A weak support for the estimations and predictions was found in the circular dichroism (CD) spectrum of hybrid **44*55**. Nor an exciton coupled signal neither certain indications of a slightly induced signal in the range between 450 nm and 300 nm was found.[129] Other aromatic building blocks with the triple bond linker mode, showed an intense CD response in the area where the chromophores absorbed after incorporation into DNA hybrids. Exciton coupled (pyrene)[120] and induced (fluorene)[63] CD signals were found. The result found here might be an indication that the transitions moments in the two BTD units were in line and not twisted.

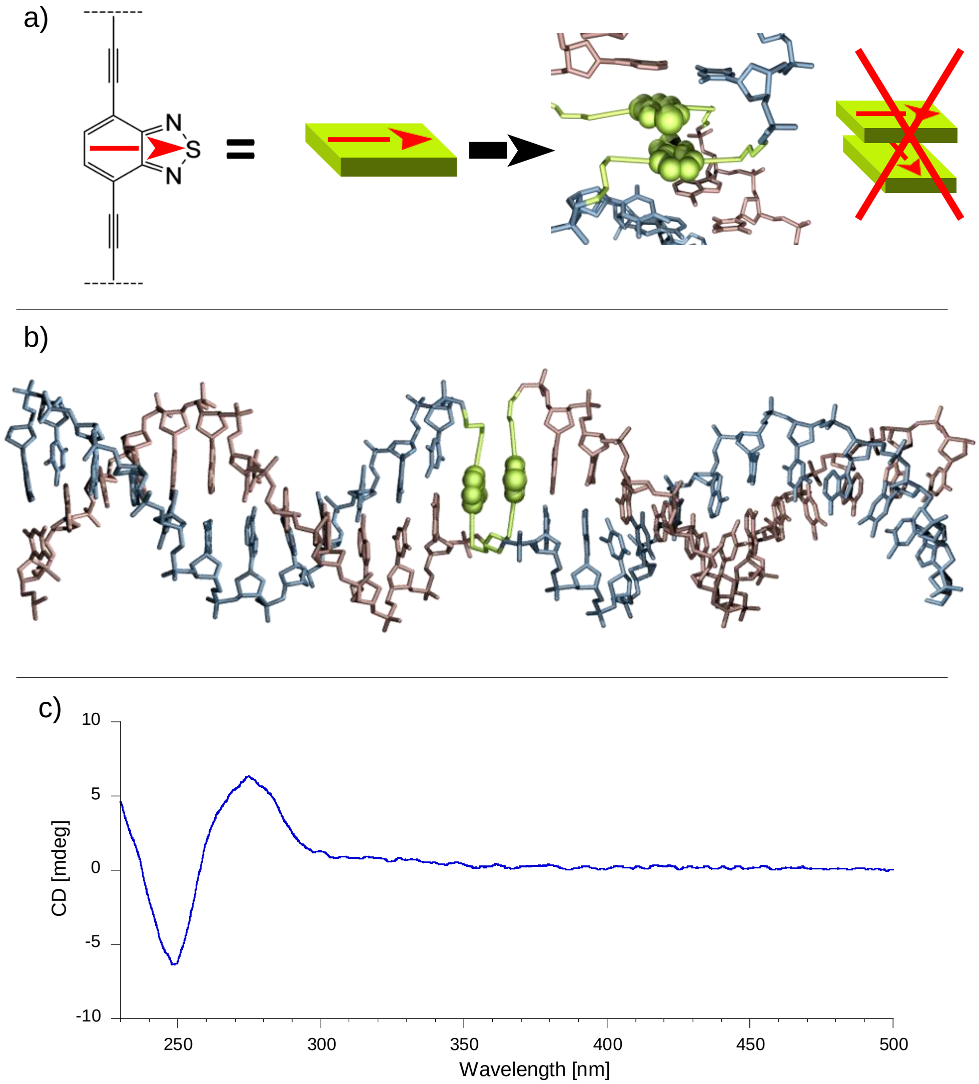

Figure 50. (a) The high electronic polarization from the phenyl part to the thiadiazole of BTD is indicated by the red arrow. Molecular modeling revealed a high tendency of the BTD units to be stacked collinearly with the polarization in contrary directions. (b) An amber – minimized *HyperChem®* [110] model supported the assumptions. The **W** units are shown in olive. (c) Circular dichroism spectrum of hybrid **44*****55**. A signal from normal B-shaped DNA was detected in the range between 300 nm and 240 nm whereas in the region between 450 nm and 300 nm no signal at all was detected. A signal would be an indication of twisted transition moments (twisted chromophores).

The UV/VIS spectra of oligonucleotides and all hybrids were determined. Some selected samples are shown (**Figure 51**a/b). The two single strands only differed in their modification in the middle of the sequence as **44** (**Figure 51**a, black line) had **W** in this position and **54** (**Figure 51**a, red line) had **V**. The lowest energy absorbance bands of the two chromophores were well separated. Single strand **44** had a maximum at 400 nm and **54** at 320 nm. A selective excitation of **W** at 400 nm for fluorescence experiments was possible. UV/VIS spectra from hybrids were in line with the spectra from single strands and no additional special features were found. Hybrid **44*****55** (**Figure 51**b, blue line) had the highest absorbance at 400 nm as two **W** units were present. The high absorbance intensity at 320 nm of hybrid **54*55** (red line) was expected as **W** and **V** were perent. A slight hypochromic effect of **W** at 400 nm is seen in this hybrid (**Figure 51**b, red line). If the absorbance values of hybrid **54*55** and **52*55** (black line) at 400 nm were compared it was found that **54*55** was slightly less intense. Both hybrids had **W** in the same strand an only the unit facing **W** was different (C or **V**). This slight hypochromic effect could be a sign of interstrand stacking interactions between **W** and **V**.

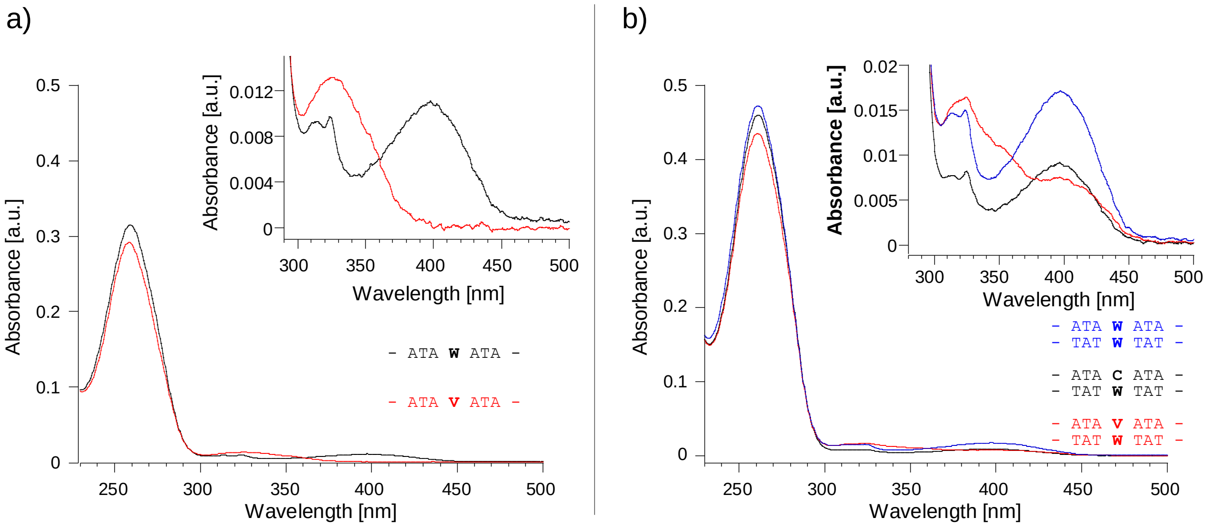

Figure 51. UV/VIS spectra of selected single strands and hybrids. (a) Single strand **44** (black line) was a representative sample for an oligonucleotide with one **W** unit whereas **54** (red line) was shown as representative for the incorporation of one **V** unit. As can be seen, selective excitation of **W** at 400 nm was possible. (b) Three selected hybrids with a **W***C (**52*55**, black line), a **V*W** (**54*55**, red line) and a **W*W** (**44*55**, blue line) combination.

The steady-state fluorescence emission curves (excitation at 400 nm for all combinations) of all hybrids were measured and some selected spectra are shown (**Figure** 52a-c). The question was which influence the position of **W** in the sequences and the unit facing **W** in the counter strand (natural base or other BTD unit) will have on the fluorescence emission efficiency. A strong dependence was predicted based on the analysis of the preliminary results.

Figure 52a represents the curves of hybrids when the position of **W** was kept constant and only the natural base in the counter strand was shuffled (all combinations of **55** with natural DNA bases in the counter strand). The second plot (**Figure** 52b) summarizes the data where the natural base was constant (C in the counter strand) and **W** was in different environments. The last plot (**Figure** 52c) shows tree combinations of **W** facing another BTD unit (**W*W** combinations and a **W*V** combination). The quantum yield of **W** in all hybrids was calculated and plotted as a function of the partner **B** in the counter strand (**Figure** 52d). Overall, the position of all emission curves was constant at 500 nm (maximum emission intensity) irrespective of the partner in the counter strand or the position of **W** in the sequences. In contrast to this uniform result, the intensities of the emission curves were very different and changed strongly. These results were interesting and required further discussion.

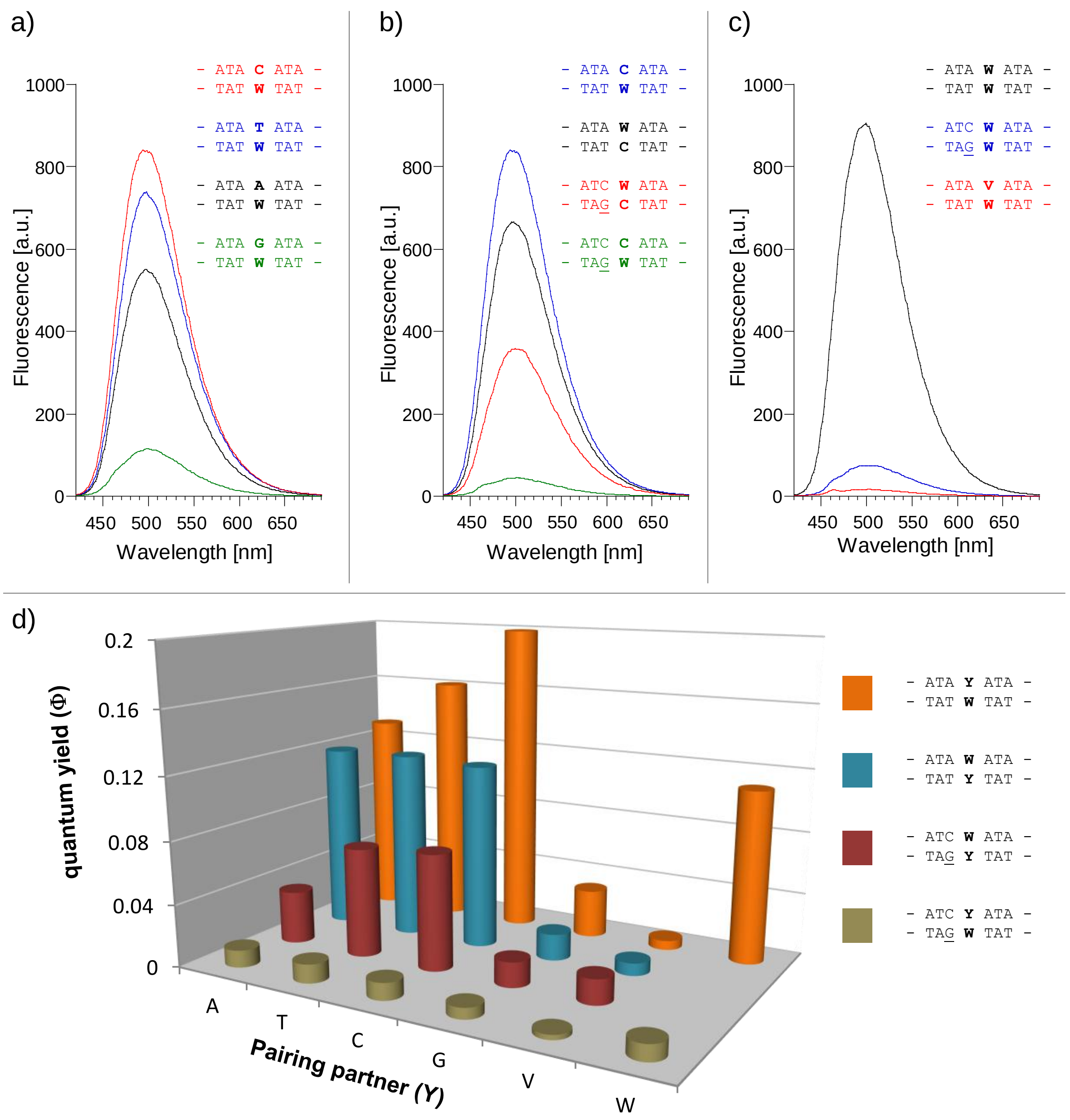

Figure 52. (a-c) Fluorescence emission curves of selected hybrids after excitation at 400 nm. (d) Quantum yields of **W** in all hybrids as a function of the partner **Y** in the counter strand.

The influence of the DNA base in the counter strand facing **W** was investigated first. A closer look at the emission data of hybrids from pool 2 (**Figure 52**a) revealed that the order of emission intensities was following the same ranking as the oxidation potential of the DNA bases. The base with the highest oxidation potential (cytosine C) had the least influence on the fluorescence emission of **W** whereas guanine (G), with the lowest oxidation potential of all four bases, had the highest quenching effect. These results can be explained together with the mechanism of fluorescence quenching by electron transfer and the corresponding calculations (**Table 9**). The situation with G in the counter strand was straight forward. An exergonic process was predicted for charge separation between G and **W** which was reflected by the low quantum yield of hybrid **53*55** (G***W**). Even if the ΔG_{CS} value between adenine (A) and **W** was slightly endergonic (**Table 9**), charge separation between the two molecules seemed to be still possible as the fluorescence was quenched as well. Calculations based on the *Weller* equation only gave a rough estimation of the kinetics for charge separation. Some facts are not considered in the equation, for example the slightly changed solvent polarity (acetonitrile vs. water) and the changes in the environment of the molecules after DNA hybrid formation. These slight changes obviously allowed charge separation between A and **W** despite the calculated slight endergonic free *Gibbs* energy. If the fluorescence data of the hybrid with thymine (T) next to **W** (hybrid **51*55**) were compared to the data with C in this position (hybrid **52*55**), also T in the counter strand still showed a certain fluorescence quenching effect on **W**.

The next step was to find out which influence the microenvironment of **W** in the different sequences had on the emission efficiency. The influence of the bases was shown to be important. The neighboring bases of **W** were different in each pool and therefore considerable changes in the fluorescence emission were expected. In pool 1 **W** was between two adenines (purine bases) and in pool 2 between two thymines (pyrimidine bases). Pool 3 and 4 had mixed purine-pyrimidine sequences directly next to **W**. From the chart (**Figure 52**d) it became evident, that the emission of **W** highly depended on the microenviroment formed by the surrounding bases. In pool 1 the emission of **W** was influenced by intrastrand interactions with the neighboring A units. Only the presence of G in the counter strand next to **W** could even further quench the emission of **W**. Other bases in the counter strand had no effect. In pool 2 **W** was between two T units. No such strong intrastrand effect as in pool 1 was found and all bases in the counter strand next to **W** influenced the fluorescence emission according to their oxidation potentials. Pool 3 and 4 had a GC base pair directly next to the position of **W**. The presence of G quenched the emission of **W** by a considerable amount. In pool 3, G was in the counter strand diagonally opposite to **W**. Even though the fluorescence was quenched compared to the emission of hybrids from pool 1 and 2, certain recognition and differentiation modes for the four bases were still possible. This was not the case for hybrids in pool 4. The direct neighborhood of G in the same strand severely quenched the emission of **W**.

The fluorescence emission behavior of hybrids with two BTD units (**W***W** and **W***V** combinations) were interesting because of several reasons. First, the reduction potential of **V** was low. Hence, an important effect on the fluorescence emission was expected. Second, the interaction between two BTD units promised to reveal information about the exact orientation and organization between the stacking BTD units as the *syn*- form of [2.2](4,7)benzothiadiazolophanes (bicyclic, dimeric molecule where two BTD units are held in close proximity by a short C2-linkers) was reported to show a highly quenched fluorescence emission compared to the *anti*-conformation.[130]

As already mentioned, the emission maxima for all hybrids was at 500 nm, thus, no excimer or exciplex fluorescence emission was found for hybrids with two BTD units. **Figure 52**d summarizes the quantum yields for all these hybrids. Apparently, a very strong fluorescence quenching effect of **V** on the emission of **W** was detected. This strong interaction was not further amplified by the presence of G. Compared to the quantum yield of the most efficient combination discussed above (hybrid **52*55** with a C***W** combination and quantum yield of approximately 0.2) the replacement of C by **V** caused a virtual shut-down of the fluorescence emission and an ON/OFF behavior was postulated. The exact reason for this result and the quenching mechanism between **W** and **V** needs further analysis. Two **W** units next to each other in hybrid **44*55** had the brightest (because the highest intensity was detected) fluorescence emission of all combinations even though the quantum yield was almost divided by a factor of two compared to the best combination (**52*55**). A certain amount of self-quenching was found. This self-quenching was by far not as severe as reported for the *syn*-conformation of [2.2](4,7)benzothiadiazolophane. In this study the collinear and parallel placement of the two BTD rings (thiadiazole part in same direction) highly quenched the fluorescence emission. Such a strong effect was not seen in hybrid **44*55**. This supported the assumptions of parallel BTD units in the DNA hybrids (see **Figure 50**a). Based on all the spectroscopic data gained so far it was concluded that the thiadiazole part must point into contrary directions and did not interact with each other.

3.4.4 Summary

Two new building blocks, **W** and **V**, were design, synthesized and incorporated into DNA oligonucleotides and their spectroscopic properties were analyzed. The fluorescence properties were of specific interest, as the use of **W** or **V** for additional antenna hybrids was envisioned. Building block **V** had interesting redox properties in the monomeric state (compound **41**). The very low reduction potential of **41** caused a fully quenched fluorescence emission after introduction into DNA hybrids. Building block **W** on the other hand showed fluorescence emission properties that highly depended on the DNA base environment (**Figure 52**d and **Figure 53**). The strong interstrand interactions of two artificial units next to each other and the resulting DNA hybrid stabilization were remarkable. Nevertheless, none of the two units formed emissive exciplex or excimer species. The properties and the behavior of **W** in DNA hybrids were encouraging and let to the design of a different antenna system based on pyrene **S** and BTD **W** (chapter 3.5).

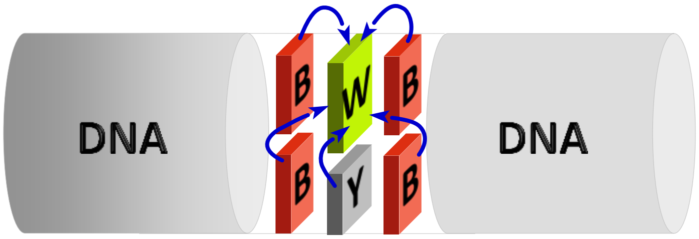

Figure 53. Summary of chapter 3.4. The new building block **W** was incorporated into DNA double strands and the fluorescence was analyzed. The microenvironment formed by the DNA bases highly influenced the fluorescence emission efficiency.

3.4.4.1 Note on other non-nucleosidic building blocks derivatived from BTD

The scaffold of 2,1,3-benzothiadiazole was shown to be an interesting and versatile unit for the synthesis of new non-nucleosidic building blocks for the incorporation into DNA oligonucleotide. The extension of the pool of BTD-derived units could lead to interesting studies and results with a broad interest. A starting point for the broadening of building blocks availability is shown briefly in the following (**Figure 54** and **Figure 55**). Some of the presented derivatives were already synthesized (see experimental part, synthetic work was partially performed by K. Uhlmann which is gratefully acknowledged).

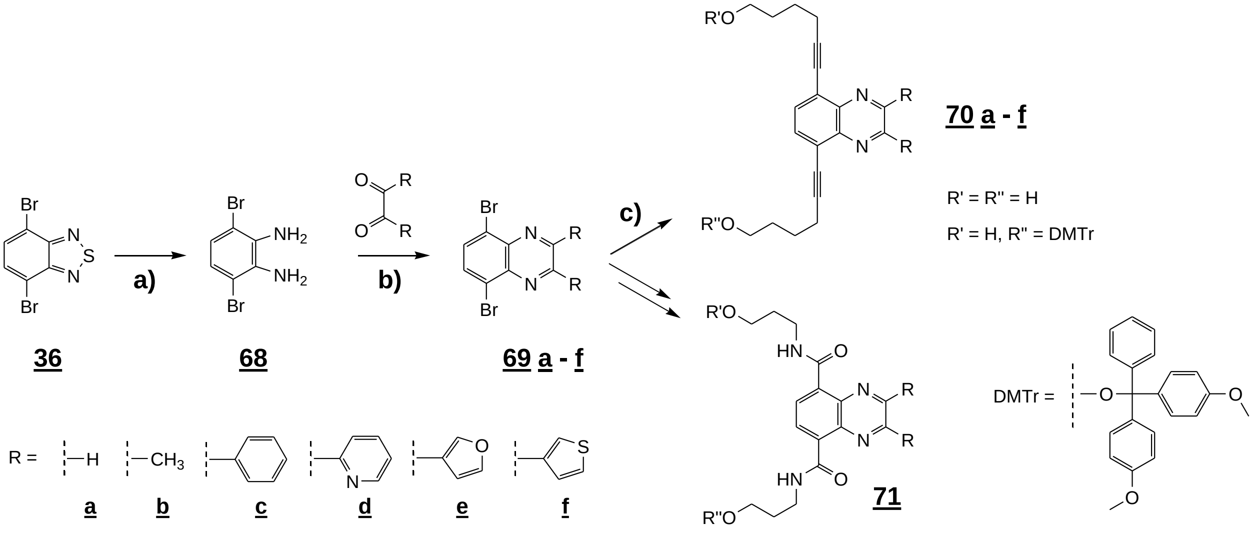

Figure 54. Synthetic route to new building blocks based on the scaffold of quinoxaline (details see experimental part). Reagents and conditions: (a) sodium borohydrate, EtOH, 0 °C to RT overnight; (b) EtOH, cat. HCl, reflux, 1 – 10 hrs. (c) 5-hexyn-1-ol, Cu(I)I, bis(triphenylphosphine)palladium(II) dichloride, Et_3N, dioxane, 60 °C, 1 h.

The thiadiazole ring of BTD was opened by treating **36** with sodium borohydrate. The resulting 3,6-dibromo-1,2-diaminobenzene **68** was partially unstable, thus, subsequent condensation with a diketone was necessary. The resulting new aromatic core scaffold was a quinoxaline (**69**a-f). The versatility which could be introduced in this step was broad. A huge variety of diketones is commercially available. This provides many different 2,3-disubstituted quinoxaline units (see experimental part). Triple bond linker units were introduced by converting the 5,8-dibromo substituted quinoxaline via a *Sonogashira* reaction to the 5,8-dihexynyl substituted diols. The introduction of 5,8-dicarboxamide linker units (**71**), in analogy to the reported route for BTD, would be an interesting and rather simple alternative but wasn't tried yet.

A different approach to extend the study of this chapter was to replace one single atom in the basic BTD scaffold. Replacing sulfur by oxygen seems to be at first sight naive as the two elements often show comparable properties. However, several studies showed that in certain applications, differences between 2,1,3-benzothiadiazole (BTD) and 2,1,3-benzoxadiazole (BOD) existed. Some steps towards the successful synthesis of BOD-based new building blocks were already prepared (**Figure 55**).

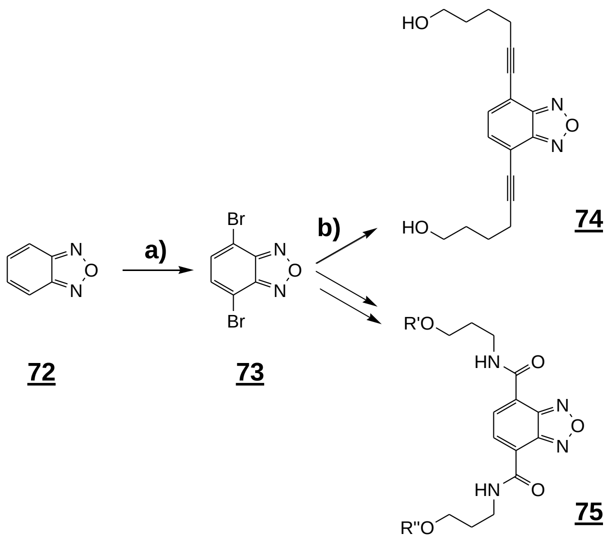

Figure 55. Synthetic route to 2,1,3-benzoxadiazole (BOD) based building blocks (details see experimental part). Reagents and conditions: (a) 2,1,3-benzoxadiazole **72**, Fe, Br_2, 90 °C, 2 hrs; (b) 5-hexyn-1-ol, Cu(I)I, bis(triphenylphosphine)palladium(II) dichloride, Et_3N, dioxane, 60 °C, 1 h. The preparation of **75** was not yet tried and is only presented as an alternative.

3.5 Energy transfer in a pyrene stack – Quenching of the pyrene excimer by **W**

The topic of light-harvesting antennas based on DNA-assembled phenanthrene and pyrene units showed remarkable and interesting features (chapter 3.1 – 3.3). Energy transfer along the π-arrays reached by this approach was different from previous architectures. Nevertheless, certain drawbacks were still present. Light absorption at 320 nm was rather in the near UV region of the electromagnetic spectrum. Sunlight has its highest intensity between 390 nm and 750 nm in the visible region of the electromagnetic spectrum. The maximum intensity is at approximately 500 nm. Thus, a system which works at 320 nm is not perfectly aligned and optimized for the use as “Sunlight-harvester”.

The design of the hybrids in chapter 3.1 – 3.3 was based on phenanthrene units as light absorbers (at 320 nm) and the phenanthrene-pyrene exciplex as reporter (fluorescence emission at 450 nm). The absorbance maxima of absorber units and the reporter unit were separated by approximately 40 nm. The exciplex between **S** and **P** represented a special case. To find a similar exciplex with two new chromophores could easily lead to highly extended studies. The two new chromophores would have to match the described properties, especially red-shifted absorption and fluorescence emission compared to the **SP**-exciplex was crucial. A more straight forward approach was to replace **P** as absorber in the core segment by the former reporter unit (pyrene **S**). The newly synthesized **W** unit built the new reporter unit. The strong electron accepting properties of **W** (see chapter 3.4) could have a beneficial effect on the energy transfer in the π-array. So far, only a few studies existed where pyrene in combination with BTD was used.[117]

The absorbance properties of the two units were in line with previously used building blocks. Pyrene **S** had a maximum absorbance around 360 nm and dihexynyl-BTD **W** around 400 nm. Thus, the combination of **S** and **W** also resulted in a red-shift of 40 nm (**Figure 56**a). The blue line at the bottom (**Figure 56**a) represented the absorbance spectrum of hybrids from the previous chapters (3.1 – 3.3) whereas the green line predicted the spectrum of a new hybrid from this chapter. The red-shift is obvious. In comparison to phenanthrene as light harvesting units, certain disadvantages in the use of pyrene were expected. Phenanthrene did not show the tendency to form excimers (chapter 3.1). There are only a few examples of phenanthrene excimers in the literature.[98] Retrospectively, this fact was a big advantage for the systems in chapter 3.1 – 3.3. Relaxation of an excited **P** unit to the ground state by monomer emission (between 380 nm and 410 nm) was, from the energetic point of view, of a higher level than exciplex emission. Formation of an exciplex stabilized the excited states of the two partners in the excited complex and relaxation to the ground states by fluorescence emission took place from a lower energy level (450 nm, **Figure 56**b). An even higher stabilization takes place when an excimer was formed. When the pyrene excimer relaxed back to the ground state, fluorescence emission at 500 nm was observed. This revealed that the excimer was even stronger stabilized and was lying at a lower energy level compared to the pyrene-phenanthrene exciplex (**Figure 56**b). The red-shift of the fluorescence emission from monomer to exciplex and excimer is a measure of the stabilization in the excited states. A simplified picture is drawn which shows the problem of using pyrene in the antenna part (**Figure 56**c). The exciplex in chapter 3.1 and 3.2 acted as energy trap. A stabilized situation was reached when the excited **P** unit formed an exciplex with **S**. It was concluded that excitation was transported to the point of lowest energy (**Figure 56**c top). The replacement of **P** units by **S** units proposes the formation of excimers in the antenna part and, thus, a potential stabilization of the excited states. Whatever is placed at the end of the **S**-array cannot further stabilize the excited states in comparison to the potential excimers. The excimers in the antenna part can act as energy traps (sicks) which would decrease the transfer efficiency.

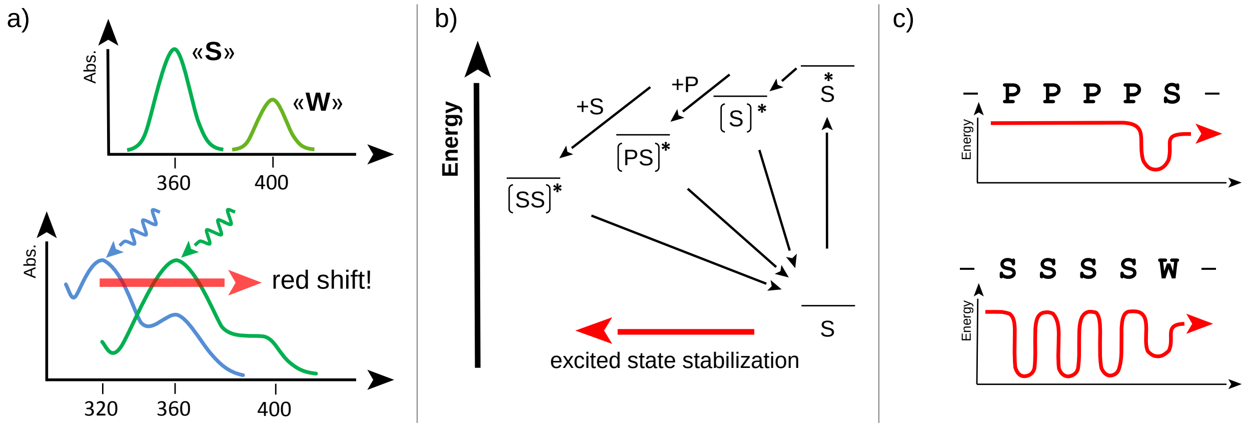

Figure 56. (a) Lowest energy absorbance of pyrene **S** and dihexynyl-BTD **W** (top) and the expected red-shift of the excitation wavelength (bottom). The blue line represents the absorbance spectrum of previous hybrids, the green line stands for new hybrids with **S** and **W**. (b) Arbitrary energy diagram where **S** is excited to **S*** and relaxes back to the ground state via different routes: monomer emission, exciplex formation in the presence of a **P** unit and excimer formation in the presence of a second **S** unit. The higher stabilization in the different intermediate states is in the order excimer > exciplex > monomer. (c) **PS**-exciplex formation trapped excitation energy from **P** in antenna hybrids (top). **S** units can form excimers in the antenna part. Thus, energy traps are generated which can lower the transfer efficiency (bottom).

3.5.1 System design

The system design was kept perfectly constant in terms of flanking DNA segments and core segment. The phenanthrene units (**P**) from the former design in chapter 3.1 – 3.3 were replaced by pyrene units (**S**) and the pyrene unit from the former design was replaced by a BTD unit (**W**) (**Figure 57**). In previous chapters the relevant properties were most significantly seen in hybrids with four light absorbing units (e.g. hybrid **21*****22**, **29*****30** and **29*****35**). Two units were often not enough to see the desired effects whereas hybrids with eight units did not further change the results compared to hybrids with four units. It was decided to synthesize three new hybrids, one hybrid with an AT base pair next to the core segment and one hybrid with the GC base pair in this position. As a control, one hybrid without the reporter unit **W** was synthesized. All three hybrids had four **S** units in the core segment, two in each strand. Also in these hybrids, the abasic site analogue φ was introduced to keep the length of the strand constant and to reduce positional isomers of **W** (**Figure 57**).

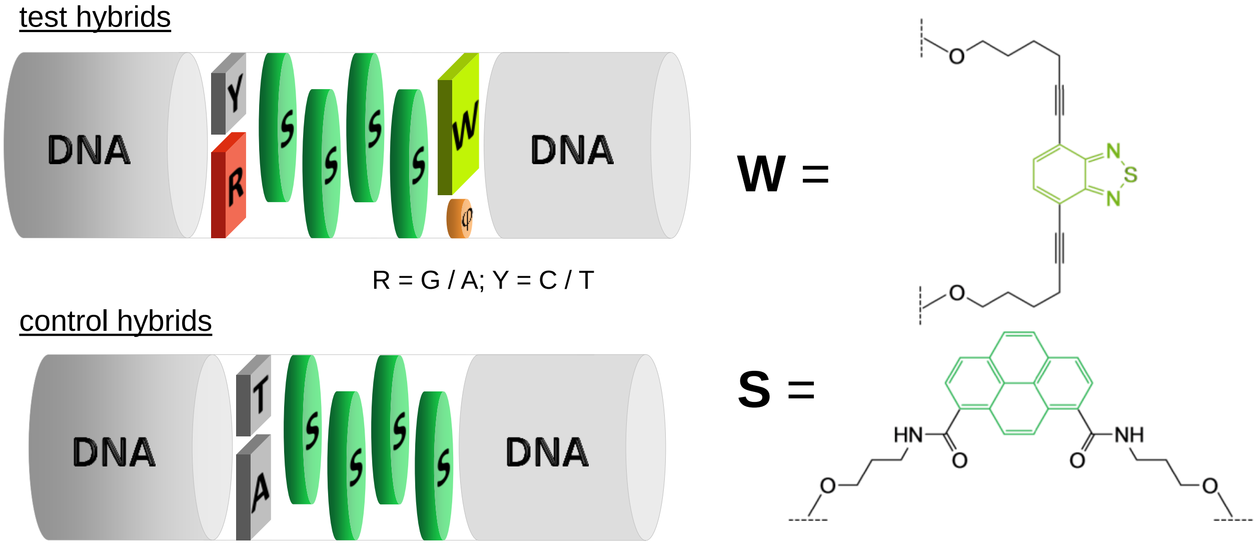

Figure 57. System design with pyrene units **S** and the dihexynyl-BTD unit **W** in the core segment. Next to the core, an AT or a GC base pair was placed. In the control hybrid the **W***φ pair was omitted.

3.5.2 Spectroscopic investigation and discussion

The melting temperature (Tm) values were measured (**Table 12**). They did not show any anomalies compared to the values of hybrids from chapters 3.1 to 3.3. They were in the expected range. The replacement of the AT base pair in hybrid **76*77** by a GC base pair stabilized hybrid **78*79** by 4.0 °C. This was in analogy to the previously found stabilization of a GC base pair.

Table 12. Oligonucleotides **76** – **81**, hybrids and the corresponding Tm values

Nr.	*Sequence*	*ε value (260 nm)*	*Mass [g/mol]*	*Tm [°C]*[a]
76	5'- TAA TAA TAA ATA **S S W** ATA AAT AAT AAT	354125	8706.3	36.0
77	3'- ATT ATT ATT TAT **S S**φ TAT TTA TTA TTA	283600	8423.3	
78	5'- TAA TAA TAA ATC **S S W** ATA AAT AAT AAT	346225	8681.9	40.0
79	3'- ATT ATT ATT TAG **S S**φ TAT TTA TTA TTA	286300	8450.1	
80	5'- TAA TAA TAA ATA **S S** ATA AAT AAT AAT	334000	8315.8	38.0
81	3'- ATT ATT ATT TAT **S S** TAT TTA TTA TTA	283600	8243.7	

[a] 1 μM DNA double strand (2 μM total oligonucleotide concentration), 100 mM sodium chloride, 10 mM sodium phosphate buffer at pH 7.0

The absorption profiles of the three hybrids were recorded (**Figure 58**). Two important regions were present, the DNA region between 300 nm and 220 nm and the chromophore region between 500 nm and 300 nm. The chromophore region seemed to be less interesting in these hybrids compared to the UV/VIS spectra from chapter 3.1 – 3.3. Only one significant absorbance maximum was found. The second view revealed that hybrid **76*77** and **78*79** had a very slight shoulder between 390 nm and 460 nm compared to hybrid **80***81 which lacked this feature. This shoulder was attributed to the presence of **W** in the two mentioned hybrids. The broad and structureless absorbance band centered at 355 nm was attributed to the **S** units. A marginal difference in the absorbance intensity was found between **76***77 and the two other hybrids **78***79 and **80***81. The **W** unit had a very low absorptivity compared to the four **S** units. The UV/VIS specta showed that selective excitation of **W** might be difficult. A selective excitation at wavelength longer than 420 nm could be possible. Nevertheless the small ε-value at this wavelength might cause difficulties in the detection limit of fluorescence. It was decided that the fluorescence emission after excitation at 355 nm was measured to get a first feeling for the properties.

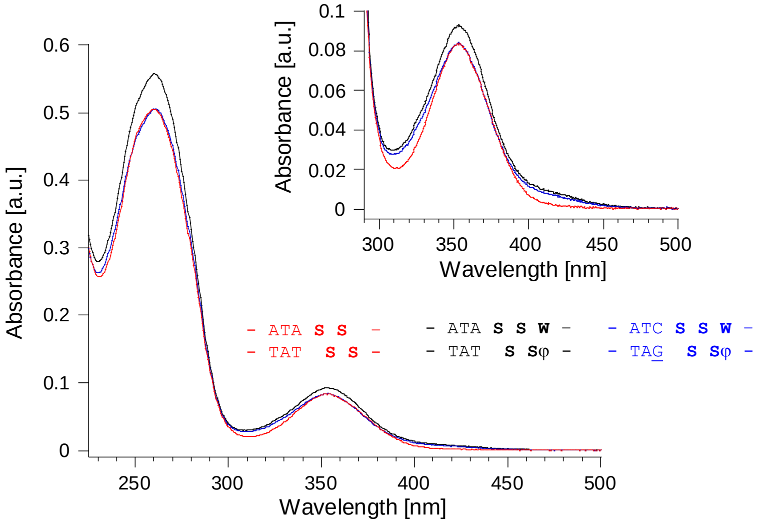

Figure 58. UV/VIS absorbance profiles of hybrids **76*77**, **78*79** and **80*81**. The inset showed the enlarged region of the chromophores.

The investigation of the first single strands in chapter 3.1 showed that phenanthrene units in close proximity to pyrene units formed an exciplex and that this fluorescent species was the actual reporter signal for the antenna system. The exciplex reported the interaction between the antenna part (the **P** units) and the reporter unit **S**. The records of the emission spectra of the first two single strands **76** and **77** from chapter 3.5 therefore quickly revealed which spectroscopic response had to be followed in this chapter.

The first important results in this chapter were found when **76** and **77** were investigated. Single strand **77** included two **S** units in the sequence and had two distinct emission bands, one centered at 400 nm and the second, slightly more intense and broader, centered at 500 nm (**Figure 59**a, blue line). From chapter 3.3 it was known that these two bands corresponded to pyrene monomer (400 nm) and pyrene excimer (500 nm) fluorescence emission. Single strand **76** (**Figure 59**a, black line) on the other hand had a highly quenched emission spectrum compared to single strand **77**. The most significant difference, besides the different base next to the **S** units, was the presence of **W** in the sequence. No signs of a new fluorescent species were seen which revealed, as a first benchmark, that a fluorescent exciplex between **S** and **W** was not present. The spectroscopic response which had to be followed in chapter 3.4 was rather the high quenching effect of **W** on the **S**-excimer and **S**-monomer emission. Hybridization of the two single strands to form hybrid **76*****77** gave the second interesting and important result in this chapter (**Figure 59**a, red line). The emission intensity of hybrid **76*****77** after excitation at 355 nm was slightly increased compared to single strand **76** alone, overall the emission was highly quenched compared to single strand **77**. The absorbance spectrum (**Figure 51**, chapter 3.4) indicated that the **W** unit had at 350 nm a minimum absorbance band. It was expected that excitation of **S** at 355 nm let to a marginal emission from **W**. The combination of **76** and **77** to hybrid **76*****77** influenced the excimer formation in both strands and a strong interstrand interaction was expected.

The introduction of a GC base pair next to the core segment in hybrids from chapter 3.2 resulted in a constant reduction of the exciplex emission after excitation of the antenna part. The DNA base guanine (G) acted as excitation energy trap. A similar effect was expected in hybrid **78*****79**. This hybrid only differed from hybrid **76*****77** in the base pair next to the core segment. Single strand **79** where the pyrene excimer was next to G had a slightly less intense emission curve (**Figure 59**b, blue line) compared to single strand **77**. The quenching effect of the **W** unit on the pyrene excimer emission was as well present (single strand **78**). The emission intensity of hybrid **78*****79** was decreased by 40 % compared to **76*****77**. This decrease was slightly more severe than between hybrid **21*****22** and **29*****30** in chapter 3.2 (27 %).

The control hybrid **80*****81** was tested in the same way. The two single strands **80** and **81** showed almost superimposable emission curves and only differed in the pyrene monomer emission intensities. Hybrid **80*****81** had a very broad pyrene excimer emission band and pyrene monomer emission almost disappeared (**Figure 59**c).

The interesting comparison between the two hybrids with the **W** unit (**76*****77** and **78*****79**) and the control hybrid **80*****81** was made (**Figure 59**d). An impressive decrease of the excimer band at 500 nm was found in the two hybrids where **W** was introduced compared to the control hybrid. Of course, the GC base pair in **78*****79** caused an even higher decrease. Overall the effect of **W** was impressive. Hybrid **76*****77** showed an excimer emission intensity which was reduced by approximately 92 % compared to **80*****81** (**Table 13**). The introduction of a single building block had such a severe influence on the pyrene excimer emission. Nevertheless, concerning the energy transfer efficiency certain drawbacks were found. It was mentioned before that the important spectroscopic response was the quenching effect of **W** on the pyrene excimer emission. Hence, it was concluded that the remaining amount of pyrene excimer emission in hybrid **76*****77** and **78*****79** was the percentage of inefficient energy transfer to the reporter unit (see later).

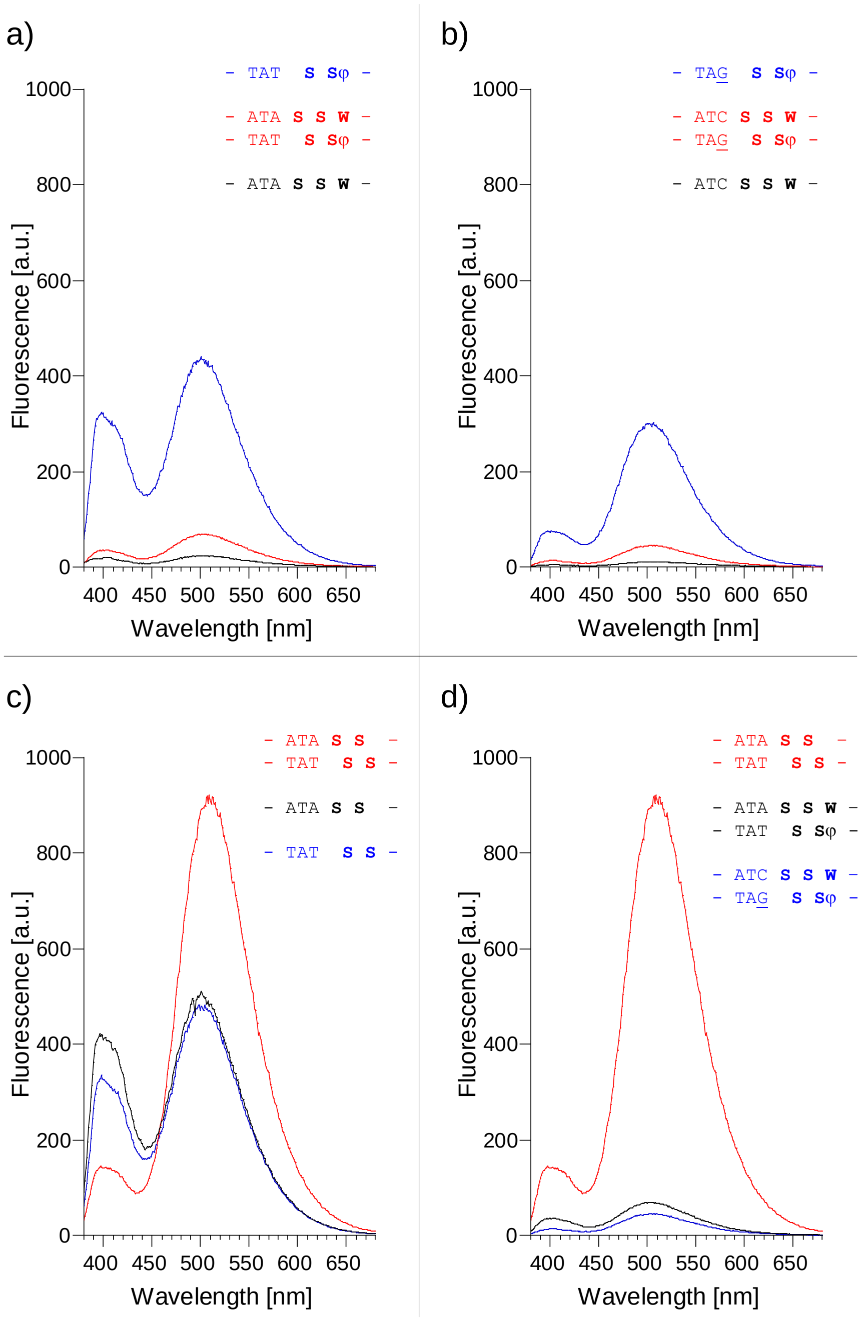

Figure 59. Fluorescence emission spectra of all single strands and the corresponding hybrids from chapter 3.5 (after excitation at 355 nm). (a) Set from hybrid **76*77**. (b) Set from hybrid **78*79**. (c) Set from hybrid **80*81**. (d) Summary of the emission properties from the three new hybrids.

The actual interaction between **S** and **W** could not be further analyzed with the used equipment. Generally an exciplex formation could be cautiously stated. Exciplex formation does not necessarily imply fluorescence emission. An exciplex is in principle a charge transfer complex in which the polarity between the partners is different.[68] A strong charge transfer state stands for a strongly polar exciplex with almost located charges whereas weak polarization within the excited complex stands for a certain delocalization and a weak polarization. Exciplexes with weak polarization are also called 'excimer-like' exciplexes.[70, 71] The dynamics within the complex also influence the decay pathway.[72, 131]

Table 13. Spectroscopic properties of hybrid **76*77**, **78*79** and **80*81**

	80*81	***76*77***	***78*79***
a.u.c (excitation at 355 nm)	92482.0	8434.5	5028.2
relative quantum yield (a.u.c·/ Abs.)	$11.1\cdot10^5$	$0.9\cdot10^5$	$0.6\cdot10^5$
rel.quantum yield per **S** unit	$27.9\cdot10^4$	$2.3\cdot10^4$	$1.5\cdot10^4$
total quenching efficiency [%]	-	91.8	94.6
Em. Intensity at 500 nm	921.6	69.6	45.5
Quenching efficiency [%]	-	92.3	95.0

First of all a reason for the strong quenching of pyrene excimer emission in the presence of **W** had to be found. From previous studies it was well known that pyrene excimer emission of two units in a DNA strand could be quenched by the placement of two perylenebisimide (PDI) units in the counter strand next to them (**Figure 60**a).[61, 64, 132] Spectroscopic analysis revealed an interaction between the two PDI units and the two pyrene units. Insertion of the two PDI units between the two pyrene units was stated which suggested a 'mechanical' quenching of the excimer emission. Hybrids **76*77** and **78*79** placed the **W** unit on top of an **S**-stack. Therefore, 'mechanical' quenching was no longer possible (**Figure 60**b).

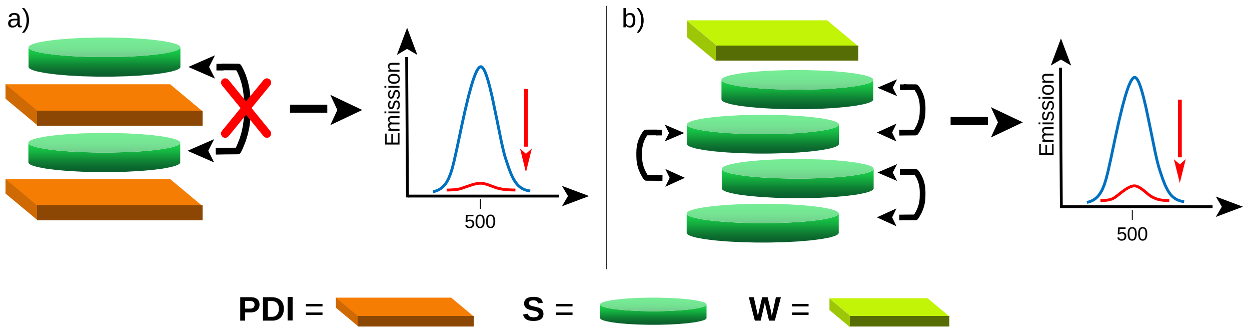

Figure 60. (a) The architecture prohibited excimer formation by insertion of two PDI units between two pyrene units. The strong pyrene excimer emission (blue line) in the absence of PDI was strongly quenched in the presence (red line) of PDI. (b) Pyrene excimer formation was in principle allowed by the architecture as **W** was on top of the stack and no disruption took place. Nevertheless excimer emission was highly quenched in the presence of **W** (red line) compared to examples where **W** was missing (blue line).

The strong quenching effect of the pyrene excimer fluorescence emission was performed with one single **W** unit against four **S** units. This was surprising. Only one **S** unit was interacting with the **W** unit and the three remaining **S** units could in principle freely form excimers. This fact made the result even more attractive. Based on all data from the last chapters and assuming that the excitation energy transfer between **S** units was comparable to the transfer between **P** units, a mechanism for the results in this chapter was postulated (**Figure 61**).

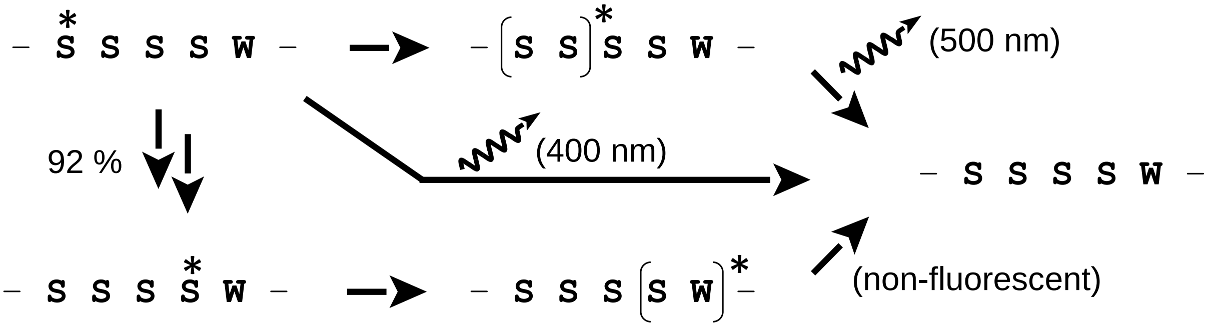

Figure 61. Postulated mechanism for the results in chapter 3.5. The interaction between **S** and **W** and the non-fluorescent relaxation was formulated like the exciplexes in the last chapters. 92 % of all excitation relaxed via this pathway. Exciplex formation does not necessarily need to be the case in this example but is the most straight forward explanation.

The excitation of pyrene **S** could take three main routes. First of all direct back relaxation to the ground state by monomer emission at 400 nm was observed. As explained in chapter 3.3 an excited **S** unit could interact with a second **S** unit in the ground state and form an excimer state. This second pathway relaxed back to the ground state by excimer emission at 500 nm. Obviously, more than one possibility existed for an excited **S** unit to from an excimer. After each excitation energy transfer step to the next **S** unit, a new possibility to form an excimer arose. Comparison of the emission spectrum of hybrid **80*81** and **76*77** revealed that a major part of the excitation energy in **S** units in hybrid **76*77** relaxed via a different route and did not form excimers. It was concluded, that excitation energy was transported to the **S** unit next to **W**. Here, an interaction between **S** and **W** took place. Whether this interaction was the formation of an exciplex or not was not yet experimentally proofed. However, this scenario could well be possible. Non-fluorescent relaxation to the ground state terminated the process.

In chapter 3.1 and 3.2 the analysis of the efficiency was rather difficult. The reporter and thus the spectroscopic response of energy transfer was the exciplex fluorescence emission. The linear increase of the emission intensity was a sign for a very efficient process. The possible side reactions like pyrene or phenanthrene monomer emission were not found or were covered by the intense and broad exciplex emission curve. Nevertheless other indications, like the linear increase of the emission intensities at 450 nm and 500 nm with the identical slope as the linear increase of the overall emission intensity (area under the curve), supported the very efficient energy transfer process from **P** to the **PS**-exciplex. In chapter 3.5 the energy transfer efficiency was less difficult to determine. The reporting spectroscopic response was the fluorescence quenching of the interaction between **S** and **W** (exciplex formation was cautiously proposed). Excitation energy which was not transported to the exciplex between **S** and **W** formed excimers. It was concluded that the emission at 500 nm was a sign of an inefficient process. Hybrid **76*77** was quenched by a ratio of 92 % compared to the control hybrid **80*81**. This suggested that 8 % of excitation were not transported to the exciplex. Still, 92 % efficiency was a very good value.

Figure 56 showed that the formation of an excimer stabilizes the excited complex between two molecules. Overall, only 8 % of the excited species were not transported to the exciplex between **S** and **W** and they relaxed beforehand via monomer of excimer emission. This fact could be another sign of a considerable amount of delocalization of the excitation energy over the whole π-array. **Figure 62** summarizes the results from chapter 3.5.

3.5.3 Summary

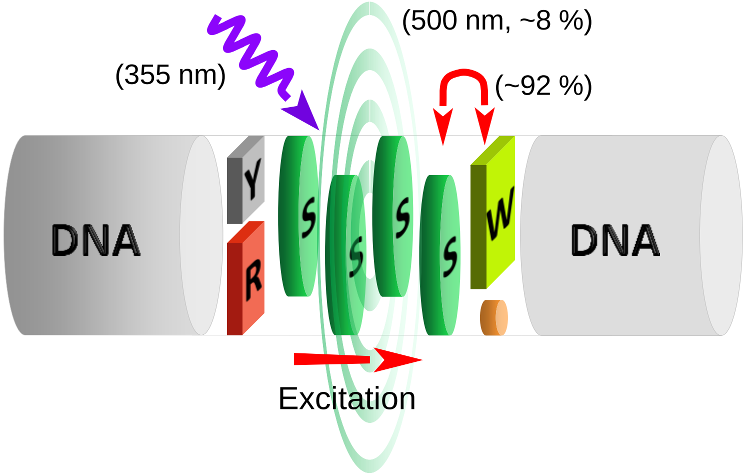

Figure 62. Summary of the findings in chapter 3.5. After excitation of the pyrene units at 355 nm the excitation energy was transferred via the π-stack to the **S** unit next to **W**. The interaction between **W** and **S** let to a non-fluorescent relaxation to the ground states.

In conclusion, a second system for light harvesting was constructed and described. In comparison to the previous system, where light was absorbed by phenanthrene units and the energy was transported to a phenanthrene-pyrene exciplex, light absorption was performed by pyrene units and the excitation energy was transported to a pyrene-dihexynyl BTD exciplex. Relaxation and energy conversion was non-fluorescent. Because of the beneficial excimer formation in the antenna part, energy transfer to the exciplex was less efficient compared to the previous design in chapter 3.1 and 3.2.

4. Summary

The thesis was separated into two main parts. In the first section, fundamental aspects of the light harvesting and energy transferring properties of DNA-assembled phenanthrene (**P**) stacks were investigated and studied in details (**Figure 63** and **Figure 64**). It was found that absorption of light at 320 nm let to a unidirectional energy transfer towards a phenanthrene-pyrene exciplex. The exciplex converted the absorbed energy to light which was emitted at 450 nm. The fluorescence emission intensity of this **PS**-exciplex increased linearly by increasing the number of introduced **P** units. No signs of inefficiency in the energy transfer steps were found based on the used techniques. The fluorescence emission spectra lacked phenanthrene as well as pyrene monomer emission signals (chapter 3.1). The study was extended and the influence of a second energy-converting channel was studied. A GC base pair next to the core segment was introduced to challenge the central position of the exciplex as main energy acceptor. The fluorescence emission spectra revealed that the energy of one **P** unit was trapped by guanine. The excitation energy of all other **P** units was still transported to the **PS**-exciplex (chapter 3.2). This supported the findings of a previous study where the inner units in an extended pyrene array were insultated from DNA bases by the outer neighbors.

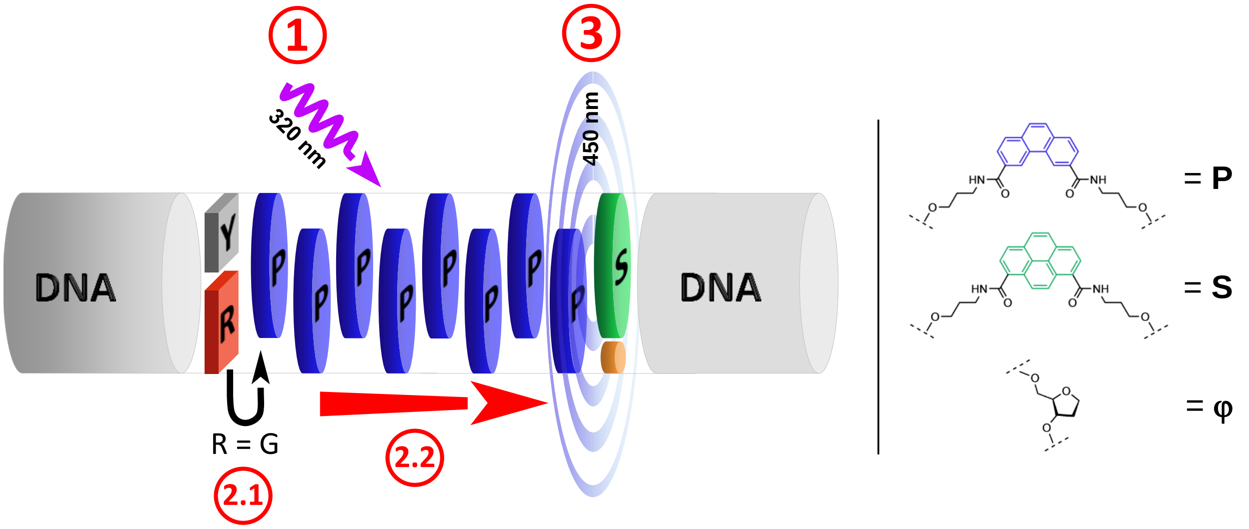

Figure 63. Excitation energy transfer in a phenanthrene (**P**) stack. (1) Excitation of up to eight **P** units at 320 nm, (2.1) in the presence of guanine (G) the excitation of one **P** unit was quenched, (2.2) excitation energy transfer via the π-array, (3) formation of a **PS**-exciplex and relaxation by fluorescence emission at 450 nm.

In the course of this study the question arose whether the excitation energy was completely trapped by the exciplex or if it was possible to further propagate it to another acceptor. The background of this question built the formulation of a mechanism where the excited state was transported from **S** to **P** and further on to the other end of the **P** stack. It was found that indeed a delocalization of the excitation energy between **P** and **S** was present. Formation of a pyrene excimer species after excitation at 320 nm was highly increased in the presence of **P** units (chapter 3.3).

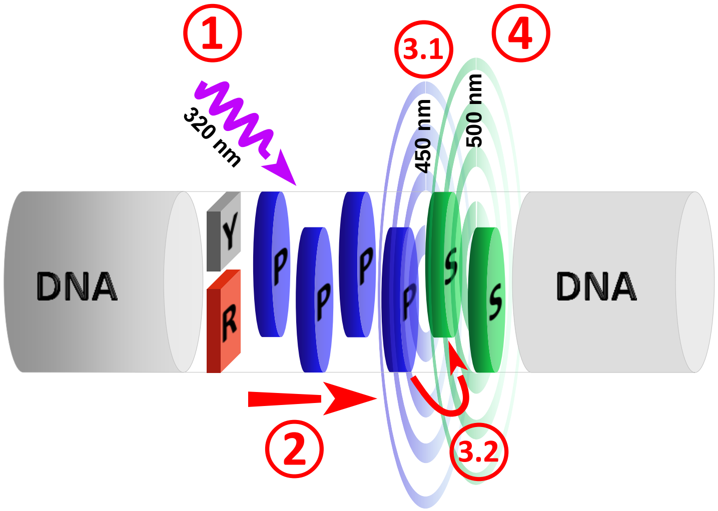

Figure 64. Probing the delocalization of the excited state between phenanthrene (**P**) and pyrene (**S**). (1) Excitation at 320 nm of up to four **P** units, (2) excitation energy transfer via the π-array, (3.1) exciplex formation between an excited **P** and **S** and fluorescence emission at 450 nm, (3.2) excitation transfer from **P** to **S**, (4) excimer formation between an excited **S** and a second **S** unit and relaxation by fluorescence emission at 500 nm.

The second section of the thesis dealt with the expansion of the system (**Figure 65** and **Figure 66**). The question was whether other chromophores could do the same job as phenanthrene and pyrene did. As a superior goal the use of pyrene units as light absorbing and energy transferring array was envisioned. First new chromophores were needed to red-shift the absorbance spectrum of the hybrids. 2,1,3-Benzothiadiazole (BTD) molecules proposed an ideal new unit for this purpose. 4,7-Dihexynyl BTD (**W**) and 4,7-dicarboxamide BTD (**V**) were synthesized and analyzed before and after incorporation into DNA oligonucleotides. They showed interesting and particular fluorescence emission properties in different environments. In addition, the high DNA hybrid stabilization effect of two opposing BTD units was exceptional (chapter 3.4).

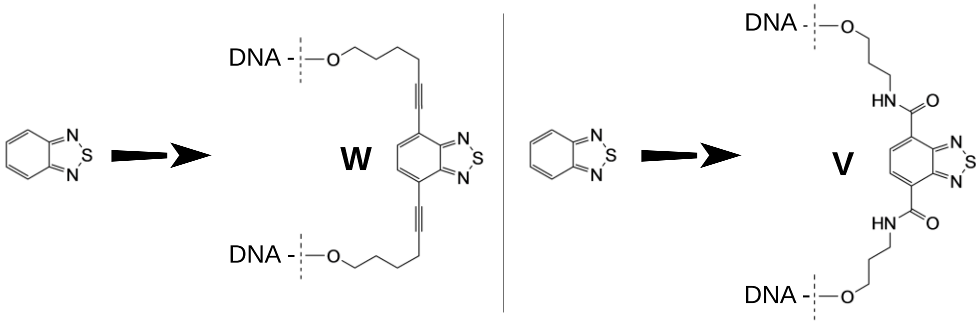

Figure 65. The introduced 4,7-dihexynyl BTD (**W**) and 4,7-dicarboxamide BTD (**V**) building blocks.

In the last chapter the combination of the two sections was undertaken. Even if the excited state interactions between **W** and **S** were not described before, a clear effect was seen. A high fluorescence emission quenching of **W** on **S** was found. As a consequence hybrids with four **S** units and one **W** unit on one end of the stack showed highly quenched pyrene excimer emission curves. This efficient fluorescence quenching was ascribed to the energy transfer from **S** to the excited state complex between **S** and **W** (chapter 3.5).

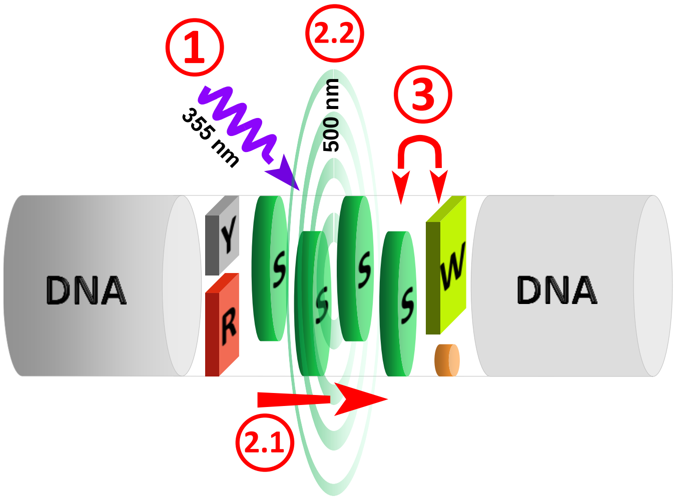

Figure 66. Excitation energy transfer in a pyrene (**S**) stack. (1) Excitation at 355 nm, (2.1) excitation energy transfer via the π-array, (2.2) partial loss of transfer efficiency by excimer formation between **S** units, (3) formation of a non-fluorescent state between **S** and 4,7-dihexynyl BTD (**W**).

5. Outlook and Conclusion

Besides the substantial amount of knowledge about ‘outer shell’ – properties (structure and shape) of extended π-arrays built with non-nucleosidic aromatic building blocks, an additional data point dealing with ‘inner shell’ – phenomena (transfer) was generated. In chapter 3 it was possible to show that extended arrays of phenanthrene building blocks were able to act as light harvesting entity and to transfer energy to a defined position. The described DNA-based antenns are particularly interesting because of several reasons. (**1**) The system combines light harvesting and energy transfer which is important and of current interest, not only because of potential applications as source for energy production but also as additional mimic of natural photosynthesis. (**2**) The very high efficiency of energy transfer reached wih this inicial study is promsising and can be well compared to the top excamples of the field. (**3**) The general DNA approach gives rise to the preparation of higher ordered structures and thus to extended functions and properties. (**4**) The synthesis of the oligomers is fast and no time-consuming and demanding steps are required. The characterization is clear and no misleading or wrong conclusions are possible. (**5**) The non-nucleosidic aromatic building blocks are ready-to-use within several synthetic steps. The availability of similar building blocks is broad and extendable as has been shown in chapter 3.4. (**6**) The approach with its basic and simple design is unique. Chapter 3.5 showed that also other units in the light absorbing part were able to do the job. Thus, further expansion of the system to other chromophores is likely to be possible. Nevertheless, some aspects and results remained untouched and additional studies are required to understand them. (**1**) The time-resolved analysis of the light absorption, energy transfer and light emission in the core segment of the hybrids is crucial and needs to be analyzed. This would answer many questions: What time frame is required for the individual steps? Is the system as efficient as steady-state spectroscopy revealed? Are there differences in the dynamics of the process when the number of **P** units is changed? (**2**) The study of **W** and **V** as fluorophores and especially the interaction between each other remained on a preliminary stage. Further analysis is also required here. (**3**) The analysis of the high quenching effect of **W** on the excimer and monomer of **S** was not extended.

In the following, some ideas are given on how the topic could be advanced. The list of potential new studies is by far not complete. Numerous other attempts are possible. One can define four major areas where potential additional tasks could start: (**1**) Further study of the basic design, (**2**) expansion of the basic design, (**3**) expansion of global system and (**4**) applications of the global system.

(**1**) Further study of the basic design

The basic design remains constant as introduced in chapter 3.1. The core segment is still built out of the light absorbing **P** units and the energy collecting phenanthrene-pyrene exciplex. The difference is made by the introduction of DNA base pairs in the energy collecting **P**-stack which is afterwards separated into two equal sections. The question is whether this break is virtually a barrier that prevents excitation energy to move to the exciplex or if the passage to the exciplex is not disturbed by the additional base pair. Irrespective of the outcome, this study might answer some interesting questions. From DNA charge transfer studies it is known that electrons can move across AT tracts in DNA hybrids. Is this as well possible for excitation in **P**-stacks? This study could give additional information about the interplay between the **P** units (**Figure 6**).

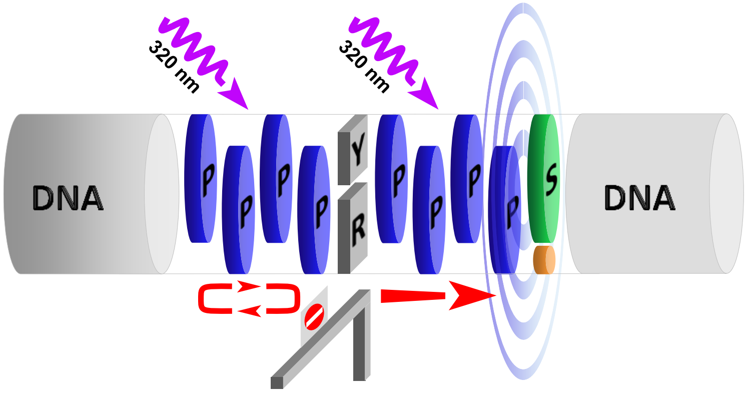

Figure 67. Breaking the phenanthrene stack. What will be the consequences of the insertion of a break in the middle of the light harvesting and energy transferring **P**-stack? Does a DNA base pair act as a barrier? Is the excitation energy on one side lost?

(**2**) Expansion of the basic design

The basic design is kept constant. The cascade introduced in chapter 3.1 is light absorption, energy transfer to the exciplex followed by fluorescence emission. The task is to expand this three-step-cascade by an additional step. To prove that the collected energy and the amplified fluorescence emission can be used for additional reactions, a first trial would be to introduce a FRET acceptor as end-group of the DNA hybrid (see the introduction 1.4 the example from *Kool*). The collected energy represented in the intense fluorescence emission of the exciplex would thus be used to excite a FRET acceptor (**Figure 68**).

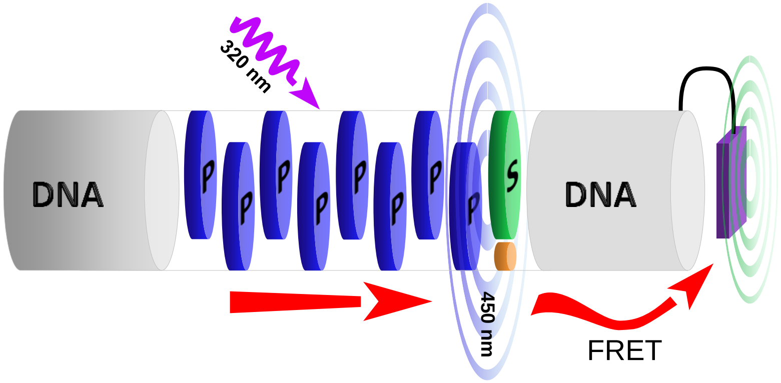

Figure 68. Introduction of a FRET acceptor into the DNA hybrid. In the hybrids described in this thesis the collected energy from the **P**-stack is 'lost' by fluorescence emission. The idea is to further use the generated light by exciting a FRET-acceptor. This would make an additional step in the cascade.

(**3**) Expansion of the global system

Chapter 3.4 and 3.5 dealt with the idea of extending the study to other chromophores and different combinations in the light collecting segment of the core. One straight forward approach is to use the two building blocks introduced in chapter 3.4 and to synthesize an antenna with **W** units as light absorbers and a **V** unit in the collection center. Not only the advantage of having a first system which is excitable in the visible region of light but also the fact that BTD units are often used in photovoltaic systems makes this purpose interesting (**Figure 69**).

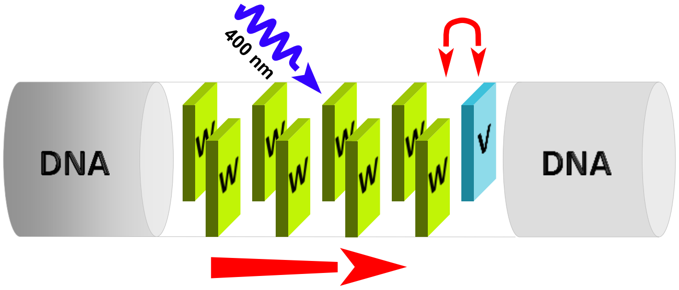

Figure 69. Light harvesting by **W** and collection in the **WV** excited complex. Even if the interaction between **W** and **V** was not fully understood and was not fluorescent, this setup could cause impressive results. In addition excitation in the visible region of light would be possible.

(**4**) Applications of the global system

The three proposals before are mainly direct consequences of the results summarized in this thesis. There are no major uncertainties concerning feasibility, complexity and outcome of these studies. The last proposal on the other hand is highly speculative. The goal is to prepare a supramolecular assembly with a metal complex in the center. The ligands of this metal complex are chimeric. They contain the direct ligand of the metal ion as well as an antenna unit. DNA is entirely discarded from this approach (**Figure 70**).

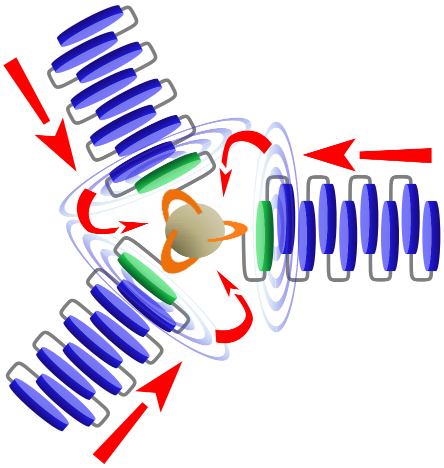

Figure 70. Light harvesting metal complex. The antennas are used as ligand of a metal complex (sphere in the middle). The ligand could be phenathroline units. A FRET mechanism would take place.

6. Experimental Part

Table 14. Abbreviations in the experimental part

Solvents		***Salts***	
Dichloromethan	DCM	Aluminum trichloride	$AlCl_3$
Diethylether	Et_2O	Ammonium chloride	NH_4Cl
Ethanol	EtOH	Iron trichloride	$FeCl_3$
Ethyl acetate	EA	Magnesium sulfate	$MgSO_4$
Hexane	hex	Sodium carbonate	Na_2CO_3
Methanol	MeOH	Sodium chloride	NaCl
N,*N*-dimethylformamide	DMF	Sodium hydrogencarbonate	$NaHCO_3$
Reagents		***Other***	
Hydrochloric acid	HCl	Hours	hrs.
O-(benzotriazol-1-yl)-*N*,*N*,*N'*,*N'*-tetramethyluroniumhexafluoro-phosphate	HBTU	minutes	min.
Sodium hypochlorite	NaOCl	room temperature	RT
Triethylamine	Et_3N	Saturated solution in water	sat.
4,4'-dimethoxytriphenylmethyl chloride	DMT-Cl		

5.1 General information

Organic reactions. Chemicals for the organic reactions were of the highest available quality (95-99 % purity) from different suppliers (mainly AlfaAeasar, Sigma-Aldrich, Acros and TCI). Dry solvents from the solvent drying line (Leumann group) were used for normal organic reactions. Silica from Sigma-Aldrich and distilled technical solvents were used for column chromatography.

Oligonucleotide synthesis. The natural nucleotide phosphoramidite building blocks were purchased from SAFC® Proligo® (Hamburg, Germany). The abasic site analogue φ phosphoramidite building block was purchased from Glen Research® (Virginia, USA). All modified oligonucleotides were synthesized on an Applied Biosystems 394-DNA/RNA synthesizer using standard synthetic procedure ('trityl-off' mode). All chemicals and solvents for the DNA synthesis were purchased from SAFC® Proligo®. CPG solid supports (controlled pore glass, modified with the corresponding first DNA base) were from Glen Research®. The coupling time for the artificial building blocks was elongated to two minutes. The coupling yields for all building blocks per single step were between 90 % and 99 % ('trityl assay'). Cleavage from the solid support and final deprotection was done by treatment of the CPG-oligonucleotide with 30% NH_4OH solution at 55 °C for 2 hours. All oligonucleotides were purified on a Shimadzu AT-10 HPLC (LiChrospher 100 RP-18, 5 μm column from Merck; eluent A = TEAAc buffer (Et_3N/HOAc 0.1

M, pH 7.0), eluent B = 80 % MeCN, 20 % TEAAc buffer) with an eluatation time of 20 minutes (different gardients between 10 -35 % solvent B concentration). Fully natural oligonucleotides were purchased from *Microsynth* (Balgach, Switzerland).

5.2 Analysis

NMR experiments were performed on a *Bruker Avance 300*. Accurate mass determination experiments were performed on an *LTQ Orbitrap XL* with nanospray ionization (NSI) in the positive mode

LC–MS experiments with oligonucleotides were performed on a Shimadzu LC-20AT high performance liquid chromatograph (equipped with a Waters XTerra® MS C18 3.5 μm 2.1x100 mm column; the eluent was A = 50 mM ammonium formate and B = acetonitrile LC-MS Chromasolv® from Sigma-Aldrich, the gradient was 0-50 % B over 10 min) coupled to a Shimadzu SPD-M20A UV/VIS photodiode array detector (PDA) and a Shimadzu LCMS-2010EV. All LC-MS data were analyzed with Shimadzu LCMSsolutions software.

The ε-values for oligonucleotide concentration determination at 260 nm were: dA = 15300 $M^{-1}cm^{-1}$, dG = 11700 $M^{-1}cm^{-1}$, dC = 7400 $M^{-1}cm^{-1}$, T = 9000 $M^{-1}cm^{-1}$, **S** = 8600 $M^{-1}cm^{-1}$, **P** = 26900 $M^{-1}cm^{-1}$, **W** = 20125 $M^{-1}cm^{-1}$, **V** = 9146 $M^{-1}cm^{-1}$.

All experiments with oligonucleotides were carried out in 100 mM aqueous sodium chloride and 10 mM sodium phosphate buffer at pH 7.0. UV/VIS absorbance and UV/VIS-assisted thermal denaturation experiments were carried out on a *Varian Cary-100* Bio-UV/VIS spectrophotometer equipped with a *Varian Cary* block temperature controller and all data were collected with *Varian* WinUV software. Melting temperature values (Tm) were determined from the 1st derivative of the second cooling ramp (cooling-heating-cooling cycles in the temperature range of 10-90°C, temperature gradient of 0.5 °C/min, optic path length of 10 mm). Fluorescence data were collected on a *Varian Cary Eclipse* fluorescence spectrophotometer using quartz cuvettes. *Varian Eclipse* software was used to investigate the fluorescence. The cyclic volrammetry experiments were carried out on a *Metrohm* 663 VA Stand with a PGStat 20 (Decurtins group). The scan speed was 100 mV/sec in acetonitrile with 0.1 M tetrabutylammonium hexafluorophosphate. All collected data were plotted and analysed using *KaleidaGraph* (*Synergy* Software). Molecular modelling was done with *HyperChem* (Hypercube Inc.) in the *Amber* force field.

5.3 Synthetic procedures

Compound **2**

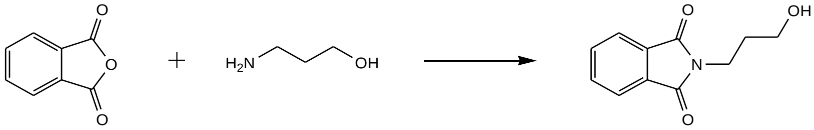

Phthalic anhydride (20 g, 135 mmol) and 3-hydroxypropylamine **1** (10.32 ml, 135 mmol) were mixed in a flask and heated to 140 °C. The reaction mixture was stirred at that temperature for 1 hour and then cooled down to RT. Compound **2** was pure enough to be further used. ^{1}H NMR (300 MHz, $CDCl_3$): δ 7.94-7.68 (m, 4 H), 3.91-3.81 (m, 2 H), 3.62 (t, J = 5.77 Hz, 2 H), 2.90-2.30 (s br, 1 H), 1.95-1.83 (m, 2 H).

Compound **3**

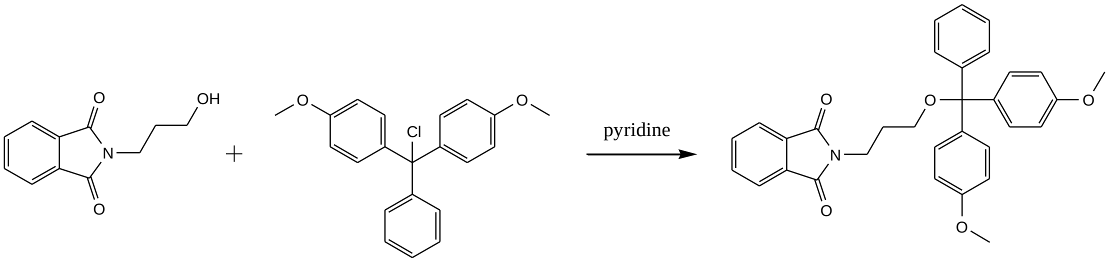

Compound **2** (10 g, 48.7 mmol) and DMT-Cl (17.3 g, 51.1 mmol) were dissolved in dry pyridine (100 ml) and stirred at RT overnight. The reaction mixture was diluted with EA:Hex (200 ml 1:1) and was washed with twice 10% aqueous citric acid and once with sat. aqueous $NaHCO_3$. The organic layer was dried over $MgSO_4$ and was evaporated under reduced pressure. The crude product was stored in the fridge overnight. The residue was then suspended in hexane. Compound **3** was filtered off as yellowish solid (21.7 g, 87 %). ^{1}H NMR (300 MHz, $CDCl_3$): δ 7.84-7.67 (m, 4 H), 7.43-7-13 (m, 9 H), 6.82-6.74 (m, 4H), 3.84-3.74 (m, 8 H), 3.15 (t, J = 6.02 Hz, 2 H), 2.06-1.93 (m, 2 H).

Compound **4**

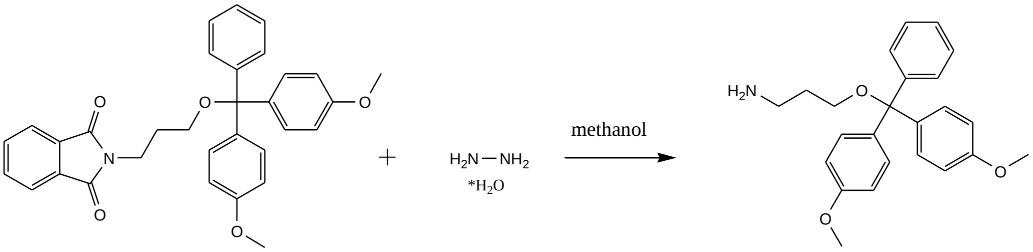

Compound **3** (15 g, 29.5 mmol) was dissolved in MeOH (250 ml) and hydrazine monohydrate (7.2 ml, 147.8 mmol) was added. The reaction mixture was heated up to 50˚C and was stirred at that temperature overnight. The reaction mixture was filtered and the filtrate was concentrated under reduced pressure. The remaining solution was diluted with DCM and was filtered again. The organic layer was washed with twice 1 M aqueous potassium carbonate and was dried over $MgSO_4$. The organic layer was evaporated under reduced pressure. Compound **4** (10 g yellowish oil, 89 %) was pure enough to be further used. ^{1}H NMR (300 MHz, $CDCl_3$): δ 7.48-7.16 (m, 9 H), 6.88-6.78 (m, 4 H), 3.80 (s, 6 H), 3.15 (t, J = 6.14 Hz, 2 H), 2.90-2.76 (m, 2 H), 1.83-1.68 (m, 2 H), 1.60-1.20 (s br, 2 H)

Wittig-intermediate for compound **7**

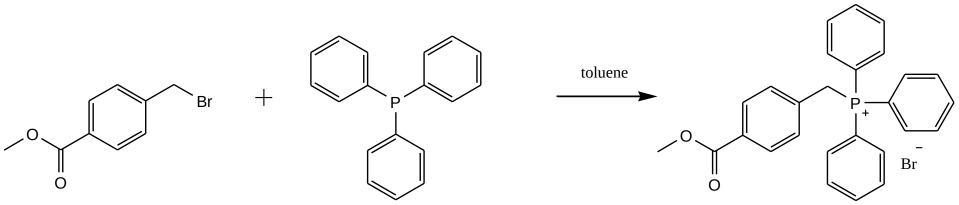

Methyl-4-(bromomethyl)benzoate **5** (15 g, 65.5 mmol) and triphenylphosphine (18.9 g, 72.1 mmol) were dissolved in toluene (150 ml). The reaction mixture was refluxed for 5 hrs. The reaction mixture was cooled down to RT and then placed in an ice bath. The precipitate was filtered off, washed with toluene and dried. The phosphonium salt was isolated as white solid (31.7 g, 98 %). ^{1}H NMR (300 MHz, $CDCl_3$):

Compound **7**

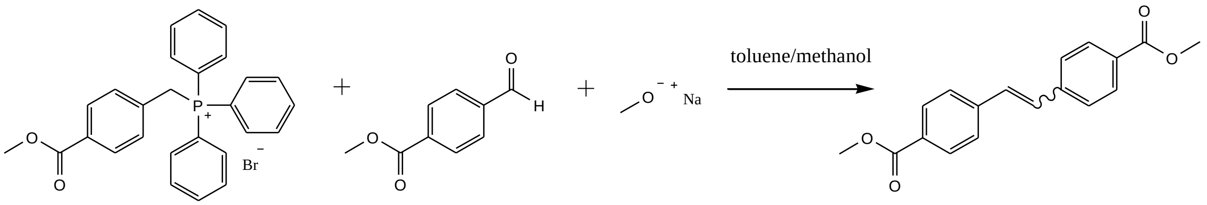

The phosphonium intermediate (30 g, 61.1 mmol) and methyl-4-formylbeozoate **6** (12.1 g, 73.3 mmol) were dissolved in MeOH (114 ml) and toluene (57 ml). Sodium methoxide (25 % w/w in MeOH, 15.1 ml, 67.2 mmol) was added dropwise during one hour at 0 °C. The reaction mixture was slowly warmed to RT and stirred at that temperature for 30 min. and then refluxed for one hour. The reaction mixture was cooled down to RT and then stored in the refrigerator for 3 hrs. The precipitate was filtered off and washed with ice cold MeOH:toluene (2:1). Compound **7** was isolated as white solid (12.7 g, 70 %, cis:trans 3:2). The isomers were separated by washing the filter several times with MeOH:toluene (2:1). The filter was the pure trans isomer. The filtrate (washings) was evaporated to a small volume and cooled to 0 °C. The precipitate was filtered off and gave the pure cis isomer. ^{1}H NMR (300 MHz, $CDCl_3$) cis-isomer: δ 7.89 (d, 4 H, *J* = 8.48 Hz), 7.26 (d, 4 H, *J* = 8.48 Hz), 6.71 (s, 2 H), 3.89 (s, 6 H). trans-isomer: δ 8.04 (d, 4 H, *J* = 8.29 Hz), 7.59 (d, 4 H, *J* = 8.47), 7.23 (s, 2 H), 3.93 (s, 6 H).

Compound **8**

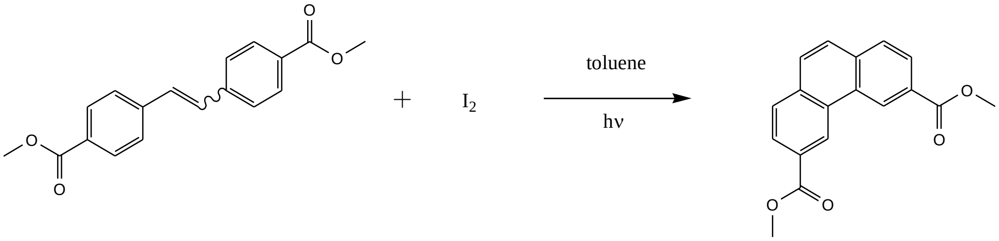

Compound **7** (5.7 g, 19.2 mmol) and iodine (540 mg, 2.1 mmol) were dissolved in toluene (4000 ml) and a stream of air was carefully bubbled through the solution. The solution was irradiated with a medium pressure mercury lamp for 4 days (completion of the reaction controlled by NMR). The reaction mixture was washed with aqueous sodium thiosulfate and was dried over $MgSO_4$. The organic layer was evaporated under reduced pressure. The residue was dissolved in hot DCM (45 ml). The solution was cooled down to RT and MeOH (22 ml) was added. The solution was placed in the fridge. Compound **8** was isolated as yellowish needles (3.2 g, 56 %). ^{1}H NMR (300 MHz, $CDCl_3$): δ 9.45 (d, J = 1.18 Hz, 2 H), 8.24 (dd, J_1 = 1.52 Hz, J_2 = 8.31 Hz, 2 H), 7.94 (d, J = 8.33 Hz, 2 H), 7.85 (s, 2 H), 4.06 (s, 6 H).

Compound **9**

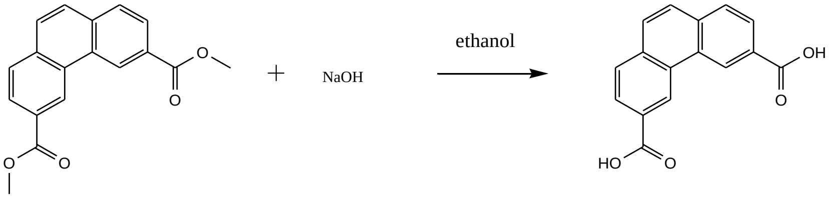

Compound **8** (3 g, 10.2 mmol) was suspended in ethanol (200 ml) and 2.0 M aqueous sodium hydroxide (15.3 ml) was added. The reaction mixture was refluxed for 1 hour. The solvent was evaporated under reduced pressure. The residue was suspended in water (200 ml) and was acidified with 2.0 M aqueous HCl to pH 2. The aqueous layer was filtered off and the product was dried. Compound **9** was isolated as white solid (2.67 g, 98 %). ^{1}H NMR (300 MHz, DMSO): δ 13.33 (s br, 2 H), 9.35 (s, 2 H), 8.25-8.12 (m, 4 H), 8.09 (s, 2 H).

Compound **10**

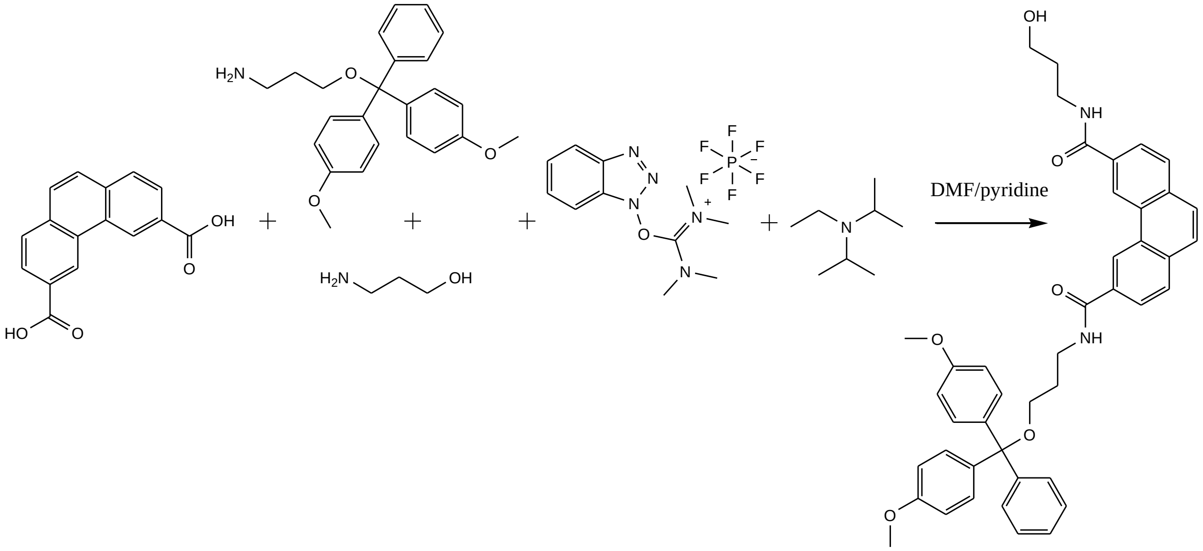

Compound **9** (1 g, 3.76 mmol) was dissolved in dry DMF (19 ml) under argon. *N*,*N*-diisopropylethylamine (3.2 ml, 18.78 mmol) was added. Compound **4** (1.41 g, 3.76 mmol) and 3-hydroxypropylamine **1** (286 µl, 3.76 mmol) were dissolved in dry pyridine (7 ml) and were added to the reaction mixture. HBTU (3.13 g, 8.27 mmol) was added to the reaction mixture. The reaction mixture was stirred at RT for 2 hrs. The reaction mixture was diluted with EA (200 ml) and was washed with three times 10% aqueous citric acid and once with sat. aqueous $NaHCO_3$. The organic layer was dried over $MgSO_4$, filtered and evaporated under reduced pressure. The crude product was purified by column chromatography (DCM:MeOH 96:4 with 2% Et_3N). Compound **10** was isolated as white foam (797 mg, 31 %).

Compound **11**

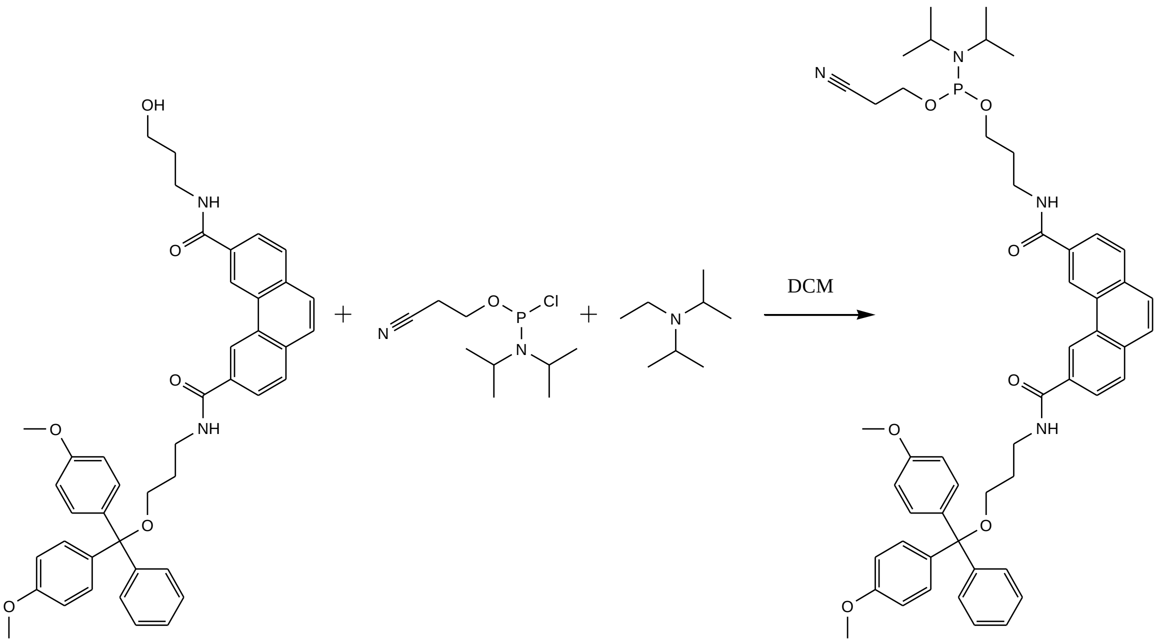

Compound **10** (900 mg, 1.32 mmol) was dissolved in dry DCM (20 ml) and *N*,*N*-diisopropylethylamine (788 μl, 4.61 mmol) was added. 2-Cyanoethyl *N*,*N*-diisopropylchloro-phosphoramidite (195 μl, 1.32 mmol) was added dropwise. The reaction mixture was stirred at RT for 2 hours. The reaction mixture was diluted with EA and was washed once with sat. aqueous $NaHCO_3$. The organic layer was dried over $MgSO_4$ and was evaporated under reduced pressure. The crude product was purified by column chromatography (EA with 2% Et_3N). Compound **11** was isolated as white foam (523 mg, 45%). ^{1}H NMR (300 MHz, $CDCl_3$): δ 9.16 (d, J = 14.73 Hz, 2H), 8.06-7.68 (m, 6 H), 7.45-7.12 (m, 9 H), 6.99-6.88 (m, 2 H), 6.79-6.73 (m, 4 H), 3.96-3.48 (m, 16 H), 3.33 (t, J = 5.42 Hz, 2 H), 2.59 (t, J = 6.27 Hz, 2 H), 2.10-1.92 (m, 4 H), 1.20-1.08 (m, 12 H). ^{31}P NMR (300 MHz, $CDCl_3$): δ 148.22

Compound **13**

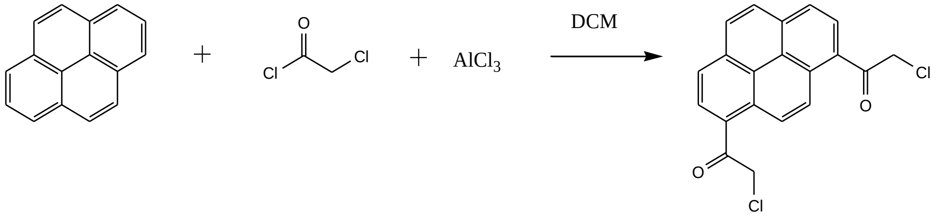

Pyrene **12** (25 g, 124 mmol) was dissolved in DCM (500 ml) and cooled down to 0°C. $AlCl_3$ (49.6 g, 372 mmol) was slowly added. The resulting dark suspension was stirred at 0°C for 10 min. Chloroacetyl chloride (29.6 ml, 372 mmol) was added drop wise during 45 min. The reaction mixture was stirred at 0°C during 20 min. and then heated up to RT and stirred over night. The reaction mixture was cooled down to 0°C and 2.0 M aqueous HCl (120 ml) were added dropwise during 40 min. The reaction mixture was stirred for 30 min. at 0°C. DCM was evaporated under reduced pressure. The remaining aqueous suspension was filtered. The filter was washed with hot water (washing with water was continued until there was no more foam and the product decayed). The filter was suspended in DCM (150 ml) and stirred at RT for 50 min. and then filtered. This treatment was repeated once. The filter was then again suspended in DCM (500 ml), stirred at 35 °C for 1 hour and filtered. The filtrate was evaporated to a volume of ca. 20 ml. The precipitate was filtered off. Compound **13** was isolated as red-brownish solid. The extraction procedure was repeated five times. ^{1}H NMR (300 MHz, DMSO): δ 8.85 (s, 2H); 8.69 (d, J = 8.1 Hz, 2H); 8.51 (d, J = 8.1 Hz, 2H); 8.40 (s, 2H); 5.44 (s, 4H)

Compound **14**

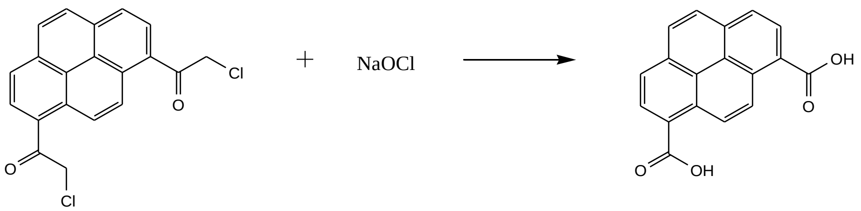

Compound **13** (1 g, 2.82 mmol) was suspended in water (4.4 ml) and n-butanol (0.8 ml). Na_2CO_3 (89.5 mg, 0.8 mmol) and EtOH (0.5 ml) were added with stirring, NaOCl (0.87 ml, 10-13% active chlorine) was added. The reaction mixture was heated up to 90˚C and stirred at that temperature for 20 min. NaOCl (7.54 ml, 10-13% active chlorine) was added slowly. The reaction mixture was then diluted with water (6.4 ml) after 90 min. and stirred at 90˚C for additional 2 h. The reaction mixture was filtered twice. The filter was washed with hot water. The filtrate was acidified with conc. HCl (36%) to pH 1. The precipitate was filtered off and the filter was washed three with hot water. The product was dried. Compound **14** was isolated as yellow solid (748 mg, 91%). ^{1}H NMR (300 MHz, DMSO): δ 13.46 (s br, 2H); 9.31 (s, 2H); 8.65 (d, J = 8.1 Hz); 8.45 (d, J = 8.1 Hz, 2H); 8.38 (s, 2H).

Compound **15**

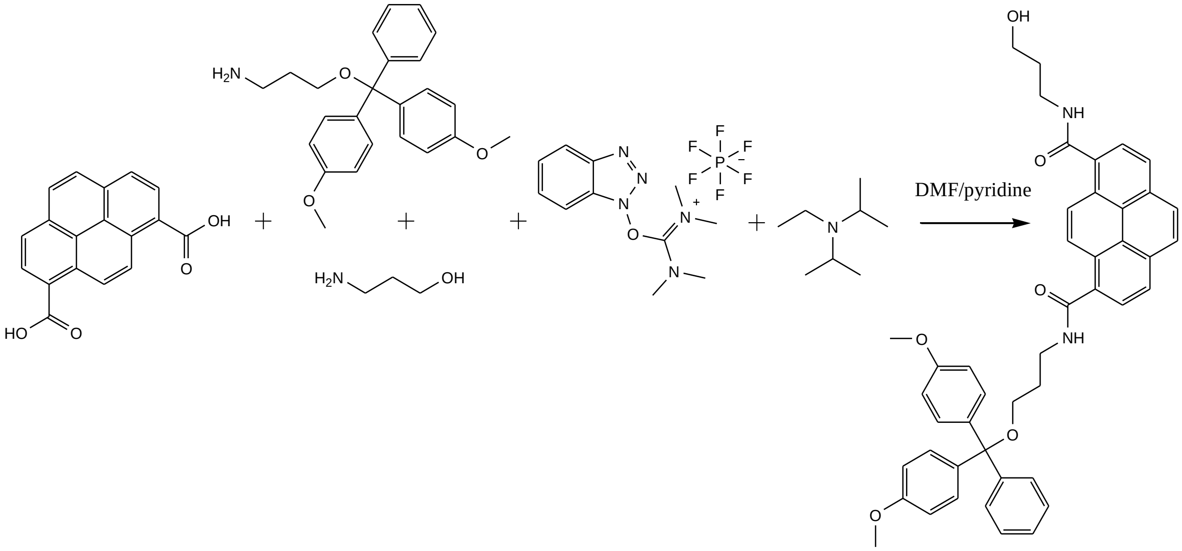

Compound **14** (1 g, 3.44 mmol) was dissolved in dry DMF (17.4 ml) under argon. *N*,*N*-diisopropylethylamine (2.94 ml, 17.22 mmol) was added. Compound **4** (1.3 g, 3.44 mmol) and 3-hydroxypropylamine **1** (0.2 ml, 3.44 mmol) were dissolved in pyridine (7 ml) and added to the reaction mixture. HBTU (2.87 g, 7.58 mmol) was added to the reaction mixture. The mixture was stirred at RT for 2 hrs. The reaction mixture was diluted with EA and was extracted with twice 10% aqueous citric acid and once with sat. aqueous $NaHCO_3$. The organic layer was dried over $MgSO_4$, filtered and evaporated under reduced pressure. The crude product was purified by column chromatography (DCM:MeOH 96:4 with 2% Et_3N). The product was diluted with a minimum amount of dichloromethane and was added dropwise to ice cold diethyl ether. Compound **15** was filtered off as yellowish solid (909 mg, 37%). ^1H NMR (300 MHz, CDCl3): δ 8.36 - 8.17 (m, 2H); 7.89 - 7.49 (m, 7H); 7.39 - 6.95 (m, 7H); 6.63 - 6.54 (m, 4H); 3.95 - 3.67 (m, 7H); 3.61 - 3.26 (m, 9H); 2.10 - 1.85 (m, 4H).

Compound **16**

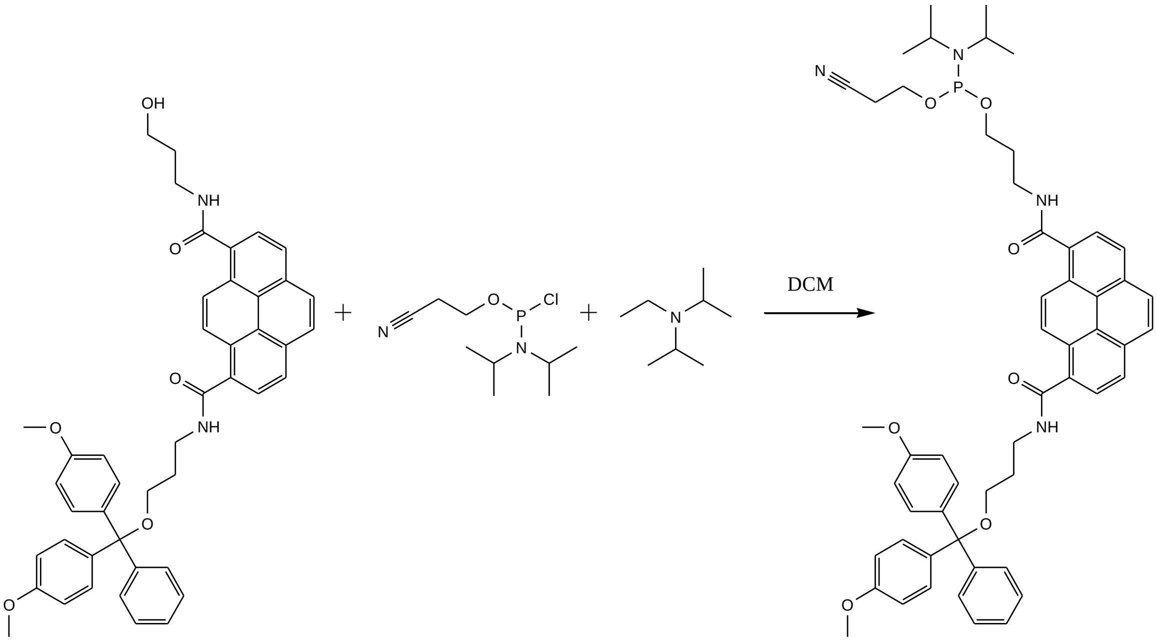

Compound **15** (1 g, 1.41 mmol) was dissolved in dry DCM (20 ml) and *N*,*N*-diisopropylethylamine (0.84 ml, 4.95 mmol) was added. 2-Cyanoethyl N,N-diisopropylchloro-phosphoramidite (0.21 ml, 1.41 mmol) was added dropwise. The reaction mixture was stirred at RT for 2 hrs. The reaction mixture was diluted with DCM and was extracted once with sat. aqueous $NaHCO_3$. The organic layer was dried over $MgSO_4$ and evaporated under reduced pressure. The crude product was purified by column chromatography (DCM:EA 1:1 with 2% Et_3N). The product was dissolved in a minimum amount of dichloromethane and was added dropwise to cold cyclohexane. Compound **16** was filtered off as yellowish solid (715 mg, 55 %). ^{1}H NMR (300 MHz, $CDCl_3$): δ 8.64 - 8.53 (m, 2H); 8.22 - 7.91 (m, 6H); 7.35 - 7.00 (m, 9H); 6.83 - 6.72 (m, 2H); 6.64 - 6.56 (m, 4H); 3.98 - 3.25 (m, 18H); 2.43 - 2.25 (m, 2H); 2.12 - 1.94 (m, 4H); 1.10 - 0.99 (m, 12H).

4,7-Dihexynyl BTD diol (**37**)

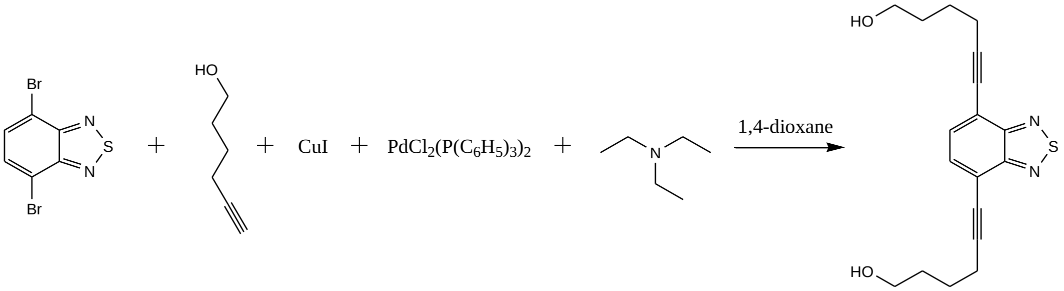

A solution of 4,7-dibromo-2,1,3-benzothiazole **36** (700 mg, 2.38 mmol), 5-hexyn-1-ol (580 µl, 5.24 mmol) and Et3N (1.46 ml, 10.48 mmol) in 1,4-dioxane (15 ml) was degassed for 5 min with a stream of argon directly into the solution. Bis(triphenylphosphine)-palladium(II) dichloride (84 mg, 0.12 mmol) and copper(I)iodide (27 mg, 0.14 mmol) were added at once. The suspension was stirred at 60 °C for one hour. The reaction mixture was diluted with EA and was three times extracted with sat. aqueous NH_4Cl and twice with sat. aqueous NaCl. The organic layer was dried over $MgSO_4$, filtered and evaporated under reduced pressure. The crude product was purified by column chromatography (EA/DCM 1:1). Compound **37** was isolated as orange solid (721 mg, 92 %; Rf = 0.22 in EA/DCM 1:1). ^{1}H NMR (300 MHz, $CDCl_3$): δ = 7.59 (s, 2 H), 3.81-3.71 (m, 4 H), 2.69-2.60 (m, 4 H), 1.85-1.76 (m, 8 H), 1.68-1.55 (m, 2H). ^{13}C NMR (300 MHz, $CDCl_3$): δ = 154.8, 132.4, 117.3, 98.7, 77.4, 62.4, 32.1, 25.0, 19.9). HR MS (NSI): calculated for $C_{18}H_{20}N_2O_2S$ $[M]^+$ 328.12, found 329.13 $[M+H]^+$.

Mono-DMT protected 4,7-dihexynyl BTD (**38**)

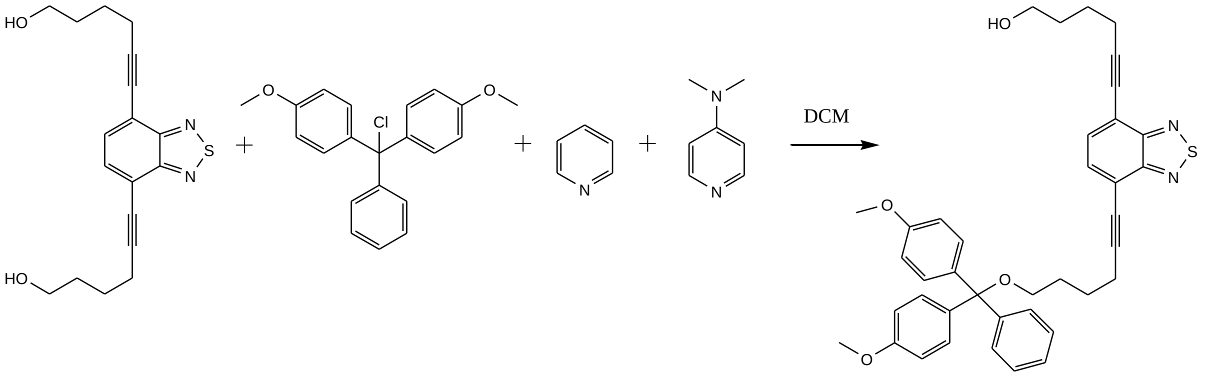

To a solution of **37** (600 mg, 1.82 mmol), pyridine (180 µl, 2.19 mmol) and 4-(dimethylamino)pyridine (33 mg, 0.27 mmol) in dry DCM (13 ml), DMT-Cl (618 mg, 1.82 mmol) in dry DCM (13 ml) was added dropwise over three hours at RT. The reaction mixture was stirred at RT for an additional hour. The reaction mixture was diluted with EA and was extracted twice with sat. aqueous NH_4Cl, once with sat. aqueous $NaHCO_3$ and once with sat. aqueous NaCl. The organic layer was dried over $MgSO_4$, filtered and evaporated under reduced pressure. The crude product was purified by column chromatography (EA/hex 4:3 with 2% Et_3N). Compound **38** was isolated as yellow gel (525 mg, 45 %). ^{1}H NMR (300 MHz, $CDCl_3$): δ = 7.58 (m, 2H), 7.47-7.40 (m, 2H), 7.37–7.15 (m, 7 H), 6.85-6.77 (m, 4 H), 3.81-3.71 (m, 8 H), 3.13 (t, J = 5.65 Hz, 2 H), 2.69-2.53 (m, 4 H), 1.90-1.72 (m, 8 H), 1.49 (s br, 1 H). ^{13}C (300 MHz, $CDCl_3$): δ = 158.5, 154.8, 145.5, 136.8, 132.4, 130.2, 128.4, 127.8, 126.7, 117.5, 117.3, 113.1, 99.0, 98.6, 85.9, 77.4, 77.0, 63.0, 62.5, 55.3, 32.1, 29.6, 25.8, 25.0, 20.0, 19.9. HR MS (NSI): calculated for $C_{39}H_{38}N_2O_4S$ $[M]^+$ 630.26, found 653.24 $[M+Na]^+$.

4-7-dihexynyl BTD phosphoramidite (39)

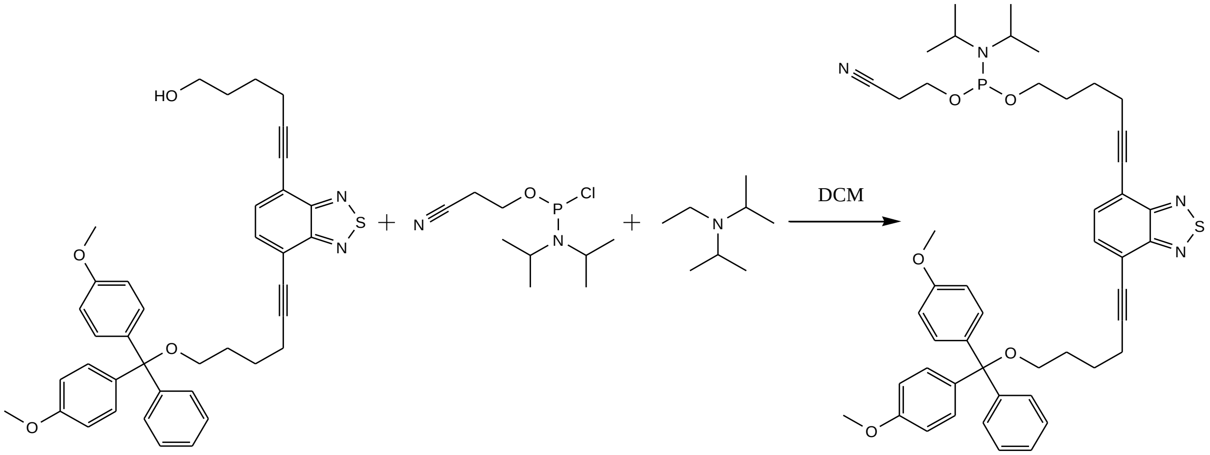

To a solution of compound **38** (500 mg, 0.79 mmol) and N,N-diisopropylethylamine (270 µl, 1.59 mmol) in dry dichloromethane (16 ml), 2-cyanoethyl N,N-diisopropylchlorophosphoramidite (130 µl, 0.87 mmol) was added dropwise. The reaction mixture was stirred at RT for one hour. The reaction mixture was evaporated under reduced pressure and the crude product was purified by column chromatography (EA/hex 1:1 with 2% Et_3N). Compound **39** was isolated as yellow gel (598 mg, 90 %). ^{1}H NMR (300 MHz, $CDCl_3$): δ = 7.66-7.52 (m, 2 H), 7.49-7.40 (m, 2 H), 7.38-7.14 (m, 7 H), 6.87-6.74 (m, 4 H), 3.96-3.50 (m, 12 H), 3.13 (t, J = 5.63 Hz, 2 H), 2.72-2.50 (m, 6 H), 1.96-1.68 (m, 8 H), 1.20 (s, 3H), 1.19 (s, 3H), 1.18 (s, 3H), 1.17 (s, 3H). ^{13}C (300 MHz, $CDCl_3$) δ = 158.5, 154.8, 145.5, 136.8, 132.5, 132.4, 130.2, 128.3, 127.8 126.7, 117.7, 117.5, 117.3, 113.1, 98.9, 98.5, 85.9, 77.4, 77.0, 63.4, 63.2, 63.0, 58.6, 58.3, 55.3, 43.3, 43.1 30.6, 30.5, 29.6, 25.8, 25.3, 24.83, 24.78, 24.74, 24.68, 20.6, 20.5, 20.0, 19.8. ^{31}P NMR (300 MHz, $CDCl_3$): δ = 147.6. HR MS (NSI): calculated for $C_{48}H_{55}N_4O_5PS$ [M]+ 830.36, found 831.37 [M+H]+.

4,7-Dicarbonitrile BTD (40)

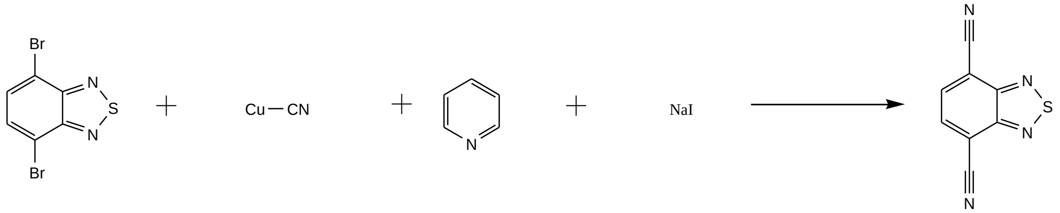

4,7-Dibromo-2,1,3-benzothiadiazole **36** (600 mg, 2.04 mmol), copper(I)cyanide (731 mg, 8.17 mmol), pyridine (1.31 ml, 16.34 mmol) and sodium iodide (30 mg, 0.20 mmol) were suspended in dry DMF (12 ml). The reaction mixture was degassed for 5 min. with a stream of argon directly into the reaction mixture. The reaction mixture was heated at 180 °C for 6 hrs under an atmosphere of argon. The reaction mixture was cooled down and 10 ml of $FeCl_3$ in 6 % HCl were added (5 g $FeCl_3$, 4 ml conc. HCl 32 %, 16 ml water). The reaction mixture was stirred at 100 °C for 30 min. The reaction mixture was diluted with

EA and was extracted once with sat. aqueous NaCl, twice with sat. aqueous NH_4Cl and once with sat. aqueous $NaHCO_3$. The organic layer was dried over $MgSO_4$ and was evaporated under reduced pressure. The crude product was purified by column chromatography (DCM). Compound **40** was isolated as brown solid (304 mg, 80 %). ^{1}H NMR (300 MHz, $CDCl_3$): δ 8.13 (s, 2H).

4,7-Dicarboxylic acid BTD (41)

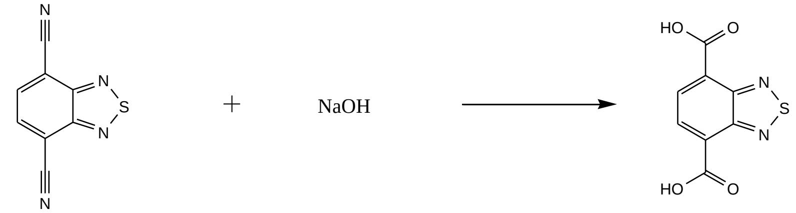

Compound **40** (270 mg, 1.45 mmol) was dissolved in 25 % aqueous NaOH (9 ml. Composition: 6.25 g NaOH, 18.75 g H_2O) and was refluxed for 2 hrs. The reaction mixture was acidified with conc. HCl to pH 1 on ice. The brown slurry was centrifuged to precipitate the product. The product was washed with water and was dried. Compound **41** was isolated as brown solid (277 mg, 85 %). ^{1}H NMR (300 MHz, DMSO): δ 13.64 (s br, 2 H); 8.33 (s, 2 H).

Mono-DMT protected 4,7-dicarboxamide BTD (42)

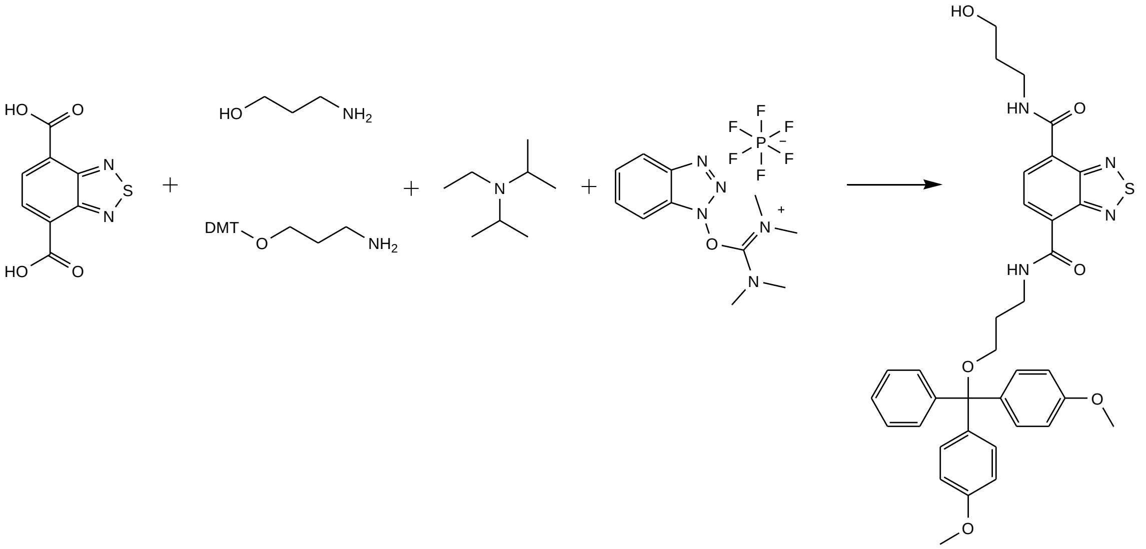

To a solution of compound **41** (250 mg, 1.12 mmol) and N,N-diisopropylethylamine (765 µl, 4.46 mmol) in dry DMF (4 ml) under argon, compound **4** (421 mg, 1.12 mmol) and 3-hydroxypropylamine **1** (85 µl, 1.12 mmol) in dry DMF (4 ml) were added. HBTU (931 mg, 2.46 mmol) was added at once to the reaction mixture. The mixture was stirred at RT for two hrs. The reaction mixture was diluted with EA and was extracted once with sat. aqueous NH_4Cl, sat aqueous $NaHCO_3$ and once with sat. aqueous NaCl. The organic phase was dried over $MgSO_4$, filtered and evaporated under reduced pressure. The crude product was purified by column chromatography (EA with 2 % Et_3N, changed to EA/MeOH 95:5 with 2 % Et_3N after the bis-DMT protected product was eluated). Compound **42** was isolated as brownish foam (240 mg, 33 %). ^1H NMR (300 MHz, $CDCl_3$): δ = 9.23 (t, J = 6.22 Hz, 1 H); 9.02 (t, J = 5.37 Hz, 1 H); 8.79-8.66 (m, 2 H); 7.48-7.11 (m, 9 H); 6.78-6.67 (m, 4 H); 3.91-3.60 (m, 12 H); 3.29 (t, J = 5.84 Hz, 2 H); 3.10 (t, J = 6.50 Hz, 1 H); 2.09-1.83 (m, 4 H). ^{13}C NMR (300 MHz, $CDCl_3$): δ = 163.8, 162.4, 158.5, 152.2, 152.2, 145.1, 136.4, 133.3, 132.9, 130.2, 128.4, 127.9, 127.2, 126.9, 113.1, 86.3, 77.4, 61.6, 59.4, 55.3, 38.3, 36.8, 32.8, 29.8. HR MS (NSI): calculated for $C_{35}H_{36}N_4O_6S$ $[M]^+$ 640.24, found 663.22 $[M+Na]^+$.

4,7-Dicarboxamide BTD phosphoramidite (**43**)

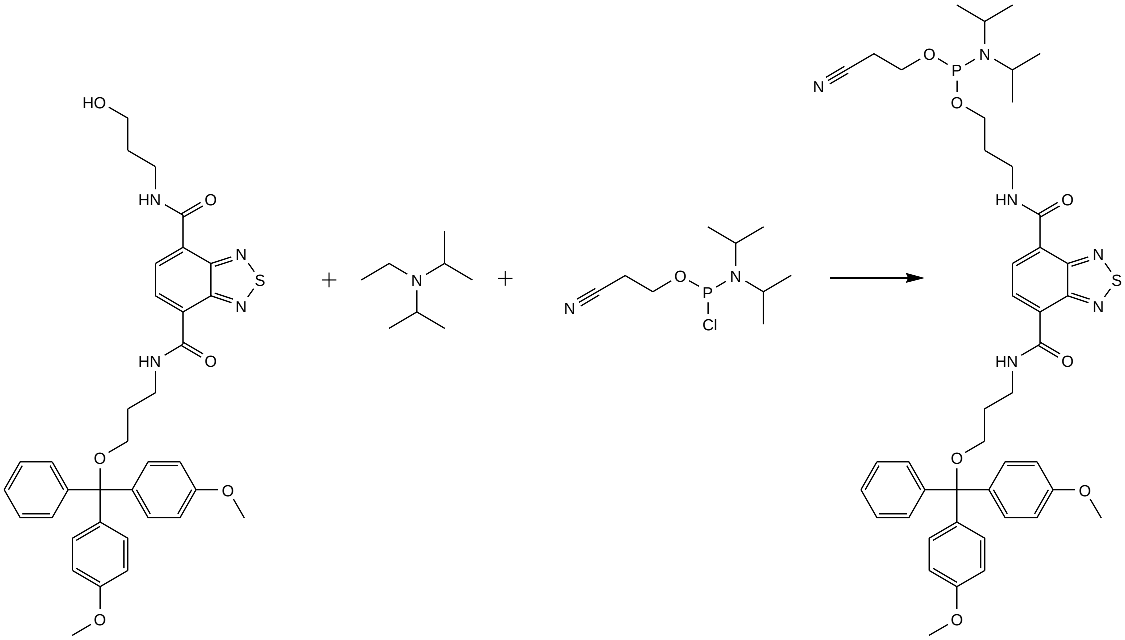

To a solution of compound **42** (200 mg, 0.31 mmol) and N,N-diisopropylethylamine (110 µl, 0.63 mmol) in dry DCM (6 ml), 2-cyanoethyl N,N-diisopropylchlorophosphoramidite (51 µl, 0.34 mmol) was added dropwise. The reaction mixture was stirred at RT for one hour. The reaction mixture was evaporated under reduced pressure and the crude product was purified by column chromatography (EA with 2 % Et3N). Compound **43** was isolated as brownish foam (200 mg, 75 %). ^1H NMR (300 MHz, $CDCl_3$): δ = 9.16 (t, J = 5.56 Hz, 1 H); 9.06 (t, J = 5.37 Hz, 1 H); 8.79-8.63 (m, 2 H); 7.46-7.05 (m, 9 H); 6.78-6.70 (m, 4 H); 3.96-3.53 (m, 16 H); 3.32 (t, J = 5.84 Hz, 2 H); 2.68 (t, J = 6.31 Hz, 2 H); 2.14-1.90 (m, 4 H); 1.21 (s, 3 H), 1.20 (s, 3 H), 1.19 (s, 3 H), 1.17 (s, 3 H). ^{13}C NMR (300 MHz, $CDCl_3$): δ 162.7, 162.5, 158.5, 152.2, 145.1, 136.4, 133.0, 132.9, 130.2, 128.4, 128.1, 127.8, 127.7, 126.9, 117.7, 113.1, 86.3, 77.4, 61.5, 61.3, 58.7, 58.4, 55.3, 43.3, 43.2, 38.2, 37.5, 31.2, 31.1, 29.8, 24.8, 24.7, 20.6, 20.5. ^{31}P NMR (300 MHz, $CDCl_3$): δ 147.9. HR MS (NSI): calculated for $C_{44}H_{53}N_6O_7PS$ $[M]^+$ 840.34, found 863.33 $[M+Na]^+$.

1,2-diamino-3,6-dibromobenzene (**68**)

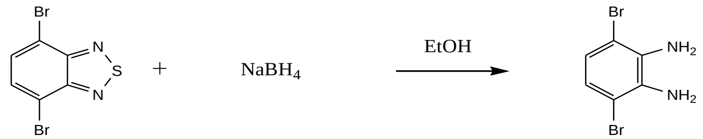

To a suspension of 4,7-dibromo-2,1,3-benzothiazole**36** (1117 mg, 3.8 mmol) in EtOH (50 ml), sodium borohydride (2660 mg, 70.3 mmol) was added portionwise at 0 °C. The reaction mixture was stirred for 20 hrs at RT. After evaporation of the solvent, water (60 ml) was added. The aqueous phase was extracted with Et_2O. The organic phase was washed with sat. aqueous NaCl. The organic layer was dried over $MgSO_4$ and evaporated under reduced pressure. Compound **68** was used without further purification. ^{1}H NMR (300 MHz, $CDCl_3$): δ 6.85 (s, 2 H), 3.89 (s br, 4 H).

5,8-dibromo-2,3-difuranylquinoxaline (**69 a-f**). Representative procedure for the preparation of the quinoxaline core.

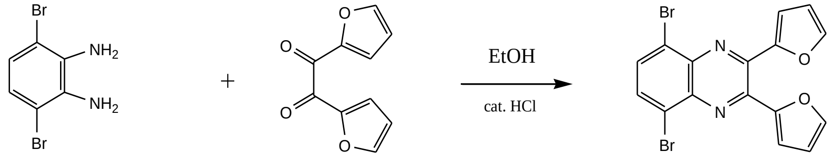

2,2'-Furil (1000 mg, 5.26 mmol), compound **68** (1538 mg, 5.79 mmol) and a catalytic amount of HCI (one drop) in EtOH (35 ml) were refluxed for several hours (reaction progress followed by TLC). The precipitate was collected and slightly washed with cold EtOH. Compound **69e** was isolated as yellow solid (1805 mg, 92 %). ^{1}H NMR (300 MHz, $CDCl_3$): δ 7.88 (s, 2 H), 7.63 (m, 2 H), 6.98 (m, 2 H), 6.60 (m, 2 H). **5,8-dibromoquinoxaline** (**69a**): δ 9.02 (s, 2H), 8.01 (s, 2H). **5,8-dibromo-2,3-dimethylquinoxaline** (**69b**): δ 7.84 (s, 2 H), 2.83 (s, 6 H). **5,8-dibromo-2,3-diphenylquinoxaline** (**69c**): δ 7.92 (s, 2 H), 7.70-7.62 (m, 4 H), 7.45-7.32 (m, 6 H). **5,8-dibromo-2,3-dipyridylquinoxaline** (**69d**): δ 8.33-8.24 (m, 4 H), 7.98 (s, 2 H), 7.95-7.86 (m, 2 H), 7.30-7.23 (m, 2 H). **5,8-dibromo-2,3-dithiophenylquinoxaline** (**69f**): δ 7.84 (s, 2 H), 7.55 (dd, J^1 = 5.09 Hz, J^2 = 1.13 Hz, 2 H), 7.48 (dd, J^1 = 3.77 Hz, J^2 = 0.94 Hz, 2 H), 7.05 (dd, J^1 = 5.08 Hz, J^2 = 3.77 Hz, 2 H).

5,8-dihexynyl-2,3-difuranylquinoxaline diol (**70 a-f**). Representative procedure for the preparation of 5,8-dihexynyl substituted quinoxaline diols.

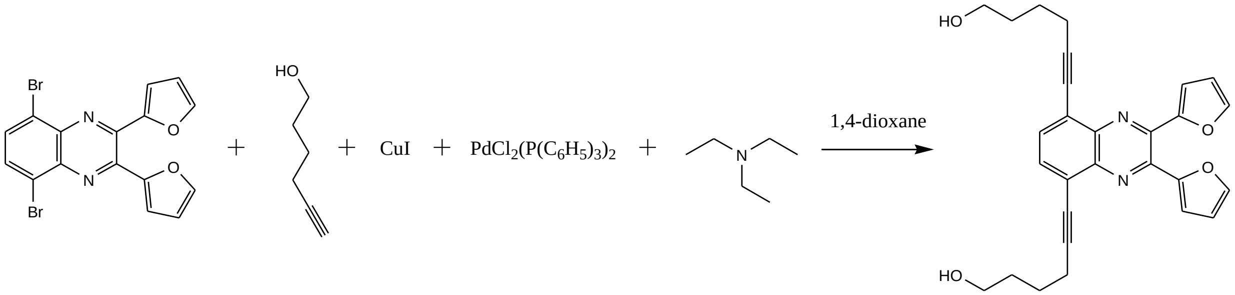

A suspension of compound **69e** (483 mg, 1.15 mmol), 5-hexyn-1-ol (282 µl, 2.53 mmol) and Et_3N (705 µl, 5.06 mmol) in 1,4-dioxane (15 ml) was degassed with a stream of argon into the solution for 30 min. Bis(triphenylphosphine)-palladium(II) dichloride (35 mg, 0.05 mmol) and copper(I) iodide (11 mg, 0.06) were added at once. The suspension was stirred at 60 °C for 8 hrs. The reaction mixture was filtered over a pad of celite and was evaporated under reduced pressure. The residue was dissolved in app. 100 ml DCM and was washed twice with 10 % aqueous citric acid and once with sat. aqueous $NaHCO_3$. The organic phase was dried over $MgSO_4$ and was evaporated under reduced pressure. The crude product was purified by column chromatography (EA:DCM 1:1). Compound **70e** was isolated as orange solid (244 mg, 47 %). ^{1}H NMR (300 MHz, $CDCl_3$): δ 7.72 (s, 2 H), 7.60 (dd, J^1 = 1.70 Hz, J^2 = 0.75 Hz, 2 H), 6.86 (dd, J^1 = 3.58 Hz, J^2 = 0.57 Hz, 2 H), 6.57 (dd, J^1 = 3.39 Hz, J^2 = 1.70 Hz, 2 H), 3.78 (q, J = 5.33 Hz, 4 H), 2.67 (t, J = 6.50 Hz, 4 H), 1.97-1.75 (m, 8 H), 1.49 (t, J = 5.18 Hz, 2 H). **5,8-dihexynyl-quinoxaline diol** (**70a**): δ 8.94 (s, 2 H), 7.81 (s, 2 H), 3.79 (s br, 4 H), 2.70-2.61 (m, 4 H), 2.06 (s br, 2 H), 1.91-1.71 (m, 8 H). **5,8-dihexynyl-2,3-dimethylquinoxaline diol** (**70b**): δ 7.70 (s, 2H), 3.83 (q, J = 5.33 Hz, 4 H), 2.78 (s, 6 H), 2.65 (t, J = 6.31 Hz, 4 H), 2.28 (t, J = 5.56 Hz, 2 H), 1.96-1.75 (m, 8 H). **5,8-dihexynyl-2,3-diphenylquinoxaline diol** (**70c**): δ 7.75 (s, 2 H), 7.65-7.58 (m, 4 H), 7.41-7.29 (m, 6 H), 3.72 (q, J = 5.96 Hz, 4 H), 2.65 (t, J = 6.50 Hz, 4 H), 1.96-1.73 (m, 8 H). **5,8-dihexynyl-2,3-dipyridylquinoxaline diol** (**70d**): δ 8.35-8.29 (m, 2 H), 8.17-8.08 (m, 2 H), 7.89-7.77 (m, 4 H), 7.29-7.19 (m, 2 H), 3.79-3.68 (m, 4 H), 2.65 (t, J = 6.50 Hz, 4 H), 1.95-1.75 (m, 8 H), 1.71 (s br, 2 H). **5,8-dihexynyl-2,3-dithiophenylquinoxaline diol** (**70f**): 7.68 (s, 2 H), 7.51 (dd, J^1 = 4.99 Hz, J^2 = 1.04 Hz, 2 H), 7.39 (dd, J^1 = 3.67 Hz, J^2 = 1.04 Hz, 2 H), 7.03 (dd, J^1 = 5.09 Hz, J^2 = 3.78 Hz, 2 H), 3.81-3.70 (m, 4 H), 2.66 (t, J = 6.50 Hz, 4 H), 1.96-1.75 (m, 8 H), 1.38 (s br, 2 H).

4,7-Dibromobenzoxodiazole (BOD) (**73**)

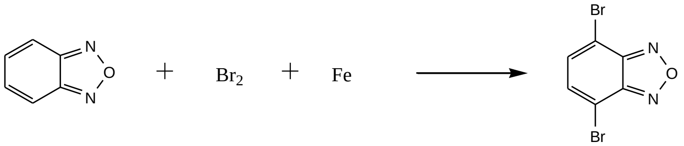

Benzofurazane **72** (2000 mg, 16.65 mmol) and iron (186 mg, 3.33 mmol) were mixed and heated to 90 °C. Bromine (2.53 ml, 49.1 mmol) was added dropwise to the reaction mixture. The reaction mixture was stirred at 90 °C for 1.5 hrs. The reaction mixture was poured onto ice water. A sodium thiosulfate solution was added and the mixture was extracted with EA. The organic layer was separated and dried over $MgSO_4$. The organic layer was evaporated under reduced pressure. The crude product was recrystallized from EtOH. Compound **73** was isolated as brown needles (3.96 g, 85 %). ^{1}H NMR (300 MHz, $CDCl_3$): δ 7.51 (s, 2 H).

4,7-dihexynyl BOD diol (**74**)

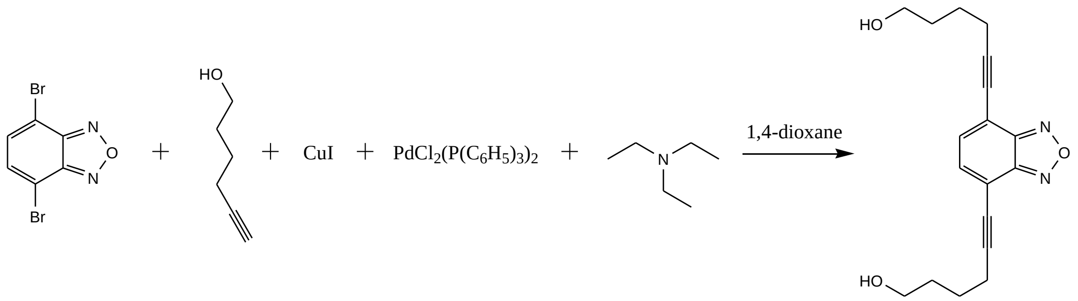

A solution of 4,7-dibromo-2,1,3-benzoxazole **72** (700 mg, 2.52 mmol), 5-hexyn-1-ol (611 µl, 5.54 mmol) and Et_3N (1.54 ml, 11.1 mmol) in 1,4-dioxane (10 ml) was degassed with a stream of argon into the solution for 5 min. Bis(triphenylphosphine)-palladium(II) dichloride (88 mg, 0.13 mmol) and copper(I) iodide (28 mg, 0.15 mmol) were added at once. The suspension was stirred at 60 °C for 1 hour. The reaction mixture was diluted with EA and was extracted twice with sat. aqueous NH_4Cl and once with sat. aqueous NaCl. The organic layer was dried over $MgSO_4$ and was evaporated under reduced pressure. The crude product was purified by column chromatography (EA:hex 4:1). Compound **73** was isolated as yellow solid (584 mg, 74 %). ^{1}H NMR (300 MHz, $CDCl_3$): δ 7.36 (s, 2 H), 3.79-3.69 (m ,4 H), 2.64-2.56 (m, 4 H), 1.83-1.73 (m, 8 H).

7. Appendix

7.1 ^{1}H NMR spectra of BTD-based building blocks

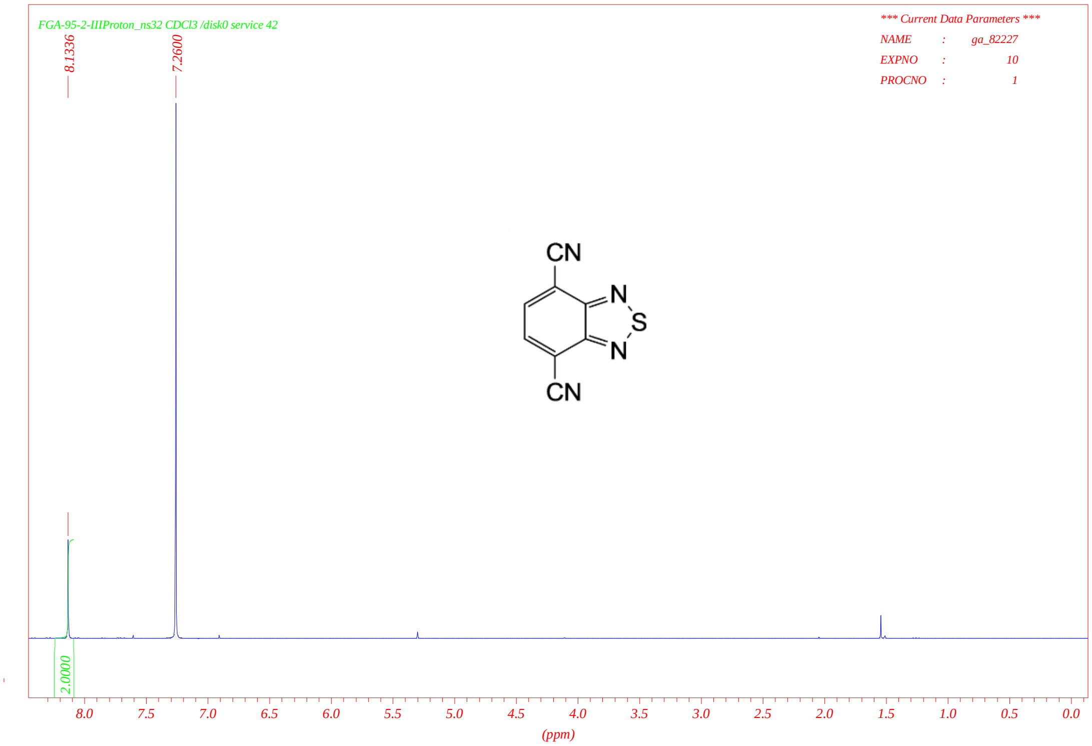

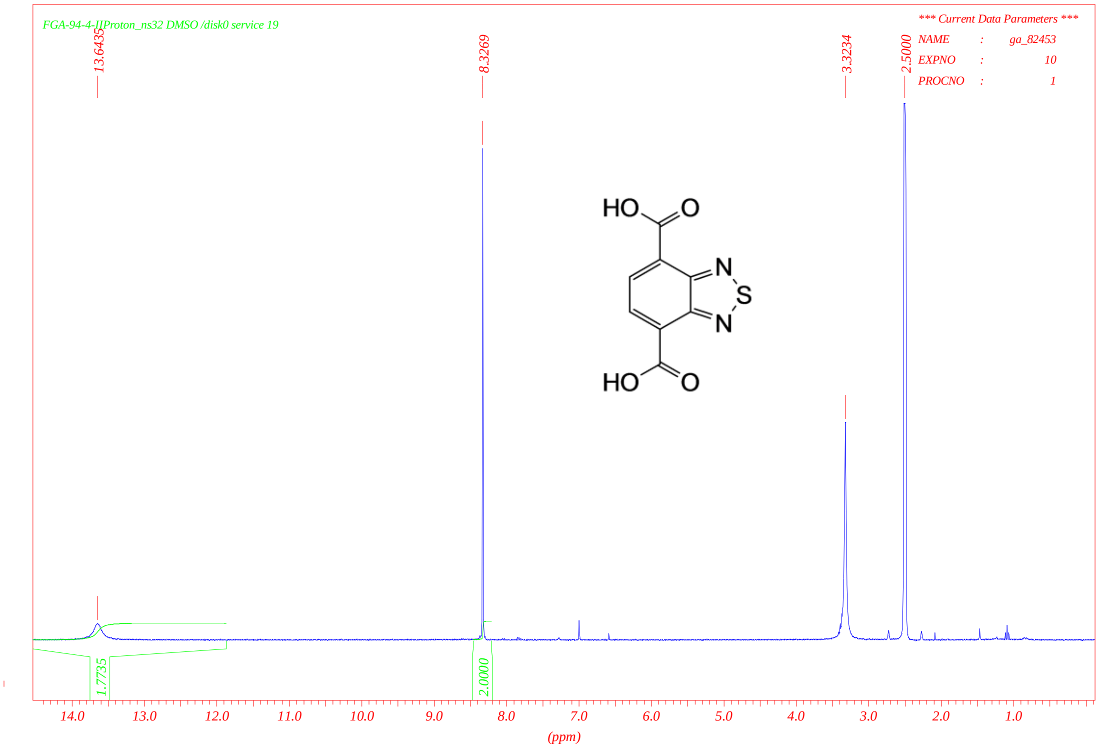

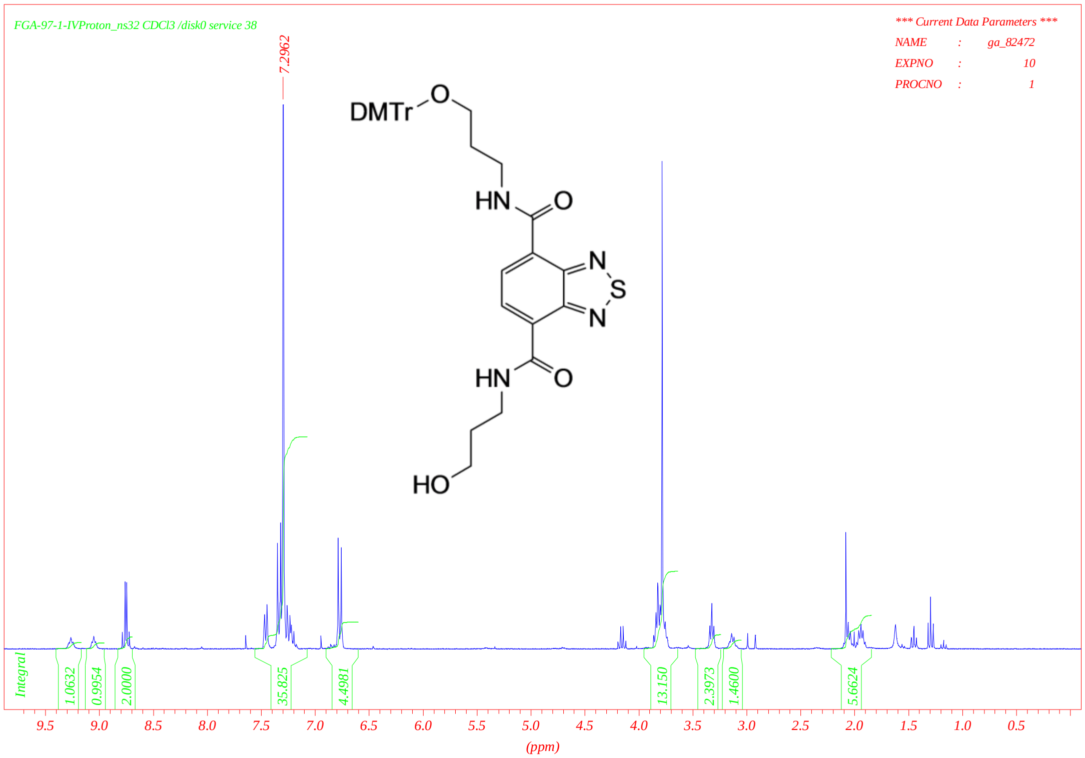
FGA-97-1-IVProton_ns32 CDCl3 /disk0 service 38
*** Current Data Parameters ***
NAME : ga_82472
EXPNO : 10
PROCNO : 1
7.2962
DMTr
O
HN
O
N
S
N
HN
O
HO
Integral
1.0632
0.9954
2.0000
35.825
4.4981
13.150
2.3973
1.4600
5.6624
9.5
9.0
8.5
8.0
7.5
7.0
6.5
6.0
5.5
5.0
4.5
4.0
3.5
3.0
2.5
2.0
1.5
1.0
0.5
(ppm)

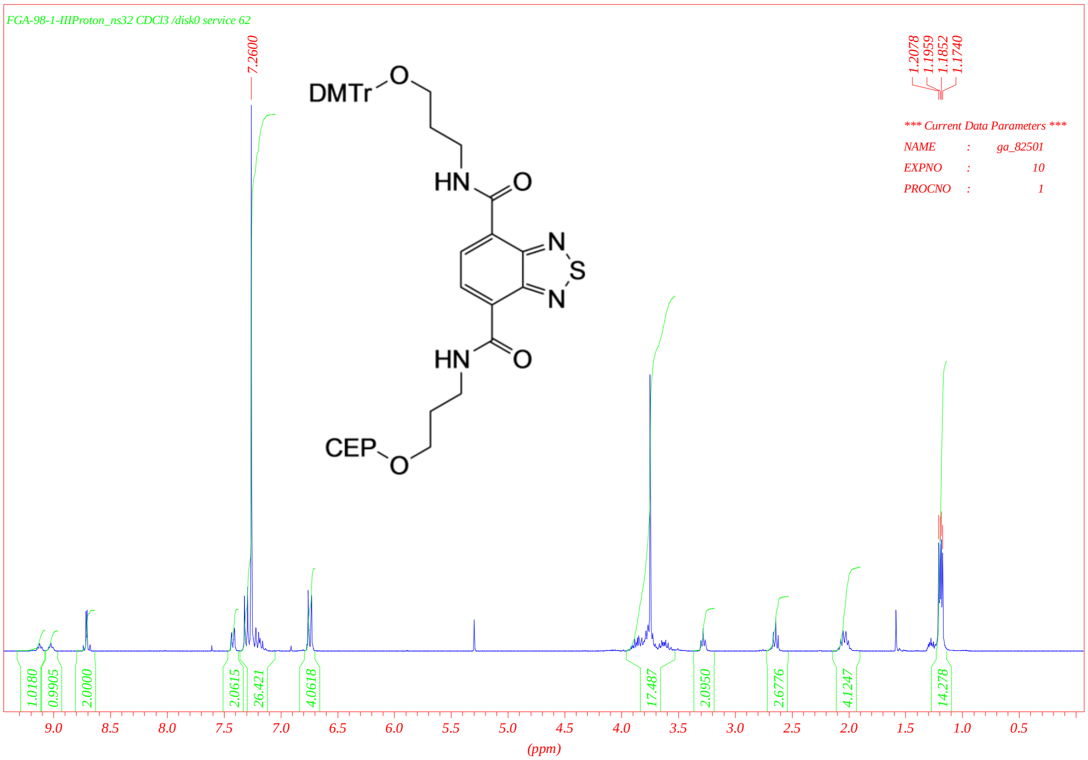
FGA-98-1-IIIProton_ns32 CDCl3 /disk0 service 62
7.2600
1.2078
1.1959
1.1852
1.1740
*** Current Data Parameters ***
NAME : ga_82501
EXPNO : 10
PROCNO : 1
DMTr
O
HN
O
N
S
N
HN
O
CEP
O
1.0180
0.9905
2.0000
2.0615
26.421
4.0618
17.487
2.0950
2.6776
4.1247
14.278
9.0
8.5
8.0
7.5
7.0
6.5
6.0
5.5
5.0
4.5
4.0
3.5
3.0
2.5
2.0
1.5
1.0
0.5
(ppm)

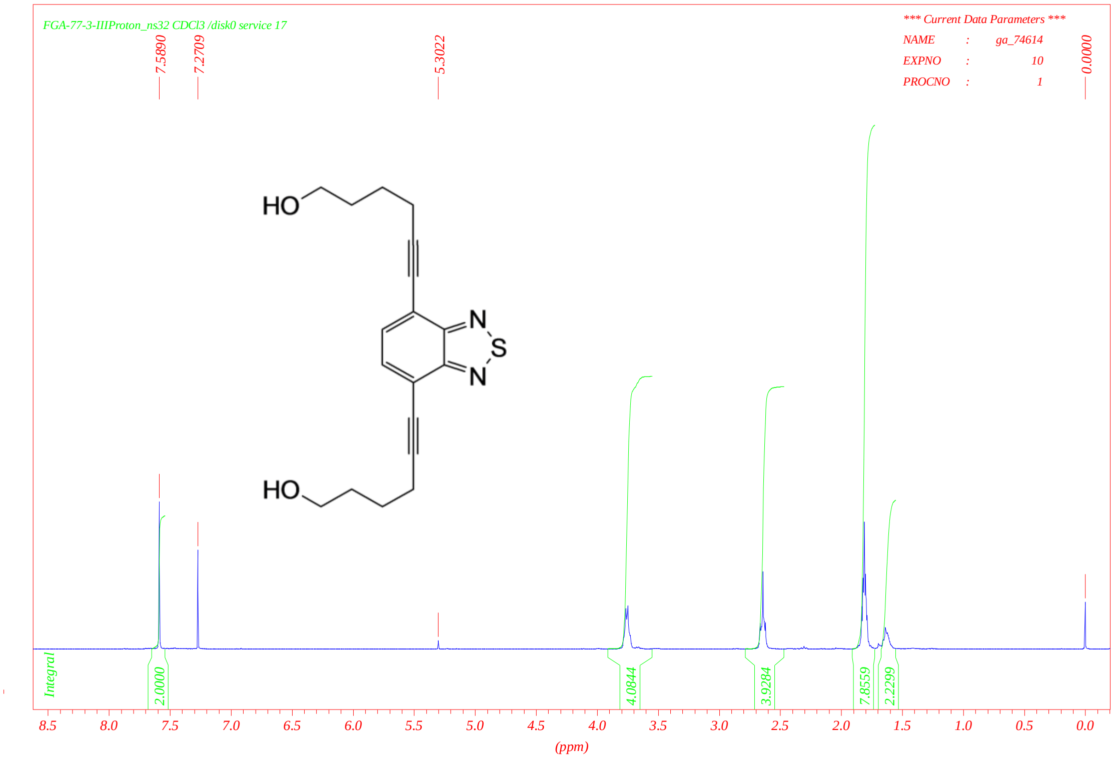
FGA-77-3-IIIProton_ns32 CDCl3 /disk0 service 17
*** Current Data Parameters ***
NAME : ga_74614
EXPNO : 10
PROCNO : 1
7.5890
7.2709
5.3022
0.0000
HO
N
S
N
HO
Integral
2.0000
4.0844
3.9284
7.8559
2.2299
8.5
8.0
7.5
7.0
6.5
6.0
5.5
5.0
4.5
4.0
3.5
3.0
2.5
2.0
1.5
1.0
0.5
0.0
(ppm)

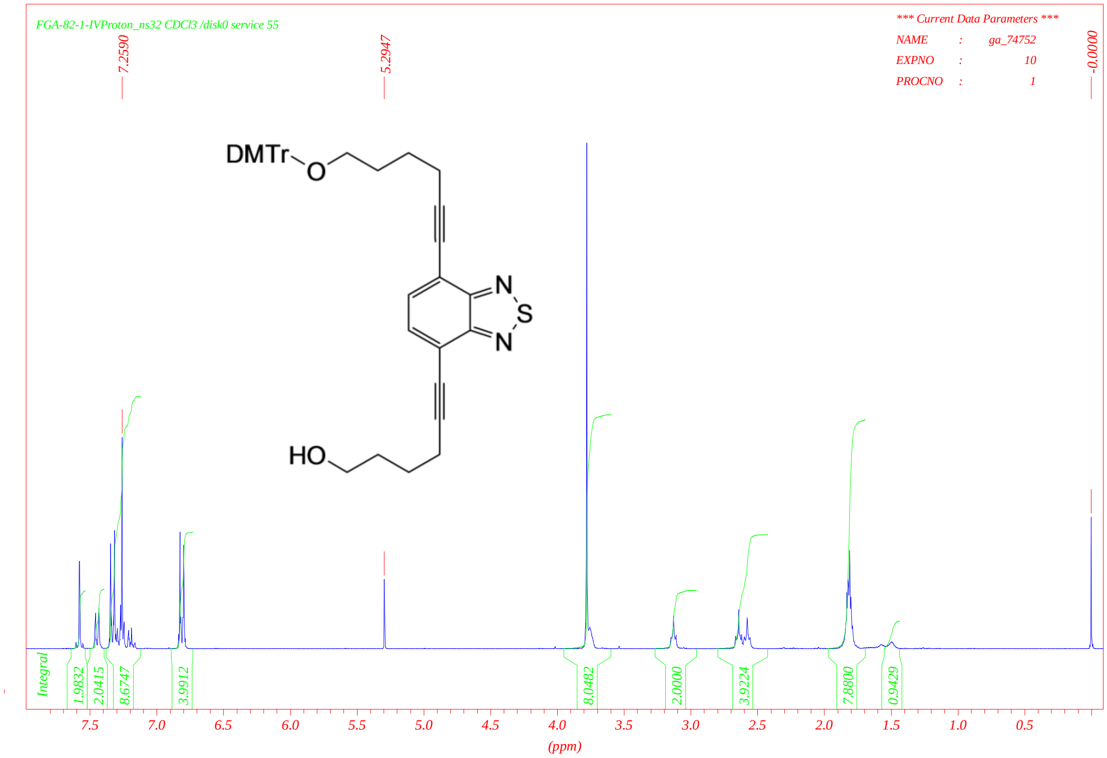
FGA-82-1-IVProton_ns32 CDCl3 /disk0 service 55
*** Current Data Parameters ***
NAME : ga_74752
EXPNO : 10
PROCNO : 1
7.2590
5.2947
-0.0000
DMTr
O
N
S
N
HO
Integral
1.9832
2.0415
8.6747
3.9912
8.0482
2.0000
3.9224
7.8800
0.9429
7.5
7.0
6.5
6.0
5.5
5.0
4.5
4.0
3.5
3.0
2.5
2.0
1.5
1.0
0.5
(ppm)

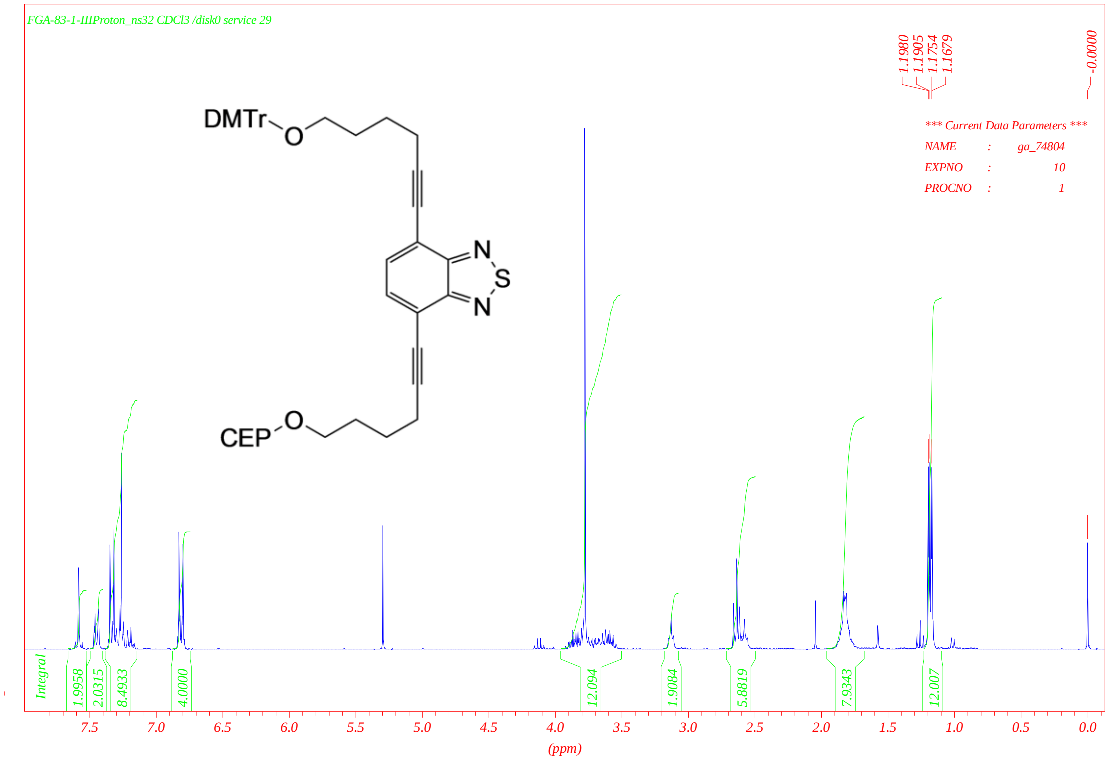
FGA-83-1-IIIProton_ns32 CDCl3 /disk0 service 29
DMTr
O
N
S
N
CEP
O
1.1980
1.1905
1.1754
1.1679
-0.0000
*** Current Data Parameters ***
NAME : ga_74804
EXPNO : 10
PROCNO : 1
Integral
1.9958
2.0315
8.4933
4.0000
12.094
1.9084
5.8819
7.9343
12.007
7.5
7.0
6.5
6.0
5.5
5.0
4.5
4.0
3.5
3.0
2.5
2.0
1.5
1.0
0.5
0.0
(ppm)

7.2 Mass spectrometry (LC – MS) data of modified oligonucleotides

Table 15. LC-MS data of all oligonucleotides from chapter 3.1 – 3.5

	17 ***5970.1 g/mol*** $C_{204}H_{248}N_{68}O_{110}P_{18}$		***18*** ***5665.8 g/mol*** $C_{185}H_{236}N_{60}O_{113}P_{18}$		***19*** ***6412.5 g/mol*** $C_{226}H_{271}N_{70}O_{116}P_{19}$		***20*** ***6108.2 g/mol*** $C_{207}H_{259}N_{62}O_{119}P_{19}$		***21*** ***6855.0 g/mol*** $C_{248}H_{294}N_{72}O_{122}P_{20}$	
Z	found (m/z)	calc. (m/z)	found (m/z)	calc. (m/z)	found (m/z)	calc. (m/z)	found (m/z)	calc. (m/z)	found (m/z)	calc. (m/z)
-5	1193.5	1193.0	1132.1	1132.2	1281.5	1281.5	1220.6	1220.6	1369.8	1370.0
-6	994.00	994.0	943.4	943.3	1067.8	1067.8	1017.2	1017.0	1141.3	1141.5
-7	851.9	851.9	808.3	808.4	915.3	915.1	871.7	871.6	978.4	978.3
-8	745.5	745.3	707.3	707.2	800.7	800.6	762.4	762.5	856.0	855.9
-9			628.7	628.5	711.6	711.5	677.9	677.7	760.6	760.7
-10									684.5	684.5

	22 ***6550.6 g/mol*** $C_{229}H_{282}N_{64}O_{125}P_{20}$		***23*** ***7739.7 g/mol*** $C_{292}H_{340}N_{76}O_{134}P_{22}$		***24*** ***7435.4 g/mol*** $C_{273}H_{328}N_{68}O_{137}P_{22}$		***25*** ***5955.1 g/mol*** $C_{203}H_{247}N_{69}O_{109}P_{18}$		***26*** ***5681.8 g/mol*** $C_{185}H_{236}N_{60}O_{114}P_{18}$	
Z	found (m/z)	calc. (m/z)	found (m/z)	calc. (m/z)	found (m/z)	calc. (m/z)	found (m/z)	calc. (m/z)	found (m/z)	calc. (m/z)
-5	1308.8	1309.1					1190.0	1190.0	1134.9	1135.4
-6	1090.8	1090.8	1289.0	1289.0	1238.2	1238.2	991.5	991.5	945.9	946.0
-7	935.0	934.8	1104.9	1104.7	1061.3	1061.2	849.7	849.7	810.6	810.7
-8	817.7	817.8	966.5	966.5	928.5	928.4	743.3	743.4	709.1	709.2
-9	726.9	726.8	859.0	859.0	825.3	825.2			630.4	630.3
-10	654.2	654.1	772.8	773.0	742.5	742.5				

	27 ***6397.5 g/mol*** $C_{225}H_{270}N_{71}O_{115}P_{19}$		***28*** ***6124.2 g/mol*** $C_{207}H_{259}N_{62}O_{120}P_{19}$		***29*** ***6839.9 g/mol*** $C_{247}H_{293}N_{73}O_{121}P_{20}$		***30*** ***6566.6 g/mol*** $C_{229}H_{282}N_{64}O_{126}P_{20}$		***31*** ***7724.7 g/mol*** $C_{291}H_{339}N_{77}O_{133}P_{22}$	
Z	found (m/z)	calc. (m/z)	found (m/z)	calc. (m/z)	found (m/z)	calc. (m/z)	found (m/z)	calc. (m/z)	found (m/z)	calc. (m/z)
-5	1277.9	1278.5	1223.9	1223.8	1367.4	1367.0	1312.0	1312.3		
-6	1065.4	1065.3	1019.6	1019.7	1138.8	1139.0	1093.4	1093.4	1286.0	1286.5
-7	912.9	912.9	873.9	873.9	976.0	976.1	937.3	937.1	1102.0	1102.5
-8	798.7	798.7	764.5	764.5	854.0	854.0	819.7	819.8	964.6	964.6
-9	710.1	709.8	679.1	679.5	759.2	759.0	728.7	728.6	857.1	857.3
-10					682.8	683.0	655.9	655.7	771.5	771.5

	32 ***7451.4 g/mol*** $C_{273}H_{328}N_{68}O_{138}P_{22}$		***33*** ***5968.1 g/mol*** $C_{204}H_{250}N_{62}O_{115}P_{18}$		***34*** ***6410.5 g/mol*** $C_{226}H_{273}N_{64}O_{121}P_{19}$		***35*** ***6852.9 g/mol*** $C_{248}H_{296}N_{66}O_{127}P_{20}$		***44*** [a] ***7773.4 g/mol*** $C_{258}H_{316}N_{98}O_{138}P_{24}S_1$	
Z	found (m/z)	calc. (m/z)	found (m/z)	calc. (m/z)	found (m/z)	calc. (m/z)	found (m/z)	calc. (m/z)	found (m/z)	calc. (m/z)
-5			1193.1	1192.6	1281.0	1281.1	1369.0	1369.6		
-6	1240.7	1240.9	993.8	993.7	1067.3	1067.4	1140.9	1141.2	1294.4	1294.6
-7	1063.1	1063.5	851.6	851.6	914.9	914.8	978.1	978.0	1109.4	1109.5
-8	930.3	930.4	744.9	745.0	800.3	800.3	856.0	855.6	970.8	970.7
-9	827.2	826.9	662.1	662.1			761.0	760.4	862.6	862.7
-10	744.4	744.1					684.6	684.3	776.2	776.3
-11									705.4	705.7

	45 ***7624.1 g/mol*** $C_{250}H_{317}N_{77}O_{155}P_{24}$		***46*** ***7615.0 g/mol*** $C_{250}H_{318}N_{74}O_{157}P_{24}$		***47*** ***7600.0 g/mol*** $C_{249}H_{317}N_{75}O_{156}P_{24}$		***48*** ***7640.1 g/mol*** $C_{250}H_{317}N_{77}O_{156}P_{24}$		***49*** ***7711.2 g/mol*** $C_{254}H_{322}N_{76}O_{156}P_{24}S_{1}$	
Z	found (m/z)	calc. (m/z)	found (m/z)	calc. (m/z)	found (m/z)	calc. (m/z)	found (m/z)	calc. (m/z)	found (m/z)	calc. (m/z)
-6					1265.55	1265.7			1284.15	1284.2
-7	1087.75	1088.1	1086.75	1086.9	1084.75	1084.7	1090.35	1090.4	1100.40	1100.6
-8	951.85	952.0	950.65	950.9	948.95	949.0	953.60	954.0	962.70	962.9
-9	845.80	846.1	845.05	845.1	843.45	843.4	847.80	847.9	855.80	855.8
-10	761.45	761.4	760.45	760.5	759.15	759.0	763.10	763.0	770.25	770.1
-11	693.70	692.1	691.15	691.3	689.85	689.9	693.35	693.5	700.25	700.0

	50 ***7696.2 g/mol*** $C_{250}H_{309}N_{101}O_{139}P_{24}$		***51*** ***7687.2 g/mol*** $C_{250}H_{310}N_{98}O_{141}P_{24}$		***52*** ***7672.1 g/mol*** $C_{249}H_{309}N_{99}O_{140}P_{24}$		***53*** ***7712.2 g/mol*** $C_{250}H_{309}N_{101}O_{140}P_{24}$		***54*** ***7783.3 g/mol*** $C_{254}H_{314}N_{100}O_{140}P_{24}S_{1}$	
Z	found (m/z)	calc. (m/z)	found (m/z)	calc. (m/z)	found (m/z)	calc. (m/z)	found (m/z)	calc. (m/z)	found (m/z)	calc. (m/z)
-6					1277.45	1277.7			1295.70	1296.2
-7	1098.60	1098.5	1096.2	1097.2	1094.80	1095.0	1100.50	1100.7	1110.70	1110.9
-8	960.95	961.0	960.25	959.9	957.90	958.0	962.90	963.0	971.90	971.9
-9	854.15	854.1	853.05	853.1	851.50	851.5	856.05	855.9	863.85	863.8
-10	768.60	768.6	767.60	767.7	766.15	766.2	770.40	770.2		
-11	698.25	698.7	698.15	697.6	696.65	696.5	699.75	700.1		

	55 ***7701.3 g/mol*** $C_{258}H_{324}N_{74}O_{154}P_{24}S_{1}$		***56*** [a] ***7749.3 g/mol*** $C_{257}H_{316}N_{96}O_{139}P_{24}S_{1}$		***57*** ***7649.1 g/mol*** $C_{250}H_{316}N_{80}O_{154}P_{24}$		***58*** ***7640.1 g/mol*** $C_{250}H_{317}N_{77}O_{156}P_{24}$		***59*** ***7625.1 g/mol*** $C_{249}H_{316}N_{78}O_{155}P_{24}$	
Z	found (m/z)	calc. (m/z)	found (m/z)	calc. (m/z)	found (m/z)	calc. (m/z)	found (m/z)	calc. (m/z)	found (m/z)	calc. (m/z)
-6	1282.75	1282.5	1290.6	1290.6	1273.25	1273.8	1072.10	1272.3		
-7	1099.20	1099.2	1105.6	1106.0	1091.85	1091.7	1090.45	1090.4	1088.0	1088.3
-8	961.70	961.7	967.6	967.7	955.15	955.1	953.90	954.0	952.25	952.1
-9	854.75	854.7	860.2	860.0	848.90	848.9	847.90	847.9	846.30	846.2
-10	769.10	769.1	774.2	773.9	763.90	763.9	763.05	763.0	761.35	761.5
-11	699.10	699.1	703.4	703.5	694.3	694.4	693.55	693.5	692.2	692.2

	60 ***7665.1 g/mol*** $C_{250}H_{316}N_{80}O_{155}P_{24}$		***61*** ***7736.2 g/mol*** $C_{254}H_{321}N_{79}O_{155}P_{24}S_{1}$		***62*** ***7672.1 g/mol*** $C_{249}H_{309}N_{99}O_{140}P_{24}$		***63*** ***7663.1 g/mol*** $C_{249}H_{310}N_{96}O_{142}P_{24}$		***64*** ***7648.1 g/mol*** $C_{248}H_{309}N_{97}O_{141}P_{24}$	
Z	found (m/z)	calc. (m/z)	found (m/z)	calc. (m/z)	found (m/z)	calc. (m/z)	found (m/z)	calc. (m/z)	found (m/z)	calc. (m/z)
-6	1275.95	1276.5	1288.55	1288.4	1277.20	1277.7				
-7	1093.85	1094.0	1104.1	1104.2	1094.90	1095.0	1094.15	1093.7	1091.45	1091.6
-8	957.05	957.1	966.0	966.0	958.05	958.0	956.80	956.9	954.95	955.0
-9	850.65	850.7	858.35	858.6	851.35	851.5	850.40	850.5	848.80	848.8
-10	765.55	765.5	772.50	772.6	766.15	766.2	765.35	765.3	763.65	763.8
-11	695.65	695.8	702.45	702.3	696.45	696.5				

	65 ***7688.1 g/mol*** $C_{249}H_{309}N_{99}O_{141}P_{24}$		***66*** ***7759.3 g/mol*** $C_{253}H_{314}N_{98}O_{141}P_{24}S_1$		***67*** ***7726.3 g/mol*** $C_{258}H_{323}N_{77}O_{153}P_{24}S_1$		***76*** [a] ***8706.2 g/mol*** $C_{306}H_{362}N_{102}O_{150}P_{26}S_1$		***77*** [a] ***8423.8 g/mol*** $C_{293}H_{360}N_{76}O_{167}P_{26}$	
Z	found (m/z)	calc. (m/z)	found (m/z)	calc. (m/z)	found (m/z)	calc. (m/z)	found (m/z)	calc. (m/z)	found (m/z)	calc. (m/z)
-6					1287.35	1286.7				
-7	1096.90	1097.3	1107.55	1107.5	1102.70	1102.7			1202.4	1202.4
-8	959.95	960.0	968.95	968.9	964.60	964.8	1087.0	1087.3	1052.2	1052.0
-9	853.15	853.2	861.05	861.1	857.3	857.5	966.4	966.4	935.5	935.0
-10	767.80	767.8	775.10	774.9	771.7	771.6	869.4	869.6	841.4	841.4
-11					701.25	701.4	790.2	790.5	764.8	764.8

	78 [a] ***8682.2 g/mol*** $C_{305}H_{362}N_{100}O_{151}P_{26}S_1$		***79*** [a] ***8448.8 g/mol*** $C_{293}H_{359}N_{79}O_{166}P_{26}$		***80*** ***8315.8 g/mol*** $C_{288}H_{343}N_{100}O_{146}P_{25}$		***81*** ***8243.7 g/mol*** $C_{288}H_{351}N_{76}O_{162}P_{25}$	
Z	found (m/z)	calc. (m/z)	found (m/z)	calc. (m/z)	found (m/z)	calc. (m/z)	found (m/z)	calc. (m/z)
-7	1239.2	1239.3	1206.0	1206.0	1187.0	1187.0	1176.6	1176.7
-8	1084.4	1084.3	1055.2	1055.1	1038.4	1038.5	1029.4	1029.5
-9	963.6	963.7	937.3	937.8	922.9	923.0	914.9	915.0
-10	867.0	867.2	843.8	843.9	830.6	830.6	823.4	823.4
-11	788.2	788.3			755.3	755.0	748.3	748.4

[a] determined with ESI-MS

7.3 LC – MS spectra of modified oligonucleotides

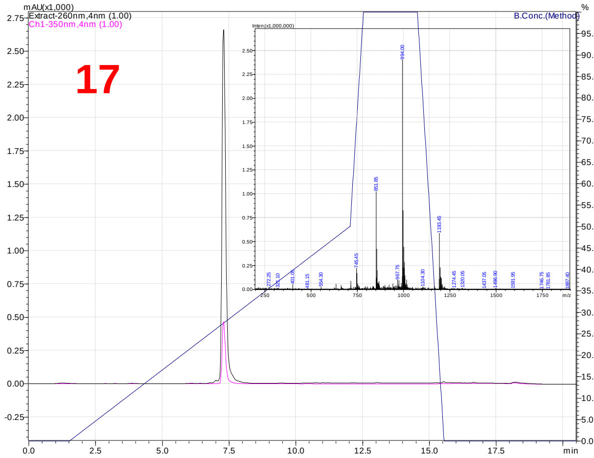

17

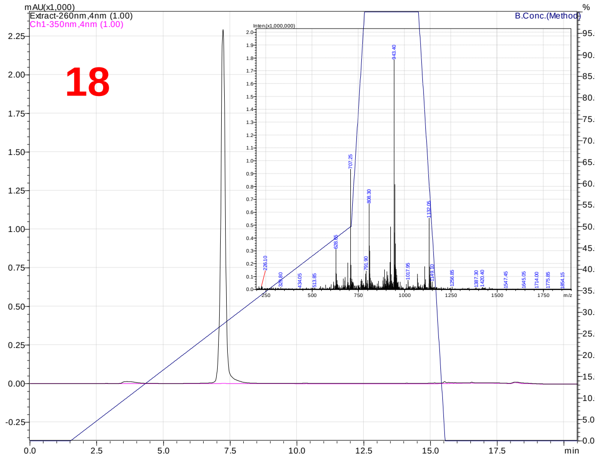

18

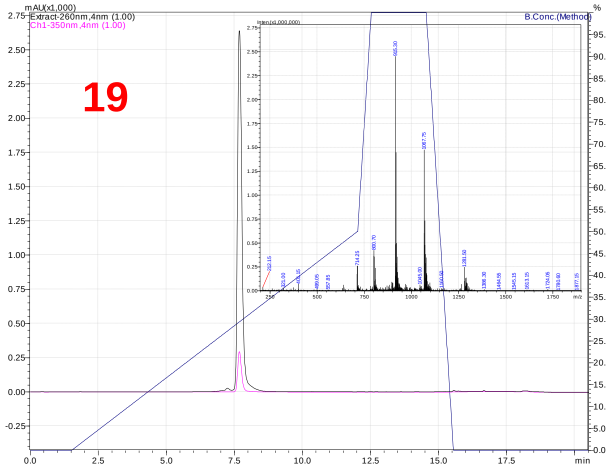

19

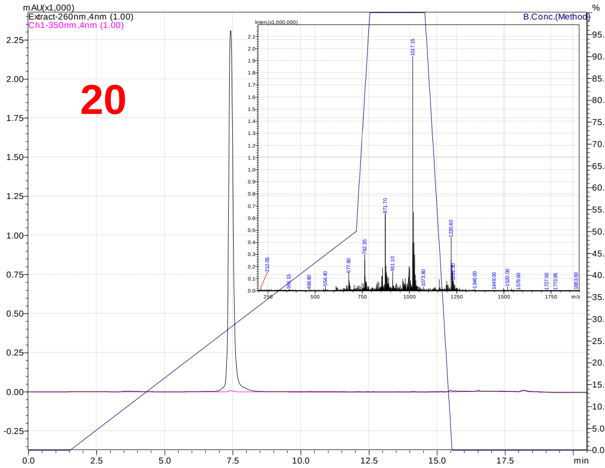

20

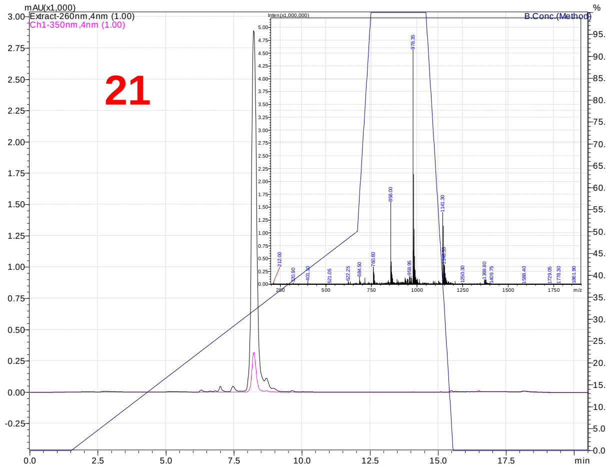

21

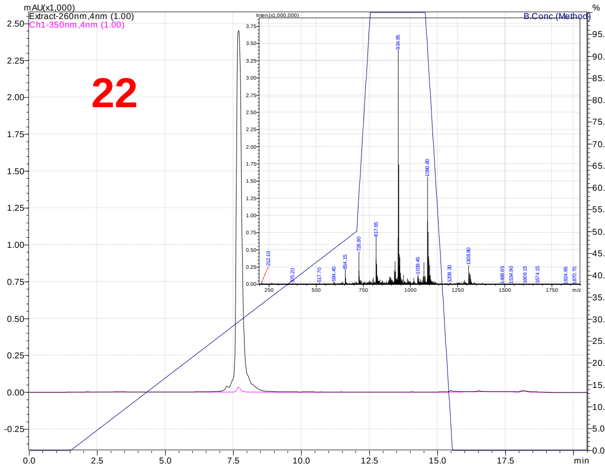

22

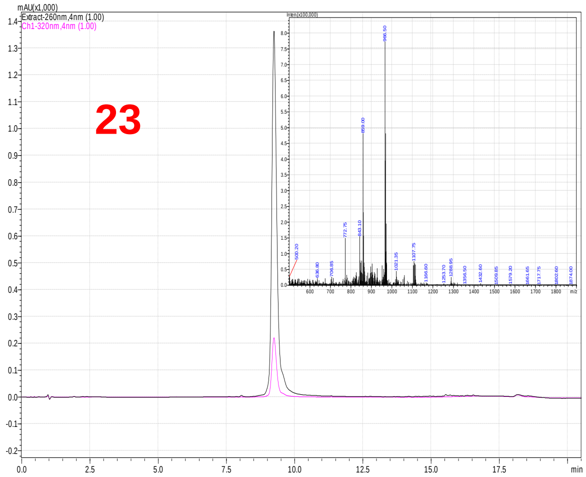
mAU(x1,000)
Extract-260nm,4nm (1.00)
Ch1-320nm,4nm (1.00)
23
min
m/z

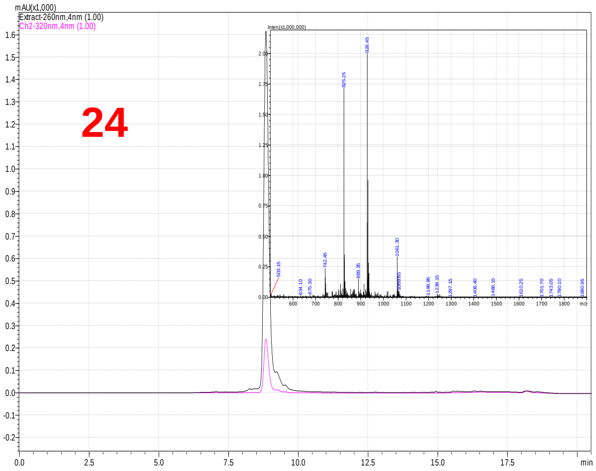
mAU(x1,000)
Extract-260nm,4nm (1.00)
Ch2-320nm,4nm (1.00)
24
min
m/z

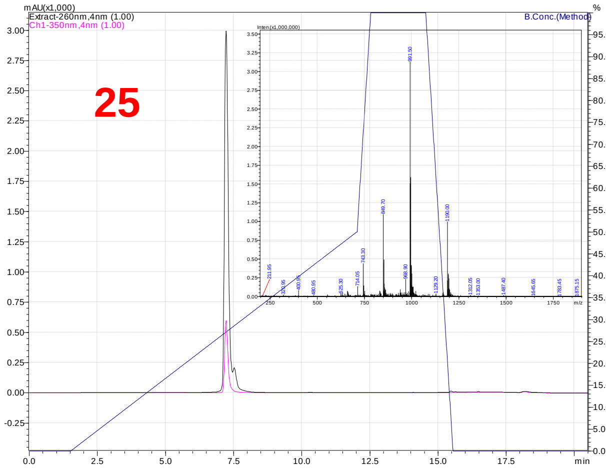
mAU(x1,000)
Extract-260nm,4nm (1.00)
Ch1-350nm,4nm (1.00)
B.Conc.(Method)
%
25
min
m/z

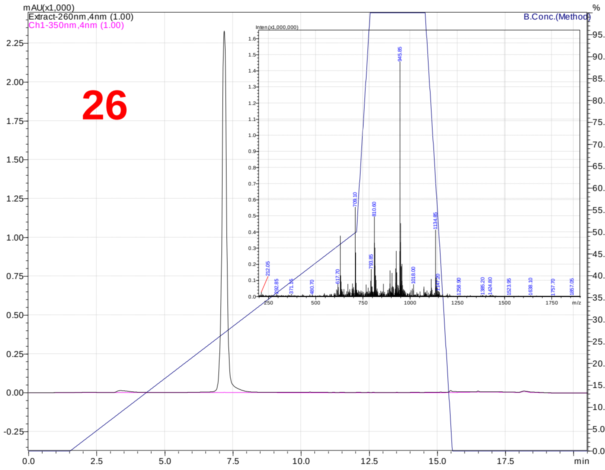
mAU(x1,000)
Extract-260nm,4nm (1.00)
Ch1-350nm,4nm (1.00)
B.Conc.(Method)
%
26
min
m/z

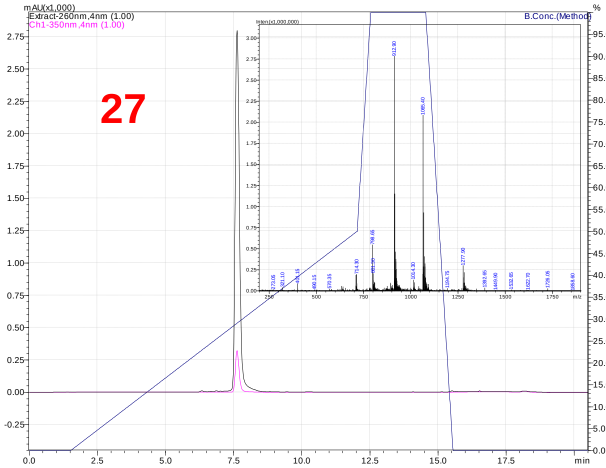
mAU(x1,000)
Extract-260nm,4nm (1.00)
Ch1-350nm,4nm (1.00)
B.Conc.(Method)
%
27
min
m/z

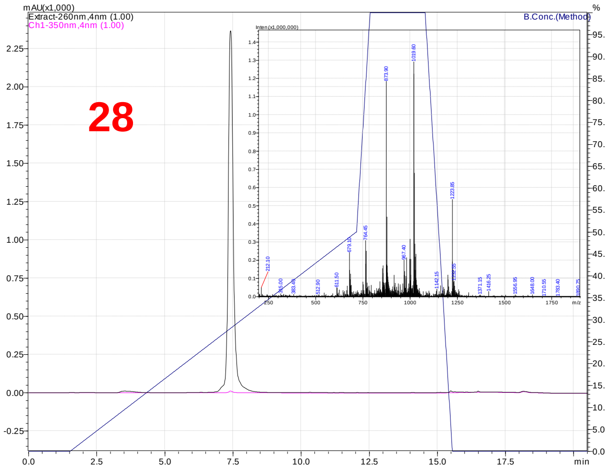
mAU(x1,000)
Extract-260nm,4nm (1.00)
Ch1-350nm,4nm (1.00)
B.Conc.(Method)
%
28
min
m/z

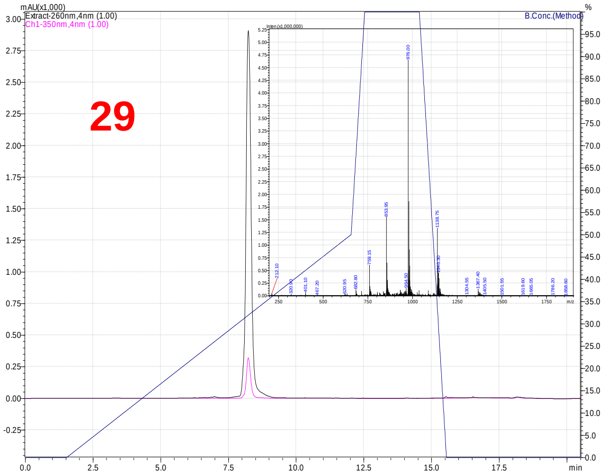
29

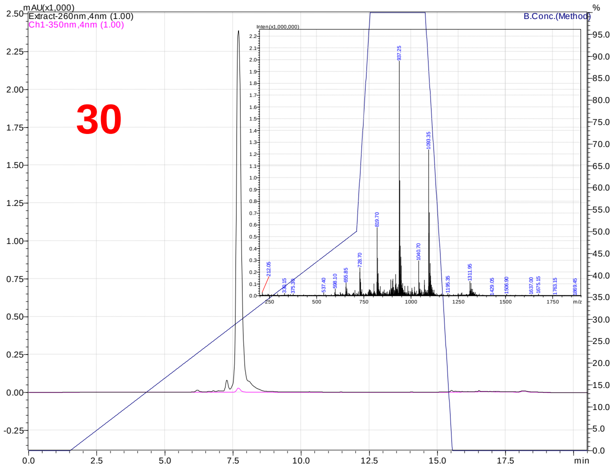
30

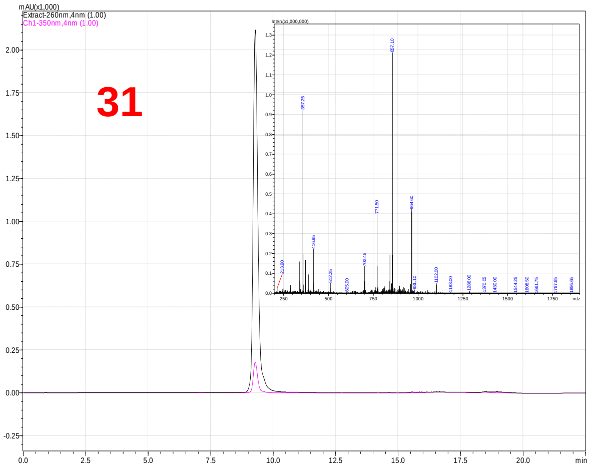
31

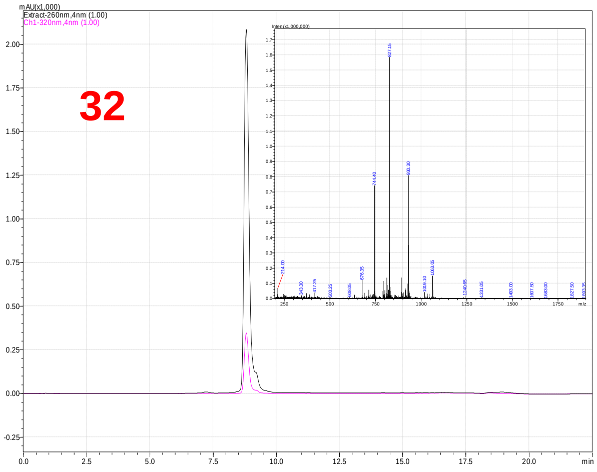
32

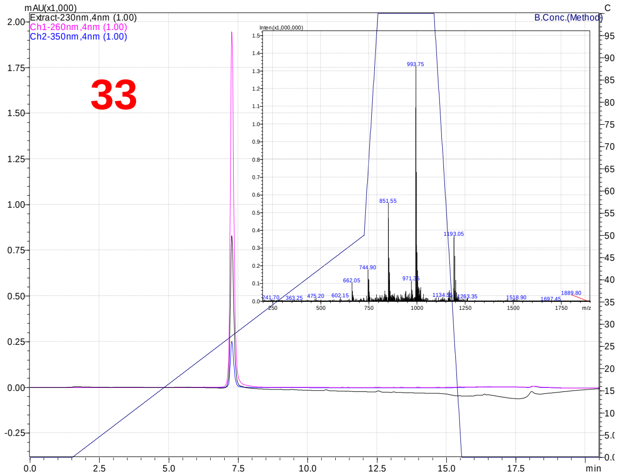
33

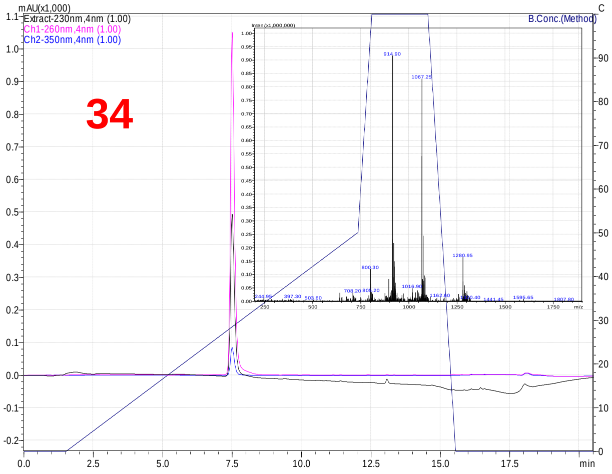
34

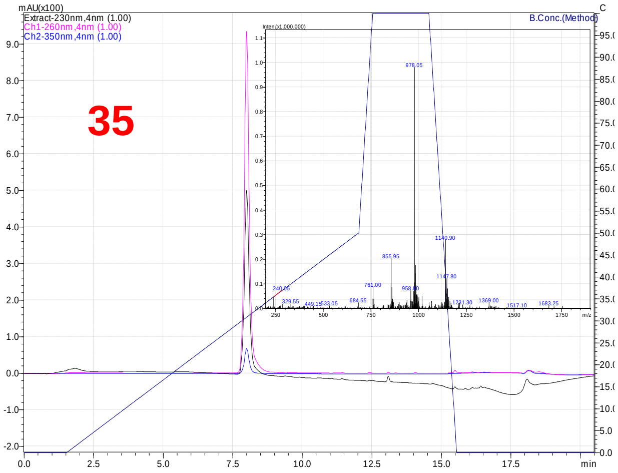
35

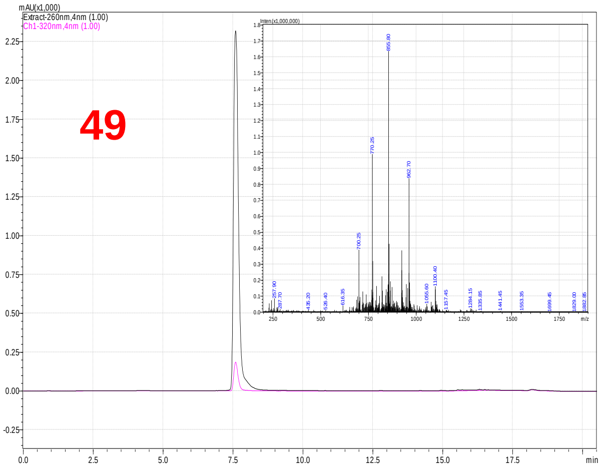
49

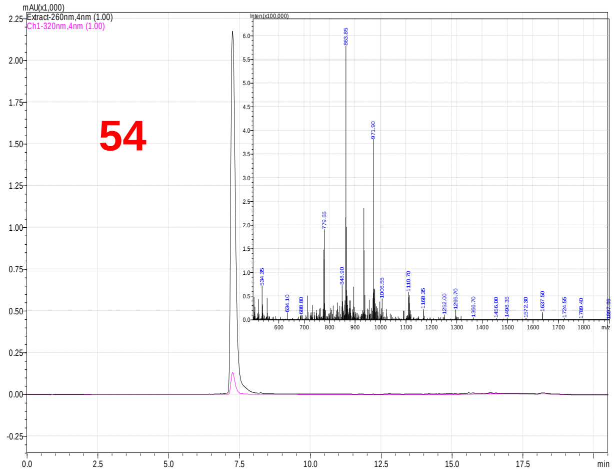
54

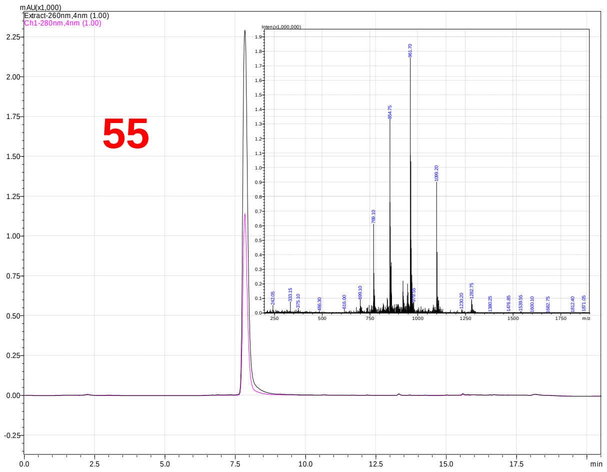
55

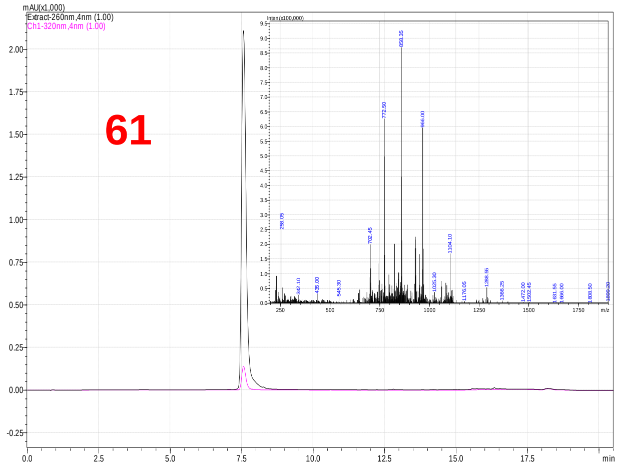
61

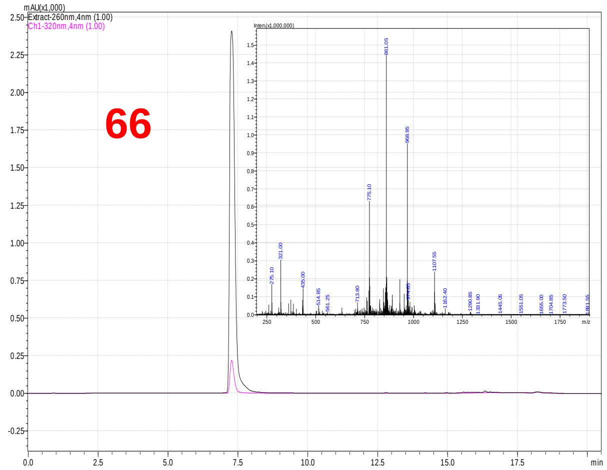
66

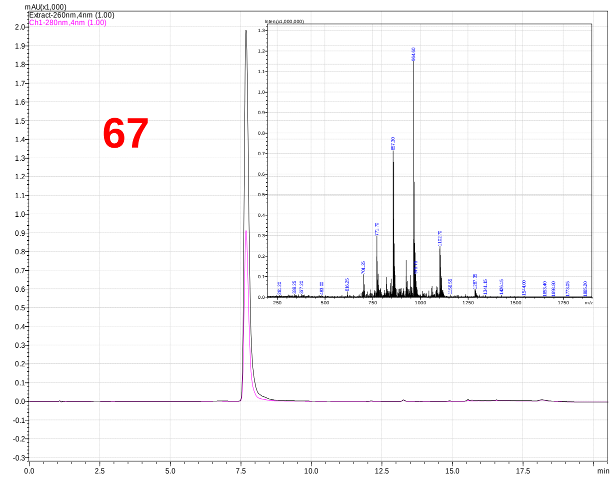
67
mAU(x1,000)
Extract-260nm,4nm (1.00)
Ch1-280nm,4nm (1.00)
Inten.(x1,000,000)
min
m/z

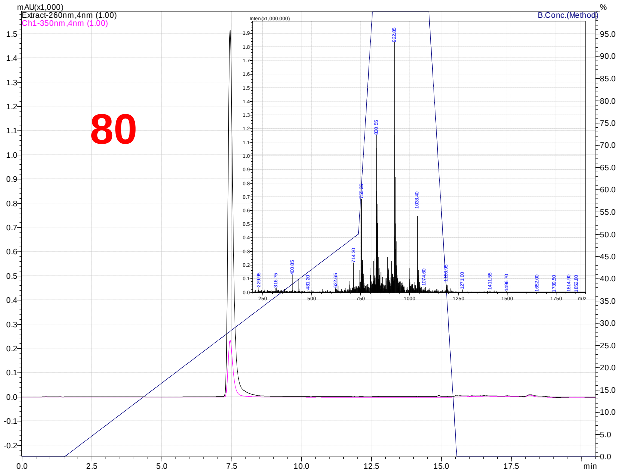
80
mAU(x1,000)
Extract-260nm,4nm (1.00)
Ch1-350nm,4nm (1.00)
B.Conc.(Method)
%
Inten.(x1,000,000)
min
m/z

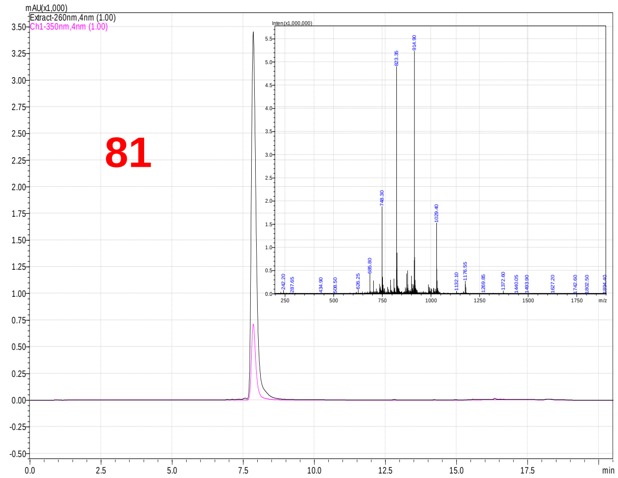
81
mAU(x1,000)
Extract-260nm,4nm (1.00)
Ch1-350nm,4nm (1.00)
Inten.(x1,000,000)
min
m/z

8. References

[1] J. D. Watson, F. H. C. Crick, *Nature* **1953**, *171*, 737-738; J. D. Watson, F. H. C. Crick, *Nature* **1953**, *171*, 964-967.

[2] F. H. Portugal, J. S. Cohen, *A Century of DNA - A History of the Discovery of the Structure and Function of the Genetic Substance*, The MIT Press, **1980**.

[3] S. L. Beaucage, M. H. Caruthers, *Tetrahedron Letters* **1981**, *22*, 1859-1862; M. H. Caruthers, *Science* **1985**, *230*, 281-285; S. Agrawal, *Protocols for Oligonucleotides and Analogs*, Humana Press, New Yersey, **1993**.

[4] J. C. Venter et. al., *Science* **2001**, *291*, 1304-1351.

[5] V. A. Bloomfield, D. M. Crothers, I. Tinoco, *Nucleic Acids - Structures, Properties and Functions*, University Science Books, **2000**.

[6] E. T. Kool, *Chemical Reviews* **1997**, *97*, 1473-1487.

[7] A. H. J. Wang, G. J. Quigley, F. J. Kolpak, J. L. Crawford, J. H. Vanboom, G. Vandermarel, A. Rich, *Nature* **1979**, *282*, 680-686; R. E. Dickerson, *Methods in Enzymology* **1992**, *211*, 67-111.

[8] L. Pauling, R. B. Corey, *Proceedings of the National Academy of Sciences of the United States of America* **1953**, *39*, 84-97; J. T. Davis, *Angewandte Chemie-International Edition* **2004**, *43*, 668-698.

[9] S. Burge, G. N. Parkinson, P. Hazel, A. K. Todd, S. Neidle, *Nucleic Acids Research* **2006**, *34*, 5402-5415.

[10] L. H. Hurley, *Nature Reviews Cancer* **2002**, *2*, 188-200.

[11] O. Khakshoor, E. T. Kool, *Chemical Communications* **2011**, *47*, 7018-7024.

[12] A. A. Henry, F. E. Romesberg, *Current Opinion in Chemical Biology* **2003**, *7*, 727-733; S. A. Benner, *Accounts of Chemical Research* **2004**, *37*, 784-797; S. A. Benner, A. M. Sismour, *Nature Reviews Genetics* **2005**, *6*, 533-543; F. Wojciechowski, C. J. Leumann, *Chemical Society Reviews* **2011**, *40*, 5669-5679.

[13] E. T. Kool, *Accounts of Chemical Research* **2002**, *35*, 936-943; N. Venkatesan, Y. J. Seo, B. H. Kim, *Chemical Society Reviews* **2008**, *37*, 648-663.

[14] A. Eschenmoser, *Science* **1999**, *284*, 2118-2124.

[15] C. J. Leumann, *Bioorganic & Medicinal Chemistry* **2002**, *10*, 841-854.

[16] A. A. Koshkin, S. K. Singh, P. Nielsen, V. K. Rajwanshi, R. Kumar, M. Meldgaard, C. E. Olsen, J. Wengel, *Tetrahedron* **1998**, *54*, 3607-3630; H. Kaur, B. R. Babu, S. Maiti, *Chemical Reviews* **2007**, *107*, 4672-4697.

[17] E. Meggers, L. Zhang, *Accounts of Chemical Research* **2010**, *43*, 1092-1102.

[18] P. E. Nielsen, M. Egholm, R. H. Berg, O. Buchardt, *Science* **1991**, *254*, 1497-1500; P. E. Nielsen, M. Egholm, O. Buchardt, *Bioconjugate Chemistry* **1994**, *5*, 3-7; B. Hyrup, P. E. Nielsen, *Bioorganic & Medicinal Chemistry* **1996**, *4*, 5-23.

[19] S. Gryaznov, J. K. Chen, *Journal of the American Chemical Society* **1994**, *116*, 3143-3144; A. Demesmaeker, A. Waldner, J. Lebreton, P. Hoffmann, V. Fritsch, R. M. Wolf, S. M. Freier, *Angewandte Chemie-International Edition in English* **1994**, *33*, 226-229; C. Richert, A. L. Roughton, S. A. Benner, *Journal of the American Chemical Society* **1996**, *118*, 4518-4531; H. Kashida, X. G. Liang, H. Asanuma, *Current Organic Chemistry* **2009**, *13*, 1065-1084.

[20] D. R. Duckett, D. M. J. Lilley, *Embo Journal* **1990**, *9*, 1659-1664.

[21] A. I. H. Murchie, R. M. Clegg, E. Vonkitzing, D. R. Duckett, S. Diekmann, D. M. J. Lilley, *Nature* **1989**, *341*, 763-766.

[22] N. C. Seeman, *Nature* **2003**, *421*, 427-431; C. Lin, Y. Liu, H. Yan, *Biochemistry* **2009**, *48*, 1663-1674; B. Sacca, C. M. Niemeyer, *Angewandte Chemie-International Edition* **2012**, *51*, 58-66.

[23] J. J. Storhoff, C. A. Mirkin, *Chemical Reviews* **1999**, *99*, 1849-1862; N. L. Rosi, C. A. Mirkin, *Chemical Reviews* **2005**, *105*, 1547-1562; U. Feldkamp, C. M. Niemeyer, *Angewandte Chemie-International Edition* **2006**, *45*, 1856-1876; H. Liu, D. Liu, *Chemical Communications* **2009**,

2625-2636; S. K. Silverman, *Angewandte Chemie-International Edition* **2010**, *49*, 7180-7201; H. Yang, K. L. Metera, H. F. Sleiman, *Coordination Chemistry Reviews* **2010**, *254*, 2403-2415; C. K. McLaughlin, G. D. Hamblin, H. F. Sleiman, *Chemical Society Reviews* **2011**, *40*, 5647-5656.

[24] G. H. Krause, E. Weis, *Annual Review of Plant Physiology and Plant Molecular Biology* **1991**, *42*, 313-349.

[25] Govindjee, *Photosynthesis: Energy conversion by plants and bacteria*, Academic Press, **1982**.

[26] R. M. Christie, *Colour Chemistry*, The Royal Society of Chemistry, **2001**; H. Zollinger, *Color Chemistry: Syntheses, Properties and Applications of Organic Dyes and Pigments*, Verlag Helvetica Chimica Acta, **2003**.

[27] G. Feher, J. P. Allen, M. Y. Okamura, D. C. Rees, *Nature* **1989**, *339*, 111-116; I. McConnell, G. H. Li, G. W. Brudvig, *Chemistry & Biology* **2010**, *17*, 434-447.

[28] J. Elemans, R. Van Hameren, R. J. M. Nolte, A. E. Rowan, *Advanced Materials* **2006**, *18*, 1251-1266.

[29] Y. C. Cheng, G. R. Fleming, in *Annual Review of Physical Chemistry, Vol. 60*, Annual Reviews, Palo Alto, **2009**, pp. 241-262; H. Tamiaki, *Coordination Chemistry Reviews* **1996**, *148*, 183-197.

[30] G. D. Scholes, *Nature Physics* **2010**, *6*, 402-403.

[31] J. M. Lehn, *Science* **2002**, *295*, 2400-2403.

[32] F. J. M. Hoeben, P. Jonkheijm, E. W. Meijer, A. Schenning, *Chemical Reviews* **2005**, *105*, 1491-1546; T. F. A. De Greef, M. M. J. Smulders, M. Wolffs, A. Schenning, R. P. Sijbesma, E. W. Meijer, *Chemical Reviews* **2009**, *109*, 5687-5754; D. Gonzalez-Rodriguez, A. Schenning, *Chemistry of Materials* **2011**, *23*, 310-325.

[33] C. A. Hunter, J. K. M. Sanders, *Journal of the American Chemical Society* **1990**, *112*, 5525-5534; C. A. Hunter, K. R. Lawson, J. Perkins, C. J. Urch, *Journal of the Chemical Society-Perkin Transactions 2* **2001**, 651-669.

[34] A. Schenning, E. W. Meijer, *Chemical Communications* **2005**, 3245-3258.

[35] D. K. Smith, F. Diederich, *Chemistry-a European Journal* **1998**, *4*, 1353-1361; A. W. Bosman, H. M. Janssen, E. W. Meijer, *Chemical Reviews* **1999**, *99*, 1665-1688; S. M. Grayson, J. M. J. Frechet, *Chemical Reviews* **2001**, *101*, 3819-3867; F. C. De Schryver, T. Vosch, M. Cotlet, M. Van der Auweraer, K. Mullen, J. Hofkens, *Accounts of Chemical Research* **2005**, *38*, 514-522.

[36] S. Xie, A. Natansohn, P. Rochon, *Chemistry of Materials* **1993**, *5*, 403-411; Y. Furusho, E. Yashima, *Chemical Record* **2007**, *7*, 1-11; E. Yashima, K. Maeda, Y. Furusho, *Accounts of Chemical Research* **2008**, *41*, 1166-1180.

[37] E. Schwartz, S. Le Gac, J. Cornelissen, R. J. M. Nolte, A. E. Rowan, *Chemical Society Reviews* **2010**, *39*, 1576-1599.

[38] V. L. Malinovskii, D. Wenger, R. Haner, *Chemical Society Reviews* **2010**, *39*, 410-422.

[39] J. N. Wilson, E. T. Kool, *Organic & Biomolecular Chemistry* **2006**, *4*, 4265-4274; R. Varghese, H. A. Wagenknecht, *Chemical Communications* **2009**, 2615-2624; T. J. Bandy, A. Brewer, J. R. Burns, G. Marth, T. Nguyen, E. Stulz, *Chemical Society Reviews* **2011**, *40*, 138-148; M. E. Ostergaard, P. J. Hrdlicka, *Chemical Society Reviews* **2011**, *40*, 5771-5788; C. Dohno, K. Nakatani, *Chemical Society Reviews* **2011**, *40*, 5718-5729.

[40] M. H. Caruthers, *Accounts of Chemical Research* **1991**, *24*, 278-284.

[41] R. X. F. Ren, N. C. Chaudhuri, P. L. Paris, S. Rumney, E. T. Kool, *Journal of the American Chemical Society* **1996**, *118*, 7671-7678; K. M. Guckian, B. A. Schweitzer, R. X. F. Ren, C. J. Sheils, P. L. Paris, D. C. Tahmassebi, E. T. Kool, *Journal of the American Chemical Society* **1996**, *118*, 8182-8183.

[42] T. J. Matray, E. T. Kool, *Journal of the American Chemical Society* **1998**, *120*, 6191-6192.

[43] P. L. Paris, J. M. Langenhan, E. T. Kool, *Nucleic Acids Research* **1998**, *26*, 3789-3793.

[44] E. T. Kool, J. C. Morales, K. M. Guckian, *Angewandte Chemie-International Edition* **2000**, *39*, 990-1009.

[45] J. M. Gao, C. Strassler, D. Tahmassebi, E. T. Kool, *Journal of the American Chemical Society* **2002**, *124*, 11590-11591; A. Cuppoletti, Y. J. Cho, J. S. Park, C. Strassler, E. T. Kool,

Bioconjugate Chemistry **2005**, *16*, 528-534; Y. N. Teo, J. N. Wilson, E. T. Kool, *Journal of the American Chemical Society* **2009**, *131*, 3923-3933.

[46] J. Guo, S. Wang, N. Dai, Y. N. Teo, E. T. Kool, *Proceedings of the National Academy of Sciences of the United States of America* **2011**, *108*, 3493-3498.

[47] N. Amann, E. Pandurski, T. Fiebig, H. A. Wagenknecht, *Chemistry-a European Journal* **2002**, *8*, 4877-4883.

[48] H. A. Wagenknecht, *Angewandte Chemie-International Edition* **2003**, *42*, 2454-2460.

[49] P. Kaden, E. Mayer-Enthart, A. Trifonov, T. Fiebig, H. A. Wagenknecht, *Angewandte Chemie-International Edition* **2005**, *44*, 1637-1639.

[50] E. Mayer-Enthart, H. A. Wagenknecht, *Angewandte Chemie-International Edition* **2006**, *45*, 3372-3375.

[51] E. Mayer-Enthart, C. Wagner, J. Barbaric, H. A. Wagenknecht, *Tetrahedron* **2007**, *63*, 3434-3439.

[52] L. A. Fendt, I. Bouamaied, S. Thoni, N. Amiot, E. Stulz, *Journal of the American Chemical Society* **2007**, *129*, 15319-15329.

[53] S. M. Langenegger, R. Haner, *Chemical Communications* **2004**, 2792-2793.

[54] S. M. Langenegger, R. Haner, *Helvetica Chimica Acta* **2002**, *85*, 3414-3421.

[55] S. M. Langenegger, R. Haner, *Chembiochem* **2005**, *6*, 2149-2152.

[56] V. L. Malinovskii, F. Samain, R. Haner, *Angewandte Chemie-International Edition* **2007**, *46*, 4464-4467.

[57] R. Haner, F. Samain, V. L. Malinovskii, *Chemistry-a European Journal* **2009**, *15*, 5701-5708.

[58] R. Haner, F. Garo, D. Wenger, V. L. Malinovskii, *Journal of the American Chemical Society* **2010**, *132*, 7466-7471.

[59] S. M. Langenegger, R. Haner, *Bioorganic & Medicinal Chemistry Letters* **2006**, *16*, 5062-5065.

[60] S. M. Langenegger, R. Häner, *Vol. Case UB-06/076 (24.09.04)*, **2004**; I. Trkulja, S. M. Biner, S. M. Langenegger, R. Haner, *Chembiochem* **2007**, *8*, 25-27.

[61] R. Haner, S. M. Biner, S. M. Langenegger, T. Meng, V. L. Malinovskii, *Angewandte Chemie-International Edition* **2010**, *49*, 1227-1230.

[62] I. Trkulja, R. Haner, *Bioconjugate Chemistry* **2007**, *18*, 289-292.

[63] D. Wenger, V. L. Malinovskii, R. Haener, *Chemical Communications* **2011**, *47*, 3168-3170.

[64] N. Bouquin, V. L. Malinovskii, R. Haner, *Chemical Communications* **2008**, 1974-1976.

[65] J. B. Birks, *Reports on Progress in Physics* **1975**, *38*, 903-974.

[66] F. M. Winnik, *Chemical Reviews* **1993**, *93*, 587-614.

[67] Ottoleng.M, *Accounts of Chemical Research* **1973**, *6*, 153-160.

[68] M. Gordon, D. R. Arnold, P. de Mayo, *The Exciplex*, Academic Press Inc., **1975**.

[69] R. A. Caldwell, D. Creed, H. Ohta, *Journal of the American Chemical Society* **1975**, *97*, 3246-3247.

[70] D. Creed, R. A. Caldwell, H. Ohta, D. C. Demarco, *Journal of the American Chemical Society* **1977**, *99*, 277-278.

[71] R. A. Caldwell, D. Creed, D. C. Demarco, L. A. Melton, H. Ohta, P. H. Wine, *Journal of the American Chemical Society* **1980**, *102*, 2369-2377.

[72] S. S. Khokhlova, A. I. Burshtein, *Journal of Physical Chemistry A* **2010**, *114*, 11506-11512.

[73] I. Trkulja, R. Haner, *Journal of the American Chemical Society* **2007**, *129*, 7982-7989.

[74] R. van Grondelle, V. I. Novoderezhkin, *Physical Chemistry Chemical Physics* **2006**, *8*, 793-807; T. Renger, *Photosynthesis Research* **2009**, *102*, 471-485.

[75] S. E. Webber, *Chemical Reviews* **1990**, *90*, 1469-1482; M. A. Fox, *Accounts of Chemical Research* **1992**, *25*, 569-574; D. Gust, T. A. Moore, A. L. Moore, *Accounts of Chemical Research* **1993**, *26*, 198-205; D. Gust, T. A. Moore, A. L. Moore, *Accounts of Chemical Research* **2001**, *34*, 40-48; N. Aratani, D. Kim, A. Osuka, *Accounts of Chemical Research* **2009**, *42*, 1922-1934; D. Gust, T. A. Moore, A. L. Moore, *Accounts of Chemical Research* **2009**, *42*, 1890-1898; W.-S. Li, T. Aida, *Chemical Reviews* **2009**, *109*, 6047-6076.

[76] R. W. Wagner, J. S. Lindsey, *Journal of the American Chemical Society* **1994**, *116*, 9759-9760; M. S. Vollmer, F. Wurthner, F. Effenberger, P. Emele, D. U. Meyer, T. Stumpfig, H. Port, H. C.

Wolf, *Chemistry-a European Journal* **1998**, *4*, 260-269; A. Harriman, J. P. Rostron, M. Cesario, G. Ulrich, R. Ziessel, *Journal of Physical Chemistry A* **2006**, *110*, 7994-8002.

[77] T. Forster, *Annalen Der Physik* **1948**, *2*, 55-75.

[78] R. M. Clegg, A. I. H. Murchie, A. Zechel, C. Carlberg, S. Diekmann, D. M. J. Lilley, *Biochemistry* **1992**, *31*, 4846-4856.

[79] R. M. Clegg, A. I. H. Murchie, A. Zechel, D. M. J. Lilley, *Proceedings of the National Academy of Sciences of the United States of America* **1993**, *90*, 2994-2998.

[80] S. Kawahara, T. Uchimaru, S. Murata, *Chemical Communications* **1999**, 563-564.

[81] S. Vyawahare, S. Eyal, K. D. Mathews, S. R. Quake, *Nano Letters* **2004**, *4*, 1035-1039.

[82] Y. Ohya, K. Yabuki, M. Hashimoto, A. Nakajima, T. Ouchi, *Bioconjugate Chemistry* **2003**, *14*, 1057-1066.

[83] M. Heilemann, P. Tinnefeld, G. S. Mosteiro, M. Garcia-Parajo, N. F. Van Hulst, M. Sauer, *Journal of the American Chemical Society* **2004**, *126*, 6514-6515; G. Sanchez-Mosteiro, E. M. H. P. van Dijk, J. Hernando, M. Heilemann, P. Tinnefeld, M. Sauer, F. Koberlin, M. Patting, M. Wahl, R. Erdmann, N. F. van Hulst, M. F. Garcia-Parajo, *Journal of Physical Chemistry B* **2006**, *110*, 26349-26353.

[84] Y. N. Teo, E. T. Kool, *Bioconjugate Chemistry* **2009**, *20*, 2371-2380.

[85] A. Ruiz-Carretero, P. G. A. Janssen, A. Kaeser, A. P. H. J. Schenning, *Chemical Communications* **2011**, *47*, 4340-4347; A. Ruiz-Carretero, P. G. A. Janssen, A. L. Stevens, M. Surin, L. M. Herz, A. P. H. J. Schenning, *Chemical Communications* **2011**, *47*, 884-886.

[86] V. A. Galievsky, V. L. Malinovskii, A. S. Stasheuski, F. Samain, K. A. Zachariasse, R. Haener, V. S. Chirvony, *Photochemical & Photobiological Sciences* **2009**, *8*, 1448-1454.

[87] A. Stutz, S. M. Langenegger, R. Haner, *Helvetica Chimica Acta* **2003**, *86*, 3156-3163.

[88] N. R. Markham, A. Wright, L. S. Zuker, M. Zuker, http://mfold.rna.albany.edu/.

[89] F. Samain, V. L. Malinovskii, S. M. Langenegger, R. Haner, *Bioorganic & Medicinal Chemistry* **2008**, *16*, 27-33.

[90] I. Tinoco, *Journal of the American Chemical Society* **1960**, *82*, 4785-4790.

[91] L. A. Marky, K. J. Breslauer, *Biopolymers* **1987**, *26*, 1601-1620.

[92] S. M. Langenegger, R. Haner, *Chemistry & Biodiversity* **2004**, *1*, 259-264.

[93] J. R. Lakowicz, *Principles of Fluorescence Spectroscopy*, Plenum Publishing Corporation, **1999**.

[94] P. Daublain, K. Siegmund, M. Hariharan, J. Vura-Weis, M. R. Wasielewski, F. D. Lewis, V. Shafiovich, Q. Wang, M. Raytchev, T. Fiebig, *Photochemical & Photobiological Sciences* **2008**, *7*, 1501-1508.

[95] F. D. Lewis, R. S. Kalgutkar, Y. S. Wu, X. Y. Liu, J. Q. Liu, R. T. Hayes, S. E. Miller, M. R. Wasielewski, *Journal of the American Chemical Society* **2000**, *122*, 12346-12351.

[96] P. Lianos, S. Georghiou, *Photochemistry and Photobiology* **1979**, *29*, 13-21.

[97] K. Yamana, R. Iwase, S. Furutani, H. Tsuchida, H. Zako, T. Yamaoka, A. Murakami, *Nucleic Acids Research* **1999**, *27*, 2387-2392; T. Kawai, M. Ikegami, T. Arai, *Chemical Communications* **2004**, 824-825.

[98] Y. Nakamura, T. Tsuihiji, T. Mita, T. Minowa, S. Tobita, H. Shizuka, J. Nishimura, *Journal of the American Chemical Society* **1996**, *118*, 1006-1012; Y. Nakamura, T. Fujii, S. Sugita, J. Nishimura, *Chemistry Letters* **1999**, 1039-1040.

[99] H. Beens, A. Weller, *Chemical Physics Letters* **1968**, *2*, 140-142; G. Briegleb, H. Schuster, W. Herre, *Chemical Physics Letters* **1969**, *4*, 53-58; J. Saltiel, D. E. Townsend, B. D. Watson, P. Shannon, *Journal of the American Chemical Society* **1975**, *97*, 5688-5695.

[100] Y. Masaki, Y. Uehara, S. Yanagida, C. Pac, *Chemistry Letters* **1992**, 315-318; F. D. Lewis, R. S. Kalgutkar, T. L. Kurth, *Journal of Physical Chemistry A* **2004**, *108*, 1425-1434.

[101] T. Forster, *Naturwissenschaften* **1946**, *33*, 166-175.

[102] S. H. Lin, W. Z. Xiao, W. Dietz, *Physical Review E* **1993**, *47*, 3698-3706; G. D. Scholes, X. J. Jordanides, G. R. Fleming, *Journal of Physical Chemistry B* **2001**, *105*, 1640-1651; G. D. Scholes, G. Rumbles, *Nature Materials* **2006**, *5*, 683-696; D. Beljonne, C. Curutchet, G. D. Scholes, R. J. Silbey, *Journal of Physical Chemistry B* **2009**, *113*, 6583-6599.

[103] M. Nakamura, Y. Murakami, K. Sasa, H. Hayashi, K. Yamana, *Journal of the American Chemical Society* **2008**, *130*, 6904-+; H. Kashida, K. Sekiguchi, X. G. Liang, H. Asanuma, *Journal of the American Chemical Society* **2010**, *132*, 6223-6230.

[104] C. A. M. Seidel, A. Schulz, M. H. M. Sauer, *Journal of Physical Chemistry* **1996**, *100*, 5541-5553.

[105] J. P. Knemeyer, N. Marme, M. Sauer, *Analytical Chemistry* **2000**, *72*, 3717-3724; S. Doose, H. Neuweiler, M. Sauer, *Chemphyschem* **2009**, *10*, 1389-1398.

[106] F. D. Lewis, R. L. Letsinger, M. R. Wasielewski, *Accounts of Chemical Research* **2001**, *34*, 159-170.

[107] T. Heinlein, J. P. Knemeyer, O. Piestert, M. Sauer, *Journal of Physical Chemistry B* **2003**, *107*, 7957-7964.

[108] F. D. Lewis, T. F. Wu, Y. F. Zhang, R. L. Letsinger, S. R. Greenfield, M. R. Wasielewski, *Science* **1997**, *277*, 673-676; F. D. Lewis, M. R. Wasielewski, *Topics in Current Chemisty* **2004**, *236*, 45-65.

[109] C. Behrens, L. T. Burgdorf, A. Schwogler, T. Carell, *Angewandte Chemie-International Edition* **2002**, *41*, 1763-+; T. Ito, S. E. Rokita, *Journal of the American Chemical Society* **2003**, *125*, 11480-11481.

[110] Hypercube, Gainsvillle, USA, *HyperChem Release 8.5*.

[111] J. C. Genereux, J. K. Barton, *Chemical Reviews* **2010**, *110*, 1642-1662; M. Bixon, B. Giese, S. Wessely, T. Langenbacher, M. E. Michel-Beyerle, J. Jortner, *Proceedings of the National Academy of Sciences of the United States of America* **1999**, *96*, 11713-11716; P. T. Henderson, D. Jones, G. Hampikian, Y. Z. Kan, G. B. Schuster, *Proceedings of the National Academy of Sciences of the United States of America* **1999**, *96*, 8353-8358.

[112] *International Union of Pure and Applied Chemistry (IUPAC)*, goldbook.iupac.org.

[113] F. Vollmer, W. Rettig, E. Birckner, *Journal of Fluorescence* **1994**, *4*, 65-69.

[114] J. Peet, J. Y. Kim, N. E. Coates, W. L. Ma, D. Moses, A. J. Heeger, G. C. Bazan, *Nature Materials* **2007**, *6*, 497-500; S. H. Park, A. Roy, S. Beaupre, S. Cho, N. Coates, J. S. Moon, D. Moses, M. Leclerc, K. Lee, A. J. Heeger, *Nature Photonics* **2009**, *3*, 297-U295.

[115] M. Karikomi, C. Kitamura, S. Tanaka, Y. Yamashita, *Journal of the American Chemical Society* **1995**, *117*, 6791-6792; B. Liu, G. C. Bazan, *Proceedings of the National Academy of Sciences of the United States of America* **2005**, *102*, 589-593; F. Schluetter, A. Wild, A. Winter, M. D. Hager, A. Baumgaertel, C. Friebe, U. S. Schubert, *Macromolecules* **2010**, *43*, 2759-2771.

[116] J. M. Raimundo, P. Blanchard, H. Brisset, S. Akoudad, J. Roncali, *Chemical Communications* **2000**, 939-940; K. Susumu, T. V. Duncan, M. J. Therien, *Journal of the American Chemical Society* **2005**, *127*, 5186-5195.

[117] C.-H. Chen, J. T. Lin, M.-C. P. Yeh, *Organic Letters* **2006**, *8*, 2233-2236.

[118] M. J. Edelmann, J. M. Raimundo, N. F. Utesch, F. Diederich, C. Boudon, J. P. Gisselbrecht, M. Gross, *Helvetica Chimica Acta* **2002**, *85*, 2195-2213; X. Zhang, H. Gorohmaru, M. Kadowaki, T. Kobayashi, T. Ishi-i, T. Thiemann, S. Mataka, *Journal of Materials Chemistry* **2004**, *14*, 1901-1904; S. Kato, T. Matsumoto, T. Ishi, T. Thiemann, M. Shigeiwa, H. Gorohmaru, S. Maeda, Y. Yamashita, S. Mataka, *Chemical Communications* **2004**, 2342-2343; K. R. J. Thomas, J. T. Lin, M. Velusamy, Y. T. Tao, C. H. Chuen, *Advanced Functional Materials* **2004**, *14*, 83-90; F. F. D. Oliveira, D. Santos, A. A. M. Lapis, J. R. Correa, A. F. Gomes, F. C. Gozzo, P. F. Moreira, V. C. de Oliveira, F. H. Quina, B. A. D. Neto, *Bioorganic & Medicinal Chemistry Letters* **2010**, *20*, 6001-6007.

[119] C. Kitamura, K. Saito, M. Ouchi, A. Yoneda, Y. Yamashita, *Journal of Chemical Research-S* **2002**, 511-513; M. Akhtaruzzaman, M. Tomura, J. Nishida, Y. Yamashita, *Journal of Organic Chemistry* **2004**, *69*, 2953-2958; A. L. Appleton, S. Miao, S. M. Brombosz, N. J. Berger, S. Barlow, S. R. Marder, B. M. Lawrence, K. I. Hardcastle, U. H. F. Bunz, *Organic Letters* **2009**, *11*, 5222-5225.

[120] H. Bittermann, D. Siegemund, V. L. Malinovskii, R. Haner, *Journal of the American Chemical Society* **2008**, *130*, 15285-15287.

[121] K. Pilgram, R. D. Skiles, *Journal of Heterocyclic Chemistry* **1974**, *11*, 777-780; R. H. Schieferstein, K. Pilgram, *Journal of Agricultural and Food Chemistry* **1975**, *23*, 392-395.

[122] K. Pilgram, *Journal of Heterocyclic Chemistry* **1974**, *11*, 835-837.

[123] A. D. Malakhov, M. V. Skorobogatyi, I. A. Prokhorenko, S. V. Gontarev, D. T. Kozhich, D. A. Stetsenko, I. A. Stepanova, Z. O. Shenkarev, Y. A. Berlin, V. A. Korshun, *European Journal of Organic Chemistry* **2004**, 1298-1307; H. Maeda, T. Maeda, K. Mizuno, K. Fujimoto, H. Shimizu, M. Inouye, *Chemistry-a European Journal* **2006**, *12*, 824-831; T. H. Huang, Y. J. Chen, S. S. Lo, W. N. Yen, C. L. Mai, M. C. Kuo, C. Y. Yeh, *Dalton Transactions* **2006**, 2207-2213.

[124] C. J. Grubb, D. J. ColeHamilton, M. K. Whittlesey, *Journal of the Chemical Society-Faraday Transactions* **1996**, *92*, 5005-5012.

[125] G. B. Schuster, *Accounts of Chemical Research* **2000**, *33*, 253-260; B. Giese, *Accounts of Chemical Research* **2000**, *33*, 631-636; S. A. E. Marras, *Molecular Biotechnology* **2008**, *38*, 247-255; U. Asseline, *Current Organic Chemistry* **2006**, *10*, 491-518.

[126] X. Chen, P. F. Sullivan, *Pharmacogenomics Journal* **2003**, *3*, 77-96; A. Okamoto, Y. Saito, I. Saito, *Journal of Photochemistry and Photobiology C-Photochemistry Reviews* **2005**, *6*, 108-122; K. M. Wang, Z. W. Tang, C. Y. J. Yang, Y. M. Kim, X. H. Fang, W. Li, Y. R. Wu, C. D. Medley, Z. H. Cao, J. Li, P. Colon, H. Lin, W. H. Tan, *Angewandte Chemie-International Edition* **2009**, *48*, 856-870.

[127] D. Rehm, A. Weller, *Israel Journal of Chemistry* **1970**, *8*, 259-271.

[128] Z. R. Grabowski, A. Grabowska, *Zeitschrift Fur Physikalische Chemie-Frankfurt* **1976**, *101*, 197-208.

[129] R. W. Woody, N. Berova, *Circular Dichroism - Principles and Applications*, Wiley-VCH, **2000**; N. Berova, L. Di Bari, G. Pescitelli, *Chemical Society Reviews* **2007**, *36*, 914-931.

[130] M. Watanabe, K. Goto, M. Fujitsuka, S. Tojo, T. Majima, T. Shinmyozu, *Bulletin of the Chemical Society of Japan* **2010**, *83*, 1155-1161.

[131] S. G. Fedorenko, A. I. Burshtein, *Journal of Physical Chemistry A* **2010**, *114*, 4558-4569.

[132] S. M. Biner, R. Haener, *Chembiochem* **2011**, *12*, 2733-2736.

Erklärung

gemäss Art. 28. Abs 2 RSL 05

Name/Vorname:	Garo, Florian
Matrikelnummer:	03-108-818
Studiengang:	Chemistry and Molecular Sciences
Art der Arbeit:	Dissertation
Titel der Arbeit:	Energy transfer in a DNA-based π-array – On the use as light-harvesting antenna systems
Leiter der Arbeit:	Prof. Dr. Robert Häner

Ich erkläre hiermit, dass ich diese Arbeit selbständig verfasst und keine anderen als die angegebenen Quellen benutzt habe. Alle Stellen, die wörtlich oder sinngemäss aus Quellen entnommen wurden, habe ich als solche gekennzeichnet. Mir ist bekannt dass andernfalls der Senat gemäss Artikel 36 Absatz 1 Buchstabe o des Gesetzes vom 5. September 1996 über die Universität zum Entzug des auf Grund dieser Arbeit verliehenen Titels berechtigt ist.

…………………………..…………………………….
Ort/Datum

………………………………………………
Unterschrift

Curriculum Vitae

Persönliche Daten

Name/Vorname:	Garo, Florian
Geburtsdatum:	24.03.1983
Heimatort:	Tschugg BE

Ausbildung

01/2009 – 06/2012	Doktorarbeit, Universität Bern, Prof. Dr. Robert Häner
10/2007 – 11/2008	Masterstudium, Universität Bern, Masterarbeit bei Prof. Dr. Robert Häner
10/2003 – 06/2006	Bachelorstudium, Universität Bern

Praktikum

08/2006 – 08/2007	Syngenta Crop Protection AG, Basel

Wissenschaftliche Artikel

- F.Garo, R. Häner, **2012** *(manuskript in preparation)*
- F. Garo, R. Häner, *Eur. J. Org. Chem.* **2012**, *(accepted)*
- F. Garo, R. Häner, *Angew. Chem. Int. Ed*. **2012**, *51*, 916-919
- R. Häner, F. Garo, D. Wenger, V.L. Malinovskii, *J. Am. Chem. Soc*. **2010**, *132* (21), 7466-7471
- C.-H. Huang, A. Parish, F. Samain, F. Garo, R. Häner, J. R. Morrow, *Bioconjug. Chem.* **2010**, *21*, 476–482